Investigation of molecular pathogenesis of amyotrophic lateral sclerosis and mouse models of neurodegeneration

A thesis presented in partial fulfilment of the requirements for the degree of Doctor of Philosophy to the University of London

By

Ruth Chia Pek Sim

Department of Neurodegenerative Disease
Institute of Neurology
University College London

ProQuest LLC
789 East Eisenhower Parkway
P.O. Box 1346
Ann Arbor, MI 48106-1346

Declaration

I hereby declare that this thesis is my own work and effort, and that it has not been submitted anywhere for any award. Wherever contributions of others are involved, every effort is made to indicate this clearly, with due reference to the literature, and acknowledgement of collaborative research and discussions.

Abstract

Amyotrophic lateral sclerosis (ALS) is a neurodegenerative disease affecting motor neurons causing a progressive fatal loss of motor function. Superoxide dismutase 1 (SOD1) was the first gene in which mutations were found to be causative in some familial ALS cases. To date, more than 140 genetic variants, with good evidence for pathogenicity in around 30 of these, have been identified in *SOD1* to be causative in ALS. Although we now know that mutations in *SOD1* cause the protein to acquire some unknown toxic function(s), the mechanism that leads to disease is unknown. The work presented in this thesis investigates novel aspects of mutant SOD1 (mutSOD1) protein misfolding and axonal transport defects implicated in ALS and neurodegeneration.

We hypothesize that different mutSOD1s have varying tendencies to aggregate, and it is the initial nucleation event of aggregation leading to formation of a stable protein 'seed' that is the critical point in the misfolding pathway similar to prion disease. To test this hypothesis, fibrillization assays with varying solvent conditions (pH and chaotrope concentration) were undertaken. It was demonstrated *in vitro* that misfolding of the normal cellular SOD1 protein leads to the formation of amyloid fibrils which possess the ability to seed the formation of further fibrils in an autocatalytic cascade. In order to demonstrate the relevance of these findings to *in vivo* disease, the effects of seeding fibrillization reactions with tissue homogenates obtained from transgenic ALS mouse models (tgSOD1^{G93A}) that overexpress mutant forms of the human SOD1 gene were investigated. A similar seeding effect was found using tissue homogenates as with fibrils from recombinant protein, and tissue homogenate from tgSOD1^{G93A} also seeded fibrillization of wild type protein in the assay. These novel findings may provide new insights to the disease mechanism of ALS both in familial and sporadic disease.

Legs at odd angles (Loa) is a motor and sensory neuron degeneration mouse model with a mutation in the cytoplasmic dynein heavy chain. Dynein is a molecular motor and plays a role in axonal transport in motor neurons. Loa heterozygotes

(*Loa/+*) show no impairment in the axonal transport rate of embryonic motor neurons, whereas tgSOD1^{G93A} had a slower retrograde axonal transport rate in comparison to their wildtype littermates. When *Loa/+* mice were crossed to tgSOD1^{G93A} mice, the resulting double heterozygote progeny (*Loa/+*,SOD1^{G93A}) had an improved disease phenotype compared to the tgSOD1^{G93A} parent accompanied by an increased in retrograde transport rate. In an attempt to better understand the rescue effect of mutant dynein and disease mechanisms in tgSOD1^{G93A}, another mouse model allelic to Loa known as the Abnormal rear legs (Arl) was investigated with the objective of working with an alternative mouse model with a more impaired axonal transport function. Although Arl heterozygotes (*Arl/+*) have a more severe phenotype at the histopathological level, there was no significant impairment in the axonal transport rate.

Mariusz is potentially another mouse model for motor neuron degeneration. Mariusz was produced by the mouse ENU Mutagenesis Program in Harwell. Preliminary phenotypic characterization and genome wide mapping was carried out in Harwell. Initial behavioral analyses results showed interesting neurological defects in these mice and the initial location of the mutation was mapped to a 80Mb region on the proximal end of Chromosome 18. The main work carried out on Mariusz in this thesis was the critical region mapping of the initial location of the mutation. The critical region was narrowed to 2.5Mb containing 16 genes, 5 of which were identified to be high priority candidate genes. Mutations in these candidate genes in humans have been implicated in different diseases involving motor function. More strikingly, Mariusz mice displayed some phenotypes paralleling clinical features seen in some human neurodegenerative diseases, and thus serving as another potential model for understanding the diverging mechanisms in causing neurodegeneration.

Table of contents

List of figures

List of tables

List of videos

Abbreviations

Å	Angstrom unit
a.u.	Arbitrary unit
Ac-nLPnLD-AMC	Acetyl-L-norleucyl-L-prolyl-L-norleucyl-L-aspartyl-(7-amino-4-methylcoumarin)
AEBSF	4-(2-aminoethyl)-benzenesulfonyl fluoride
AGE	Agarose gel electrophoresis
ALS	Amyotrophic lateral sclerosis
ALS-P/D	Amyotrophic lateral sclerosis with parkinson and dementia complex
ANG	Angiogenin *gene*
ApoE	Apolipoprotein E *gene*
Arl	Abnormal rear legs
ATP	Adenosine triphosphate
ATPγS	5'-(γ-thio) triphosphate
AUC	Analytical ultracentrifugation
BB	Bromophenol blue
BCA	Bichoninic acid
β–ME	β-mercaptoethanol
Boc-LRR-AMC	Boc-Leu-Arg-Arg-(7-amino-4-methylcoumarin)
BSSG	beta-sitosterol beta-D-glucoside
CD	Circular dichroism
cDNA	complementary DNA
CF	5(6)-carboxyfluorescein
CHMP2B	Charged multivesicular body protein 2b *gene*
CNS	Central nervous system
CNTF	Cilliary neurotrophic factor *gene*
cs	cross-seeded
DAPI	4',6-diamidino-2-phenylindole
DCTN1	Dynactin 1 *gene*
DJ1	DJ1 *gene*
DMEM	Dulbecco's Modified Eagle's Medium
DMSO	Dimethyl sulfoxide
DNA	Deoxyribonucleic acid
dNTP	Deoxyribonucleotide triphosphate
DSF	Differential scanning fluorimetry
DTNB	5,5'-dithiobis-(2-nitrobenzoic acid)
DTT	Dithiothreitol
DYNC1H1	Dynein heavy chain
DYNC1I	Dynein intermediate chain
EAAT	Excitatory amino acid transporter

EDTA	Ethylenediaminetetraacetic acid
EM	Electron microscope
fALS	familial ALS
FAM	5'-fluorescein-CE phosphoramidite
FBS	Fetal bovine serum
GdnHCl	Guanidine hydrochloride
GFP	Green-fluorescent protein
HEX	5'-hexachloro-fluorescein-CE phosphoramidite
HFE	Hemochromatosis *gene*
HSP	Heat shock protein
IF	Intermediate filament
IPTG	Isopropyl-ß-D-thiogalactopyranoside
LB	Luria bertani
Loa	Legs at odd angle
LM	Light microscope
MAPK	Mitogen activated protein kinase
MBR	Metal-binding region
MoRAG	Mouse Reaching and Grasping
mSOD1	Mouse SOD1
mutSOD1	Mutant SOD1
MWCO	Molecular weight cut-off
MWM	Molecular weight marker
NEDLI	E3 ubiquitin ligase
NEFH	Neurofilament heavy chain *gene*
NF	Neurofilament
NF-H	Neurofilament heavy chain
NF-L	Neurofilament light chain
NF-M	Neurofilament medium chain
NGF	Nerve growth factor
Ni-NTA	Nickel ion immobilized nitrilotriacetic acid
NMDA	N-methyl-D-aspartate
non-tg^{wt}	Non-transgenic wildtype
OD	Optical density
OMIM™	Online *Mendelian Inheritance in Man*
PC	Phosphotidylcholine
PE	Phosphotidylethanolamine
P/S	Penicillin/streptomycin
PBS	Phosphate buffered saline
PCR	Polymerase chain reaction
PRPH	Peripherin *gene*
rAT	Retrograde axonal transport
RFU	Relative fluorescence unit
RMSD	Root-mean-square deviation

ROS	Reactive oxygen species
ROX	6-carboxy-X-rhodamine
sALS	sporadic ALS
SDS	Sodium dodecyl sulphate
SDS-PAGE	SDS-polyacrylamide gel electrophoresis
SE	Sedmentation equilibrium
SETX	Senataxin *gene*
SNP	Single nucleotide polymorphism
SOD1	Superoxide dismutase 1
ss	self-seeded
S-S	Disulphide bond
Suc-LLVY-AMC	N-Succinyl-Leu-Leu-Val-Tyr-(7-amino-4-methylcoumarin)
SV	Sedimentation velocity
TARDBP	TAR DNA binding protein *gene*
TDP-43	TAR DNA binding protein
TeNT	Tetanus neurotoxin
TET	5'-tetrachloro-fluorescein-CE phosphoramidite
tgNF	Transgenic NF overexpressor
tgSOD1	Transgenic mouse overexpressing SOD1 (wildtype or mutant as denoted with superscript 'wtSOD1' or 'mut')
ThT	Thioflavin-T
Tm	Melting temperature
UPS	Ubiquitin-proteasome pathway
VAPB	VAMP (vesicle-associated membrane protein)-associated protein B and C *gene*
VEGF	Vasoendothelial growth factor *gene*
WTL	Wildtype-like
wtSOD1	Wildtype SOD1
YFP	Yellow-fluorescent protein

Acknowledgment

My heartfelt thanks to Lizzy for being a great mentor, for trusting my instinct when it came to planning and doing the experiments, for giving me the independence to run with the project and for believing that I can do all the protein stuff despite being based in a genetics lab. To Lizzy, I would not have journeyed this far in the last 4 years if you had not encouraged me to keep going – THANK YOU.

To all past and present members of the Fisher's lab – I thank you for the good times in the lab, all the chatting and laughing and tea breaks! And yet we still accomplished so much good science together. Special thanks to Fran and Marie, my coffee buddies...never failing me when I needed (or don't need!) that caffeine break. You girls make the PhD journey less lonely and a lot more fun.

To the people in the Protein Lab a.k.a. Jacko's lab – Mark, Sam, Howard. Thank you for accommodating me into your lab space, allowing me to help myself with many reagents and for teaching me how to purify my first protein prep! I would not have grown over 200L of *E.coli* and prepped more than 400mg of proteins without you. To Jacko, my protein supervisor, thank you for intentionally leaving me to learn on my own....as much as it was difficult, you've moulded me to be a stronger person when it came to having to battle my way around getting things done in the lab.

To Clarkey, special thanks to you for taking me under your wings on all things protein. I enjoyed the moments we talked about science, proteins and thermodynamics! Thank you for always keeping a look out for me...

To Papa and Mummy, this one is for you. I wouldn't be who I am today without you. To my sisters, thank you for being the outlet for me to do other non-science stuff whenever I am home...

AND above all, to my God, Jesus my saviour, for giving me life, love and grace. For without Your grace, I wouldn't be here today.

Chapter 1 Introduction

1.1 Neurodegenerative disorders of the central nervous system (CNS)

Any pathological conditions involving components of the brain or the spinal cord, whether in neuronal or non-neuronal cells, are referred to as disorders of the CNS. Neurodegenerative disorders refer to conditions primarily affecting neurons, causing either loss of structure or function. These are a large group of neurological disorders with heterogeneous clinical and pathological expressions affecting specific subsets of neurons in specific functional anatomic systems. These disorders usually arise for unknown reasons and have a progressive development. Therefore, CNS conditions which are not primarily neuronal disease are not considered to be neurodegenerative disorders (e.g. multiple sclerosis, neoplasm, metabolic defects).

Classically, neurodegenerative diseases are divided to groups based on their neuropathological hallmarks of predominant clinical features (phenotype effects e.g. movement or cognitive involvement) and the topography of predominant lesion (e.g. cerebral cortex, basal ganglia, brain stem and cerebellum and spinal cord). However, such classification is often complicated by the overlap in the clinical presentation and similarities in some molecular characteristics of the disease (e.g. presence and type of inclusions, degree of gliosis in specific brain areas) (Figure 1.1) (Bertram and Tanzi 2005). Among the hundreds of different neurodegenerative diseases, some of the most common are Alzheimer disease (AD), Parkinson disease (PD), Lewy body dementia (LBD), frontotemporal dementia (FTD), Huntington disease (HD) and amyotrophic lateral sclerosis (ALS), and prion diseases. Based on the molecular approach of classification, the diseases listed above all share a common neuropathological hallmark of having inclusions in the affected area (so they are collectively known as protein misfolding diseases) (reviewed in Gregersen *et al.* 2006 and they can be sub-categorized based on the make-up of the inclusion bodies. Examples of this molecular category are trinucleotide repeat diseases (e.g. HD, spinal cerebellar atrophy), prion diseases

Figure 1.1. Overview of the anatomical location and macroscopic and microscopic changes characteristic of some neurodegenerative disorders. The full neuropathological spectrum of these disorders is much more complex than depicted here. When there is more than one characteristic histopathological feature, these are depicted from left to right, as indicated in the labels listing microscopic changes (e.g. 2 panels for AD depict an Aβ plaque [left] and neurofibrillary tangles [right]). (Figure and legend adapted from Bertram and Tanzi 2005). (PD = Parkinson's disease, AD = Alzheimer's disease, FTD = frontotemporal dementia, LBD = Lewy Body Disease, HD = Huntington's disease, ALS = amyotrophic lateral sclerosis)

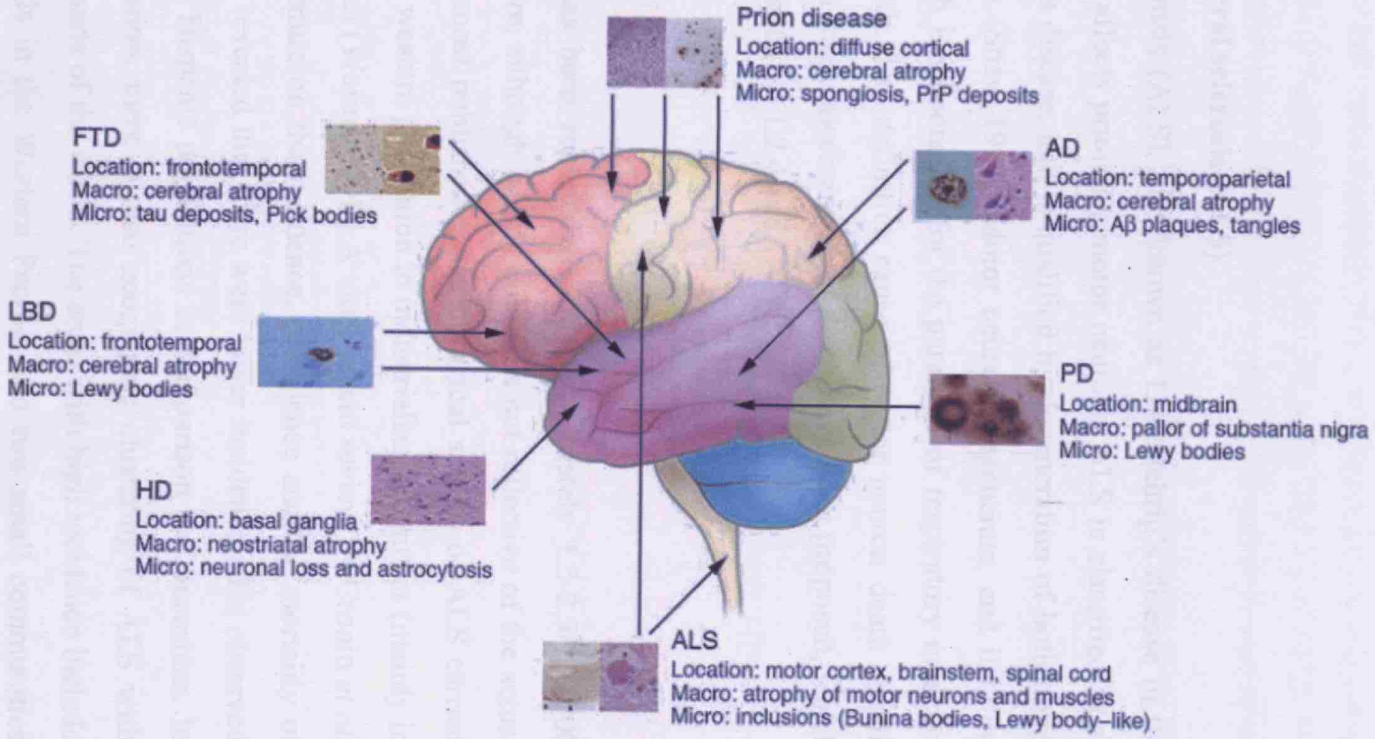

(e.g. Creutzfeldt-Jakob disease, fetal familial insomnia), synucleopathies (e.g. PD, LBD), and tauopathies (e.g. FTD). Because theses diseases share the same molecular defect (e.g. protein misfolding), by understanding the disease mechanism in one disease, it may be possible to also understand the pathogenesis of other diseases within the same category. Of the neurodegenerative diseases mentioned, the focus of this thesis is primarily on the disorders of a selective group of neurons innervating muscles, called motor neurons, which for unknown reasons degenerate giving rise to the disease known as amyotrophic lateral sclerosis (ALS).

1.2 Amyotrophic lateral sclerosis (ALS)

Amyotrophic lateral sclerosis (ALS), also known as Lou Gehrig's disease in the USA, is a disease which affects primarily motor neurons. ALS is classified as an adult-onset motor neurons disease, and is qualified by degeneration of both upper and lower motor neurons (Shaw 1999). Motor neurons degenerate, and it is the death of these cells which is responsible for the paralysis of respiratory muscles, ultimately leading to death. The definitive cause of motor neuron death is still largely unknown although many mechanisms of death have been proposed, which will be presented in more detail in 1.2.4 and 1.4.

1.2.1 Epidemiology

The incidence of ALS has been reported to be approximately 1.5-2.5/100,000 people per year. This figure, although widely quoted is not reflective of the actual global incidence because most published epidemiological studies of ALS carried out are biased towards the western population in industrialized countries (mainly in North America and Europe) (Worms 2001). A more recent review by Cronin *et al.* (2007) of the known literature on the incidence, prevalence and the mortality of ALS across all ethnicities revealed that there were lower incidence rates observed in the Asian, African and Hispanic populations in comparison to Caucasians. In addition to ethnicity variation, there is also geographic clustering of ALS with higher incidence in some parts of the world. The areas with high incidence include Guam, the Mariana Islands in the Western Pacific, and two small communities

(Kozagawa in Wakayama Prefecture and Hobara in Mie Prefecture) in the Kii peninsula of Japan (Lavine *et al.* 1991;Yoshida *et al.* 1998;Plato *et al.* 2003;Okumura 2003;Kihira *et al.* 2008). The incidence in these regions in the 1960s was reported to be 50-100 fold higher than elsewhere in the world, but the incidence rates have been declining over the last 40 - 50 years, although still slightly higher than the reported global incidence (Chancellor and Warlow 1992;Roman 1996;Plato *et al.* 2003;Kihira *et al.* 2008).

The majority of ALS cases, approximately 90%, are sporadic (sALS) with unknown cause whereas the remaining 10% are familial cases (fALS), of which 10-20% of all fALS have been linked to mutations in the SOD1 gene (Rosen *et al.* 1993) (described in 1.3.1). There is a higher incidence of ALS in men than in women with an approximate ratio of 1.5:1 (Gubbay *et al.* 1985;Haverkamp *et al.* 1995;Worms 2001;Logroscino *et al.* 2008), but this gender ratio decreases to 1:1 with age (more apparent after the age of 70 years) (Li *et al.* 1990;Haverkamp *et al.* 1995;Strong 2003;Logroscino *et al.* 2008). The reported median age of onset in most studies is between 56 and 63 years with exception of juvenile ALS which typically has onset age of less than 25 years (Rosen 1978;Gubbay *et al.* 1985;Haverkamp *et al.* 1995;Worms 2001). Coincident with the preponderance of men to be affected with ALS more than women, the age of onset also appears to follow a similar pattern where the age of onset of disease symptoms in men is earlier than women by an average of 3-4 years (Gubbay *et al.* 1985;Li *et al.* 1990;Logroscino *et al.* 2008).

The prognosis of ALS is death which happens usually within 2-5 years after the first symptoms of onset (Gubbay *et al.* 1985;Li *et al.* 1990;Haverkamp *et al.* 1995;Worms 2001;Zoccolella *et al.* 2008) with a 50% survival at 3 years, 20% survival at 5 years and 10% survival at 10 years (Talbot 2004). Survival has also been shown to somewhat correlate to the presenting clinical symptom at onset, where it has been observed that patients with bulbar symptoms, compared to loss of limb functions, were more likely to have a more rapid disease progression (Jablecki *et al.* 1989;Brooks 1991;Haverkamp *et al.* 1995;del Aguila *et al.* 2003;Ravits *et al.* 2007b;Zoccolella *et al.* 2008).

1.2.2 Diagnosis and pathology

There are no specific tests which are available for use in the diagnosis of ALS. Diagnosis is based on the history and prospective physical examination, supplemented by electrophysiological and muscle biopsy findings to rule out other conditions that may mimic the disease (e.g. lymphoma, spondylotic myelopathy) (Swash and Leigh 1992). Based on the El Escorial diagnosis criteria established by the World Federation of Neurology (WFN), for a patient to be diagnosed as having ALS, degeneration of the upper and lower motor neurons must be evident in three defined areas (brainstem, brachial, thorax and trunk, or crural) presenting as a progressive spread of symptoms within a region or to other regions over time (Swash and Leigh 1992).

1.2.2.1 Clinical features

ALS is a disease which affects upper and lower motor neurons. Damage to upper motor neurons (motor neurons that make up the corticospinal or corticobulbar pathways) presents itself clinically as muscle weakness, spasticity, stiffness and brisk reflexes, whereas damage to lower motor neurons (anterior horn cells and cranial nerve nuclei) is clinically observed as weakness in skeletal muscles accompanied by muscular atrophy, cramping, fasciculation, flaccidity and suppression of reflexes (Traynor *et al.* 2000). Patients with these features with a mid-life onset accompanied by a rapid disease progression are recognized as having 'classical ALS', whereas all other clinical or phenotype deviants are called atypical ALS.

Motor neuron degeneration

Approximately 25% of patients will present initially with primary bulbar involvement (Gubbay *et al.* 1985;Li *et al.* 1990;Haverkamp *et al.* 1995;del Aguila *et al.* 2003). Some of the more common physical findings indicative of bulbar involvement include tongue weakness, atrophy and fasciculation, deficient elevation of the laryngohyoid complex with swallowing, deficits in buccal tone, lip movements and velopharyngeal function (Lindsay and Bone 1992;Piao *et al.* 2003). While motor functions are progressively lost during the course of the

disease, ALS patients usually have preserved oculomotor muscles, sensory and autonomic functions, and voluntary sphincters of the bowel and bladder functions (Mannen *et al.* 1977;Mannen *et al.* 1982;Mannen 2000). The preservation of these functions suggests that the motor neurons innervating these muscles are spared in ALS. The oculomotor muscles are innervated by cranial nerves III, IV and V1 from the oculomotor nuclei in the brainstem, and the bladder and bowel sphincter muscles are innervated by motor neurons from the nucleus of Onufrowicz in the second and third sacral segments of the spinal cord (Pullen *et al.* 1997;Kandel *et al.* 2000;Mannen 2000). However, there are increasing reports on the observation of ophthalmoplegia and more subtle eye movement abnormalities and involvement of the Onufrowicz nucleus in ALS patients, especially in patients whose disease duration has been prolonged by means of assisted ventilation (Hayashi *et al.* 1987;Hayashi and Kato 1989;Hayashi *et al.* 1991;Carvalho *et al.* 1995). These observations were supported by histological evidence showing that inclusions characteristic of ALS (e.g. Bunina bodies, ubiquitinated inclusions, spheroids) do occur in the oculomotor and Onufrowicz nuclei without overt neuronal loss when examined at autopsy (Okamoto *et al.* 1991b;Bergmann 1993;Bergmann *et al.* 1995;Kihira *et al.* 1997;Mannen 2000).

Involvement of extra-motor CNS areas

Sensory and cognitive involvement was initially thought not to be a feature of ALS. However, there is increasing evidence that these functions are also affected in the degenerative disease course.

Several neuropsychological studies performed on ALS patients (with no prior dementia diagnosis) revealed that about 30-60% of these patients had clinically significant cognitive impairment more typically associated with frontotemporal type defects (diminished word generation, impaired memory, alterations in behavior, impairment of facial expression recognition, abstract reasoning and problem solving) (Massman *et al.* 1996;Strong *et al.* 1999;Portet *et al.* 2001;Lomen-Hoerth *et al.* 2003;Schmolck *et al.* 2007;Wheaton *et al.* 2007;Zimmerman *et al.* 2007a). Many of these clinical findings were supported by histological evidence showing degeneration of neurons in extra-motors areas

(Okamoto *et al.* 1991c;Wightman *et al.* 1992;Kawashima *et al.* 2001;Wilson *et al.* 2001;Mackenzie and Feldman 2003;Neumann *et al.* 2006) and neuroimaging studies showing global and regional atrophy of the frontal and temporal lobes of the brain (Ellis *et al.* 2001;Chang *et al.* 2005;Mezzapesa *et al.* 2007). Examples include reports showing inclusions which were positive for ubiquitin and TDP-43 but negative for tau and α-synuclein in neurons in the neocortex, cingulate gyrus, entorhinal cortex, hippocampus and amygdala accompanied by cortical spongiosis and gliosis in the non-motor brain areas of ALS patients (Okamoto *et al.* 1991c;Wightman *et al.* 1992;Kawashima *et al.* 2001;Wilson *et al.* 2001;Mackenzie and Feldman 2003;Neumann *et al.* 2006). These studies showed that ubiquitin-positive inclusions were present in both cognitively impaired and cognitively intact patients with ALS indicating that cognitive dysfunction may be an under recognized subclinical pathology.

In other studies, parkinsonism symptoms (e.g. bradykinesia, tremor, gait abnormalities), although rarely but unlikely due to chance, were also seen in ALS patients and was accompanied by neuropathological findings of nigral neuronal loss (Kato *et al.* 1993;Williams *et al.* 1995;Qureshi *et al.* 1996;Desai and Swash 1999;Zoccolella *et al.* 2002).

1.2.2.2 Histological and cytological features

Spinal cord

The main neuropathological feature of ALS is the loss of motor neurons in the CNS which parallels the appearance of clinical symptoms in patients. Neuronal loss is macroscopically seen as atrophy of the spinal cord and ventral roots, and degeneration and scarring of the corticospinal tract. Microscopically, remaining motor neurons in the ventral horn appear shrunken, show signs of apoptosis, and processes close to cell bodies are affected showing chromatolysis with diminished or distorted dendritic arborisation (Hirano 1991;Martin 1999). Gliosis is also often seen in areas of neuronal loss and several types of inclusions have been found to occur with varying degrees of specificity for ALS (Leigh and Swash 1991; de Girolami *et al.* 1999;Katayama *et al.* 1999;Kato *et al.* 2000;Sasaki *et al.* 2001;Piao *et al.*.2003;Schiffer and Fiano 2004). Descriptions of the different types of cellular inclusions found in spinal cord of ALS patients are summarized in Table 1.1 and illustrated in Figures 1.2 to 1.9.

Table 1.1. Cellular inclusions found in spinal cord of ALS patients. AHCs = anterior horn cells; ALS = amyotrophic lateral sclerosis; NFs = neurofilaments; Ⓟ+ve = phosphorylated, Ⓟ–ve = nonphosphorylated epitopes. (Compiled from (Leigh *et al.* 1989;Sasaki *et al.* 2001;Kato 2008)).

Inclusion	Site	LM appearance (stained with H&E unless stated otherwise)	EM appearance	Component protein/description	Specificity
Bunina bodies (BB)	AHCs (cytoplasm and dendrites, not found in axon)	Eosinophilic, rounded or elongated, single or arranged in small beaded chains, 1-4μm diameter	Complex, variable; vesicles with filamentous tubules, 70-80 nm diameter, small vesicles, electron dense granules	Cystatin C	Considered most specific for ALS; but rare in SOD1-linked familial ALS
Lewy body-like hyaline inclusions (LBHI)	AHCs and astrocytes	Eosinophilic core with paler peripheral halo, 7-20μm diameter	Granule-coated fibrils of 15-25 nm diameter surrounded by 10nm NFs.	NFs (Ⓟ+ve and Ⓟ–ve epitopes) SOD1 (wildtype and mutant)	Specific for SOD1-linked familial ALS
Skein-like inclusions (SLI)	AHCs	Hardly visible or detected as faintly eosinophilic when stained with H&E (Only detected when stained with ubiquitin)	Bundles of filaments with granules, 15-25nm.	Ubiquitin (-ve for SOD1)	Characteristic for sporadic ALS but not specific

Inclusion	Site	LM appearance (stained with H&E unless stated otherwise)	EM appearance	Component protein/description	Specificity
Hyaline bodies (HyB)	AHCs in spinal grey matter	Homogeneous, eosinophilic, argyrophilic conglomerates	Masses of 10 nm filaments	NFs (Ⓟ+ve Ⓟ–ve epitopes)	Not seen in controls; present in some sporadic and familial cases
Basophilic bodies (BaB)	AHCs	Basophilic, 'globoid' or 'asteroid' shapes, 3-4μm diameter (but can vary in size)	Complex, irregular chains containing filamentous or 'fuzzy' structures, with rough ER, glycogen, small vesicles and mitochondria; possibly related to Bunina bodies (?)	Ubiquitin, (-ve for NFs, phosphorylated tau, cystatin C)	Majority of ALS cases; not seen in controls
Spheroids (Sp)	AHCs (proximal axons and perikaryon)	Rounded swellings, 10-100μm diameter, hyaline, eosinophilic, argyrophilic	Masses of 10 nm filaments	NFs (Ⓟ+ve and Ⓟ–ve epitopes)	Nonspecific; seen in most controls and ALS cases

Inclusion	Site	LM appearance (stained with H&E unless stated otherwise)	EM appearance	Component protein/description	Specificity
Hirano bodies (HiB)	AHCs (Perikarya and dendrites); axons in spinal grey matter	Eosinophilic rod-shaped bodies, 4-6μm diameter	Lattice-like or parallel arrays of fine 6-10 nm filaments	Actin, α-actinin, tau, tropomyosin, vinculin	Non-specific
Granulovacuolar degeneration (GVD)	AHCs	Clear vacuoles, 3-5μm diameter containing 1μm granules	Membrane-bound inclusions with dense granular core	NFs (Ⓟ+ve epitopes) tubulin	Seen in Guamanian ALS-P/D

Figure 1.2. Bunina bodies (BB) in the anterior horn cells in the lumbar cord of amyotrophic lateral sclerosis. a) H&E staining; b) cystatin C immunoreactivities are seen in the Bunina bodies in an anterior horn cell and its dendrites (Scale bar = 10 μm); c) Electron microscopic features of a typical Bunina body. Bunina bodies, though they seem to be complicated in structure, consist mainly of two elements, one amorphous material and the other tubular and vesicular structures. Large and typical Bunina bodies consist of electron-dense amorphous material surrounded by a few tubular and vesicular structures, sometimes with a central clear area containing 10 nm filaments and other cellular organelles (Scale bar = 2 μm) (Okamoto *et al.* 2008).

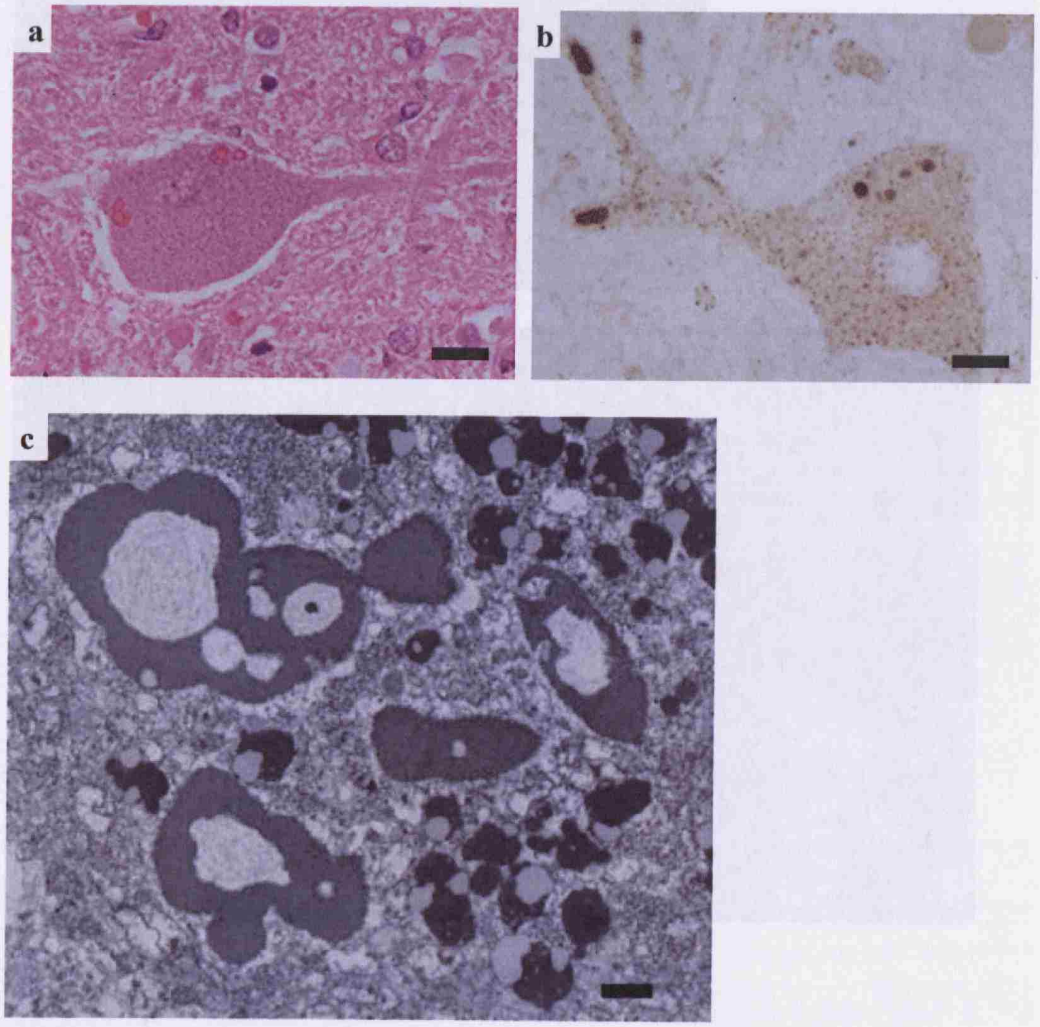

Figure 1.3. Lewy body-like hyaline inclusions (LBHI) in the cytoplasm of an anterior horn cell. a) H&E staining; swollen cytoplasm of an anterior horn cell containing multiple Lewy body-like hyaline inclusions, 650x magnification; b) Electron microscopic appearance of LBHI. Inclusions contain 13 to 25nm filamentous structures and vesicles of various sizes, 23500x magnification (Sasaki *et al.* 1989).

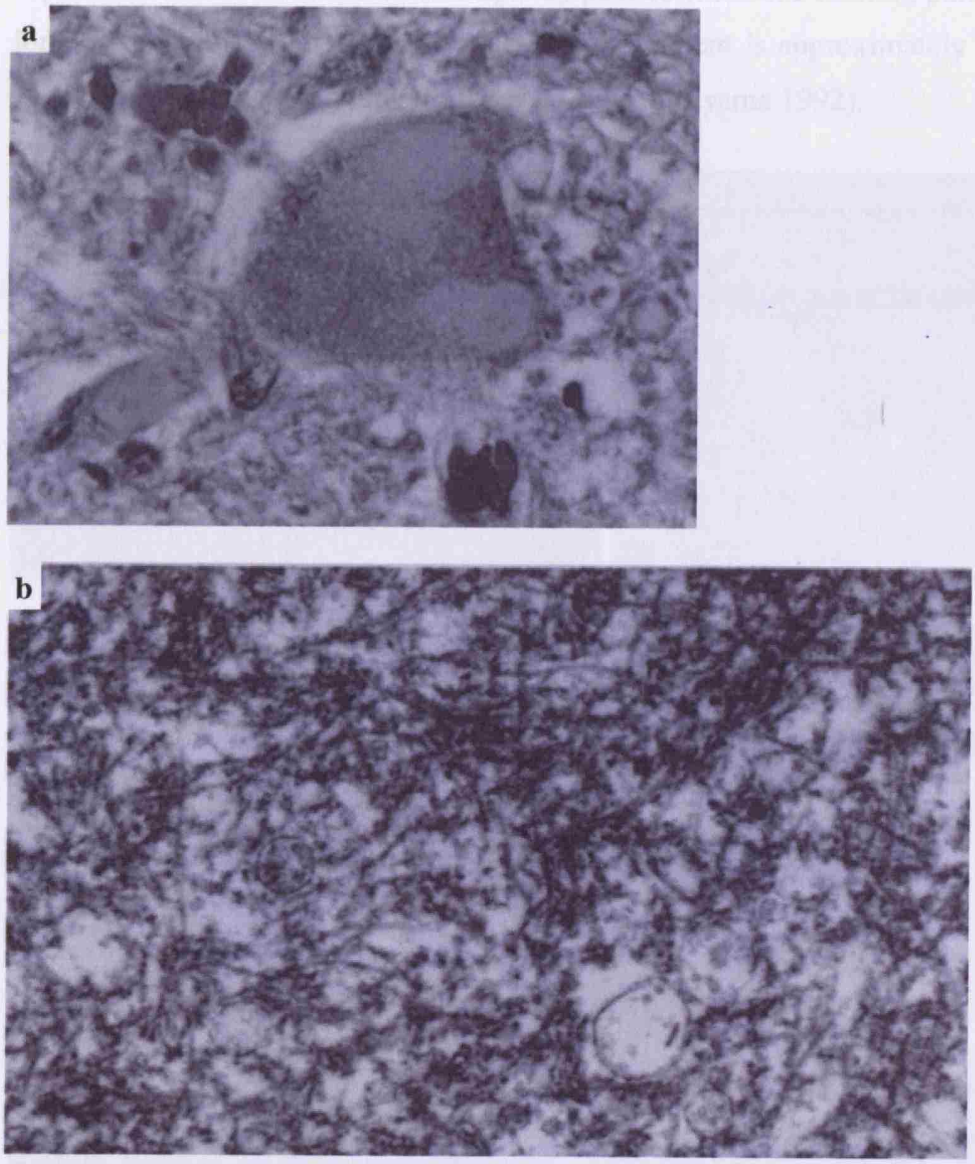

Figure 1.4. Skein-like inclusions (SLI). a) H&E staining; SLIs (arrows) were usually visualized by ubiquitin immunostaining, though some were recognized by H&E staining, showing eosinophilic tint, and linear or curvilinear structures (Scale bar = 12.5 μm) (Sasaki *et al.* 2006); b) Ubiquitin immunohistochemistry; Anterior horn in the spinal cord of an ALS patient showing threads of skein, ubiquitin-positive inclusions, 240x magnification (Adamek *et al.* 2002); c) A skein-like inclusion consists of bundles of compactly packed filaments running parallel to the longitudinal axis without fine granules. Each filament is approximately 15-25 nm in diameter, 51300x magnification (Sasaki and Maruyama 1992).

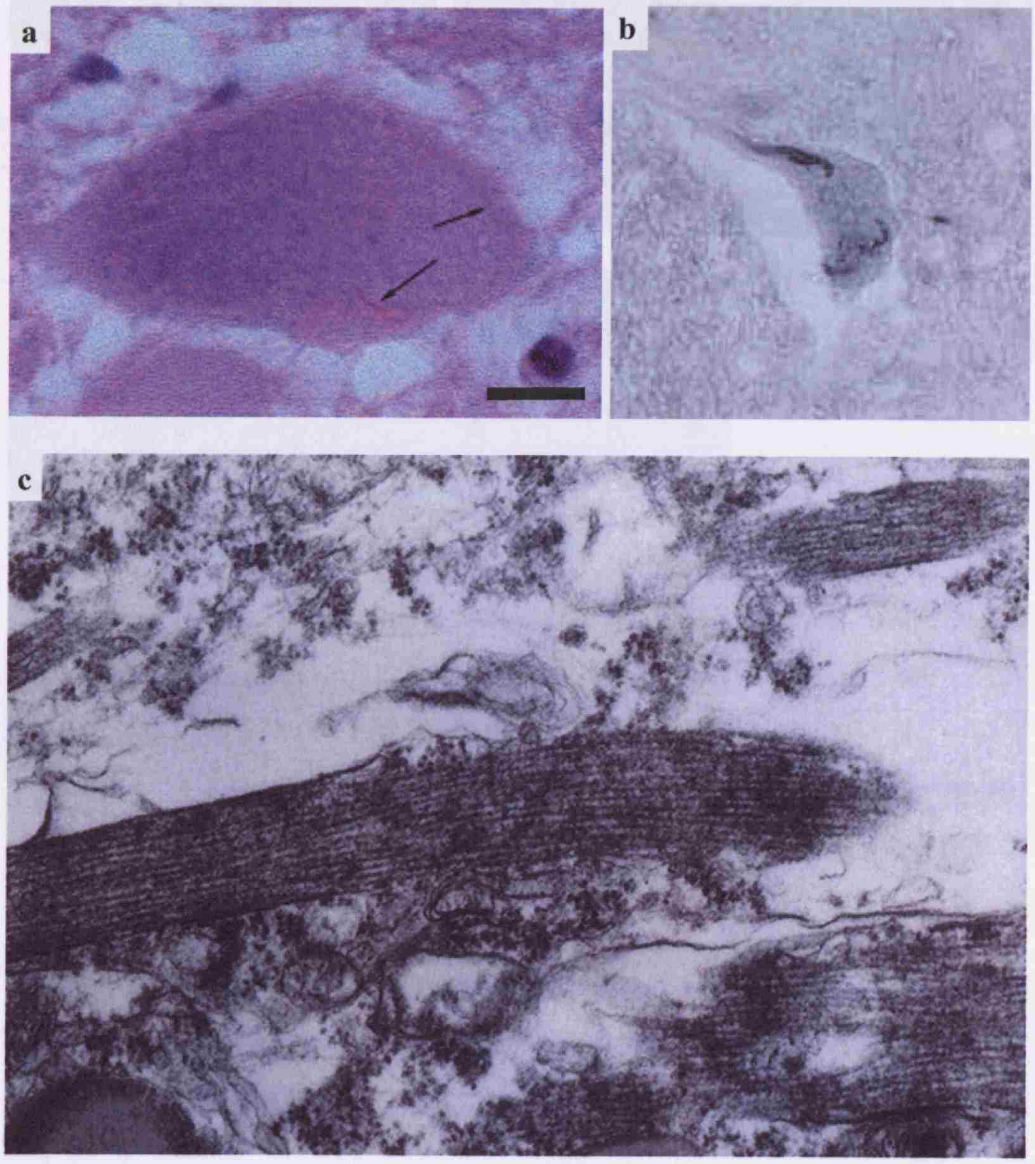

Figure 1.5. Hyaline bodies (HyB). a) H&E with luxol fast blue labeling of hyaline conglomerate inclusion (Xiao *et al.* 2006);. b) Toluidine blue A staining; Hyaline inclusion (arrow) with darkly stained core, 650x magnification; c) Electron microscopic examination of conglomerate inclusion in the perikarya of the anterior horn. The conglomerate inclusion consists of 10-nm neurofilament, 12000x magnification. Nuc: nucleus (Scale bar=1 μm) (Katayama *et al.* 1999).

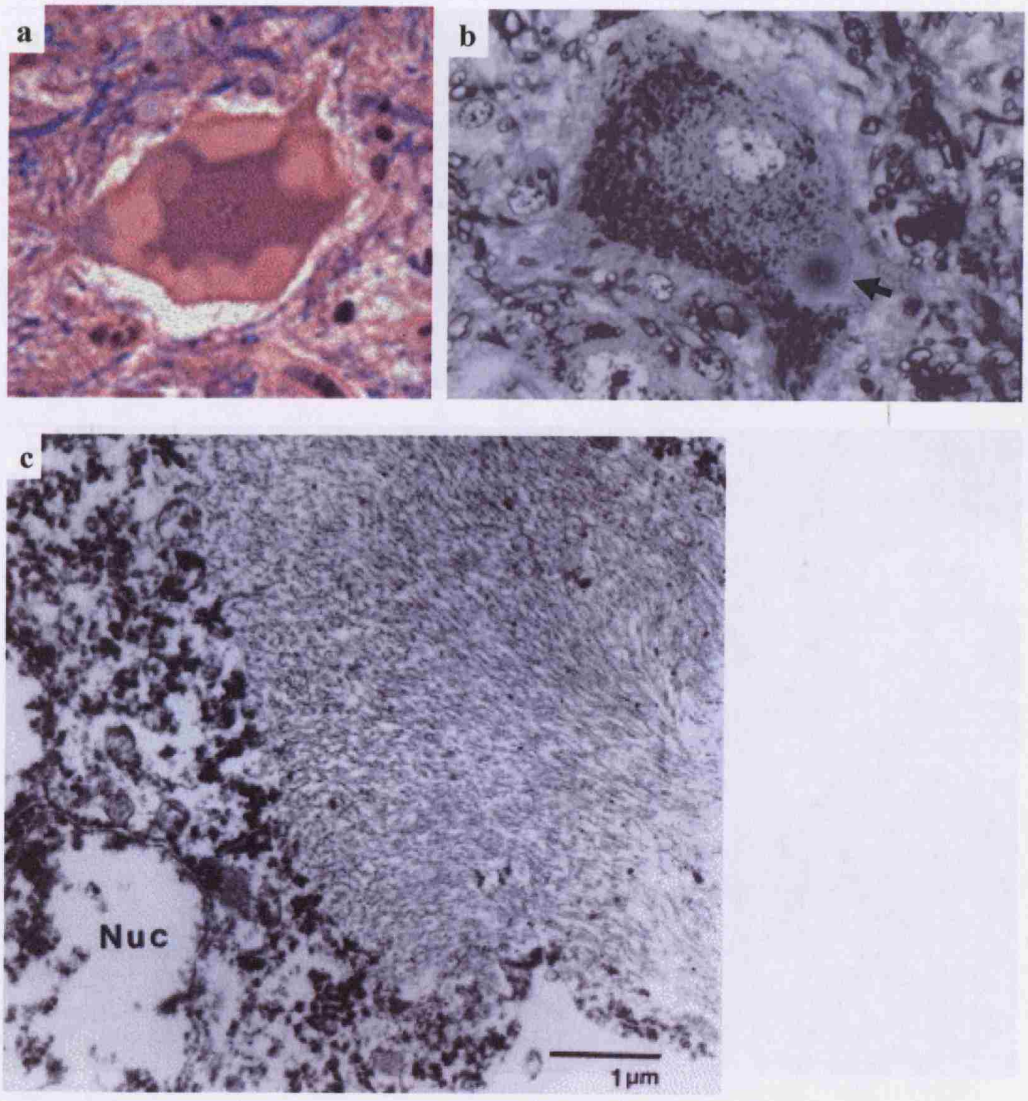

Figure 1.6. Basophilic bodies (BaB). a) H&E staining of BaB (arrow) b) The same neuron as in 'a' showing BaB immunostained for ubiquitin (arrow), 640x magnification (Sasaki *et al.* 2001); c) Electron microscopic examination of BaB. BaB consists of thick filamentous structure associated with granules. A tubular structure is observed among granule-associated filaments (arrowheads), 51300x magnification (Sasaki *et al.* 2001).

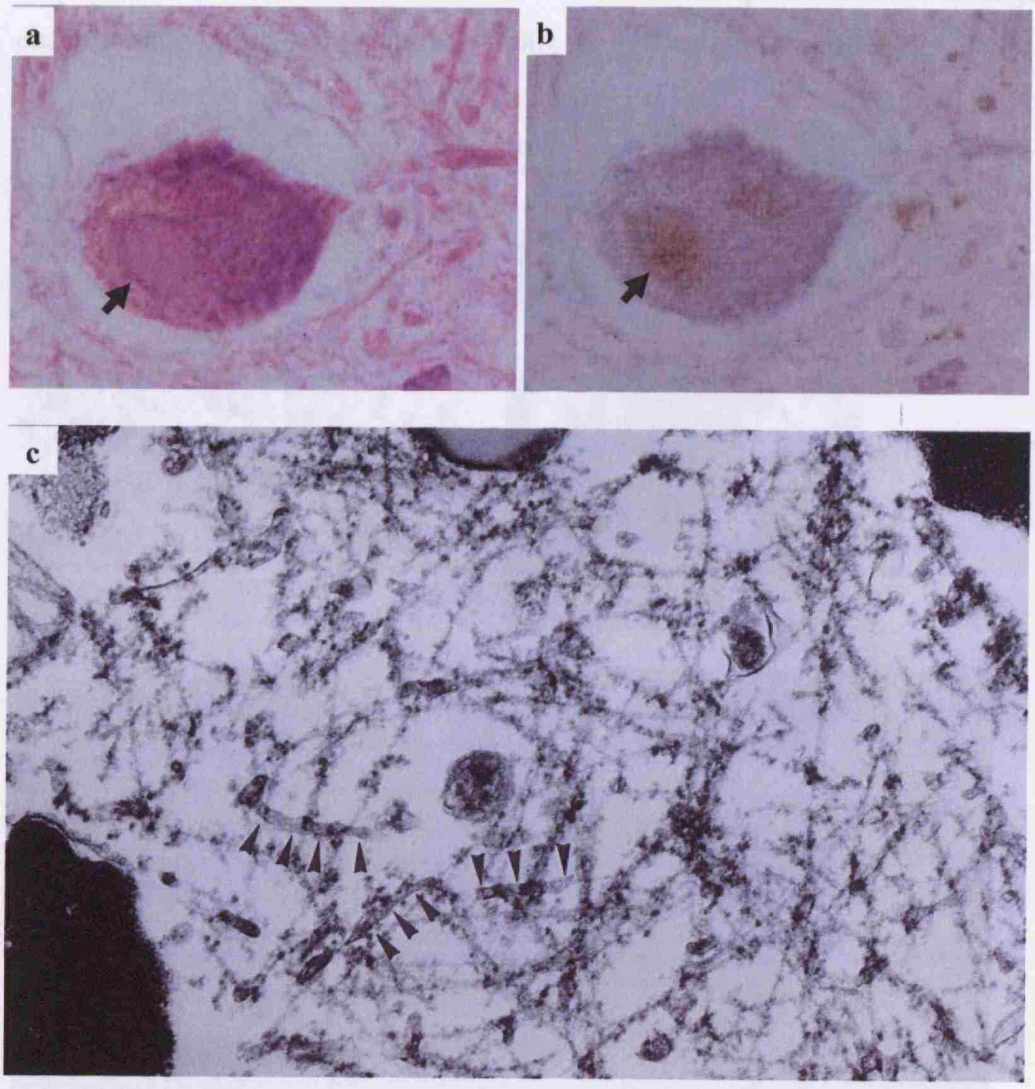

Figure 1.7. Spheroids (Sp) in the anterior if the lumbar cord. a) H&E staining, 350x magnification; b) Bielschowsky Silver impregnation, 700x magnification. (Hirano *et al.* 1984). The spheroids were argyrophilic and identified as pale, eosinophilic or sometimes faintly basophilic structures containing a wavy or whorl-like pattern of fine fibrils in H&E stain; c) Electron microscopic examination of spheroids. Increased number of 10nm neurofilaments in the perikaryon of an anterior horn cell in ALS. The bundles of NFs in the spheroids were arranged in a characteristic interwoven pattern, 38000x magnification (Hirano *et al.* 1984).

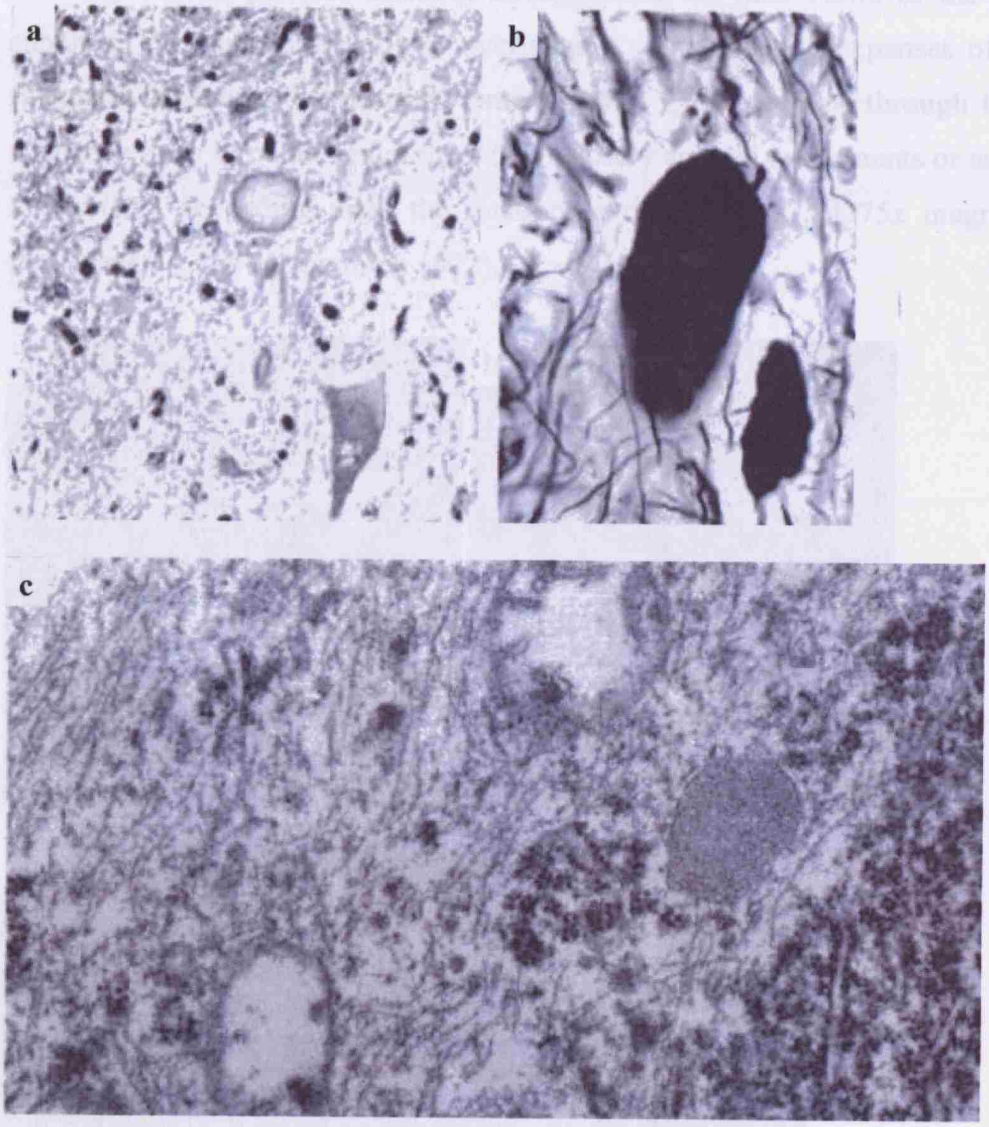

Figure 1.8. Hirano bodies (HiB). a) H&E staining; light micrograph of the hippocampal cortex illustrating a spindle-shaped juxtaganglionie Hirano body (arrow), granulovacuolar bodies and fragments of neurofibrillary tangles, 408x magnification. With H&E, the Hirano bodies appeared as eosinophilic, spindle-shaped to spheroidal structures in the neuropil and adjacent to the pyramidal cells. (Schochet, Jr. and McCormick 1972). Electron microscopic examination of b) anterior horn cells showing a large spindle-shaped Hirano body adjacent to the perikaryon of a neuron, 8250x magnification; c) sections through the Hirano bodies showing various patterns filament arrangements. *En face* views of the strata or subunits, each consisting of two overlapping or intersecting expanses of parallel filaments produce a lattice work pattern (LW). Cross sections through the strata appear as rows of punctate densities (PD) closely applied to filaments or as broader fibrils (BF) depending upon the rotation of the subunits, 84375x magnification (Schochet, Jr. and McCormick 1972).

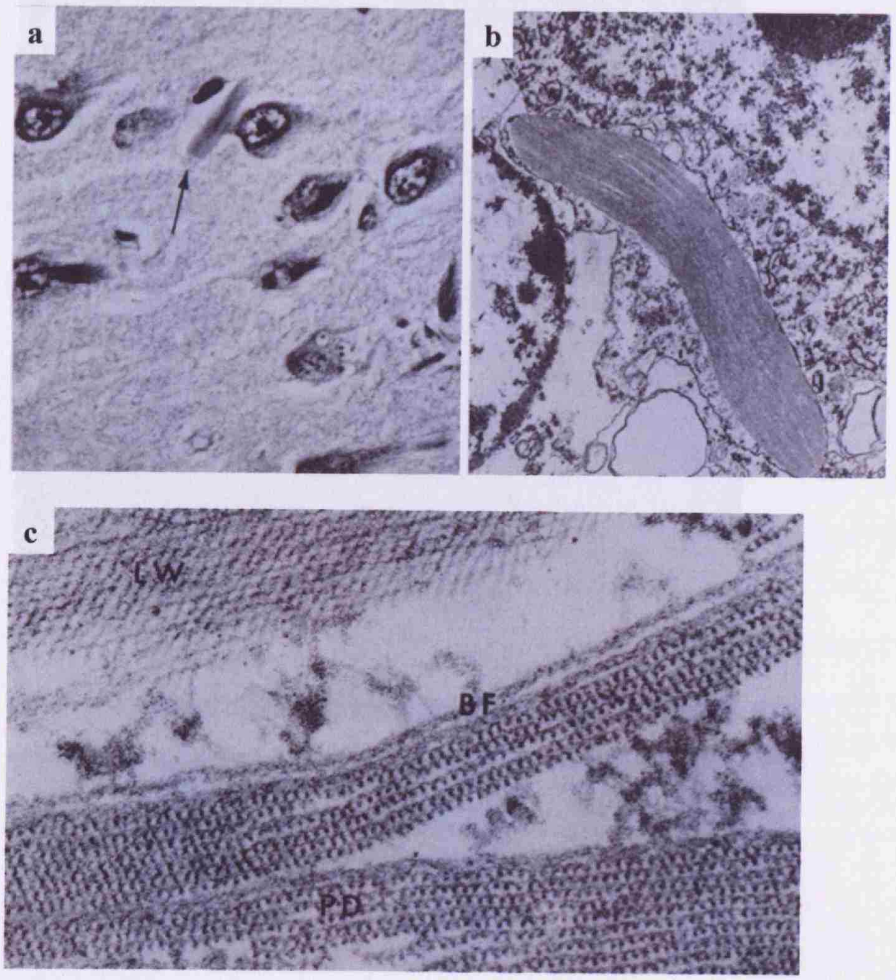

Figure 1.9. Granulovacuolar degeneration (GVD). a) H&E staining; GVD (arrow) appear as clear vacuoles containing granules, 3380x magnification. (Sasaki *et al.* 1998a); b) Electron microscopic examination of GVD showing slight-to-moderate amounts of electron-dense material surrounded by a two-layered membrane which closely resembles smooth endoplasmic reticulum. Direct connections between the inner material and neuronal cytoplasm are clearly seen. Filamentous structures are not seen in the inner material, 24400x magnification (Okamoto *et al.* 1991a).

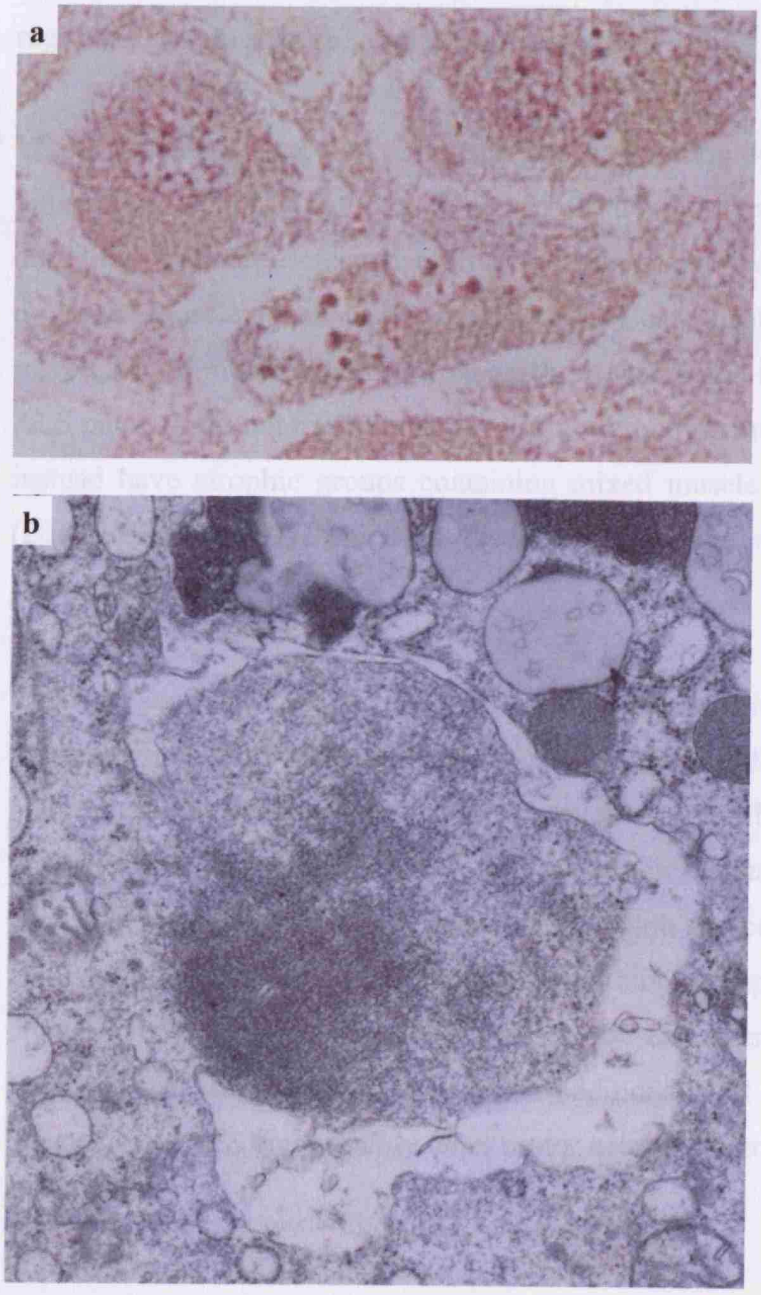

Muscles

Usually in normal muscles which have been denervated, reinnervation by sprouting from remaining intact axons will cause the muscles to regain their normal size but may result in a change in their physiologic type (two main types: slow (type I) and fast (type II)) in response to the activity pattern of the reinnervating axon (Pette 2001). Fiber types are usually distributed randomly in a checkerboard pattern throughout the muscles, which when denervation and reinnervation occurs, is usually accompanied by a change in the checkerboard pattern to a non-random regrouping of muscle fiber types (Morris 1969).

In ALS patients, atrophy of muscles is a common feature due to the loss of innervation of motor neurons. When motor neurons innervating a muscle bundle die, the physiologic response from neighbouring axons is to reinnervate the orphaned muscle fibers in the bundle and so as expected, exhibit a non-random regrouping of muscle fiber type. Recently, it was found that muscles biopsies from ALS patients, do not have the non-random regrouping muscle fiber type pattern but instead have atrophic groups containing mixed muscle fiber types (Figure 1.10) (Baloh *et al.* 2007) which is distinctive in comparison to other causes of denervation.

This was suggestive of the inability of sprouting axons in ALS to change the fiber type of reinnervated muscle fibers possibly via the inability to generate appropriate patterns of activity to convert the reinnervated muscle fiber to their type, as shown in single-fiber electromyography (EMG) where individual motor units in ALS had abnormal patterns of activity (Daube 2000). Baloh and colleagues have shown that the pattern of innervation, in terms of having more groups of atrophic muscle with mixed fiber type, seen in ALS appears to be characteristic for this disease and proposed that this could be used as an additional tool for early and differential diagnosis for ALS and possibly other motor neuron disorders.

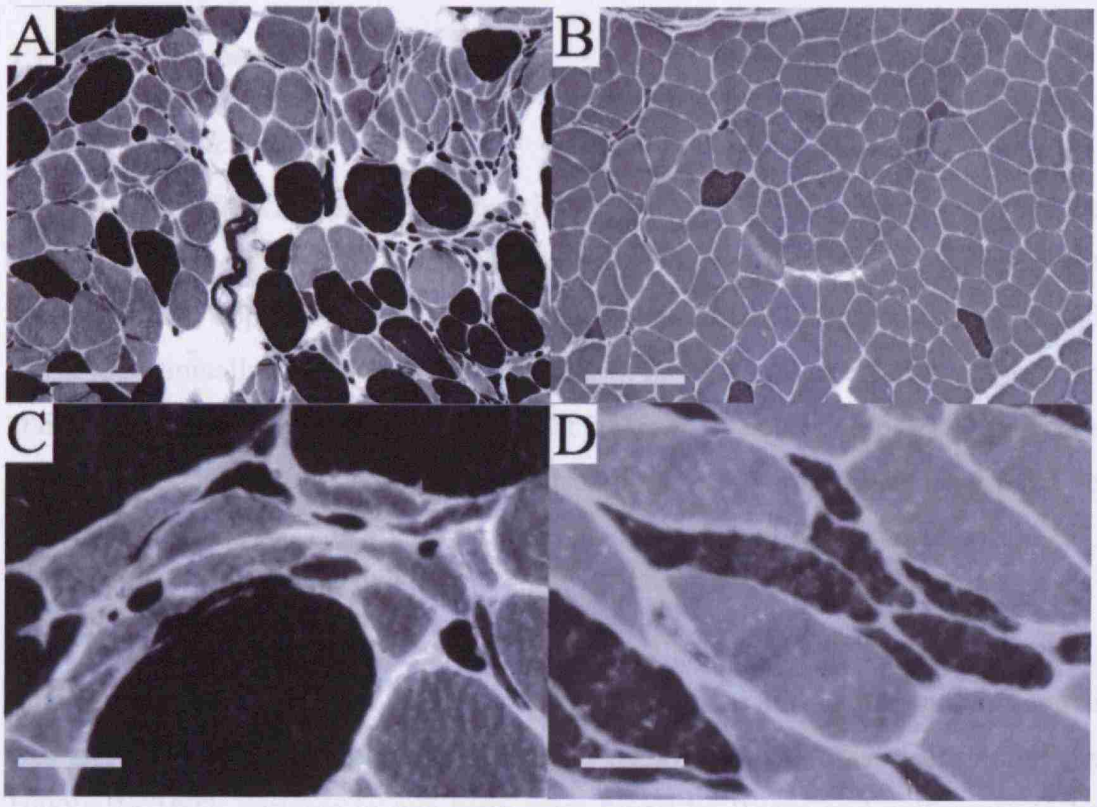

Figure 1.10. Distinctive pattern of muscle innervation and reinnervation in ALS muscles. (A,C) Muscle biopsies from patients with ALS, (B) X-linked spinal bulbar muscular atrophy (X-SBMA), and (D) polyneuropathy stained with ATPase pH 9.4 (Light staining = Type I fibers; dark staining = Type II fibers). In ALS muscle at low power (A), frequent groups of atrophic fibers contain mixed fiber types. This is seen at higher magnification in (C). SBMA biopsies (B) showed type I predominance and less frequent atrophic groups than in ALS muscle. In polyneuropathy (D), grouped atrophic fibers were less common than in ALS, and when present more commonly contained fibers of the same type. (Scale bars in the upper panels = 200 μm and in the lower panels = 25 μm). (Figure and legend from Baloh *et al.* 2007).

1.2.3 Disease cause(s) and risks

1.2.3.1 Genetics

Familial ALS (fALS) makes up approximately 10-20% of all ALS cases, with the rest being sporadic (sALS) in the absence of a positive family history. The onset age of fALS is approximately 10 years earlier than sALS, but otherwise fALS and sALS are clinically indistinguishable with both having similar disease progression and neuropathologically, both have similar patterns of neuronal loss and presence of inclusions. Due to the similarities in disease manifestation, this has led many to hypothesize that fALS and sALS may share a common pathogenic mechanism.

Familial genes and loci associated with ALS

Since the description of ALS by Charcot and Aran in the mid 1800's, nothing much was known about the genetic and molecular pathogenesis of this disease until the 1990's. In 1993, variants in one gene were found by Rosen and colleagues to be causative in 10-20% of fALS cases. The gene was superoxide dismutase 1 (*SOD1*) (Rosen *et al.* 1993). Initially found to be causative mainly in familial cases, there are now increasing numbers of sporadic cases found to also have mutations in SOD1 (approximately 2-3% of sALS) (Suthers *et al.* 1994;Andersen 2001;Alexander *et al.* 2002;Obata *et al.* 2005;Corrado *et al.* 2006;Gros-Louis *et al.* 2006;Eisen *et al.* 2008;Luquin *et al.* 2008).

A recent search carried using the term 'ALS' on OMIMTM (Online Mendelian Inheritance in Man (OMIMTM) is a continuously updated catalogue of human genes and genetic disorders) returned with more than 90 genes or loci which in some ways are associated with ALS. Of this list, only 13 loci are linked to fALS with pathogenic mutations found in 8 genes (SOD1, Alsin, SETX, VAPB, ANG, TARDBP, CHMP2B, and DJ1). The remaining 5 loci (ALS2;18q21, ALS5;15q15.1, ALS6;16q12, ALS7;20p13 and ALS-FTD;9q21), although have been detected by means of linkage in families (single or pooled families), the underlying gene defects have not yet been found (Table 1.2).

Table 1.2. Genes and loci linked to familial ALS. (AD = autosomal dominant, AR = autosomal recessive).

Disorder	Location	Gene	Inheritance / onset type	Features	Reference
ALS1	21q22.1	*SOD1*	AD/AR; adult	Classical ALS; inheritance pattern, disease onset and progression varies depending on mutation and population studied	Rosen *et al.* 1993
ALS2	2q33	*ALS2* (Alsin)	AR; juvenile	Early onset, <25 years; slow disease progression	Ben *et al.* 1990; Hentati *et al.* 1994; Yang *et al.* 2001
ALS3	18q21	Unknown	AD; adult	Classical ALS; slightly earlier onset	Hand *et al.* 2002
ALS4	9q34	*SETX* (Senataxin)	AD; juvenile	Early onset, <25 years; slow disease progression and long disease duration; normal lifespan	Rabin *et al.* 1999; De Jonghe *et al.* 2002; Chen *et al.* 2004
ALS5	15q15.1-q21.1	Unknown	AR; juvenile	Early onset; disease progression varies depending population background of which the families were studied	Hentati *et al.* 1998
ALS6	16q12	Unknown	AD; adult	Classical ALS; short disease duration; signs of FTD in some patients	Abalkhail *et al.* 2003; Ruddy *et al.* 2003; Sapp *et al.* 2003
ALS7	20p13	Unknown	AD; adult	Classical ALS; short disease duration	Sapp *et al.* 2003

Disorder	Location	Gene	Inheritance / onset type	Features	Reference
ALS8	20q13.3	*VAPB*	AD; adult	Early onset but not juvenile; slow disease progression; heterogeneous clinical phenotype (mix of classical and atypical ALS)	Nishimura *et al.* 2004a; Nishimura *et al.* 2004b; Mitne-Neto *et al.* 2007
ALS9	14q11	*ANG*	AD; adult	Classical ALS; higher preponderance for bulbar onset; shows wide phenotypic variability (causative in some fALS, but is considered a risk factor gene in sALS)	Hayward *et al.* 1999; Greenway *et al.* 2004; Greenway *et al.* 2006; Wu *et al.* 2007; Gellera *et al.* 2008
ALS10	1p36.2	*TARDBP*	AD; adult	Classical ALS	Kabashi *et al.* 2008; Sreedharan *et al.* 2008; Van Deerlin *et al.* 2008; Yokoseki *et al.* 2008
ALS-FTD1	9q21-q22	Unknown	AD; adult	Classical ALS with FTD phenotype	Hosler *et al.* 2000
ALS-CHMP2B related	3p11.2	*CHMP2B*	AD; adult	Classical ALS with no dementia; lower motor neuron predominant	Parkinson *et al.* 2006
ALS-Parkinson/ dementia complex	1p36	*DJ1*	AD; adult	Early onset-borderline juvenile/adult; complex phenotype of Parkinson, dementia with classical ALS features	Annesi *et al.* 2005

Susceptibility or risk factor genes

In addition to the genes linked to fALS, several genes have also been identified via association studies as susceptibility or risk factor genes in ALS. Due to the small sample size and heterogeneity of the sampled population studied, most of these association studies gave results which were inconclusive (variable results from association studies conducted by different groups on the same gene), nevertheless still hold true for the specific population studied. The main genes best studied are *PRPH* (peripherin), *NEFH* (neurofilament heavy chain, NF-H), *DCTN1* (dynactin 1), *VEGF* (vasoendothelial growth factor), *HFE* (hemochromatosis), *CNTF* (cilliary neurotrophic factor), and *ApoE* (apolipoprotein E) (Table 1.3).

Table 1.3. Susceptibility or risk factor genes associated with ALS.

Gene	Location	Description	Reference
PRPH (Peripherin)	12q12-q13	Peripherin is a neuronal specific cytoskeletal protein. In ALS, inclusions in spinal cord of ALS patients have found to be immunoreactive to peripherin. A frameshift deletion and missense mutations in the *PRPH* gene were found in two sALS cases from two association studies.	Gros-Louis *et al.* 2004; Leung *et al.* 2004
NEFH (Neurofilament heavy chain)	22q12.1-q13.1	Similar to peripherin, NEFH is an intermediate filament specific to neurons. NEFH has been found in many types of inclusions in spinal cord of ALS patients. Several deletion and insertion mutations in the repeat motifs of the NEFH tail domain (phosphorylation sites) have been found in cases of sALS and fALS. Although mutations were found in *NEFH,* no linkage was reported in fALS cases. It is thought that the variation in the number of repeat motif is responsible for the phenotypic variability of disease in fALS cases.	Figlewicz *et al.* 1994; Tomkins *et al.* 1998; Al-Chalabi *et al.* 1999
DCTN1 (Dynactin)	2p13	DCTN1 is large macromolecular complex (10 subunits) required for dynein-mediated retrograde axonal transport. Five missense mutations have been found in patients with predominantly lower motor neuron disease and in patients diagnosed with probable ALS. Clinical features and progression were variable between unrelated individuals and between individuals within the same family. This was suggestive of incomplete penetrance of these mutations on phenotype and may contribute as a susceptibility factor rather than being causative.	Puls *et al.* 2003; Munch *et al.* 2004; Munch *et al.* 2005

Gene	Location	Description	Reference
VEGF (Vascular endothelial growth factor)	6p12	VEGF is a growth factor responsible for promoting neovasculaturization. Expression of VEGF is partly regulated by hypoxia. Mice with targeted deletion of the hypoxia-response element (HRE) of *VEGF* gave rise to a disease-phenotype resembling ALS. This has led to the hypothesis that VEGF might play a role in causing ALS. Reports from association studies carried out on *VEGF* and sALS were not always reproducible, where some showed positive association to increased susceptibility in developing ALS while others showed otherwise. In a more recent report and the largest association study to date, it was shown that three common *VEGF* gene variations in the promoter region (-2578C/A, -1154G/A and -634G/C) showed no significant association with ALS. However, subgroup analyses by gender revealed that the -2578AA genotype linked to reduced VEGF levels, was associated with increased susceptibility to ALS in male patients.	Lambrechts *et al.* 2003; Chen *et al.* 2006; Fernandez-Santiago *et al.* 2006; Brockington *et al.* 2007; Chen *et al.* 2007; Lambrechts *et al.* 2008
HFE (Hemochromatosis)	6p21.3	*HFE* is an iron metabolism gene which has been associated with several neurodegenerative diseases. Due to the high oxidative capacity of iron, dysregulation of iron was thought to play a role in ALS pathogenesis. Association studies on sALS cases have shown that of the two most common mutations in *HFE* (*H63D* and *C282Y*), *H63D* mutation was found to be associated with an increased risk of developing ALS with a preponderance for a later onset.	Wang *et al.* 2004; Goodall *et al.* 2005; Sutedja *et al.* 2007

Gene	Location	Description	Reference
CNTF (Ciliary neurotrophic factor)	11q.12.2	The *CNTF* gene codes for a trophic factor which main role is to promote neuronal survival. A null polymorphism in *CNTF* gene, caused by a 1bp insertion in the intronic sequence of the gene, has been reported to exist in the population mainly in the heterozygous state. In the spinal cord of ALS patients, reduced levels of CNTF have been reported. In studying the effect of null mutation in the *CNTF* gene, the *CNTF* gene in mice was knocked-out which resulted in motor neuron loss. Based on these findings, it was speculated that mutations in the CNTF gene may be a susceptibility factor for ALS, but to date, no studies were able to show such association. Instead, in one family studied (SOD1-linked fALS), the CNTF null mutation was found to exert its effect as a disease phenotype modifier causing an earlier onset of disease. However, this result was not replicated in other studies.	Masu *et al.* 1993; Takahashi *et al.* 1994; Anand *et al.* 1995; Giess *et al.* 1998; Al-Chalabi *et al.* 2003
ApoE (Apolipoprotein E)	19q13.2	The ε4 allele of *ApoE (APOE4)* has been reported to be to be associated with other neurodegenerative diseases, such as Alzheimer's and Parkinson's disease. Therefore, it was speculated that this allele might also be a risk factor for ALS. Variable results were obtained from association studies conducted making it difficult to draw any conclusion on *APOE4* as a risk factor for ALS. It is generally accepted that the overall effect, if any, of the *APOE4* genotype on susceptibility and disease phenotype is not significant.	Mui *et al.* 1995 Moulard *et al.* 1996 Siddique *et al.* 1998

1.2.3.2 Exogenous factors

An example of how environmental factors could contribute to the development of ALS is the chronic consumption of flour made from cycad seeds and flying foxes (considered a delicacy) by the indigenous population of Guam, the Chomorros, as part of their diet (ALS cases in Guam are termed Guamanian-ALS because it was considered to be a variant of the more typical form of ALS reported elsewhere in the world) (Cox and Sacks 2002). A link was first observed via epidemiological studies tracking the change in their diet pattern over the years. It was found that when the Chomorros started to reduce consumption of cycad-based flour and flying foxes, the incidence rate of ALS on the island also started to decline, which strongly suggests that developing Guamanian-ALS was caused by something they ate (Spencer *et al.* 2005). It was soon shown that cycad seeds contain a neurotoxin beta-sitosterol beta-D-glucoside (BSSG), now experimentally proven to be toxic to neurons *in vivo* and *in vitro* (Khabazian *et al.* 2002;Wilson *et al.* 2002;Shaw and Wilson 2003). BSSG, the water-insoluble neurotoxin, remained in the flour made from these seeds even after washing and flying foxes which feed on cycad seeds for food accumulate BSSG in their muscles (Banack and Cox 2003). Thus, chronic consumption of the flour and flying foxes may have caused the Chomorros to be chronically exposed to BSSG, resulting in a progressive build up of the neurotoxin to a level which is toxic to neurons, thereby causing cell death (Murch *et al.* 2004;Ince and Codd 2005) and development of ALS. Although the genetic contribution to disease pathogenesis cannot be excluded, here, it clearly shows that the main etiologic agent could be an environmental neurotoxin.

Many epidemiological studies to dissect the possible exogenous factors that might cause or confer susceptibility to developing ALS have been carried out over the years. However, results from such studies have been variable. Some risk factors suggested include exposure to heavy metals and trace elements (e.g. lead, mercury, selenium, aluminium), exposure to chemicals, working with leather, welding, heavy labour, sports activities, trauma (mechanical, surgical or electrical), farming, smoking, alcohol, excess body mass and participation in the Persian Gulf war (Armon *et al.* 1991;Kurland *et al.* 1992;Strong and Pattee 2000;Armon

2001;Armon 2004;Armon 2005;Chio *et al.* 2005;Armon 2007). Of the many studies, the only association established as risk factors for ALS are age and gender. Apart from these two factors, no other factors were found to be conclusively associated, as risk factors, for ALS.

1.2.4 Proposed mechanisms of motor neuron death in ALS

Many mechanisms have been proposed to explain the underlying cause of motor neuron death in ALS. Some of the main themes of the mechanisms proposed are:

- glutamate excitotoxicity (Matyja *et al.* 2005; reviewed in Van Den *et al.* 2006)
- mitochondria dysfunction (Sasaki and Iwata 2007; reviewed in Albers and Beal 2000 and Dupuis *et al.* 2004)
- protein misfolding and aggregation (Wood *et al.* 2003;Baglioni *et al.* 2006; reviewed in Gregersen *et al.* 2006)
- oxidative stress (reviewed in Tu *et al.* 1997 and Cookson and Shaw 1999),
- cytoskeletal and axonal transport defect (reviewed in Chevalier-Larsen and Holzbaur 2006 and El-Kadi *et al.* 2007)

A summary for each thematic mechanism with some key findings is given in the following sections. A more detailed review of some of the molecular mechanisms involved in motor neuron death revealed from studies using the SOD1-linked ALS models is compiled in 1.4.2.

1.2.4.1 Glutamate excitotoxicity

Elevated glutamate levels, the primary excitatory neurotransmitter in the vertebrate CNS, have been observed in the CNS of some ALS patients (Plaitakis *et al.* 1988;Shaw *et al.* 1995a;Spreux-Varoquaux *et al.* 2002;Andreadou *et al.* 2008). Coupled with the knowledge that high levels of glutamate are toxic to neurons, this has led to the proposal that motor neuron death may be induced by glutamate excitotoxicity. Overactivation of glutamate receptors can prolong opening of

associated ion channels resulting in membrane depolarization in the post-synaptic motor neurons causing the opening of the Ca^{2+}/Na^{+} linked N-methyl-D-aspartate (NMDA) receptors, thereby facilitating excess calcium influx into motor neurons. The sustained increase in the intracellular calcium levels is detrimental to motor neurons because it can initiate downstream cascade of events ultimately leading to cell death (Rothstein 1995;Shaw and Ince 1997;Mattson 2003).

The activity of glutamate released into the synaptic cleft during neurotransmission is terminated by re-uptake via glutamate transporter proteins (EAAT) found on glial cells (EAAT1 and EAAT2) and on presynaptic motor neurons (EAAT3) (Figure 1.11). Thus, defects in EAATs can cause glutamate accumulation at the synapse. In affected areas of the CNS in sALS and fALS patients, a selective loss of EAAT2 has been reported (Rothstein *et al.* 1995;Fray *et al.* 1998;Sasaki *et al.* 2000), which adds support to the hypothesis. However, how EAAT2 is lost is not clear as no mutations were found in the EAAT2 gene (Meyer *et al.* 1995;Aoki *et al.* 1998;Jackson *et al.* 1999), suggesting that loss of EAAT2 is via some other mechanism which takes place post-translationally.

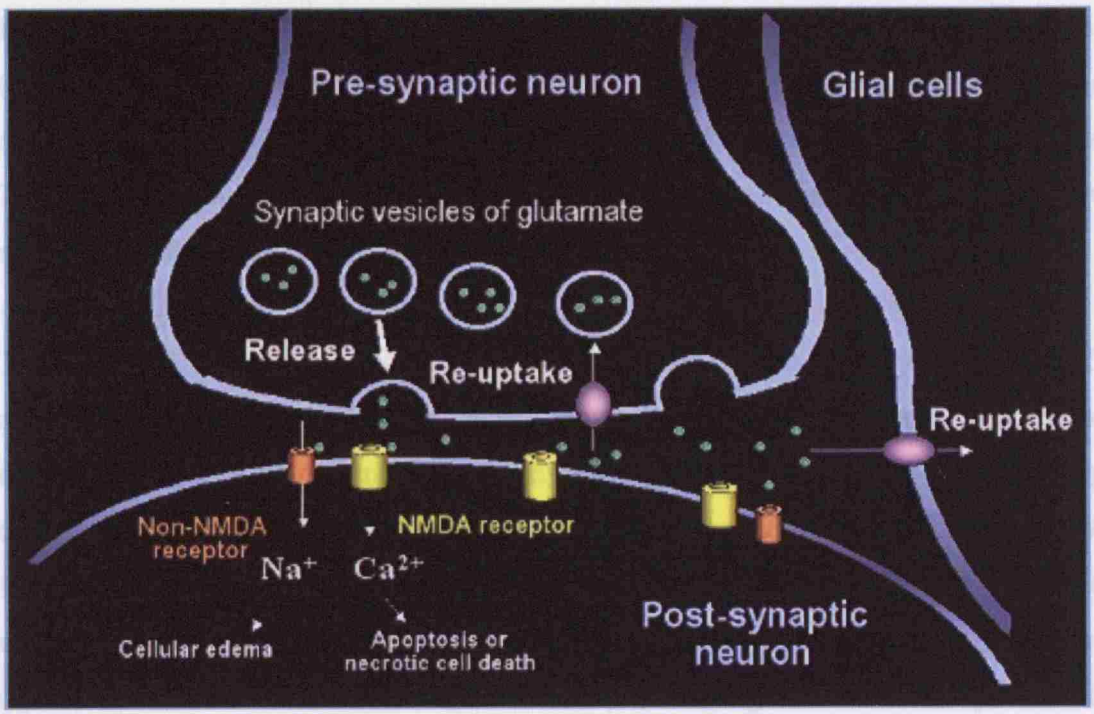

Figure 1.11. Neuronal glutamate is released from the pre-synaptic terminal into the synaptic cleft. The glutamate binding to non-NMDA receptors allows entry of Na+ into the post-synaptic neuron, resulting in cytotoxic edema. The glutamate binding to NMDA receptors allows entry of Ca^{2+} into the post-synaptic neuron resulting in necrotic cell death or apoptosis. Re-uptake of extracellular glutamate is done at the pre-synaptic terminals and adjacent glial cells.

1.2.4.2 Mitochondria dysfunction

In addition to being the 'powerhouse' of the cell in generating ATP, mitochondria also play a role in intracellular calcium buffering and regulation of apoptotic signals. Mitochondria are doubled-membrane bound organelles (inner and outer membrane) with most of their function dependent on this membrane organisation. An example of the importance of this membrane organisation is in the generation of high proton concentration in the inter-membrane space for the maintenance of a proton gradient across the inner mitochondria membrane and the matrix for ATP production via the electron transport embedded in the inner mitochondrial membrane. Mitochondrial membrane damage may also lead to a reduction in the ability to sequester calcium or may cause an outflow of calcium from mitochondrial internal storage causing a toxic increase in intracellular calcium

levels. Since mitochondria also contain many apoptotic signaling proteins (e.g. cytochrome c, an anti-apoptotic protein), release of these proteins into the cytoplasm due to a leaky membrane may inadvertently initiate apoptosis. Therefore, it is conceivable that damage to the membrane system can cause severe mitochondrial dysfunction.

The proposal that mitochondria might be involved in the pathogenesis of ALS stemmed from ultrastructural studies showing mitochondria abnormalities in motor neurons in some ALS patients and in the transgenic mouse model of ALS carrying an array of the *SOD1* gene with a G93A mutation ($tgSOD1^{G93A}$) (Okamoto *et al.* 1990;Hirano 1996;Sasaki and Iwata 1996;Kong and Xu 1998). The observed morphological abnormalities were accompanied by an alteration in the mitochondrial electron transfer chain activity (Bowling *et al.* 1993;Fujita *et al.* 1996;Browne *et al.* 1998;Borthwick *et al.* 1999) and aberrant calcium homeostasis (Curti *et al.* 1996;Siklos *et al.* 1996). Motor neurons are different from many neuronal and non-neuronal cell types. The most distinctive aspects of motor neurons are their asymmetry, large size, enormously elongated and thick and a high energy demand. It is likely that these characteristics are the predisposing features rendering motor neurons to be more susceptible to the adverse effects of mitochondria dysfunction. Mitochondria dysfunction compromises the metabolic state of motor neurons. In an *in vitro* model of chronic motor neuron toxicity, it was shown that manipulation of the energy status of motor neurons via chronic inhibition of mitochondria resulted in the selective death of these cells (Kaal *et al.* 2000).

1.2.4.3 Protein misfolding and aggregation

The presence of inclusions in the spinal cord of ALS patients and in transgenic mutant SOD1 mice ($tgSOD1^{mut}$) was suggestive that there maybe a failure or dysfunction in the protein quality control system in the cell, which is essential to make sure that proteins are folded properly, or if misfolded, are removed from toxic build up in the cell. Although it might be tempting to think that all protein aggregation events are bad, this might not necessary be true. In the event of failure

in the protein degradation pathway, if misfolded proteins, potentially toxic, cannot be removed then the best way to prevent these misfolded proteins from roaming free in the cell causing cellular damage is by aggregation, and this would be beneficial to the cell. However, if the property of the misfolded proteins is such that it favours aggregation over degradation, this will lead to a toxic build up of misfolded proteins. These misfolded intermediates, prior to aggregating, may have an adverse effect on other cellular components resulting in profound cellular dysfunction. In the case of ALS, the role of aggregation in disease pathogenesis is still unclear as to whether it is beneficial, harmful or just a side-product of the real underlying pathogenic disease mechanism.

The neuropathological hallmark of ALS is the presence of characteristic inclusions in the motor neurons (Chou 1997). Inclusions are present in all cases of ALS, whether familial, sporadic or SOD1-linked. Inclusions in SOD1-linked ALS and tgSOD1^{mut} are immunoreactive for SOD1, whereas inclusions in non-SOD1-linked ALS patients were not immunoreactive for SOD1. Both however, have been found to variably contain other proteins which include chaperones (copper chaperone for SOD1 (CCS), heat-shock proteins (Hsp70, Hsp40, Hsp25, αβ-crystalline), axonal transport and cytoskeletal proteins (neurofilaments, peripherin), ubiquitin-proteasome pathway proteins (dorfin, NEDLI, ubiquitin), glial fibrillary acidic protein (GFAP) and TAR DNA binding protein (TDP-43) (Corbo and Hays 1992;Bruijn *et al.* 1997;Shibata *et al.* 1998;Sasaki *et al.* 1998b;Kato *et al.* 2001;Takehisa *et al.* 2001;Watanabe *et al.* 2001;Maatkamp *et al.* 2004;Liu *et al.* 2005;Dickson *et al.* 2007;Tan *et al.* 2007;Strom *et al.* 2008). Although the implications of co-aggregation of these non-SOD1 proteins are unclear, it is possible that co-aggregation causes detrimental sequestrations of these proteins, rendering them unavailable to carry out their normal function. This can result in the dysregulation of cellular and protein homeostasis, which in the long run leads to cellular dysfunction and death.

1.2.4.4 Cytoskeletal abnormalities and axonal transport defects

If one considers the size and architecture of a motor neuron, in order for a motor neuron to function properly, an extensive, highly organised and efficient transport system is required for communication between the cell body and the distal end of the axon. It has been shown that disruption of the axonal transport in motor neurons can cause disease both in man and mouse (LaMonte *et al.* 2002;Puls *et al.* 2003;Munch *et al.* 2004;Munch *et al.* 2005) indicating the importance and existence of such a transport system. There are two important components that make up the axonal transport system. They are the cytoskeletal framework and the axonal transport cargo carriers (examples of cargoes are mitochondria, neurotransmitter vesicles, neurofilaments, and microtubules). Disruption in any one of the components will result in a defective axonal transport system.

In mature neurons, the cytoskeleton is a heterogeneous network of filamentous structures made up of three major components, which are the microtubules ('tracks' for movement of cargoes along the axon), microfilaments and intermediate filaments (components responsible for axonal scaffolding). The intermediate filaments (IFs) are made up of three sub-types of neurofilaments (NFs) – NF-H, NF-M and NF-L (the heavy, medium and light chains; with reference to their molecular weight), peripherin and α-internexin (Julien and Mushynski 1998). NFs have been implicated in ALS due to their presence in the inclusions, in the hyperphosphorylated form, found in the perikarya, proximal axon and diffusely in the cell body of motor neurons (Leigh and Swash 1991). NFs are expressed in the non-phosphorylated form, which are found in the soma and proximal dendrites and become phosphorylated as they are transported along the axon. Therefore, accumulation of hyperphosphorylated NFs in the soma is suggestive of a disruption in the processing or in the transport of NFs in motor neurons.

Deletion mutations in the *NEFH* gene of some ALS cases were first identified by Figlewicz and colleagues in 1994 (Figlewicz *et al.* 1994). These mutations were found to cause NF disorganization and selective degeneration and death of motor neurons (Julien and Mushynski 1998;Tomkins *et al.* 1998;Al-Chalabi *et al.* 1999).

Because NFs play an important role in regulating axonal calibre, it was proposed that disorganization of NFs may lead to an interference of axonal transport (Collard *et al.* 1995;Julien *et al.* 1995;Manser *et al.* 2008). However, the mechanism causing the hyperphosphorylation of NFs is currently unclear, although it was suggested that hyperphosphorylation might be mediated by p38 MAPK (mitogen activated protein kinase) (Tortarolo *et al.* 2003).

The molecular motor proteins involved in carrying cargoes along the axons are dynein and kinesin, both are multisubunit complexes responsible for retrograde (movement towards cell body) and anterograde (movement towards axon terminal) axonal transport, respectively. Mutations in the dynactin subunit p150Glued (dynactin is multiprotein complex that activates the motor function of dynein, participates in cargo and microtubule binding) were found in some ALS patients and this was demonstrative of a direct role of molecular motor dysfunction in ALS (Munch *et al.* 2004;Munch *et al.* 2005). Since, for ethical reasons, it is impossible to carry out experiments on humans to investigate if a defect in axonal transport in also seen in ALS patients, the best available evidence of such a defect was shown in the tgSOD1^{G93A} mice. Motor neurons of these mice had retrograde axonal transport defects which were already present during embryonic development (Murakami *et al.* 2001;Kieran *et al.* 2005). How mutSOD1 causes selective motor neuron degeneration in terms of causing disruption to the axonal transport machinery is presently unknown. However, these collective findings suggest that a well regulated axonal transport system in motor neurons is essential for motor neuron survival.

1.2.4.5 Oxidative stress

Reactive oxygen species (ROS) are by-products of aerobic metabolism carried out by the electron transport chain in the mitochondria, thus making the mitochondria the main ROS generator in the cell (Figure 1.12). Increase in ROS, either due to increase in production or failure to remove ROS, can lead to ROS accumulation. Excess ROS can cause oxidative damage to many cellular components, such as membrane lipids, proteins, DNA and mitochondria.

Markers of oxidative damage, such as protein carbonyl levels, lipid peroxidation, and protein glycerination, were found to be elevated in the spinal cord of sALS patients (Shaw *et al.* 1995b). 3-nitrotyrosine, a marker indicative of peroxynitrite-mediated oxidative damage, was also found to be increased in both sALS and fALS patients (Abe *et al.* 1995;Ferrante *et al.* 1997;Abe *et al.* 1997). It is currently unknown if these signs of oxidative damage seen in patients are due to oxidative stress as a primary cause in ALS pathogenesis, or merely a secondary effect arising from ALS caused by some other pathogenic mechanism. Due to the lack of specificity of ROS actions (ROS can cause damage to many cellular components), it was proposed that motor neuron degeneration may be due to cellular homeostasis dysregulation, which could initiate a cascade of cell damaging events mediated and amplified by ROS, as illustrated in Figure 1.13.

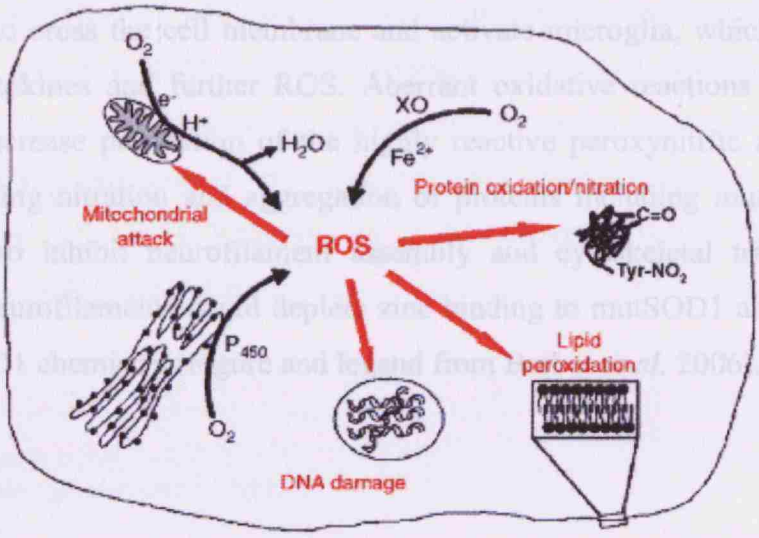

Figure 1.12. Sources of reactive oxygen species and their targets. ROS are produced during oxidative phosphorylation in mitochondria, by oxidative enzymes including cytochrome P450 in the endoplasmic reticulum, and by xanthine oxidase (XO) and reduced metal ions in the cytosol. Cellular targets attacked by ROS include DNA, proteins, membrane lipids, and mitochondria (Figure and legend from Barber *et al.* 2006).

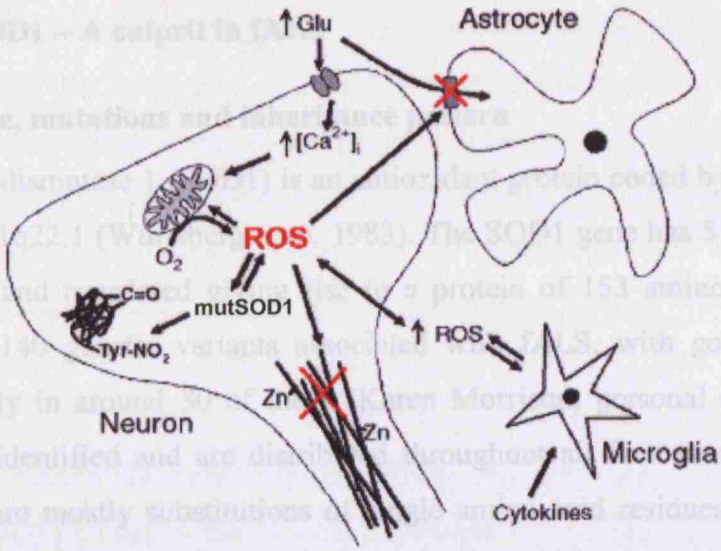

Figure 1.13. Oxidative stress potentially influences other proposed mechanisms of neurodegeneration in ALS. Excitotoxicity leads to increased intracellular calcium levels that are buffered by mitochondria leading to increased ROS production. ROS, in turn, inhibit glutamate uptake through the EAAT2 transporter in glial cells. ROS can also cross the cell membrane and activate microglia, which respond by releasing cytokines and further ROS. Aberrant oxidative reactions catalysed by mutSOD1 increase production of the highly reactive peroxynitrite and hydroxyl radical, causing nitration and aggregation of proteins including mutSOD1 itself, and may also inhibit neurofilament assembly and cytoskeletal transport. Zinc binding to neurofilaments could deplete zinc binding to mutSOD1 and exacerbate aberrant SOD1 chemistry (Figure and legend from Barber *et al.* 2006).

1.3 SOD1 – A culprit in fALS

1.3.1 Gene, mutations and inheritance pattern

Superoxide dismutase 1 (SOD1) is an antioxidant protein coded by the SOD1 gene located at 21q22.1 (Wulfsberg *et al.* 1983). The SOD1 gene has 5 exons which are transcribed and translated giving rise to a protein of 153 amino acids. To date, more than 140 genetic variants associated with fALS, with good evidence for pathogenicity in around 30 of these (Karen Morrison; personal communication), have been identified and are distributed throughout all five exons (Wroe 2008). Mutations are mostly substitutions of single amino acid residues, although some deletions, insertions and C-terminal truncations have been identified. SOD1 mutations are causative in 10-20% fALS (Gros-Louis *et al.* 2006), and have been observed in 2-3% sALS (Andersen 2001).

Except for the D90A mutation, which appears to be inherited both dominantly and recessively depending on population background, ALS caused by all other SOD1 mutations is inherited dominantly (Andersen 2006). Some mutations are found more frequently in a population than others. Two examples are the A4V and I113T mutations. A4V mutation is the most common mutation found in the USA (Cudkowicz *et al.* 1997), whereas the I113T mutation is the most common mutation in the UK (Orrell *et al.* 1999).

1.3.2 Protein properties of SOD1

1.3.2.1 Biological expression and function

SOD1 is considered a 'house-keeping' protein, thus is expressed constitutively, abundantly and ubiquitously in all cells (Zelko *et al.* 2002). SOD1 is mainly a cytosolic protein, but is also found in the nucleus, perioxisomes and mitochondrial intermembrane space of eukaryotic cells (Valentine *et al.* 2005).

SOD1 is a dimeric metalloenzyme, with each subunit containing one copper (Cu2+), one zinc (Zn2+) and an intrasubunit disulphide (S-S) bond. These post-

translational modifications of SOD1 are carried out by the copper chaperone for SOD1 (CCS) in the cytoplasm, and are the most important part of SOD1 activation (Schmidt *et al.* 2000). The main enzymatic function of SOD1 is in the scavenging of free radicals by dismutating superoxide anions (O_2^-) to hydrogen peroxide (H_2O_2), a process which is catalysed by the Cu^{2+} ligand (chemical reaction shown in equation (1) and (2) below). H_2O_2 is then removed by another enzyme, peroxidase, converting it to water and oxygen (Fridovich 1999).

$$O^{2-} + Cu^{2+} \rightarrow O_2 + Cu^{+} \quad (1)$$

$$O^{2-} + 2H^{+} + Cu^{+} \rightarrow H_2O_2 + Cu^{2+} \quad (2)$$

1.3.2.2 Structural features and protein stability of SOD1

Enzymatically active SOD1 exists as a dimer with a molecular weight of 32kDa (16kDa/subunit). Many X-ray crystal structures of SOD1 have been solved for many species (Figure 1.14), and they all show a highly conserved structure emphasizing the structural importance of this protein in carrying out its function (Valentine *et al.* 2005). Each SOD1 monomer is made up of an 8-stranded anti-parallel Greek key β-barrel fold with two prominent loops, the Zn- and electrostatic-loop, and the remainder of the monomer is interspersed with loop regions of various lengths and with the only short (-helical structure spanning residues 134-137 (Figure 1.15). The intrasubunit S-S bond is linked by oxidation of cysteine 57 (C57) located on loop IV (the longest loop) and cysteine 146 (C146) located on β-strand (β8) of the monomer. There are two other cysteine residues, C6 and C111, but these do not form any S-S bonds under normal physiological conditions. C6 is located at the hydrophobic dimer interface, whereas C111 is located on the surface of the protein exposed to the surrounding. The two monomers are held together (buried area of ~640Å2/monomer) by hydrophobic interactions, water mediated hydrogen bonding and main chain to main chain hydrogen bonding between the monomers (Elam *et al.* 2003).

The stability of SOD1 is contributed by the intrasubunit S-S bond and the occupancy of the ligand site by Zn^{2+}. SOD1 has been reported to be one of the most

stable proteins in existence when it is fully methylated with Cu^{2+} and Zn^{2+}. In the halo-state, SOD1 has a melting temperature near to boiling point of water, and does not lose its dimeric quaternary structure in 8M urea or in 1% SDS (Malinowski and Fridovich 1979;Hayward *et al.* 2002;Rodriguez *et al.* 2002). However, SOD1 loses its stability and become intrinsically disordered when in the apo- and disulfide reduced form (Rodriguez *et al.* 2005). Knowledge of how Cu and Zn are loaded into SOD1 has stemmed from *in vitro* experiments using purified SOD1, which do not reflect the true biological metal loading process *in vivo*. Thus, the actual *in vivo* metal complements of SOD1, whether all Cu^{2+} and Zn^{2+} sites are fully metallated or only partially metallated, is not known. Therefore, it is likely that a mixture of SOD1 species with varying degrees of metallation exists in cells. This means that a heterogeneous pool of SOD1 with lowered stability compared to the fully metallated SOD1 may also exist.

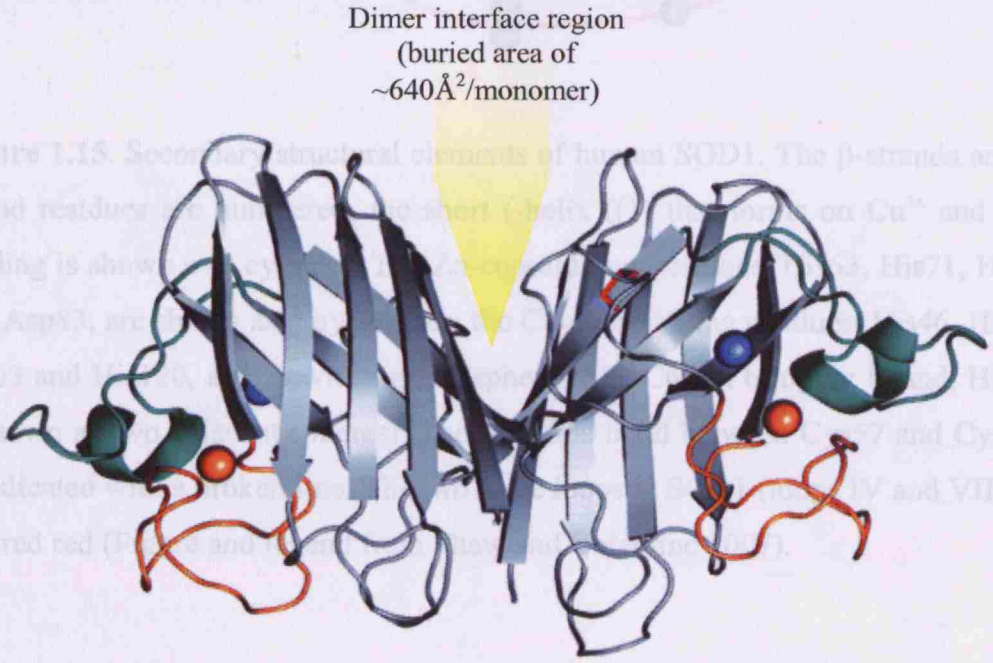

Figure 1.14. Crystal structure of metal bound dimeric human SOD1. Copper and zinc ions are shown as blue and orange spheres, respectively. The zinc loop is depicted in orange and the electrostatic loop in teal. The intrasubunit disulfide (S-S) bond is shown in red (Figure and legend from (Valentine *et al.* 2005)

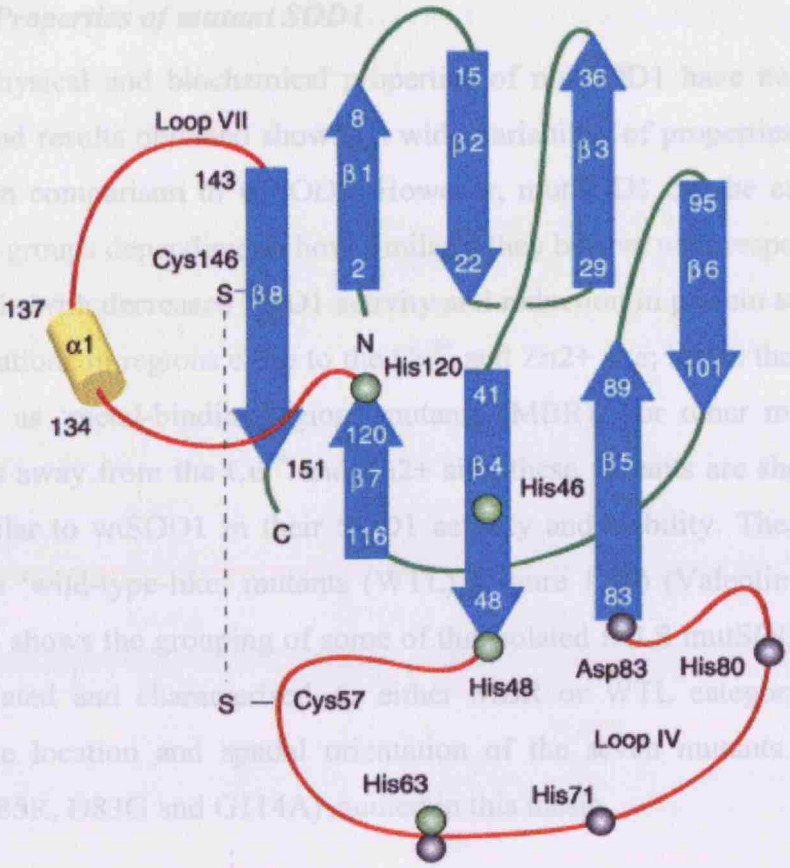

Figure 1.15. Secondary structural elements of human SOD1. The β-strands and β-strand residues are numbered; the short (-helix ((1) that forms on Cu^{2+} and Zn^{2+} binding is shown as a cylinder. The Zn-coordinating residues, His63, His71, His80 and Asp83, are shown as gray spheres; the Cu-coordinating residues, His46, His48, His63 and His120, are shown as green spheres (the Cu–Zn bridging ligand, His63, is shown as two adjacent spheres). The disulfide bond between Cys57 and Cys146 is indicated with a broken line. The two large loops in SOD1 (loops IV and VII) are colored red (Figure and legend from Shaw and Valentine 2007).

1.3.2.3 Properties of mutant SOD1

The biophysical and biochemical properties of mutSOD1 have been extensively studied and results obtained showed a wide variability of properties in the mutant variants in comparison to wtSOD1. However, mutSOD1 can be categorised into two main groups depending on how similarly they behave with respect to wtSOD1. MutSOD1s with decreased SOD1 activity and reduction in protein stability usually have mutations in regions close to the Cu^{2+} and Zn2+ site; hence these mutants are classified as 'metal-binding-region' mutants (MBR). For other mutSOD1s with mutations away from the Cu^{2+} and Zn2+ site, these variants are shown to behave very similar to wtSOD1 in their SOD1 activity and stability. These mutants are known as 'wild-type-like' mutants (WTL) (Figure 1.16) (Valentine *et al.* 2005). Table 1.4 shows the grouping of some of the isolated fALS mutSOD1, which have been isolated and characterised, to either MBR or WTL category. Figure 1.17 shows the location and spatial orientation of the seven mutants (A4V, G93A, G37R, G85R, D83G and G114A) studied in this thesis.

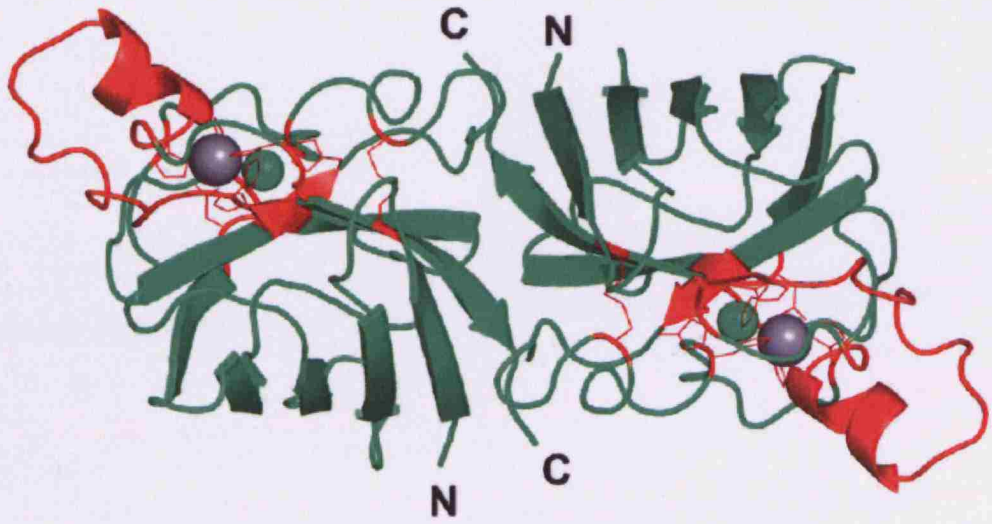

Figure 1.16. Location of MBR and WTL fALS mutants. MBR mutants refer to SOD1 mutations in and around the Cu/Zn binding sites (colored red), whereas WTL mutants refer to all other non-MBR mutations scattered throughout the (-barrel. Cu^{2+} is represented as green spheres and Zn^{2+} as grey spheres. ('C' = C-terminal, 'N' = N-terminal) (Figure from Doucette 2004).

Table 1.4. Classification of some isolated fALS mutant SOD1 proteins to WTL and MBR categories. Mutants coloured in blue are mutSOD1 studied in this thesis (Valentine *et al.* 2005).

Wild-type-like (WTL) mutants				Metal-binding-region (MBR) mutants
A4V	G72S	G93V	E133Del	H46R
V7E	D76Y	E100G	N139K	H48Q
L8Q	L84V	E100K	L144F	H80R
G37R	N86S	D101N	L144S	**D83G**
L38V	**D90A**	D101G	A145T	**G85R**
G41D	**G93A**	I113T	V148G	D124V
G41S	G93R	**G114A**	I149T	D125H
H43R	G93C	R115G		S134N
				C146R

Figure 1.17. The location and spatial orientation of the A4V, G93A, G37R, G85R, D83G and G114A mutations in SOD1. To simplify the illustration, only one subunit of the SOD1 homodimer is shown. a) SOD1 monomer showing the electrostatic loop, zinc loop and the beta-barrel structure. The C'-terminal is at the end of beta-strand 8 (labelled as β8). The vertical line represents the axis of rotation. Rotation of the SOD1 monomer 90° to the right around the axis of rotation gives rise to: b) beta-strands of the beta-barrel are labelled β1, β2, β3 and β6. c) SOD1 monomer from 'b' rotated 90(to the right around the axis of rotation. The location of A4V, G93A, G37R, G85R, D83G and G114A mutations are as labelled in b) and c). A4V is located at the buried dimer interface, G37R, D90A, G93A and G114A are located on the surface of SOD1, and D83G and G85R are buried within the monomer close to the Cu/Zn metal binding site.

(*con't* from **Figure 1.17**. The location and spatial orientation of the A4V, G93A, G37R, G85R, D83G and G114A mutations in SOD1)

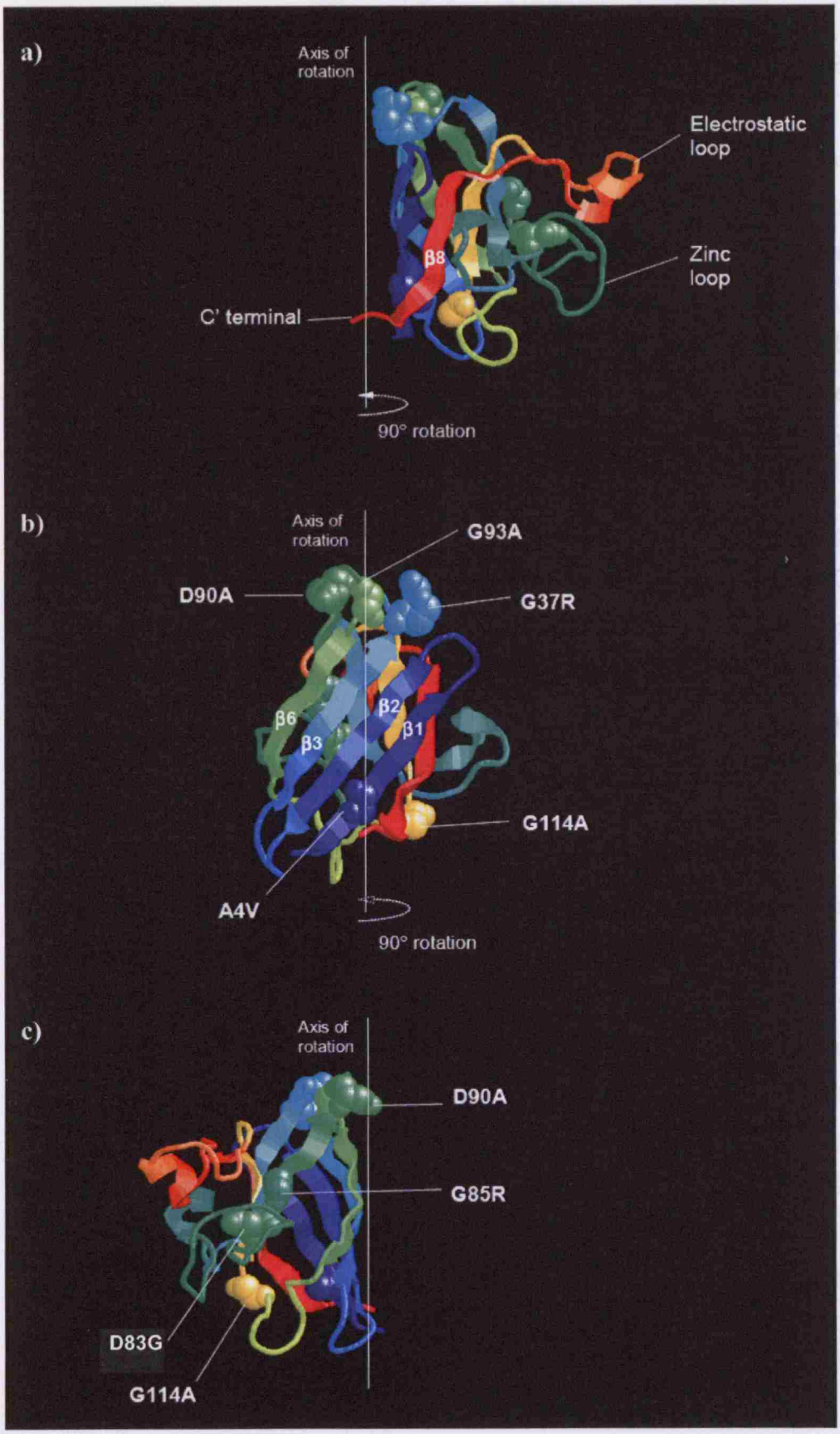

Some of the biophysical and biochemical properties of mutSOD1s which showed a significant difference compared to wtSOD1 are summarised as follow:

- Resistance to proteinase K digestion – MBR mutants are more easily digested than WTL mutants (Ratovitski *et al.* 1999).
- Protein half-life – protein half-life did not correlate to whether mutations were MBR or WTL type, although generally mutSOD1s had shorter half-life than wtSOD1 which was dependent on protein stability. However, some MBR mutants with markedly reduced stability showed comparable half-life in cells to wtSOD1 (Borchelt *et al.* 1994;Hoffman *et al.* 1996;Ratovitski *et al.* 1999).
- Sensitivity to disulfide reduction – MBR mutants are more susceptible to S-S reduction compared to WTL mutants and wtSOD1 (Tiwari and Hayward 2003)
- Thermal stability – generally all mutSOD1 showed a reduction in thermal stability, but only slight reduction in WTL mutants compared to significant reduction in MBR mutants (Rodriguez *et al.* 2002;Stathopulos *et al.* 2003).
- Chemical induced protein unfolding – all mutSOD1s with reduction in the intrasubunit S-S bond was significantly less stable than intrasubunit S-S bond reduced wtSOD1 or apo-wtSOD1. This showed that the formation of intrasubunit S-S bond is more important than Cu/Zn metallation in conferring protein stability to SOD1 (Lindberg *et al.* 2002;DiDonato *et al.* 2003;Stathopulos *et al.* 2003).
- Degree of hydrophobic exposure – mutSOD1s have a greater exposure of hydrophobic areas than wtSOD1 (Rakhit *et al.* 2002;Tiwari *et al.* 2005).
- Net charge of protein – nett charge of protein at physiological pH was variable from mutSOD1 to mutSOD1, independent of whether mutations were of MBR or WTL type. Purified recombinant Cu/Zn metallated SOD1s have an isoelectric focusing point (p*I*) value of 4.8 – 5.1. This suggests that a reduction in net charge of mutSOD1 is likely to increase the propensity of mutSOD1 to aggregate especially in cellular environment of low and fluctuating pH, as would be found in the lysosomes and in the intermembrane space of the mitochondria (Lindberg *et al.* 2005) (Figure 1.18).

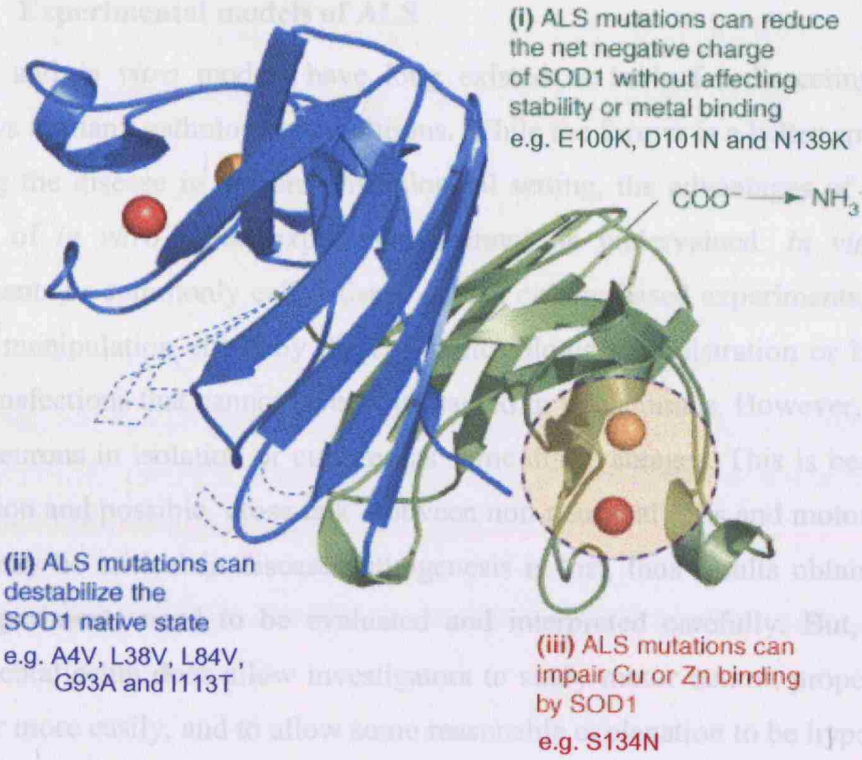

Figure 1.18. Different ALS-associated mutations of SOD1 can increase aggregation of the SOD1 polypeptide for fundamentally distinct reasons. The resulting amino acid substitutions can cause (i) a decrease in the net negative charge ($-q$) of the protein without affecting metal binding or stability of the native state (e.g. E100K, D101N and N139K); (ii) a decrease in stability of the native fold without affecting metal binding or net charge (e.g. A4V, L38V, L84V, G93A and I113T); or (iii) disruption of Cu and Zn binding without affecting the stability of the apoprotein (e.g. S134N). In addition, many mutations affect multiple determinants of aggregation. For example, G85R shows alterations in all three determinants; G37R, G93R and E100G in determinants (i) and (ii); and H46R, D124V and D125H in determinants (i) and (iii). The subunits of the wild-type holo-SOD1 dimer (PDB accession code 1HL5) are colored blue and green; Cu^{2+} and Zn^{2+} ions bound in the active site are shown as yellow and red spheres, respectively (Figure and legend from Shaw and Valentine 2007).

1.4 Experimental models of ALS

In vivo and *in vitro* models have long existed as tools for dissecting disease pathways in many pathological conditions. While the former is a better approach in studying the disease in a more physiological setting, the advantages of the latter method of *in vitro* based experiments cannot be undervalued. *In vitro* based experiments or commonly called tissue or cell culture based experiments, offer an ease of manipulation either by direct pharmacologic administration or by simple gene transfections that cannot be easily attained in live animals. However, studying motor neurons in isolation or culture has some disadvantages. This is because the connection and possible 'cross-talk' between non-neuronal cells and motor neurons which may be critical in disease pathogenesis is lost, thus results obtained from such experiments need to be evaluated and interpreted carefully. But, such an experimental setup does allow investigators to study motor neuron properties and behavior more easily, and to allow some reasonable explanation to be hypothesized from *in vitro* experiments which can then be tested in animal models. This section will mainly be focused on the available animal models used in studying ALS and some molecular clues which have been revealed from the use of these models in investigating the molecular pathogenesis of ALS.

1.4.1 Animal models

The development animal models is an important process in studying any human disease because it provides insight into the disease process in an *in vivo* setting, which otherwise is difficult to dissect in humans. An ideal animal model should be one that recapitulates the pathogenesis process giving rise to similar clinical presentations and responsiveness to disease modifying events (e.g. drug treatment, or genetic manipulation in gene-based therapy). However, it is unlikely that all aspects of a disease can be recapitulated in a single animal model due to the differences in genetic, physiology, and anatomy between human and animals. For this reason, a variety of animal models for the same disease are usually developed allowing different aspects of the disease to be investigated in alternative models should one model fail to recapitulate a certain disease phenotype. Different organisms have been used to model ALS. Among them are mice (Gurney *et al.*

1994), rats (Howland *et al.* 2002), zebra fish (Lemmens *et al.* 2007), fruit fly (Phillips *et al.* 1995) and worm (Oeda *et al.* 2001). Of these, the most widely used animal is the mouse, which will be the main focus of this sub-section.

A variety of approaches can be used to model human diseases in mice, which can be classified to three main groups. They are the intervention models (involving treatment of animals with chemicals or physical manipulation to induce neurodegeneration), spontaneous models (naturally occurring mutations in mice resembling some aspects of ALS) and genetically manipulated mouse models (overexpressors of human gene (transgenics), gene knockout and mutagenesis with N-ethyl-N-nitrosourea (ENU)).

1.4.1.1 Intervention models

Toxins

Several toxins have been reported to cause neurodegenerative lesions and motor neuron degeneration in animals resembling some aspects of ALS. Examples include β-β'-imidodiproprionitrile (IDPN), beta-sitosterol beta-D-glucoside (BSSG), β-oxaloamino-L-alanine (BOAA), kainic acid and aluminium. Of the most relevance to humans is BSSG, a neurotoxin found in cycad seeds, a type of excitotoxin with close structural similarities to glutamate (Khabazian *et al.* 2002). BSSG has been implicated in the pathogenesis of Guamanian-ALS associated with parkinsonism (P) and dementia (D), which apart from the presence of neuropathological features associated with P/D (e.g. neurofibrillary tangles), is identical to the pathological changes observed in classical ALS. In 2003, a murine model of ALS-P/D was developed (Khabazian *et al.* 2002;Wilson *et al.* 2002;Shaw and Wilson 2003) by chronically feeding mice with cycad based flour. These mice resembled many of the behavioral and neuropathological features (deficits in motor, cognitive, and sensory behaviors that correlated with the loss of neurons in specific regions of the central nervous system), observed in ALS-P/D patients and showed persistent and progressive loss of motor neurons in the lumbar spinal cord that continued to worsen even after cessation of BSSG feeding to the mice (Tabata *et al.* 2008). The development of this model has important implications in ALS

research because it provides a way of studying the interactions between genetic and environmental factors in ALS, especially in sALS, and in the identification of early events preceding motor neuron death.

Lesions

Axotomy-induced motor neuron degeneration has been a frequently used model in studying the influence of neurotrophic factors on motor neuron survival and apoptosis-mediated motor neuron death (Sendtner *et al.* 1991;Elliott 1999). However, there are limitations to this model because axotomy-induced injury results in the execution of acute cellular events and cell death which is different from the chronic and progressive motor neuron death seen in ALS.

1.4.1.2 Spontaneous models

Prior to the development of transgenic models of ALS (reviewed in 1.4.1.3), mice with naturally occurring mutations presenting with motor neuron pathology were used to study the different aspects of motor neuron degeneration. These spontaneous hereditary mice include the *mnd*, *wobbler*, *wasted* and *pmn* mice. All mouse strains showed progressive and fatal impairment of the motor system but varied in their neuropathology hallmarks and severity of disease. The main features of these mice are summarized in Table 1.5.

Table 1.5. Mice with spontaneous hereditary motor neuron pathology. (LMN = lower motor neurons/anterior horn cells, UMN = upper motor neurons, MN = motor neurons, AR = autosomal recessive, AD = autosomal dominant). (Elliott 1999;Doble and Kennel 2000).

	mnd	*wobbler*	*wasted*	*pmn*
Chromosomal linkage	8	11	2	13
Gene	*Cln8* (neuronal ceroid lipofuscinosis-8)	*Vps54* (vacuolar protein sorting 54)	*Eefla2* (translation elongation factor)	*Tbce* (tubulin-specific chaperone)
Inheritance	AD	AR	AR	AR
Clinical features, disease onset and survival	Slow progression; stiffness, atrophy and paralysis in hindlimbs; onset at 5-11 months and death at about 9-14 months	Progressive forelimb weakness and eventual denervation of diaphragm; onset at 3-4 weeks and death at around 6 months	Rapid progression of hindlimb weakness; onset at 3 weeks and death by 1 month	Rapid progression of pelvic and hindlimb weakness; onset at 2-3 weeks and death at 7 weeks
LMNs changes	Lysosomal accumulation	Vacuolization	Pronounced vacuolization	Chromatolysis
LMNs loss	Minimal loss (greater loss at later disease stage)	Prominent (mainly in cervical spinal cord)	Extensive	Limited (preserved soma size)
UMN changes/loss	Minimal loss	Some loss	Chromatolysis	Absent
Axonopathy	Absent	Present	Present	Extensive
Denervation	Unknown	Present	Present	Present

1.4.1.3 Genetically manipulated mouse models

The breakthrough in ALS research came about when mutations in the SOD1 gene were found to be causative in a sub-population of fALS patients. Since then, many transgenic animals harboring the SOD1 gene (tgSOD1), wildtype and mutants, have been developed and studied extensively. Because intermediate filament (IF) alterations and accumulations are one of the pathological hallmarks observed in motor neurons of ALS patients and tgSOD1 mice, transgenic mice expressing human neurofilament (NF) were also developed to study the role of IF (primarily neurofilament and peripherin) accumulation in the pathogenesis of SOD1 and non-SOD1 linked ALS. There are also other mouse models which have been developed to study the different aspects of motor neuron degeneration or dysfunction in ALS (e.g. Als2 knockout, Cra1 and Loa mice), but the main focus of this section will be on the genetically manipulated models of SOD1 and IFs.

SOD1 transgenics

The first tgSOD1 mouse, carrying the G93A mutation, was created in 1994 by Gurney and colleagues (Gurney *et al.* 1994), and since then many more transgenic mutant SOD1 lines have been generated (Table 1.6). Almost all lines of tgSOD1 mice share similar clinical and behavioural phenotype, disease progression pattern and neuropathological characteristics (Figure 1.19) with each other and resemble the pathology seen in ALS patients. They are summarised as follows, and tabulated in Table 1.6 (Morrison *et al.* 1998;Elliott 1999;Shibata 2001;Bendotti and Carri 2004;Julien and Kriz 2006):

- Exhibit normal motor function but develop an adult-onset hindlimb weakness (initial symptoms) which progresses over weeks to months leading to motor paralysis, neurogenic amyotrophy and ultimately death.
- Age of onset and lifespan is conversely related to gene dosage and protein level in spinal cord (i.e. net amount of SOD1 expressed, taking into account the degradation rate of SOD1. For example, stable SOD1 mutants (e.g. G37R) have a longer half-life than stability-compromised SOD1 mutant (e.g.G85R)). Lifespan is also dependent on the genetic background of the mice (e.g.

tgSOD1^{G93A} mice on the C57BL/6J genetic background have a longer lifespan in comparison to mice on the C57BL/6JxSJL background).

- Rapidity of disease progression at onset is dependent on the type of mutation.
- Mainly involves the spinal cord anterior horns and brainstem motor nuclei (white matter areas are preserved).
- Lesions in high expressor mice are more extensively distributed than those in low expressor mice, and occasionally spread into other systems, including the spinal cord posterior horns, vagal nerve dorsal nuclei, brainstem reticular formation, red nuclei, substantia nigra, interpeduncular nuclei, cerebellum, thalamus and olfactory bulb.
- Presence of intracytoplasmic vacuoles (dilated mitochondria and endoplasmic reticulum) in the soma and dendrites of motor neurons even at pre-symptomatic stage. The degree of vacuolation is dependent on gene dosage (i.e. more vacuoles found in high expressor than in low expressor mice) *Note: this feature is not seen in ALS patients.*
- At onset, motor neurons show signs of cytoskeletal disorganization (accumulation of phosphorylated neurofilaments) and formation of mutSOD1-containing ubiquitinated inclusion bodies in the soma. The number of inclusions increases as disease progresses, accompanied by a reduction in motor neuron number in the ventral horn of the spinal cord (also coincident with onset and progression of muscle weakness). Inclusions in astrocytes are more prominent in low expressor than in high expressor mice.
- At terminal stage, extensive motor neuron loss is accompanied by prominent astrocytosis.

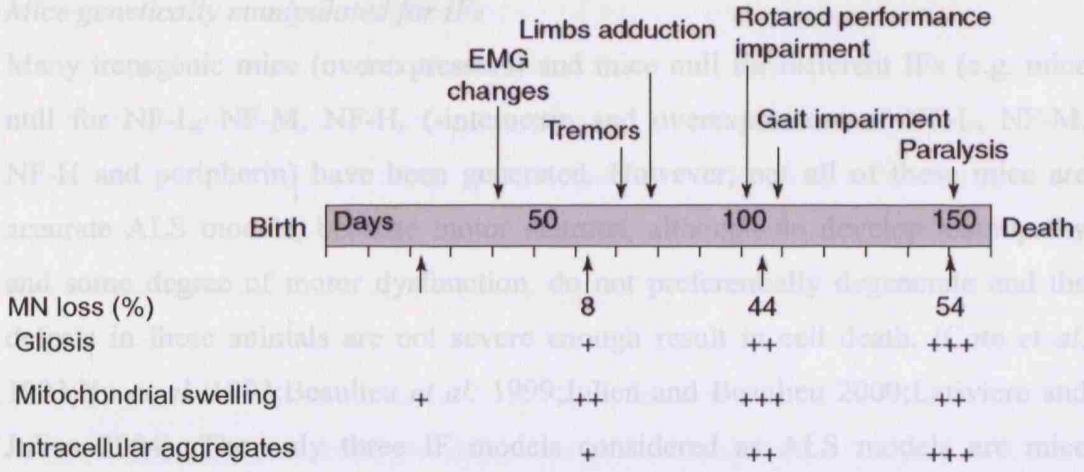

Figure 1.19. Graphical representation of the behavioural and neuropathological progression of the disease in tgSOD1^{G93A} mice. These mice develop the first signs of muscular dysfunction around two months of age, with an impairment of the evoked response tested electromyographically (EMG). Thereafter, tremors appear in the hindlimb, associated with a progressive reduction in the extension reflex when the mice are raised by the tail. At ~ 4 months of age, the mice show a progressive muscular weakness starting from the hind limb, revealed by the increasing difficulty to stay on a rotating bar and by a reduction in stride length on an inclined ramp. At this stage, more than 50% of motor neurons (MN) of the lumbar spinal cord are lost and one month later these mice die. Mitochondrial vacuolisation and the swelling of MNs are among the earliest events and are accompanied by a decreased function of the mitochondria. Later, but still at the asymptomatic stage, the tgSOD1^{G93A} mice show signs of cytoskeletal disorganization in the MNs, with the accumulation of phosphorylated neurofilaments. The accumulation of detergent-insoluble proteins and ubiquitinated intracellular inclusions are particularly evident at advanced stages of the disease. Reactive gliosis, which involves hypertrophy and the activation of astrocytes, and the proliferation and activation of microglia, is detectable with the degeneration of MNs and becomes prominent when the cell loss is remarkable. Hypertrophic astrocytes and reactive microglia are usually located around degenerating motoneurons. (Figure and legend from Bendotti and Carri 2004).

Mice genetically manipulated for IFs

Many transgenic mice (overexpressors) and mice null for different IFs (e.g. mice null for NF-L, NF-M, NF-H, (-internexin and overexpressors of NF-L, NF-M, NF-H and peripherin) have been generated. However, not all of these mice are accurate ALS models, because motor neurons, although do develop axonopathy and some degree of motor dysfunction, do not preferentially degenerate and the defects in these animals are not severe enough result in cell death. (Cote *et al.* 1993;Xu *et al.* 1993;Beaulieu *et al.* 1999;Julien and Beaulieu 2000;Lariviere and Julien 2004). The only three IF models considered as ALS models are mice overexpressing NF-L, NF-H and NF-L bearing the point mutation L394P (NF-L^{L394P} is not a mutation described in ALS, but implicated in a form of skin disease known to disrupt the cytoskeleton (Lee *et al.* 1994)).

Although most IF models do not develop an overt motor neuron degeneration phenotype, there are some molecular and behavioral abnormalities which are similar to ALS observed in patients and in the tgSOD1 mouse model. These abnormalities in selected IF models are summarized as follows:

<u>IF knockout mice:</u>

- NF-$M^{-/-}$ mice had no overt behavioral phenotype or gross structural defects in the nervous system except for a reduction in the axonal caliber for all myelinated axons in the central and peripheral nervous system (Elder *et al.* 1998). Axons lacking NF-M exhibited an increase in the axonal transport velocity of NF-L and NF-H (Jacomy *et al.* 1999) which was accompanied by an aberrant stoichiometric decrease of NF-L and an increase of NF-H levels. These changes were concurrent with an increase in the microtubule numbers and density in the axon (Elder *et al.* 1998).
- NF-$H^{-/-}$ mice had almost normal axonal caliber and no change in the number and packing density of NFs. The NFs in the axon were mostly made up of NF-L and NF-M. However, there was an increase in microtubule content and in the ratio of assembled tubulin to NF-L protein in the insoluble cytoskeletal preparation from the sciatic nerves. Axonal transport studies showed that there was an increase in transport velocity in newly synthesized NF-L and NF-M,

which corresponded to the presence of neurofilamentous swellings in motor neurons but without motor neuron loss (Zhu *et al.* 1998).

- In the double NF-M/NF-H knockout mice, the absence of NF-M and NF-H resulted in the sequestration of unassembled NF-L proteins in the neuronal perikarya. This was accompanied by a reduction in the axonal calibre of motor and sensory roots, which was equivalent to the histopathological changes seen in NF-L null mice (Jacomy *et al.* 1999). Axonal atrophy was not accompanied by axonal loss. Axons lacking NF-M and NF-H also had a reduction of NF-L and α-internexin but with an increase in microtubule content. These mice also developed hindlimb paralysis, paralleled by muscular atrophy, but was not accompanied by motor neuron loss in the spinal cord. (Elder *et al.* 1999a;Elder *et al.* 1999b).
- Peripherin knockout mice ($PRPH^{-/-}$) were viable animals without an overt motor dysfunction phenotype. These mice showed no obvious defects in the myelinated motor and ventral roots, but had a significant reduction in the number and caliber of unmyelinated sensory fibers (Lariviere *et al.* 2002).

Overexpression of NFs : In most transgenic overexpressors of NFs, although there were accumulations of NFs in the perikarya of motor neurons, these accumulations appeared to be well tolerated as there were no overt neuronal losses seen in these mice (Julien and Beaulieu 2000).

- Overexpressor NF-H mice (tgNF-H) were normal at birth but when aged, showed a progressive decline in muscle function when tested for their ability to grasp (Collard and Julien 1995). This decline in motor function was correlated to a progressive disruption of peripheral nerve function accompanied by degeneration of distal axons and muscular atrophy but without motor neuron death. These mice also had axonal transport defects (Collard *et al.* 1995) and altered axonal conductances (Kriz *et al.* 2000a).
- Motor neurons in the ventral horn of the spinal cord of mice overexpressing NF-L (tgNF-L) were found to have massive accumulations of neurofilaments, swollen perikarya, and eccentrically localized nuclei. These neuropathological

changes were accompanied by an increase in the frequency of axonal degeneration, proximal axon swelling, and severe skeletal muscle atrophy. Overexpressor NF-L mice had a more aggressive disease course than overexpressor NF-H mice. These mice had an earlier disease onset ensued by a rapid progression and death within 3-4 weeks (Xu *et al.* 1993;Doble and Kennel 2000).

- Overexpression of NF-L^{L394P} (tgNF-L^{L394P}) in mice caused massive motor neurons loss within 4 weeks after birth, accompanied by abnormal accumulations of NFs and severe neurogenic muscular atrophy. The exact toxicity is not known. These degenerative pathologies were predominantly seen in motor neurons, but sensory neurons did show some modest level of degeneration (Lee *et al.* 1994).
- Overexpressing NF-L in NF-H in mice (tgNF-L/NF-H) showed an improved neuropathological phenotype of reduced perikaryal swellings and rescue of motor neuron function, which emphasized the importance of NF stoichiometry in proper NF assembly and transport (Meier *et al.* 1999).

1.4.2 Disease molecular clues revealed from studying SOD1-linked fALS models

1.4.2.1 Mutant SOD1 confers toxicity not by loss of function but by 'toxic-gain-of-function'

It was initially thought mutSOD1s cause ALS due to loss of function. However, studies from genetically manipulated SOD1 mice revealed otherwise, that mutSOD1s cause ALS by, a yet undetermined, 'toxic-gain-of-function'. The evidence for this is:

- tgSOD1^{G93A} developed an ALS phenotype whereas mice overexpressing wtSOD1 (tgSOD1^{wtSOD1}) did not. Although tgSOD1^{wtSOD1} did not develop ALS, these mice had a characteristic set of neurodegenerative changes (swelling and vacuolization of mitochondria in neuronal processes throughout the CNS, axonal degeneration in some fiber tracts, and had moderate motor neuron loss only in aged mice of > 2 years), which apart for the absence of motor neuron loss, resembled the neuropathological changes seen in tgSOD1^{G93A} mice (Gurney *et al.* 1994;Jaarsma *et al.* 2000).
- mSOD1 knockout mice did not develop ALS, although these mice were shown to be more vulnerable to oxidative stress when axotomized (Reaume *et al.* 1996).
- Many mutations in SOD1 did not result in loss of activity (reviewed in 1.3) (Borchelt *et al.* 1994). In fact, elevated SOD1 activity, relative to non-transgenic mice, were detected in some tgSOD1^{mut} mice (e.g. tgSOD1^{G93A}, tgSOD1^{G37R}) and these mice still developed ALS (Gurney *et al.* 1994).
- Mice expressing a lower level of mutSOD1 (tgSOD1^{G93Adl}) also developed an ALS phenotype, but with a later onset and a less rapid disease progression. This demonstrated the gene dosage effect in developing ALS which would be unlikely if cell death was due to the loss of SOD1 function (Dal Canto and Gurney 1997).

1.4.2.2 Mitochondrial alterations, oxidative stress and apoptosis

mutSOD1 proteins have been reported to form aggregates on the outer membranes of mitochondria (Higgins *et al.* 2003;Liu *et al.* 2004;Vande *et al.* 2008) and the matrix (Vijayvergiya *et al.* 2005). A report by Vande *et al.* (2008) showed that mutSOD1 (G93A, H46R, G85R and G127X) was selectively deposited to the outer cytoplasmic surface of the mitochondria of the spinal cord and not mitochondria from other tissues. Interaction of mutSOD1s with the membrane was specific and deposited mutSOD1 behaved as an integral membrane protein of cross-linked misfolded SOD1 dimers (Vande *et al.* 2008). Although the functional implication of the aberrant deposition of mutSOD1s in the mitochondria membrane is yet to be investigated, these findings are important because they reflect how mutSOD1s can potentially cause selective degeneration in motor neurons via preferential interaction with spinal cord mitochondria. It was postulated by the authors that this aberrant mutSOD1 deposition may affect protein import, ionic homeostasis, mitochondrial motility, mitochondrial fission/fusion, or regulation of apoptosis (Vande *et al.* 2008).

Mitochondria are one of the main producers of reactive oxygen species (ROS) in the cells, alterations in mitochondria which might elevate the production of ROS are detrimental to the cell as this will cause oxidative damage to many cellular components, and in a positive feedback mechanism, these ROS can amplify damage to mitochondria thereby causing bioenergetic failure, alterations in the mitochondrial permeability transition pore (MPTP), leakage of cytochrome c and activation of caspases leading to apoptosis-mediated death. There is evidence showing that in tgSOD1 mice and cultured cells expressing mutSOD1, there is an increase in oxidative stress markers (Liu *et al.* 1999a;Liu *et al.* 1999b) and activation of mitochondrial regulated caspases (e.g. caspase-3) indicative of apoptosis-mediated cell death (Pasinelli *et al.* 1998;Inoue *et al.* 2003;Boston-Howes *et al.* 2006). Also, mutSOD1 in tgSOD1 mice and in ALS patients has been shown to preferentially bind to Bcl-2, an anti-apoptotic integral membrane protein of the outer mitochondrial membrane, which the authors suggest is detrimental because co-aggregation of Bcl-2 and mutSOD1 prevents Bcl-2 from executing its anti-apoptotic function hence promoting apoptosis (Mu *et al.* 1996;Pasinelli *et al.*

2004). Collectively, these results together with those published by Vande and Vijayvergiya reinforce the role of mutSOD1 in causing selective motor neuron death via mitochondria.

1.4.2.3 Importance of cytoskeletal stoichiometry in motor neuron survival

As previously described under IF mouse models in section 1.4.1.3, overexpression of any single subunit of NF in mice resulted in axonal alterations, accumulation of NFs in the soma and motor dysfunction. But, when two NFs were co-overexpressed, as in the case of tgNF-L/NF-H mice, motor neuron function was rescued (Meier *et al.* 1999). This emphasized the importance of stoichiometry between the different IFs in maintaining axonal and neuronal survival. This meant that any event that can cause loss of stoichiometry, for instance by dysregulating the expression of the different IFs or by aberrant sequestration and co-aggregation of IFs with misfolded proteins (e.g. mutSOD1), can cause motor neuron dysfunction or death. This was shown to be true indirectly via mouse crosses of tgSOD1^{G37R} and tgSOD1^{G93A} to tgNF-H, and tgSOD1^{G93A} to tgNF-L mice as this resulted in a prolonged survival in both tgSOD1^{G37R} and tgSOD1^{G93A} mice. Increase in accumulation of NFs in the perikarya of motor neurons was also observed, and it was postulated that because there was an excess of NFs in motor neurons due to overexpression, this excess of NFs could serve as a sink in sequestering toxic mutSOD1 protein from causing damage (Couillard-Despres *et al.* 1998;Kong and Xu 2000). Although the exact mechanism on how mutSOD1 causes cytoskeletal disorganization is unclear, but collectively, these results demonstrated the involvement of neurofilaments in the pathogenesis of ALS.

1.4.2.4 Axonal transport – aberrant interaction of mutSOD1 and dynein

In 2005, Kieran and colleagues crossed tgSOD1^{G93A} mice to mice named Loa, which were heterozygous for a missense mutation in the dynein heavy chain (*Dync1h1*, F580Y; also known as the Loa mutation which is acronym for Legs at odd angles) (Hafezparast *et al.* 2003). The resulting progeny from the cross, *Loa*/+,SOD1^{G93A} mice, had an extended lifespan of 20% and an improved muscular phenotype. More surprisingly is that E13.5 (refers to days of gestation)

embryonic motor neurons from *Loa*/+,SOD1^{G93A} mice had an accelerated retrograde axonal transport rate (rAT) in comparison to embryonic motor neurons from tgSOD1^{G93A} and *Loa*/+ mice, which had a reduced and normal rAT, respectively (Kieran *et al.* 2005). Following this, these cross-breeding experiments were repeated by crossing heterozygous Cra1 mice (mice with allelic mutation to Loa, Y1055C; referred to as the Cra1 mutation, acronym for Cramping) to tgSOD1^{G93A} mice and similar amelioration of phenotype (attenuated decline of both motor activity and an increase of survival time) was found in the progeny from the cross (Teuchert *et al.* 2006). There is no definitive explanation for the observed phenomenon, but it appears to be that accelerating rAT is beneficial for the survival of motor neurons (Kieran *et al.* 2005).

Following the reports on the cross-breeding experiments, research into identifying the connection between dynein and mutSOD1 and how this interaction rescues motor neuron function was intensified. The first report showing a potential interaction was published by Zhang and colleagues in 2007. They showed that dynein-heavy chain and dynein-intermediate chain, a dynein-complex responsible for retrograde axonal transport, co-aggregated with mutSOD1 in the spinal cord motor neurons and in the sciatic nerves of tgSOD1^{G93A} and tgSOD1^{G85R} mice (Zhang *et al.* 2007). In a follow up study, Strom and colleagues showed further evidence supporting the findings of Zhang *et al.* (2007), and additionally also showed that formation of large SOD1 inclusions in cultured cells expressing mutSOD1-tagged with GFP (A4V, G85R and G93A) was dependent on the association of mutSOD1-GFP with the intact dynein complex (Strom *et al.* 2008), whereas H46R-GFP and H48Q-GFP did not readily form inclusions, whether expressed in cells with an intact or disrupted dynein-dynactin complex.

These results have important implications because the demonstration of the direct "gain-of-interaction" between mutant SOD1 and dynein not only provides insights into the mechanism by which mutSOD1 could contribute to a defect in retrograde axonal transport, but also may possibly explain the results obtained from the cross-breeding experiments reported by Kieran *et al.* (2005) and Teuchert *et al.* (2006). It is reasonable to think that mutations in dynein-heavy chain (in the Loa and Cra1

mice) inhibit the interaction with mutSOD1, and in some ways yet unidentified, cause an increase in rAT which results in improved motor function phenotype and survival in tgSOD1 mice.

1.4.2.5 Non-cell autonomous death of motor neuron

The non-cell autonomous view on motor neuron death was first shown by Gong and colleagues showing that the selective expression of mutant mouse G86R SOD1 in astrocytes of transgenic mice was not sufficient to cause an ALS-like motor deficit (Gong *et al.* 2000). In another study, when mutSOD1 (G37R) was selectively expressed in motor neurons, the transgenic mice also did not show an ALS phenotype (Pramatarova *et al.* 2001). In chimeric mice and cultured cells having a mixture of both wildtype (non-transgenic) and mutSOD1-expressing cells, degeneration of mutSOD1-expressing motor neurons was delayed when these motor neurons were surrounded by healthy-wildtype non-neuronal cells. However, when wildtype motor neurons were surrounded by mutSOD1 expressing non-neuronal cells, these motor neurons also developed some neurodegenerative changes (Clement *et al.* 2003;Di Giorgio *et al.* 2007;Nagai *et al.* 2007). In similar studies investigating the effect of selective expression of mutSOD1 in microglia on motor neurons, it was demonstrated that onset of degeneration was dependent primarily on the expression of mutSOD1 in motor neurons (Beers *et al.* 2006;Boillee *et al.* 2006b;Jaarsma *et al.* 2008), but the rapidity or severity of disease progression was dependent on microglia. In mice with mutSOD1-expressing motor neurons surrounded by microglia with diminished or null expression of mutSOD1, it was found that the disease progression of these mice was significantly slowed but with no change in the onset age (Beers *et al.* 2006;Boillee *et al.* 2006b).

Recently, it was demonstrated, both in cultured cells and tgSOD1 mouse spinal cord, that despite mutSOD1 being a cytosolic protein without any organelle-targeting sequence, a fraction of mutSOD1 can be secreted to the extracellular microenvironment (Urushitani *et al.* 2006). This result has important implications because it supports the view that toxicity is transferable from one cell to another,

therefore is consistent with the findings that the disease is not strictly autonomous to motor neurons.

1.4.2.6 Failure of protein quality control and SOD1 aggregation

Toxicity of mutSOD1 has long been linked to protein misfolding and aggregation due to the presence of SOD1 immunoreactive inclusions in motor neurons and astrocytes in ALS patients, tgSOD1 mice and cultured cells expressing mutSOD1 proteins. *In vitro* characterization of many of the mutSOD1 proteins revealed that aggregation is a common property for all mutSOD1 (Shaw and Valentine 2007). It was proposed that, like other protein misfolding diseases (e.g. Prion, Alzheimer's disease), mutSOD1 confers its toxicity via first being misfolded into soluble oligomers or other misfolded species followed by aggregation forming insoluble complexes (inclusions), in which the intermediates between the misfolding and aggregation process are thought to be the damaging species to the cell (Shaw and Valentine 2007). The protein chaperone (heat shock proteins, Hsps) and ubiquitin-proteasome systems (UPS) perform many homeostatic functions within cells involving protein folding, transport and degradation of proteins, and alterations in these protein quality control systems, whether directly or indirectly, have been observed in all experimental models of SOD1 and also in ALS patients.

It has been shown that proteasome function is inhibited by the expression of mutSOD1 in cell cultures and in tgSOD1 mice (Urushitani *et al.* 2002;Puttaparthi *et al.* 2003). Although the mode of inhibition is unknown, it might be possible that inhibition may be mediated by sequestration of the proteasome to co-aggregate with mutSOD1. This is supported by *in vivo* evidence showing that inclusions found in the spinal cord of some ALS patients and tgSOD1 were immunoreactive for SOD1 (Watanabe *et al.* 2001). The inadvertent sequestration of the proteasome may further amplify SOD1 aggregation because degradation of SOD1 is mediated by the proteasome via the ubiquitin-proteasome pathway (Hoffman *et al.* 1996). Thus this may cause a buildup of misfolded SOD1 in cells which may interact aberrantly with other proteins or organelles causing dysfunction (e.g. aberrant interaction of misfolded mutSOD1s to mitochondria outer membrane as described

in 1.4.2.2; interaction with heat shock proteins as described in the next paragraph) prior to it forming aggregates. Alternatively, the presence of aggregates itself might cause physical blockade in the cell thereby impeding other cellular functions, for instance aggregates may cause physical blockade in the axons thereby impairing transport of essential cargoes between the soma and axon terminal.

Evidence of UPS involvement in motor neuron dysfunction comes from cultured neuronal and non-neuronal cells expressing mutSOD1-GFP, where mutSOD1-GFP aggregates formed in these cells consisted of an immobile-porous scaffold which allowed diffusion of some cellular proteins through the aggregates, whereas there was transient interaction with Hsp70 and sequestration of proteasomes into the aggregate scaffold. Furthermore, shown in the same and a follow up experiment, it was demonstrated that cells expressing soluble mutSOD1-GFP were more viable than cells expressing higher levels of mutSOD1-GFP in the aggregated form (Matsumoto *et al.* 2005;Matsumoto *et al.* 2006). These results show that SOD1 aggregates can act as physical blockade and as a non-specific aggregation sink aberrantly sequestering other cellular proteins. In these experiments, it appeared that cell survival was dependent on the appearance and degree of aggregate accumulation in the cell.

In tgSOD1^{G93A} and tgSOD1^{G85R}, a reduction in the chaperoning capacity in the lumbar spinal cord was detected prior to the onset of symptoms (Bruening *et al.* 1999;Tummala *et al.* 2005). Reduction in Hsp function may be explained by co-aggregation with mutSOD1, seen as co-localised inclusions in motor neurons (Watanabe *et al.* 2001;Maatkamp *et al.* 2004). The role of Hsps in ALS pathogenesis was demonstrated *in vivo* by treating tgSOD1^{G93A} mice with arimoclomol, a co-inducer of Hsps. Arimoclomol-treated mice had improved muscle function and prolonged lifespan (Kieran *et al.* 2004). Similarly, in cell culture experiments, neuronal cells co-transfected with G93A and Hsp70 or in combination of Hsp70 and Hsp40 showed a decrease in the number of intracytoplasmic aggregates and suppressed cell death in comparison to G93A only-expressing cells (Bruening *et al.* 1999;Takeuchi *et al.* 2002b). However, in cross-breeding experiments of mice overexpressing Hsp70 to tgSOD1^{G93A},

tgSOD1^{G37R} and tgSOD1^{G85R}, alleviation of disease phenotype was not seen (Liu *et al.* 2005). This discrepancy between *in vivo* and *in vitro* results suggests that upregulation of Hsp70 alone is not sufficient, but instead it requires a combinatorial upregulation of different Hsps to ameliorate the SOD1-mediated toxicity in motor neurons.

The role of protein aggregation in causing ALS is still controversial. There are contradictory reports showing that aggregation is not necessary for development of ALS. Examples include one experiment which targeted mutSOD1 to mitochondria resulting in cell death which was not accompanied by the presence of cytoplasmic inclusions (Takeuchi *et al.* 2002a), and in another, PC12 cells transduced with mutSOD1-YFP using an adenovirus showed no correlation of number of inclusions accumulated with cell survival (Lee *et al.* 2002).

1.4.2.7 Participation of wtSOD1 in the pathogenesis of ALS

Participation of wtSOD1 in the pathogenesis of ALS was first demonstrated by Jaarsma and colleagues (2000) where they crossbred tgSOD1^{G93A} to tgSOD1^{wtSOD1} to produce double-transgenic mice overexpressing wtSOD1 and G93A, tgSOD1$^{G93A/wtSOD1}$. These mice had an accelerated motor neuron death and earlier disease onset by an average of 50 days compared to tgSOD1^{G93A} but without alteration in the disease duration upon onset (Jaarsma *et al.* 2000). This experiment was repeated by another group, and they not only showed similar results of disease acceleration by co-expression of wtSOD1 with G93A and L126Z (Z refers to stop-truncation of the last 28 amino acids of SOD1), but also showed a conversion of an unaffected phenotype of the tgSOD1^{A4V} mice to an ALS phenotype seen in other tgSOD1^{mut} mice (Deng *et al.* 2006). In the tgSOD1$^{A4V/wtSOD1}$ mice, conversion to an ALS phenotype was accompanied by formation of detergent-insoluble multimeric aggregates of SOD1, which contained both mutSOD1 and wtSOD1. The authors hypothesized that wtSOD1 is converted from a soluble form to aggregated SOD1 multimers/oligomers in the double-transgenic mice and thereby contributes to exacerbation of disease. These aggregates were also found to co-localise with the α-subunit of ATP-synthase located in the inner mitochondria membrane of

vacuolated mitochondria (Deng *et al.* 2006). This suggests that motor neuron death may be mediated by impaired ATP synthesis arising from mitochondrial damage caused by mutSOD1 insoluble oligomers (Deng *et al.* 2006). More importantly, these experiments demonstrated the involvement of wtSOD1 in causing ALS suggesting that this might also be applicable in the pathogenesis of sporadic cases of ALS without mutations in SOD1.

1.5 Thesis outline

This thesis is organised in three main parts, as described below. The specific aims are given separately at the beginning of each result chapter (Chapters 3 – 8) and will not be mentioned here.

The first part (Chapters 3 – 6) presents results from work carried out on SOD1 protein. The main aim was to investigate the toxic properties of SOD1 in causing ALS.

The second part (Chapters 7 and 8) will present data from work carried out on the characterization of two mouse models with signs of neuromuscular dysfunction, which are the Mariusz and Arl mice.

The third part (Chapter 9) will be a general discussion on the implications of the present work within the broader context of ALS pathogenesis and therapeutics. Some unresolved questions on SOD1 fibrillization are also highlighted and some suggestions on how to bring this work forward are included.

Chapter 2 Materials and Methods

2.1 Materials

2.1.1 Chemicals and reagents

Chemicals and reagents used were of the highest grade. Reagent grade water, dH_2O, was from a Barnstead water purification system.

10X Tris/Glycine/SDS buffer	National Diagnostics
16% Tris/Glycine pre-cast gel	Invitrogen Life Tech.
26S proteasome	BIOMOL
4-(2-aminoethyl)-benzenesulfonyl fluoride (AEBSF)	Melford
4',6-diamidino-2-phenylindole (DAPI)	Sigma-Aldrich
5,5'-dithiobis-(2-nitrobenzoic acid) (DTNB)	Sigma-Aldrich
5(6)-carboxyfluorescein (CF)	Fluka
α-lactalbumin	Sigma-Aldrich
β-mercaptoethanol (β-ME)	Sigma-Aldrich
Absolute ethanol (C_2H_5OH)	VWR
Ac-nLPnLD-AMC	BACHEM
Agarose (electrophoresis grade)	Invitrogen
Albumin	Sigma-Aldrich
ATPγS	BIOMOL
Benzonase	BDH
Better Buffer	Microzone
Boc-LRR-AMC	BIOMOL
Bovine serum albumin (BSA)	Sigma-Aldrich
Bromophenol blue (BB)	Sigma-Aldrich
Calcium chloride ($CaCl_2$)	Sigma-Aldrich
Catalase	Sigma-Aldrich
Complete® Protease Inhibitor Cocktail Tablets	Roche
Coomassie Brilliant Blue-R	Fluka
Coomassie Brilliant Blue-G	Fluka

Copper sulphate ($CuSO_4$)	Sigma-Aldrich
Deoxyribonucleotide triphosphate (dNTP)	Promega
Dimethyl sulfoxide (DMSO)	Sigma-Aldrich
DMEM	Gibco-BRL
DNA loading buffer	Bioline
Ethidium bromide	Sigma
Ethylenediaminetetraacetic acid (EDTA)	Sigma-Aldrich
Fetal bovine serum (FBS)	Gibco-BRL
Fluorescent mounting media	Dakocytomation
Formamide	Sigma-Aldrich
Glacial acetic acid (CH_3COOH)	BDH
Glycerol	Sigma-Aldrich
Guanidine hydrochloride (GdnHCl)	Fisher
Hydrochloric acid	Fisher
Hyperladder (1, IV)	Bioline
Imidazole	Sigma-Aldrich
Isopropanol	VWR
Isopropyl-ß-D-thiogalactopyranoside (IPTG)	Ambion
Kanamycin	Gibco-BRL
Laminin	Sigma-Aldrich
LB Agar, Miller	Sigma-Aldrich
LB Broth, Miller	Sigma-Aldrich
Lipase	Sigma-Aldrich
Lipofectamine2000	Invitrogen
Lysozyme	Sigma-Aldrich
MegaBACE ET-ROX Size Standard	Amersham Biosciences
MegaBACE Loading Buffer	Amersham Biosciences
MegaBACE Long Read Matrix	Amersham Biosciences
MegaMix Blue PCR Master Mix	Microzone
Methanol (CH_30H)	Fisher
Myoglobulin	Sigma-Aldrich
Murine nerve growth factor (NGF)	Invitrogen
Nitrilotriacetic acid sepharose matrix (Ni-NTA resin)	Qiagen

Nuclei lysis solution	Promega
Oligonucleotide primers	Sigma-Genosys
Opti-MEM	Gibco-BRL
pET 28 expression vector	Novagen
Papain	Sigma-Aldrich
Paraformaldehyde (PFA)	BHD
Pepsin	Sigma-Aldrich
Penicillin/streptomycin solution (P/S)	Sigma-Aldrich
Phosphate Buffered Saline (PBS)	Sigma-Aldrich
Phosphotidylcholine (PC)	LipidProducts
Phosphotidylethanolamine (PE)	LipidProducts
Poly-D,L-ornithine	Sigma-Aldrich
Protease	Sigma-Aldrich
Proteinase K	Roche
Protein precipitation solution	Promega
SeeBlue Pre-Stained Standard	Invitrogen Life Tech.
Sephacryl 300-HR	Sigma-Aldrich
Sephadex G-50	Sigma-Aldrich
Sodium acetate (NaAc)	Sigma-Aldrich
Sodium chloride	Sigma-Aldrich
Sodium hydroxide	Sigma-Aldrich
Sodium dodecyl sulphate (SDS)	Sigma-Aldrich
Suc-LLVY-AMC	BIOMOL
SYPRO Orange	Invitrogen
Triton-X	Sigma-Aldrich
Trypsin/EDTA	Sigma-Aldrich
Trizma base (Tris)	Sigma-Aldrich
Thioflavin-T (ThT)	Sigma-Aldrich
Thrombin	Novagen
Tris/Borate/EDTA (TBE)	National Diagnostic
Uranyl acetate	Sigma-Aldrich
Zinc sulphate ($ZnSO_4$)	Sigma-Aldrich

2.1.2 Equipment

1L polypropylene centrifuge bottle	Nalgene
13mm coverslips	VWR
150mm^2 surface culture flask	Corning
3130XL Genetic Analyser	Applied Biosystem
5kDa MWCO centrifugal filter device	Millipore
96-well PCR microplate	VWR
96-well transparent flat-bottom plate	Nunc
Balance	Mettler
Beckman Optima XL-I	Beckman Coulter
Bio-Rad Bio-Logic chromatography system	Bio-Rad Laboratories
Centrifugal filter device	Amicon
Centrifuge Allegra 25R	Beckman Coulter
Cytometer	Neubauer
Chromatographic glass column	Bio-Rad Laboratories
Dialysis cassette	Pierce
DH Autoflow CO_2 Air-Jacketed Incubator	Nuaire
Electrophoresis power pack	Bio-Rad Laboratories
Electrophoresis tank	Life Technologies Inc
Epon cell	Beckman Coulter
Evolution™ RC Superspeed Refrigerated Centrifuge	Thermo Electron Corp
Fluorimeter Spectrofluor Plus	Tecan
Gilson pipettes	Anachem Ltd
Grip strength meter (GSM)	BioSeb
Heat block	Grant Instruments
Hybaid Ribolyser beads	Hybaid
Incubator shaker	Orbital
Incubator Raven	LTE Scientific
Jasco FP-750 Fluorescence Spectrometer	JASCO Corp
Jasco J-715 Circular Dichroism Spectropolarimeter	JASCO Corp
Jasco V-550 UV-Visible Spectrometer	JASCO Corp
LIPEX™ Extruder	Northern Lipids
Microcentrifuge	Eppendorf S415C

Microscope slides	VWR
Microwave	Proline
NanoDrop® ND-1000 Spectrophotometer	NanoDrop Technologies
Nucleopore polycarbonate membrane filter	Whatman
Optical PCR seal	Applied Biosystem
Peltier Thermal Cycler PTC-225	MJ Research
pH meter	Mettler-Toledo
Plate incubator shaker	GrantBio
Phase contrast microscope	Leica
Sonicator	Philip Harris Scientific
Spectrapor7 25kDa MWCO dialysis tube	Spectrum Laboratories
Spectrapor7 8kDa MWCO dialysis tube	Spectrum Laboratories
TaqMan RealTime PCR	Applied Biosystem
Tecnai T10 microscope	FEI, Eindhoven
Tissue homogeniser	Kontas
UV/VIS disposable cuvettes	Kartell
XCell SureLock™ Mini-Cell	Invitrogen
Zeiss LSM510 microscope	Zeiss

2.1.3 Commercial kits

AlexaFluor ® 555 Protein Labelling kit	Molecular Probes
BCA Assay kit	Pierce
BigDye Terminator Ready Reaction kit	Applied Biosystem
BL21 (DE3) Competent cells kit	Novagen
Plasmid Mini Prep kit	Qiagen
SOD-525 Assay kit	Oxis-Research

2.1.4 Software

Genetic Profiler v2.0	Molecular Dynamics
Grafit (version 3.0)	Erithacus Software Ltd
GraphPad InStat	GraphPad Software Inc

Jasco Standard Analysis software	JASCO Corp
Motion Analysis software	Kinetic Imaging
Sedfit Version 9.2	Sedfit
Sequence Analyser v3.0	Molecular Dynamics

2.1.5 Prepared solution

0.5M EDTA, pH8.0	148g EDTA 40g NaOH Dissolved in dH_20, pH was adjusted to 8.0 and to a final volume of 1L.
10M sodium hydroxide	400g NaOH Dissolved in 1L dH_20.
20% (w/v) SDS	200g SDS Dissolved in dH_20 by heat at 68°C with continuous stirring. pH was adjusted to 7.2 and to a final volume of 1L.
3M sodium acetate (NaAc), pH 5.2	246.1g NaAc Dissolved in dH_20, pH was adjusted to 5.2 and to a final volume of 1L.
2X SDS-PAGE loading buffer	187.5mM Tris-Cl, pH 6.8 6% (w/v) SDS 20% (v/v) glycerol 4% (v/v) β-ME 0.01% (w/v) BB

Buffer A	20mM Tris-Cl, pH 8.0 300mM NaCl
Buffer B	20mM Tris-Cl, pH 8.0 300mM NaCl 500mM imidazole
Column wash buffer (for Ni-NTA)	20mM Tris-Cl, pH 8.0 1M imidazole 6M GdnHCl
Coomassie Brilliant Blue solution	2.50g brilliant blue (50% R, 50% G) 456ml CH_3OH 88ml CH_3COOH Made up to 1L with dH_2O.
Coomassie destaining solution	50% (v/v) dH_2O 40% (v/v) CH_3OH 10% (v/v) CH_3COOH
LB Broth	40g LB broth Dissolved in 1L dH_2O. Autoclaved, and stored at room temperature.
LB Agar	25g LB agar Dissolved in 1L dH_2O. Autoclaved, and stored at room temperature.

2.2 Methods

2.2.1 General DNA protocols

2.2.1.1 DNA extraction from mouse tissue

DNA was extracted from tail biopsies (approximately 2mm long) or ear notches from mice. Tissue was digested overnight at 55°C with cell lysis buffer made up of 600µl nucleic lysis solution (Promega), 17.5µl 20mg/ml proteinase K (Roche) and 120µl 0.5M EDTA, pH8.0. Once digested, 200µl protein precipitation solution (Promega) was added to the lysis mixture and was briefly vortexed. The mixture was placed on ice for 5-10mins followed by centrifugation at 16 100rcf, at 4°C for 10mins to precipitate protein, cellular and tissue debris. Supernatant was carefully pipetted and transferred to a clean 1.5ml microcentrifuge tube. The centrifugation step was repeated as needed to remove any residual protein precipitate which may have been carried over during transfer. DNA from supernatant was precipitated by adding equal volume of isopropanol (VWR) to supernatant, approximately 600µl, and mixed by inversion or briefly vortexed. A white DNA precipitate may be observed during mixing. DNA precipitate was pelleted by centrifugation at 16 100rcf, at 4°C for 10mins. The aqueous phase was removed by pipetting or decanted carefully to ensure that the pellet was not lost. The DNA pellet was washed vigorously, with 300µl 70% (v/v) ethanol, by flicking the microcentrifuge tube with the index finger to detach the pellet from the inner wall of the tube. This was followed by centrifugation at 16 100rcf, at room temperature for 5mins. Ethanol was removed by careful pipetting and the DNA pellet was air-dried at room temperature for 1hr. Once all organic solvent was removed by evaporation, the DNA pellet was resuspended with 100µl sterile dH_2O. DNA was quantified (described in 2.2.1.3) and stored at 4°C for immediate use and -20°C or -80°C for long term storage.

2.2.1.2 DNA isolation from bacteria

Plasmid DNA was isolated from *Escherichia coli (E.coli)* using a Qiagen DNA MiniPrep Kit. The complete protocol and working principle can be obtained online from: http://www1.qiagen.com/literature/handbooks/literature.aspx?id=1000248
Briefly, this procedure is based on the alkaline lysis of bacterial cells followed by adsorption of DNA onto silica (QIAprep membrane) in the presence of high salt. In the final elution step, instead of using the manufacturer's elution buffer, dH_2O was used to elute DNA from QIAprep columns. DNA was quantified (described in 2.2.1.3) and stored at 4°C for immediate use and -20°C or -80°C for long term storage.

2.2.1.3 DNA quantification

Quantity and purity of DNA were determined using a NanoDrop® ND-1000 Spectrophotometer (Nanodrop Technologies) by measuring absorbance at 260nm and 280nm (OD_{260} and OD_{280}). The instrument users' manual can be obtained online from: http://www.nanodrop.com/techsupport/nd-1000-users-manual.pdf
Briefly, the instrument was blanked against dH_2O and UV measurements of 1µl DNA samples were taken using the operating software on the computer. $OD_{260/280}$ ratio and DNA concentrations (OD_{260} of 1.0 = 50ug/ml dsDNA) were automatically computed by the software. DNA purity was assessed by $OD_{260/280}$ ratio, with acceptable values between 1.7-2.0.

2.2.1.4 Polymerase Chain Reaction (PCR)

Unless stated otherwise, PCR was performed on a Peltier Thermal Cycler PTC-225 (MJ Research) according to the following setup:

PCR component	Working concentration	Volume/ reaction
DNA template	100 – 300ng/µl	1.0 µl
MegaMix Blue		17.0 µl
Primers (forward and reverse)	10 µM	1.0 µl /primer
dH_2O		1.0 µl
Total reaction volume		**20.0 µl**

The following PCR cycling conditions were used for all PCRs, except for variation of the annealing temperature, which was dependent on the sequence of the primers used (refer Appendix A: Mariusz primer information):

Step	Temperature (°C)	Duration	
Initial denaturation (D_i)	95	10 mins	
Denaturation (D)	94	30 secs	┐
Annealing (A)	58 – 63	30 secs	├ Repeated 30x
Extension (E)	72	45 secs	┘
Final extension (E_f)	72	10 mins	

2.2.1.5 PCR product purification with ethanol/salt precipitation

2µl 3M sodium acetate, pH 5.2 and 55µl 95% (v/v) ethanol were added to PCR products in a 96-well PCR plate. The PCR precipitate was recovered by centrifugation at 3000rcf, at 4°C for 30-40mins. Solvent was initially removed by gentle inversion of the plate, followed by further removal of residual solvent by placing the plate inverted on absorbent tissue paper. The plate was centrifuged at 100rcf, at 4°C for 1min. The PCR pellet was washed with 150µl 70% (v/v) ethanol and centrifuged at 3000rcf, at 4°C for 10mins. The solvent was removed as before and the PCR pellet was reformed by a brief maximum-speed centrifugation. The

PCR pellet was air-dried at room temperature for 10mins, followed by storage as pellet at -20°C if not used immediately, or was resuspended and mixed thoroughly with 10µl dH_2O and stored at 4°C or -20°C.

2.2.1.6 Agarose gel electrophoresis (AGE)

Appropriate volumes and concentration (% w/v) of agarose gels were prepared by dissolving agarose in 1X TBE buffer (National Diagnostic) by microwaving at high power for 1-2mins. The gel solution was allowed to cool slightly before the addition of ethidium bromide (Sigma-Aldrich). The final concentration of ethidium bromide was 0.5µg/ml. The gel solution was poured into gel casts with combs in place and was left at room temperature for 30-40mins to solidify. 0.8-1% (w/v) gels were used for electrophoresis of genomic DNA, and 2-5% (w/v) gels were used for electrophoresis of PCR products depending on the resolution requirement. Prior to electrophoresis, DNA samples were mixed with DNA loading buffer (Bioline) in 5:1 ratio of DNA sample to loading buffer. Electrophoresis was carried out in 1X TBE buffer at 90-120V/30cm, at room temperature for 30-60mins, depending on the resolution needed. Post-electrophoresis, gels were visualised and imaged on a UV transilluminator and digital imaging system (BioRad Laboratories).

2.2.1.7 Polyacrylamide: High resolution capillary array

Fluorescent-labelled PCR products were resolved on a MegaBACE 1000 DNA Analysis System (Molecular Dynamics) which utilizes capillaries filled by high-pressure nitrogen gas, with linear polyacrylamide (LPA), commercially known as MegaBACE Long Read Matrix (Amersham Biosciences). The complete users' manual describing matrix loading, software application and electrophoresis programs can be obtained online from:
https://www.genomiphi.com/aptrix/upp00919.nsf/Content/DDB0ADAE44E31D57C1256EB40044A93E/$file/Mega_manual_complete.pdf and
https://www.genomiphi.com/aptrix/upp00919.nsf/Content/BF9A773CCC39FFE0C1256EB40044AB44/$file/63004869.pdf

v2.0 software (Molecular Dynamics). PCR samples were prepared as fo
loading onto the MegaBACE:

Component	Volume
PCR samples	1.0 µl
dH_2O	3.0 µl
MegaBACE loading buffer	5.8 µl
ET-ROX (internal standard)	0.2 µl
Total volume/reaction	**10.0 µl**

2.2.1.8 Sequencing

Automated fluorescent sequencing was performed with a BigDye Te
Ready Reaction Kit (Applied Biosystem) on a 3130XL Genetic Analyser
Biosystem). Prior to sequencing PCRs, unbound primers, primer dim
unused nucleotide triphosphate (NTPs) were removed from the templ
products using a QIAgen PCR Clean Up kit according to the manuf
instructions. Sequencing PCRs were set up as follow:

PCR component	Working concentration	Volume/ reaction
DNA template	1-10 ng/µl	1.0 µl
BIG DYE		1.0 µl
Better Buffer		5.0 µl
Primers (forward OR reverse)	5 µM	0.75 µl
dH_2O		7.25 µl
Total reaction volume		**15.0 µl**

Sequencing PCR cycling conditions were:

Step	Temperature (°C)	Duration	
Denaturation (D)	96	30 secs	
Annealing (A)	50	15 secs	Repeated 30x
Extension (E)	60	3 mins	
Cooling/Hold	15	5 mins	

PCR products from this reaction were purified with ethanol/salt precipitation (as described in 2.2.1.5), and was resuspended with 20µl formamide (Sigma-Aldrich), instead of dH_2O, for loading onto the sequencer.

Sequencing reactions were kindly performed by Dr. Gareth Banks (Institute of Neurology, UCL).

2.2.2 General protein protocols

2.2.2.1 SDS-Polyacrylamide gel electrophoresis (SDS-PAGE)

Proteins were separated based on the Laemmli system on 16% Tris/Glycine pre-cast gel (Invitrogen) using an XCell SureLock™ Mini-Cell (Invitrogen) and 1X Tris/Glycine/SDS (National Diagnostic) as running buffer. Protein samples were mixed with an equal volume of 2X SDS-PAGE loading buffer to a final concentration of 2% (v/v) β-ME. Sample loading mixture was boiled at 100°C for 10-20mins prior to loading onto gel. Electrophoresis was performed at 160V, at room temperature for 90-100mins. To visualise proteins, the gel was stained with coomassie blue by soaking it in Coomassie Brilliant Blue solution for 45mins, followed by destaining with destaining solution until gel became colourless. Protein bands were visible as blue bands on gel.

2.2.2.2 Protein quantification

Protein concentration was determined using a BCA Protein Assay kit (Pierce) according to the manufacturer's protocol. Where practical, SOD1 protein was measured for absorbance at 280nm (OD_{280}) using the NanoDrop® ND-1000 Spectrophotometer. The concentration for SOD1 was calculated using an experimentally determined extinction coefficient (ε_{SOD1}) at 280nm of 10800 M^{-1} cm^{-1} (Choi *et al.* 2005). The concentration of SOD1 was calculated using the following formula:

$$\text{SOD1 concentration (M)} = OD_{280} / \varepsilon_{SOD1}$$

2.2.3 Positional cloning : Mariusz

Mariusz phenotyping and linkage analysis were performed by Professor Neil Dear (now at University of Sheffield) and colleagues at the ENU Mutagenesis Program (MRC) at Harwell. Standard phenotyping protocols used are outlined as below. The full detailed protocol can be obtained from the online MRC Harwell MouseBook: http://www.har.mrc.ac.uk/mousebook/?by=protocols

2.2.3.1 Mice behavioural screen

Grip strength

The grip strength protocol is briefly described as follow and was carried out by Dr. Sara Wells and Professor Neil Dear (MRC, Harwell).

The grip strength test was performed to assess neuromuscular function and muscular strength of the mouse using a computerized grip strength meter (GSM). This instrument is designed with a stainless steel grid-pull bar with dimensions of 10cm x 8cm (W x H), connected to a highly sensitive electronic digital force gauge. The mouse was held by the base of its tail and was gently lowered to the grid to allow proper grip of its paws (from forelimbs only or forelimbs and

hindlimbs) onto the grid. Once the grip was secured, the mouse was gently pulled backwards horizontally until the grip was released. The force applied to the grid just before the mouse loses its grip was recorded as the peak tension by the instrument. 5 measurements were taken for each mouse and the average was calculated.

Mouse reaching and grasping (MoRAG)

The MoRAG setup and protocol are briefly described as follows and testing was carried out by Dr. Valter Tucci (MRC, Harwell).

MoRAG is a test designed to assess the neurological and muscular functions of a mouse based on the ability of the mouse to perform reaching and grasping actions. Prior to conducting the test, food was withheld from mice for 16 hours. Each mouse was then placed in a plexiglass chamber. The plexiglas chamber has a dimension of 3.8cm x 6.4cm x 11.4cm (W x D x H), with a small opening in one of the walls where a feeding plane was attached. The performance of the mouse, in the chamber, in reaching and retrieving the food target on the feeding plane through the opening in the chamber was assessed. The assessment was based on a set of 25 qualitative and quantitative parameters, as listed in Table 2.1.

Wire manoeuvre

The wire manoeuvre protocol is briefly described as follows and was carried out by Dr. Sara Wells and Professor Neil Dear (MRC, Harwell).

The wire manoeuvre test was performed to assess balance ability in a mouse. The mouse was held by its tail and was slowly lowered to a horizontal steel wire with dimensions of 0.12cm x 50cm (D x L). The mouse was allowed to secure its grip on the wire with the forelimbs before leaving it fully suspended. Phenotype was scored follow:

Wire manoeuvre assessment	**Score**
Active grip strength with hindlimbs	1
Difficulty to grasp with hindlimbs	0

Table 2.1. Assessment parameters used in MoRAG.

Qualitative	Quantitative
Assessment of behaviour in the box	
- body posture	- reaching time
- activity	- number of right paw entries
- defecation	- correct reaching
- urination	- correct grasping
- vocalization	- correct retrieval
- sniffing	- distance of reaching
- grooming	
Assessment of behaviour while performing task	
- trunk displacement	
- body rotation	
- shoulder	
- movement of arm	
- tremor during reaching	
- trajectory	
- head orientation during reaching	
- hindlimbs alignment	
- grasping and retrieval related behaviours	

2.2.3.2 Linkage analysis

Linkage analysis of the backcross progeny was simplified by the use of inbred mouse strains. The founder animals (F1) were BALB/cJ x C3H/HeJ. All progeny of F1 mice mated to C3H were homozygous for the mutation which was on the BALB/cJ genetic background. Recombination events producing C3H heterozygosity or homozygosity excluded these areas indicating no linkage.

2.2.3.3 Critical region mapping

Genotyping with microsatellite markers

Initial genotyping was performed using sets of microsatellite markers developed by MIT Centre for Genome Research. Sequences and primer pairs were obtained from the Mouse Genome Informatics (MGI) database available online from: http://www.informatics.jax.org/

Markers which were informative between inbred strains of C3H/HeJ, BALB/cJ and C57BL/6J within position 41Mb - 67Mb on mouse Chromosome 18 were selected, and listed as follow:

D18Mit177	D18Mit124	D18Mit51
D18Mit202	D18Mit181	D18Mit152
D18Mit105	D18Mit52	D18Mit139
D18Mit123	D18Mit28	D18Mit161
D18Mit238	D18Mit78	D18Mit209

Where difference in allele size for an informative marker is less than 10bp (refer Appendix A), forward primers were labelled with a fluorescent tag at the 5' end with FAM, HEX, or TET. PCR products with fluorescent tags were resolved on a MegaBACE 1000 DNA Analysis System (Molecular Dynamics). All other PCR products were resolved on 4-6% (w/v) agarose depending on the product size and the resolution required. All primers were custom-made by Sigma-Genosys.

Genotyping with single nucleotide polymorphisms (SNPs)

The following SNPs were used to fine map the critical region where there were no more informative microsatellite markers available. Sequences were obtained from the Mouse Genome Informatics (MGI) database.

rs13483373	rs6338896
rs6309214	rs13483389
rs8239209	rs4231898

2.2.4 Axonal transport analysis

2.2.4.1 Motor neuron culture

Motor neurons were prepared for axonal retrograde assay as previously described by(Kieran *et al.* 2005), as outlined in paragraphs to follow. All experimental setup and imaging, except for carrier tracking, was performed by Dr. Matthew Golding at the Cancer Research UK London Research Institute.

Culture and maintenance

Motor neuron cultures were prepared from E13 spinal cord motor neurons obtained from single embryos. The spinal cord from embryos was dissected using microscalpels, harvested and transferred into a large Petri dish. It was cut into small fragments and was incubated with DNase followed by centrifugation through a 4% (w/v) BSA cushion (Arce *et al.* 1999). This BSA solution was dialyzed for 24hrs at 4°C against 1X PBS and 48hrs against Leibovitz-15 medium (Gibco-BRL), pH 7.3, using a Spectrapor7 25kDa MWCO dialysis tube (Spectrum Laboratories). Cells were resuspended in complete medium, plated onto poly-D,L-ornithine/laminin–coated 35mm glass-bottom dishes (MatTek) at a density of 60 000cells/plate, and maintained in culture for 5-7days.

2.2.4.2 Axonal retrograde transport study

Motor neurons were incubated with 40nM TeNT H_C-Alexa 488 in complete medium for 30mins at 37°C, washed three times with Dulbecco's minimum essential medium without phenol red, riboflavin, folic acid, and penicillin/streptomycin (P/S), and supplemented with 30mM Hepes-NaOH, pH 7.3. Cells were placed in a humidified chamber maintained at 37°C and were imaged every 5secs with an inverted microscope (Diaphot 300; Nikon) equipped with a Nikon 100×, 1.3 NA Plan Fluor oil-immersion objective.

Carrier tracking

Carrier tracking was performed on time-lapse sequences using the Motion Analysis software (Kinetic Imaging). Only moving carriers that could be tracked for at least four time points were considered. The distance covered by a carrier between two consecutive frames (referred to as a single movement) was used to determine its speed. Statistical analysis and curve fitting were performed using a Microsoft Excel template created by Dr. Niranjanan Nirmalananthan (Institute of Neurology, UK).

2.2.5 SOD1 protein

2.2.5.1 Production and purification

Vector and constructs

The open reading frame (ORF) sequence of the wildtype SOD1 (wtSOD1) cDNA was confirmed by sequencing an 'in house' plasmid stock, pSP64 Poly(A)Vector, containing the construct. Construct sequence was compared to available sequence (Accession no.: NM_000454) from the Nucleotide database on NCBI (http://www.ncbi.nlm.nih.gov). Using this as template, site directed mutagenesis was performed to generate constructs for seven other mutants, G93A, G37R, A4V, G85R, D83G, D90A, G114A (Figure 2.1).

a)

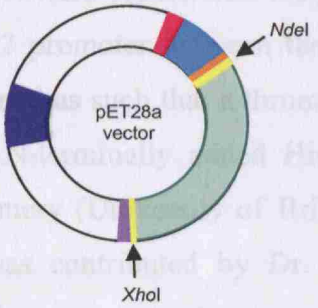

Kanamycin
T7 promoter
T7 terminator
His-Tag
Thrombin cleavage site
Met (start codon of wtSOD1 ORF)
Stop (stop codon of wtSOD1 ORF)
ORF of wildtype SOD1
cut site for Nde1 and Xho1

```
AGATCTCGATCCCGCGAAATTAATACGACTCACTATAGGGGAATTGTGAGCGGATAACAATTCCCCTC
TAGAAATAATTTTGTTTAACTTTAAGAAGGAGATATACCATGGGCAGCAGCCATCATCATCATCATCA
CAGCAGCGGCCTGGTGCCGCGC|GGCAGCCa|tATGGCGACCAAAGCCGTGTGCGTGCTGAAGGGCGAC
GGCCCAGTGCAGGGCATCATCAATTTCGAGCAGAAGGAAAGTAATGGACCAGTGAAGGTGTGGGGAAG
CATTAAAGGACTGACTGAAGGCCTGCATGGATTCCATGTTCATGAGTTTGGAGATAATACAGCAGGCT
GTACCAGTGCAGGTCCTCACTTTAATCCTCTATCCAGAAAACACGGTGGGCCAAAGGATGAAGAGAGG
CATGTTGGAGACTTGGGCAATGTGACTGCTGACAAAGATGGTGTGGCCGATGTGTCTATTGAAGATTC
TGTGATCTCACTCTCAGGAGACCATTGCATCATTGGCCGCACACTGGTGGTCCATGAAAAAGCAGATG
ACTTGGGCAAAGGTGGAAATGAAGAAAGTACAAAGACAGGAAACGCTGGAAGTCGTTTGGCTTGTGGT
GTAATTGGGATCGCCCAATAAACATTCCCTTGGATGTAGTCTGAGGCCCCTTAACTCATCTGTTATCC
TGCTAGCTGTAGAAATGTATCCTGATAAACATTAAACACTGTAATCTTAAAATGATAAC|TCGAGCAC
CACCACCACCACCACTGAGATCCGGCTGCTAACAAAGCCCGAAAGGAAGCTGAGTTGGCTGCTGCCAC
CGCTGAGCAATAACTAGCATAACCCCTTGGGGCCTCTAAACGGGTCTTGAGGGGTTTTTTG
```

b)

```
Met G S S H H H H H H S S G L V P R|G S H Met A T K A V C V L K G D
G P V Q G I I N F E Q K E S N G P V K V W G S I K G L T E G L H G F
H V H E F G D N T A G C T S A G P H F N P L S R K H G G P K D E E R
H V G D L G N V T A D K D G V A D V S I E D S V I S L S G D H C I I
G R T L V V H E K A D D L G K G G N E E S T K T G N A G S R L A C G
V I G I A Q StopT F P W Met Stop S E A P Stop L I C Y P A S C R N V
S Stop Stop T L N T V I L K Stop Stop L E H H H H H H
```

c)

Mutant SOD1	Exon	Nucleotide change	Protein change
A4V	1	GCC – GTC	Ala (A) ⇒ Val (V)
G37R	2	GGA – AGA	Gly (G) ⇒ Arg (R)
D83G	4	GAT – GGT	Asp (D) ⇒ Gly (G)
G85R	4	GGC – CGC	Gly (G) ⇒ Arg (R)
D90A	4	GAT – GCT	Asp (D) ⇒ Ala (A)
G93A	4	GGT – GCT	Gly (G) ⇒ Ala (A)
G114A	4	GGT – GCT	Gly (G) ⇒ Ala (A)

Figure 2.1. Vector and construct used for SOD1 expression. a) Schematic of pET28a vector (on the left) and sequence of wtSOD1 construct cloned into vector between *Nde*I and *Xho*I cut sites (below vector schematic). b) Protein sequence of wtSOD1. c) Site-directed mutations for G93A, G37R, G85R, A4V, D83G, D90A, and G114A.

Constructs were cloned into the pET28 expression vector (Novagen), downstream of the T7 promoter between the *Nde*I and *Xho*I restriction sites. The constructs were cloned as such that a thrombin cleavage site was created between the protein and the N-terminally added His-tag. Mutant constructs were generated by Dr. David Emery (University of Bristol). An additional construct of chimaeric GFP-G93A was contributed by Dr. James Stevens (Institute of Neurology, UCL). Received constructs were sequenced-verified with T7 primer pair:

T7 promoter	5'	TAATACGACTCACTATAGGG	3'
T7 terminator	5'	TATGCTAGTTATTGCTCAG	3'

Transformation, induction optimization and cell storage

Transformation: All constructs (G93A, G37R, A4V, G85R, D83G, D90A, G114A and GFP-G93A) were transformed into *E.coli* strain BL21 (DE3) (Novagen) according to the manufacturer's protocol. Briefly, chemically competent cells were thawed on ice in 1.5ml microcentrifuge tubes for a maximum of 30mins, followed by treatment with β-ME (1:10 dilution of 14.2M β-ME stock solution per 100µl cells) to increase transformation efficiency. Cells were incubated on ice for 10mins with interval mixing by gentle pipetting every 2mins. Approximately 1-50ng of construct was added to the cells and the cell suspension was mixed by gentle swirling, followed by incubation on ice for 30mins. Cells were heat-pulsed for 45-50secs at 42°C for optimum transformation efficiency, and were immediately placed on ice for 2mins. 0.9ml LB, pre-warmed to 42°C, was added to each transformation reaction and the reaction was incubated at 37°C for 1hr with shaking at 225-250rpm. After 1hr incubation, cells were pelleted by gentle centrifugation at 2rpm for 5mins. Approximately 750µl supernatant was removed and the cells were resuspended in the remaining supernatant by gentle pipetting. The cells were plated with a sterile spreader onto an LB agar plate containing 50µg/ml kanamycin to facilitate selection of transformants. To confirm that the bacterial colonies grown on the LB agar plate were successfully transformed, a small scale protein expression screen was performed on each colony (described

below) and plasmids were isolated (described in 2.2.1.2) for sequence verification to ensure no mutation of the construct during transformation.

Induction optimization: A small scale protein expression study was setup to screen for induction conditions that were able to yield a satisfactory quantity of soluble SOD1. Conditions screened were concentration of isopropyl-ß-D-thiogalactopyranoside (IPTG) (0.1, 0.2, 0.5 and 1.0mM final concentration), induction temperature (37°C and room temperature), and duration of induction (3, 6, 12 and 24hrs). Selected colonies from transformation plates were inoculated into 10mls LB containing 50µg/ml kanamycin. The cells were grown until the optical density at 600nm (OD_{600}) was between 0.6-1.0, followed by IPTG induction at the desired temperature and duration. Samples were taken pre- and post-induction, and protein expression was checked by comparing non-induced and induced samples by running it on SDS-PAGE (refer 2.2.2.1).

Storage: Colonies were grown in 10ml LB containing 50µg/ml kanamycin at 37°C for 4-6hrs. In a screw-cap 1.5ml microcentrifuge tube, 300µl 50% (v/v) glycerol was added to 700µl cells, and was mixed thoroughly by gentle inversions. Cells were stored at -80°C for long term storage.

Protein expression, cell harvesting and cell lysis

To make sufficient amount of protein, each construct was expressed in 10L culture. A transformant colony was inoculated into 100ml LB containing 50µg/ml kanamycin and grown overnight at 37°C. 20ml of this overnight growth was transferred to 2L LB supplemented with 50µg/ml kanamycin in a 5L Erlenmeyer flask. Cells were grown at 37°C until the OD_{600} was between 0.6-1.0. IPTG was added to a final concentration of 1mM and cells were induced at 20°C for 24hrs. Throughout growth and induction, aeration was achieved by continuous shaking at 225-250rpm. Cells were harvested by successive centrifugation and decantation of supernatant, in 1L polypropylene bottles (Nalgene) at 6000rcf, at 4°C for 30mins. Pelleted cells were frozen at -80°C until further use.

Harvested cells were resuspended with 100ml lysis buffer (Buffer A, 50U/ml benzonase, 10μg/ml lysozyme). Cells were lysed by sonication with 30-60secs bursts at 95% power for 5-6 times. The sonicated cell suspension was placed on ice between cycles to avoid increase in temperature during lysis. 200μl of crude cell lysate was sampled for SDS-PAGE, BCA assay and SOD1 assay. Cell lysate was clarified by centrifugation at 47 000rcf, at 4°C for 30mins. Supernatant containing soluble His-tagged SOD1 was transferred to a clean container and stored at 4°C temporarily. By examining the resulting pellet, the lysis procedure was repeated if cell lysis was incomplete in the first round by using a smaller volume of lysis buffer. Supernatant fractions from the first and second round of lysis were pooled.

Affinity chromatography: Ni-NTA

SOD1 was purified using metal chelate affinity chromatography, with nickel ion immobilized on a nitrilotriacetic acid sepharose matrix (Ni-NTA). Affinity purification of SOD1 on Ni-NTA was based on the high affinity of the His-tag on the SOD1 fusion protein to the nickel ions. All Ni-NTA purification was performed at room temperature using a BioRad Bio-Logic chromatography system. Purification of SOD1 involved two rounds of Ni-NTA column runs: i) removal of contaminating protein from supernatant of cell lysate and ii) removal of free His-tag after cleavage from SOD1.

Preparation of column: Approximately 100-150ml Ni-NTA resin (Qiagen) was packed into a 250ml glass column (BioRad) with dimensions of 2.5cm x 30cm (D x H). The column was equilibrated with Buffer A prior to use. Before every use, the column was prepared by flushing it with column wash buffer to remove any non-specifically bound protein, re-equilibrated with Buffer A and the OD_{280} reading from the UV detector was auto-zeroed before a sample was loaded.

First column run: Supernatant from cell lysate was loaded onto the column and the initial flow through was reloaded onto the column. After all flow through had come through the column, it was washed extensively with Buffer A until the OD_{280} reading returned to zero. The protein was eluted with a gradient of 0-60% Buffer B over 250ml. Eluted protein was collected in 3ml fractions and the protein

concentration was measured at OD_{280}. The elution profile was derived by plotting the OD_{280} for each fraction versus the corresponding fraction. Selected fractions were electrophoresed on SDS-PAGE to check for purity. Fractions with the least contaminating proteins were pooled (labelled as Ni-NTA(p1)) and His-tag was removed from the fusion protein.

Second column run: Once the His-tag was cleaved from the fusion protein, free His-tag was removed from the protein solution by a second Ni-NTA column run. Free His-tag was bound to the column whereas the SOD1 protein emerged as the flow through. The flow through was collected in fractions and the flowthrough profile was plotted as previously described for the elution profile. Selected fractions were electrophoresed on SDS-PAGE to check for purity, and pooled accordingly (labelled as Ni-NTA(p2)).

Gel filtration chromatography: Sephacryl 300-HR

Where necessary, SOD1 from the second column run (Ni-NTA(p2)) was further purified by gel filtration chromatography prior to Cu/Zn metal loading (described below). The instruction manual on media preparation and column packing can be obtained online from:
http://www.gelifesciences.co.jp/tech_support/manual/pdf/chrgfc/56119098.pdf

Approximately 100ml Sephacryl slurry was packed into a 150ml glass column (BioRad) with dimensions of 1.5cm x 100cm (D x H) and was equilibrated with gel filtration buffer (100mM Tris-Cl, pH8.0, 150mM NaCl). Prior to loading, protein sample was concentrated by ultracentrifugation using a 5kDa MWCO centrifugal filter device (Millipore). The maximum sample volume loaded was 10% of column bed volume for optimum separation of molecules. Protein sample was loaded and sample was allowed to run into the gel by gravity until the surface was almost dry. 1-2ml gel filtration buffer was then added gently to the top of the column bed without causing disruption to the gel surface. The added buffer was allowed to run into the gel as before, and this step was repeated twice before filling the column up to the top with buffer. The buffer level above the gel bed was maintained by continuous top up to maintain flow. All fractions were collected, measured for

absorbance at OD_{280}, electrophoresed on SDS-PAGE to check for purity and suitable fractions were pooled accordingly.

Dialysis, His-tag removal and Cu/Zn metal loading

Ni-NTA(p1) from the first column run was dialysed against thrombin cleavage buffer (25mM Tris-Cl, pH 8.4, 150mM NaCl) using a Spectrapor7 8kDa MWCO (Spectrum Laboratories) dialysis tube, with sample to buffer ratio of at least 1:40. Dialysis was carried out at room temperature and buffer was changed 2-3 times over 12-24hrs. Calcium chloride was added to the protein sample to a final concentration of 2.5mM before the addition of thrombin (0.5units/per mg of SOD1) to cleave off the His-tag. Cleavage was carried out for at least 18-24hrs at room temperature, with shaking at 100rpm. Digestion was terminated by addition of 4-(2-aminoethyl)-benzenesulfonyl fluoride (AEBSF) to a final concentration of 5mM and pH was reduced to 7.0 with dilute hydrochloric acid.

Purified SOD1 from the second column run (Ni-NTA(p2)) was loaded with metal by dialysis against metal loading buffer containing 150-200μM $CuSO_4$ over 3-4hrs at room temperature. This was repeated with $ZnSO_4$ in place of $CuSO_4$. After zinc loading, purified SOD1 was dialysed against storage buffer (20mM Tris-Cl, pH 7.5). Protein was stored at 4°C for immediate use and snap-frozen in liquid nitrogen for long term storage.

Determination of storage condition

The storage condition for purified SOD1 protein was determined by snap-freezing a small aliquot of the protein in liquid nitrogen followed by thawing at room temperature. The SOD1 activity of pre- and post-freeze-thawed sample was assayed and compared. Where there was no change in activity, liquid nitrogen storage for long term use was deemed suitable.

2.2.5.2 Protein characterization

SOD1 enzymatic assay

SOD1 activity was determined at relevant steps throughput purification using a commercially available kit, Bioxytech SOD-525 assay (Oxis Research) according to the manufacturer's protocol.

Thiol quantification (Ellman's assay)

To determine the accessibility and redox status of thiols in SOD1, a colorimetric reaction using 5,5'-dithiobis-(2-nitrobenzoic acid) (DTNB), also known as Ellman's reagent, was employed using modified conditions described by Ellman (1958, 1959)(Ellman 1958;Ellman 1959) and (Riddles *et al.* 1983). DTNB forms a mixed disulfide with protein thiols liberating 5-mercapto-2nitrobenzoic acid (TNB), which is a chromophore with absorption maxima at 412nm. Accessible thiols were determined under non-denaturing conditions, whereas inaccessible thiols were determined under denaturing conditions.

Reaction buffers for non-denaturing and denaturing conditions were prepared as below. Low concentration of EDTA was added as a metal chelator to prevent oxidation of free thiols.

i)	Non-denaturing reaction buffer	20mM Tris-Cl, pH7.5, 1mM EDTA
ii)	Denaturing reaction buffer	20mM Tris-Cl, pH7.5, 1mM EDTA, 6.72M GdnHCl (buffered in 20mM Tris-Cl, pH7.5)

4mg of DTNB reagent (Sigma-Aldrich) was dissolved in 1ml reaction buffer, giving a final working concentration of 10mM. Protein samples were prepared to a working concentration of approximately 1mg/ml with 20mM Tris-Cl, pH 7.5. The following (next page) were mixed together in a disposable cuvette and the reaction was incubated at room temperature for 15mins. Blank samples were prepared by adding reaction buffer to the mix in place of protein.

Component	Volume
DTNB solution	20 µl
Reaction buffer	1000 µl
Protein sample	100 µl
Total volume	**1120 µl**

The wavelength of a V-550 UV-Visible Spectrometer (Jasco) was set to 412nm and the instrument's baseline was zeroed using the blank sample. The absorbance (OD_{412}) of each sample was measured and the concentration of thiols in the sample was calculated from experimentally determined molar extinction coefficient (ε_{TNB}) of TNB (Riddles *et al.* 1979;Riddles *et al.* 1983), as shown below:

Extinction coefficient in non-denaturing reaction buffer (ε_{TNB-ND}) 14 150 M^{-1} cm^{-1}

Extinction coefficient in denaturing reaction buffer (ε_{TNB-D}) 13 700 M^{-1} cm^{-1}

Thiol concentration was calculated as follow:

Extinction coefficient, $\varepsilon_{TNB} = A / (bc)$

where A = absorbance

b = pathlength in cm

c = molar concentration (M)

Rearranging for c gives: $c = A / (b\varepsilon)$

c values calculated represent the concentration of thiols in the reaction solution. To correct for concentration of thiols in the protein sample, this value was multiplied by the dilution factor, calculated as follow:

$$\text{Dilution factor} = \frac{\text{total reaction volume (ml)}}{\text{sample volume (ml)}}$$

$$= 1.12 \text{ ml} / 0.10 \text{ ml}$$

$$= \mathbf{11.2}$$

To calculate for the number of free thiols per molecule of protein, the corrected concentration of thiols in the sample was divided by protein sample concentration.

Circular dichroism (CD)

Circular dichroism (CD) spectroscopy was performed using a J-715 Circular Dichroism Spectropolarimeter (Jasco). The secondary and tertiary structure of purified SOD1 was determined by obtaining CD spectra at far-UV (250-190nm) and near-UV (350-250nm) respectively. Far-UV and near-UV CD measurements were performed using a 0.1mm path length circular cuvette and a 10mm path length standard quartz cuvette, respectively. All data were collected using a stop resolution of 1nm, a scan speed of 50nm/min, with a 1sec response time. Measurements were performed over 10 accumulations to reduce signal to noise ratio and the baseline was corrected against the storage buffer. Protein concentrations were approximately 1.0-1.5mg/ml, and CD measurements were converted to units of molar ellipticity ([θ]). All corrections and processing were performed using the Jasco Standard Analysis Program (Jasco).

Crystallization

Purified wildtype SOD1 and 4 mutant SOD1 (G93A, G37R, A4V and G85R) were cystallized and analysed by Dr. Svetlana Antonyuk (CCLRC Daresbury Laboratory, UK). Crystallization conditions, data collection and processing were similar to published work by (Strange *et al.* 2006).

Analytical ultracentrifugation (AUC)

Dimer stability of SOD1 variants (wtSOD1, G93A, G37R, A4V, G85R, D83G, D90A, G114A and GFP-G93A) was determined by sedimentation velocity experiments using a Beckman Optima XL-I (Beckman Coulter). 400μl of protein was loaded into a double sector Epon cell with sapphire windows and centrifuged at 50 000rpm (182 000rcf at cell centre and 201 600rcf at cell bottom) at 20°C using an An-50Ti rotor. Samples were monitored immediately on reaching maximum speed using interference optics and then a further 199 scans were taken every 5mins. Every other scan was analysed using Sedfit Version 9.2, (1) using continuous size or c(s) distribution method entering no prior knowledge. Values for the partial specific volume of the protein and density and viscosity of the buffer used were calculated using Sednterp, (Hayes *et al.* 2003) and entered into the model parameters. This gave a distribution in sedimentation coefficients which was

then converted to a molar mass distribution using the c(M) distribution model. c(S) units are fringes per Svedberg, c(M) units are fringes/Da. 1 fringe is approximately 0.3mg/ml. Experimental run and fitting analyses were performed by Samantha Jones (MRC Prion Unit, UK).

Differential scanning fluorimetry (DSF)

Thermal unfolding of SOD1 variants was monitored using SYPRO Orange (Invitrogen) and was performed by using a real-time PCR (RT-PCR) instrument (Applied Biosystem). Experimental design was adapted from published protocol of (Niesen *et al.* 2007). Briefly, using a 96-well PCR plate, SYPRO Orange was mixed with protein in 1:1000 ratio with a final volume of 20µl/well (triplicates/sample and with/without 20mM EDTA at 11uM and 33uM). The plate was sealed with an Optical PCR seal (Applied Biosystem) to prevent evaporation of samples. The instrument was programmed to run with increasing temperature gradient from 19°C-95°C with 1°C increment and to hold for 60secs at every new temperature. Fluorescence was monitored using the in-built filters: FAM (492 nm) and ROX (610 nm), for excitation and emission, respectively. The fluorescence intensity was plotted as a function of temperature and curve-fitted according to the Vant Hoff equation to determine the apparent Tm value (temperature at mid-point of unfolding) using the GraFit software.

2.2.5.3 In vitro conversion of SOD1 into fibrils

To form amyloid fibrils, stock solutions of SOD1 proteins (wtSOD1, G93A, G37R, A4V, G85R, D83G, D90A, G114A and GFP-G93A) (1.3-1.5mg/ml) were diluted to a final protein concentration of 10µM in 20mM Tris-acetate buffer, with varying concentrations of GdnHCl and pH (4.0, 5.0, 7.5 and 9.0), and a final concentration of 10µM Thioflavin-T (ThT). Four Hybaid Ribolyser beads (Hybaid) were placed into each well of a 96-well transparent flat-bottom plate. 200µl reaction mixture containing diluted protein and ThT was pipetted into wells, and the plate was sealed with an Optical PCR seal (Applied Biosystem) to prevent evaporation of samples. The plate was incubated at 37°C with continuous shaking at 830rpm using a plate incubator shaker (GrantBio). The kinetics of fibril formation were monitored by

taking time point measurements of the fluorescence emission at 485nm when excited at 450nm using a fluorescence plate reader (Tecan). For seeded reactions, 2µl of preformed fibrils from spontaneous reaction or tissue homogenates was added to 200µl reaction mixture and the assay was repeated as described above. Tissue homogenates were prepared from homogenizing spinal cord samples from mice to a final concentration of 10% (w/v) in 0.5x PBS containing Complete-Mini Protease Inhibitor Cocktail (Roche) using a glass tissue homogenizer (Kontas). Tissue homogenates were aliquoted to 50µl volumes and stored at -80°C for long term storage.

The lag phase of amyloid formation was determined by fitting the time-dependent changes in the fluorescence of ThT (F) over the reaction time (t) to the following equation:

$$F = A + B/(1 + exp\,[k^* (t_m - t)]$$

where A = base level of ThT fluorescence during the lag phase

B = difference between final level of ThT fluorescence at plateau and the initial level during the lag phase

k = rate constant of fibril growth (h^{-1})

t_m = observed time at transition midpoint

The lag time (t) of fibril formation was calculated as: $t = t_m - 2/k$.

2.2.5.4 Imaging of fibrils under electron microscope

Sample preparation on carbon grids: For negative stain EM, 3.5µl of sample (fibrils or native protein) was applied to a carbon-coated, glow-discharged, 300-mesh copper grid and blotted after 2–3mins. The grids were stained with 3.5µl of 2% (w/v) uranyl acetate, blotted after 2mins and allowed to air-dry.

Imaging: Images were recorded using minimal electron dose at a magnification of 27 000× in a Tecnai T10 microscope (FEI, Eindhoven, NL) with a tungsten filament operating at 100kV. Grid preparation, analysis and imaging were performed by Dr. Howard Tattum (MRC Prion Unit, UK).

2.2.5.5 Protein labelling with Alexa Fluor 555

Proteins were labelled with Alexa Fluor 555 using the AlexaFluor® 555 Protein Labelling kit (Molecular Probes). The Alexa Fluor 555 reactive dye has a succinimidyl ester moiety which reacts efficiently with primary amines of proteins to form stable dye-protein conjugates. Alexa555-labelled proteins (which appeared light pink due to the dye) have absorption and fluorescence emission maxima of approximately 555 and 565nm, respectively. Labelling was performed according to the manufacturer's instructions with the exception of purification of labelled proteins from free dye. Instead of using the gel filtration mini-columns provided with the kit for purification of labelled-proteins, free dye was removed from labelled proteins by extensive dialysis in 1X PBS with a dialysis ratio of 5000:1 of buffer to sample. Dialysis was carried out in the dark at room temperature with 3 times buffer change over 12-24hrs. To ensure that free dye was completely removed, labelled sample was subjected to one time buffer exchange with 1X PBS by ultracentrifugation using a 5kDa MWCO membrane filter device (Millipore). Complete removal of free dye gave a clear filtrate, while labelled proteins remained light pink. Labelled proteins were stored in the dark at 4°C.

2.2.6 Proteasomal assay

Assays were performed as described in (Dantuma *et al.* 2000;Berkers *et al.* 2005;Kisselev and Goldberg 2005). 100ng of pure 26S proteasome (BIOMOL) was added to 100µl reaction buffer containing 50mM Tris-HCl, pH7.5, 10mM $MgCl_2$, 1mM DTT and 100µM ATPγS. All recombinant proteins (10µg/ml) were incubated for 1h at 37°C with pure 26S proteasome in the presence of 100µM ATPγS. Proteasome activities were then measured using 100µM Suc-LLVY-AMC (BIOMOL) for chymotrypsin-like activity, Boc-LRR-AMC (BIOMOL) for trypsin-like activity or Ac-nLPnLD-AMC (BACHEM) for caspase-like activity. Fluorescence was measured every minute for 60 min at 37°C using a TECAN 96-well plate reader ($\lambda_{ex}/\lambda_{em}$=360/465nm).

2.2.7 Liposomal assay

2.2.7.1 Production

Liposome preparation

Lipids (LipidProducts) purchased were already dissolved in 1:1 ratio of methanol: chloroform. 20mg lipid mixture of 20% (w/v) phosphotidylethanolamine (PE) and 80% (w/v) phosphotidylcholine were mixed in a 50ml round-bottom flask and gently swirled to assist evaporation of organic solvent and to form a thin lipid film. Residual organic solvent was removed by extended evaporation using a vacuum pump for 4-8hrs. Lipid composition was chosen as described to produce liposomes with neutral surface charge.

5(6)-carboxyfluorescein (CF) preparation

CF is a fluorescent dye with an excitation and emission wavelength of 492 and 517nm, respectively. The dye is membrane-impermeable and can be incorporated into liposomes. CF does not dissolve easily at neutral pH. It is only fully dissolved at pH higher than 6.8. 50mM CF was prepared by dissolving 37.6 mg CF in 2ml 20mM Tris-Cl, pH 7.5, and at this point solution appeared powdery-cloudy. To increase the pH, 20µl 10M NaOH was added initially, followed by 1µl shots of 10M NaOH to CF solution until pH was increased to 7.5. pH was measured using a pH mini-electrode (Metler-Toledo). As pH was increased, the CF solution turned dark orange, but clear, as CF powder was fully dissolved.

CF dye encapsulation

Once all organic solvent was removed, the dried lipid film was hydrated with 2ml 50mM CF. This gave a final lipid concentration of 10mg/ml, equivalent to 12.5mM lipids (average formula weight of lipid is 800). CF was encapsulated by dispersion into aqueous phase at room temperature by vigorous shaking using a Vortex mixer. Mixing was proceeded until the whole lipid film was fully dissolved indicated by an increased turbidity of the solution. Turbidity was due to increased light scattering from the formation of large multilamellar liposomes.

Extruder assembly and liposome extrusion

LIPEX™ Extruder (Northern Lipids) was assembled and lipid-CF suspension was extruded according to the manufacturer's instruction. The complete instruction manual can be obtained online from: http://www.northernlipids.com/products/documents/Extruder%20Assembly%20and%20Operating%20Manual.pdf.

Once assembled, the lipid-CF suspension was loaded into the extruder and using high-pressure oxygen-free nitrogen gas, at approximately 100kPa, the lipid-CF suspension was forced through a doubly-stacked polycarbonate membrane. 100nm pore size Nucleopore polycarbonate membrane (Whatman) was used to produce liposomes with an average size of 100nm. To ensure that the majority of liposomes extruded were of similar size, extrusion was repeated at least 10 times.

Free CF dye removal by gel filtration with Sephadex G-50

Liposomally-entrapped CF was separated from free CF by gel filtration with Sephadex G-50. Sephadex G-50 was packed into a column with dimensions of 1.5cm x 10cm (D x H), and was equilibrated with high salt buffer (20mM Tris-Cl, pH7.5, 107mM NaCl). High salt buffer (HSB) was used to balance the higher osmotic pressure in the liposome due to the encapsulated CF. As a general rule, filtered liposomes were always used on the same day as it were filtered to avoid any compromise in membrane integrity. 200µl liposome-CF was loaded and was allowed to run into the gel by gravity until the surface was almost dry. 1-2ml HSB was then added gently to the top of the column bed without causing disruption to the gel surface. The added buffer was allowed to run into the gel as before, and this step was repeated twice before filling the column up to the top with buffer. The buffer level above the gel bed was maintained by continuous top up to maintain flow. Free-CF are small molecules and migrate slower than liposomes. Fractions eluted first, approximately 1.6ml light orange-coloured suspension, were collected as these fractions contained the CF-encapsulated liposomes.

The concentration of liposomes (taken as lipid content) was estimated with the following formula:

$$\text{Liposome concentration} \approx \frac{[\ \text{volume of liposome-CF loaded on gel (ml)} \times \text{concentration of liposome-CF (mg/ml)}\ ]}{\text{volume of eluted fraction collected (ml)}}$$

$$\approx [0.2\ \text{ml} \times 10.0\ \text{mg/ml}\ ] \div 1.6\ \text{ml}$$

$$\approx \mathbf{1.25\ mg/ml}\ \text{(equivalent to 1.6 mM)}$$

Storage

Each liposome batch produced was kept in the unfiltered form and in the dark at 4°C for a maximum of one week.

2.2.7.2 Fibril effect on membrane

To test for fibril effect on membranes, fibrils were incubated with neutral liposome and checked for CF dye release, measured by a change in fluorescence. This is indicative of some sort of membrane compromise or disruption by the fibrils. Controls included were:

i) native SOD1

ii) non-SOD1 protein controls (α-lactalbumin, albumin, catalase, lipase, lysozyme, myoglobulin, papain, pepsin, protease, proteinase K, trypsin)

iii) buffer controls (20mM Tris-Cl, pH7.5, 20mM Tris-acetate, pH4.0, 20mM Tris-acetate, pH4.0 with 0.5M GdnHCl)

iv) mellitin (protein positive control known to cause disruption to membranes)

v) SDS or Triton-X (detergent control to solubilise membranes)

All protein samples were assayed at starting working concentration of 10μM.

Single concentration - end point study

Liposomes were gel filtered fresh before every use. 20µl sample was added to liposomes made up to 1ml volume at a final concentration of 0.05mg/ml in HSB. Reaction mix was pipetted directly into a disposable UV-cuvette. Sample-liposome mixture was mixed gently by pipetting, and incubated in the dark at room

temperature for 2hrs. Prior to fluorescence measurement, 1.5ml HSB was added to each sample to increase the reaction volume in the cuvette to the minimum height for the excitation light beam to pass through for measurement. Sample was excited at 492nm and emission was measured at 520nm using a FP-750 Fluorescence Spectrometer (Jasco).

2.2.8 Neurotoxicity assay

2.2.8.1 PC12 culture

The PC12 cell line was derived from the transplantable rat pheochromocytoma cells (Greene and Tischler 1976). These cells are capable of exhibiting a neuronal phenotype upon differentiation with nerve growth factor (NGF). PC12 cells were a gift from Dr. James Stevens (Institute of Neurology, UCL), and were received as frozen 1ml stock suspended in 10% (v/v) DMSO / 90% (v/v) FBS. All procedures were carried out in a tissue culture hood with aseptic technique. Unless stated otherwise, medium used throughout culture and growth conditions were:

i) 89% (v/v) DMEM / 10% (v/v) FBS, 1% (v/v) penicillin/streptomycin (P/S), pre-warmed to 37°C before use

ii) grown in a DH Autoflow CO_2 Air-Jacketed Incubator (Nuaire) at 37°C in a humid environment and 5% CO_2

Slide coating

Single round 13mm sterile coverslips were placed in each well of a 24-well tissue culture plate. Approximately 400µl 3µg/ml poly-D,L-ornithine (Sigma-Aldrich) solution was added to each well and the plate was incubated overnight at 37°C. The poly-D,L-ornithine solution was removed, replaced with 400µl 0.9mg/ml laminin and the plate was incubated at room temperature for 2hrs. The laminin solution was removed, and the sides of the plate were sealed with Parafilm. The plate was stored at -20°C until further use.

Culture and maintenance of cells

Frozen vials of cells, removed from liquid N_2 storage, were thawed rapidly in a 37°C water bath. Once thawed, cells were transferred to culture medium and pelleted by centrifugation at 160rcf at room temperature for 5mins. Medium was aspirated and the cell pellet was resuspended with 20ml of pre-warmed fresh medium. Cells were plated onto a 150cm^2 culture flask, and were grown to sub-confluency before being split 1:3 or 1:5, depending on the degree of confluency as assessed qualitatively under a phase contrast microscope. To split cells, medium was removed and 2ml trypsin/EDTA (Sigma-Aldrich), pre-warmed to 37°C, was added to the flask and was incubated at 37°C for 2mins to detach cells from the surface of the flask. Once detached, 8ml medium was added to the cells to prevent further action of trypsin/EDTA. The cells were plated onto a new flask at appropriate density. Medium was added to the cells to a final volume of 20ml.

Seeding and cell counting

Cells grown to sub-confluency were trypsinized (described above), followed by addition of 10ml medium. Cell suspension was thoroughly triturated to dissociate cell clumps to single cells. Immediately, approximately 10µl cell suspension was loaded onto each side of the counting chamber, under a cover glass, of a Neubauer cytometer (Figure 2.2(a)). The cells under the cover glass were counted under a phase contrast microscope (Figure 2.2(b)). The number of cells in 5 quadrants (each 0.04mm^2) per counting chamber was counted, and the average number of cells of the two chambers was calculated. This number was multiplied by the dilution factor to calculate the total cell density (numbers of cells/ml). The dilution factor was calculated as follow:

$$\text{Dilution factor} = \frac{\text{(conversion unit from µl to ml)}}{\text{(number of squares counted x volume per square)}}$$
$$= 1000 \div (5 \times 0.004)$$
$$= \mathbf{50\,000}$$

Cells were then seeded on poly-ornithine/laminin coated 13mm coverslips at 25 000 cells/well.

Transfection and differentiation

Seeded cells were grown overnight before transfection with pAcGFP-C1-SOD1(G93A). Lipofectamine2000 (LFA) (Invitrogen) was used to aid transfection. The standard protocol by Invitrogen was used, as outlined below:

Construct	0.8ug per well; made up to 50μl with Opti-MEM
LFA	2.0μl per well; made up to 50μl with Opti-MEM

Construct and LFA were made up in Opti-MEM as above, and were incubated at room temperature for 5mins. DNA and LFA were mixed together and the transfection mix was incubated at room temperature for 20mins. 100μl transfection mix was added to wells which were seeded with PC12 cells, and the plate was returned to the incubator. After 24hrs incubation, GFP-G93A expression was checked under a fluorescence microscope. Cells which were successfully transfected appeared green when excited with UV light. When expression of GFP-G93A was at an acceptable level, determined qualitatively by assessing the intensity of the green fluorescence, medium was changed to differentiation medium (98% (v/v) DMEM / 1% (v/v) FBS, 1% (v/v) P/S) and NGF was added to cells to a final concentration of 25nM per well. Cells were allowed to differentiate for approximately 96hrs. The medium was changed every 24-36hrs. Cells responding to NGF treatment appeared to be larger in size with more cytoplasm and have extended neurites, compared to the round morphology with little cytoplasm of undifferentiated PC12 cells.

Freezing down cells and storage

A frozen stock of PC12 cells was made by harvesting a sub-confluent flask of cells. The medium from the flask was removed, cells were trypsinized and resuspended with 6ml medium. The cell suspension was transferred to a 15ml tube and was cooled on ice for 5mins. Equal volume of pre-chilled DMSO/FBS mix in 1:5 ratio was added to the cell suspension in a drop wise manner and was mixed on ice. 1.5ml cell suspension in DMSO was transferred to a screw cap vial, and was stored at -80°C for a few days before being transferred to liquid nitrogen for long term storage.

a)

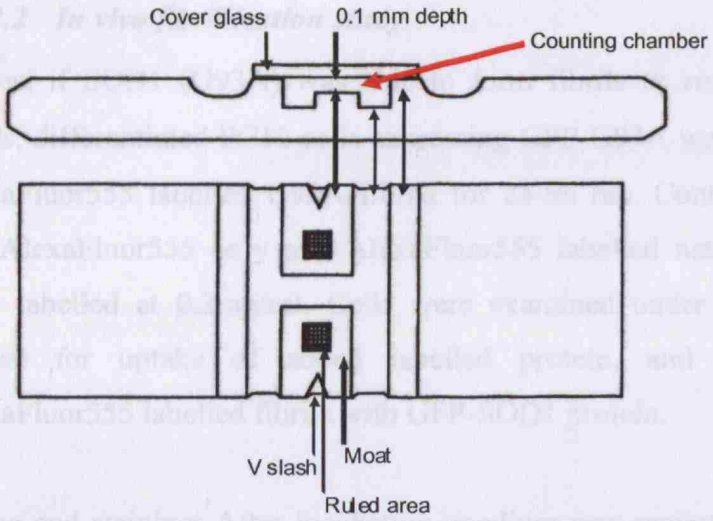

b)

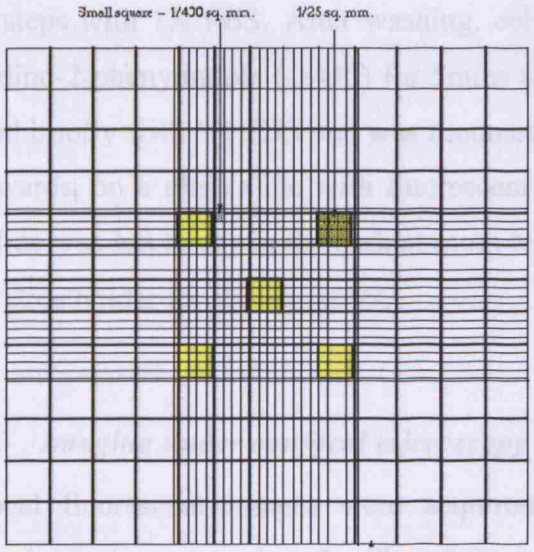

Figure 2.2. Neubauer cytometer. a) Side and top view. The counting chamber (red arrow) contains the ruled counting areas and is 0.1 mm under the cover glass, which is suspended on the raised ridges. b) Magnified ruled area in the counting chamber. Cells were counted from quadrants colored yellow (McNeely and Brown 1992).

2.2.8.2 In vivo fibrillization study

To test if SOD1 (G93A) was able to form fibrils *in vivo* when nucleated with fibrils, differentiated PC12 cells expressing GFP-G93A were incubated with 100µl AlexaFluor555 labelled G93A fibrils for 24-96 hrs. Controls included were free dye AlexaFluor555 only and AlexaFluor555 labelled native G93A. All proteins were labelled at 0.3mg/ml. Cells were examined under a confocal microscope (Zeiss) for uptake of added labelled protein, and for co-localization of AlexaFluor555 labelled fibrils with GFP-SOD1 protein.

Fixing and staining: After incubation, medium was aspirated and cells were fixed with pre-chilled 4% paraformaldehyde (PFA) for 5mins, followed by two 10mins wash steps with 1X PBS. After washing, cells were incubated with 1µg/ml 4',6-diamidino-2-phenylindole (DAPI) for 5mins to stain the nuclei. The coverslip was washed briefly with 1X PBS and was mounted, with the cell seeded surface facing downwards, on a glass slide with fluorescent mounting media (Dakocytomation). The slide was left to dry in the dark at room temperature for an hour before placing it in a slide holder for storage at 4°C.

2.2.8.3 Imaging under confocal microscopy

Confocal fluorescent images were acquired using a Zeiss LSM 510 META confocal microscope equipped with a Zeiss x63, 1.40 NA DIC Plan-Apochromat oil–immersion objective at room temperature. Fluorescence was recorded at 488nm using a 30mW Argon laser for excitation or at 543nm using 1mW HeNe laser for excitation. Image processing and editing were performed using the Zeiss LSM 5 and Adobe Photoshop software.

Chapter 3 Production and purification of superoxide dismutase 1 (SOD1)

3.1 Chapter aim

The aim of this chapter was to produce and purify proteins of eight variants and one GFP-chimaeric superoxide dismutase 1 (SOD1) for use in investigating the toxic properties of SOD1 in causing amyotrophic lateral sclerosis (ALS).

3.2 Introduction

While our genome is the blueprint of life, proteins are the basic building block of life. Proteins are responsible for the architectural framework of cells and are involved in all physiological biochemical processes, which when functioning properly sustains life but can otherwise cause diseases when dysfunctional. Proteins are encoded by genes, and it is impossible to know the functions of a gene unless the protein encoded by the gene is isolated and the biophysical and biochemical properties of the protein are studied.

A thorough structural and functional study of any protein will require tens of milligrams of that protein. A protein of interest can be isolated directly from natural sources expressing the protein, for example acetylcholine receptors from muscle tissues, but the amount isolated from a single preparation is usually very little, which means that more effort, time and money needs to be invested to ensure a sufficient amount is produced. The alternative is to express the protein using a prokaryotic (bacterial, usually *E.coli*) or eukaryotic (usually yeast, insect or mammalian cell) expression system. It is also possible to make proteins in a cell-free system or by chemical synthesis, but large scale protein production using these approaches is more expensive compared to using the cell-based systems, and therefore less favourable in academia-based laboratories where research costs are usually a concern.

The choice of which protein expression system to use depends on the intended use of the protein, whether it needs to be in the native configuration associated with or without activity or if the protein is utilized only to obtain sequence information from it. If the protein to be produced needs to be in the active form and the functionality of the protein is, for example, dependent on the post-translational modifications or the formation of disulfide bonds in acquiring the functional conformation, then expressing the target protein in an eukaryotic system would be ideal. This is because eukaryotes, in contrast to prokaryotes, are better equipped with the right machineries for post-translational modifications and have a more suitable protein folding environment within the cell. Also, in the prokaryotic system, the target protein is usually over-expressed and this over-expression, although advantageous in quantitative terms, usually causes the protein to become insoluble and form inclusion bodies. The formation of inclusion bodies is indicative of improper folding of the target protein thus making it non-functional. However, it is not impossible to produce functional proteins using a prokaryotic system. With technological advances, strategies have been developed over the years which can be used to manipulate the expression conditions to improve the yield of functional proteins from prokaryotic systems. For example, in the case of protein insolubility, the formation of inclusion bodies can be minimized by the co-expression of plasmid-encoded chaperones to aid folding of the target protein upon synthesis or by simply expressing the target protein at a lower temperature to reduce the rate of protein synthesis in the bacteria so that synthesized proteins have more time to be folded properly. An alternative to purifying functional proteins without manipulating the expression conditions is to purify the target protein directly from the inclusion bodies by *in vitro* refolding.

Protein purification is a multi-step process of fractionation to separate the target protein from the crude extract of the starting material, the source of the protein. The core of protein functionality is the specificity of the three dimensional (3D) conformation it adopts, which is dependent on the primary sequence of the protein and therefore will have its own biophysical and biochemical properties. The differences in the biophysical and biochemical properties of the mixture of proteins in the crude extract are the properties which are exploited in protein purification. In

protein purification, the concept of 'one-strategy-fits-all' does not exist because each protein is different and so a suitable purification strategy will have to be designed to suit each protein. Whether a strategy will work or not will have to be empirically determined and optimised accordingly. An ideal purification design should involve the least protein handling steps and at the same time yield the maximum amount of protein with the highest purity possible.

The human SOD1 proteins have been produced and purified using both prokaryotic (Boissinot *et al.* 1997;Leinweber *et al.* 2004;Ray *et al.* 2004) and eukaryotic expression systems (Yoo *et al.* 1999;Hayward *et al.* 2002;Rodriguez *et al.* 2002). Using either system, it has been shown that the SOD1 proteins purified were functional when assayed for their enzymatic activity. Since it is possible to obtain functional SOD1 from a prokaryotic expression system, this was the system of choice as the starting point in producing the proteins. To ensure that mutSOD1s studied were representative for both WTL and MBR mutants, in addition to wtSOD1, 5 WTL mutSOD1s (G93A (GFP- and non-GFP tagged), G37R, A4V, D90A and G114A) and 2 MBR mutSOD1 (G85R and D83G) were selected for study in this thesis. The cDNAs of SOD1, wtSOD1 and mutSOD1s, were cloned into pET28a expression vectors downstream of a nucleotide sequence encoding a string of 6 histidines (His). Expressed SOD1 was His-tagged (His-SOD1) to enable purification of SOD1 based on the affinity binding of His-SOD1 to the nickel (Ni^{2+})-immobilised resin (Ni-NTA) when fractionated on a chromatographic column. SOD1 expression in a pET expression system is based on the IPTG induction of expression of the T7 RNA polymerase (T7 RNAP) which is carried in the chromosome of *E. coli* strain BL21(DE3) (for simplicity, referred to as just *E. coli* in the remaining text of this chapter). The expression of T7 RNAP then drives the expression of SOD1 at the IPTG inducible T7/lac promoter located upstream of the cloned SOD1 cDNA. Figure 3.1 illustrates the induction mechanism of SOD1 expression in the T7 expression system (Novagen 2001).

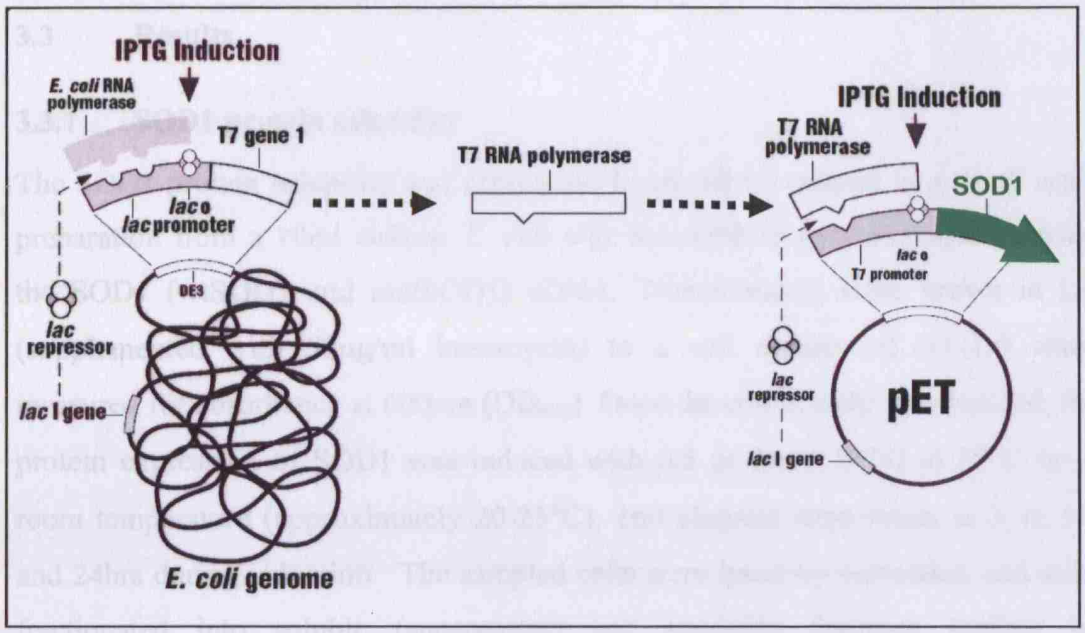

Figure 3.1. Expression of SOD1 using the T7 expression system. IPTG is an analogue of lactose (Sambrook and Russell 2001) and works by displacing a *lac* repressor from the *lac* operators upstream of the T7 RNAP and SOD1 cDNA. Once the *lac* repressor is displaced, T7 RNAP is expressed and the expressed T7 RNAP will bind to the uninhibited T7/*lac* promoter site initiating transcription of SOD1 which is then translated to produce the protein. (Figure adapted from (Novagen 2001).

3.3 Results

3.3.1 SOD1 protein solubility

The SOD1 protein solubility and expression levels were assessed in a small scale preparation from a 10ml culture. *E. coli* was transformed with plasmids carrying the SOD1 (wtSOD1 and mutSOD1) cDNA. Transformants were grown in LB (supplemented with 50μg/ml kanamycin) to a cell density of 0.6-1.0 when measured for absorbance at 600nm (OD_{600}). Once the cell density was reached, the protein expression of SOD1 was induced with 0.5 or 1mM IPTG at 37°C or at room temperature (approximately 20-25°C). 1ml aliquots were taken at 3, 6, 12, and 24hrs during induction. The sampled cells were lysed by sonication and were fractionated into soluble (supernatant) and insoluble fractions (pellet) by centrifugation. The fractions were assessed on SDS-PAGE as shown in Figure 3.2. SOD1 proteins generally have poor solubility when expressed in *E. coli* as the proteins were mainly found in the pellet fraction irrespective of the concentration of IPTG used, the duration and temperature of induction. Although there is slightly more soluble SOD1 present when expression was induced at room temperature, the overall SOD1 expression was lowered quite significantly compared to SOD1 expressed at 37°C, especially for mutSOD1. Protein solubility was assessed for wtSOD1 and four mutSOD1 (G93A, G37R, A4V and G85R). All four mutSOD1 proteins shared a common property of having a higher tendency to become insoluble compared to wtSOD1 protein, even when expression of all SOD1 variants was induced under the same conditions.

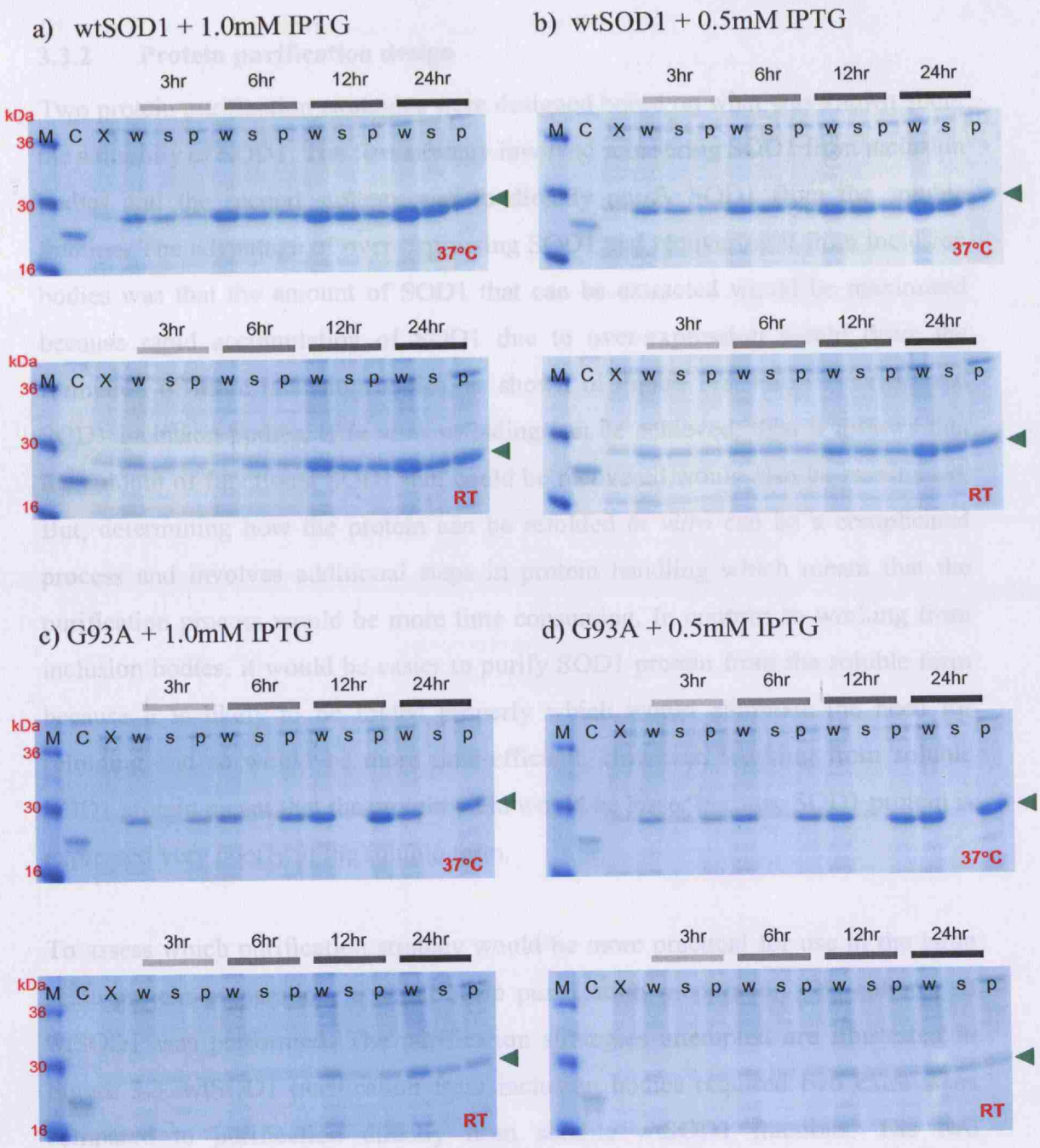

Figure 3.2. Representative SDS-PAGE gel images showing the protein solubility of SOD1 when expressed in *E.coli* under various induction conditions. Variables were IPTG concentration, duration and induction temperature. a-b) wtSOD1 c-d) G93A. (M = protein marker, C = commercial recombinant human SOD1, X = non-induced cells sample, w = whole cell lysate, s = supernatant fraction containing soluble proteins, p = pellet fraction containing insoluble proteins and cell debris, RT = room temperature, green arrow heads point to SOD1 protein).

3.3.2 Protein purification design

Two protein purification strategies were designed based on what was known about the solubility of SOD1. The first strategy involved recovering SOD1 from inclusion bodies and the second strategy was to directly purify SOD1 from the soluble fraction. The advantage of over-expressing SOD1 and recovering it from inclusion bodies was that the amount of SOD1 that can be extracted would be maximised because rapid accumulation of SOD1 due to over-expression would drive the formation of more inclusion bodies, as shown in Figure 3.2. From the extracted SOD1 inclusion bodies, if *in vitro* refolding can be achieved, then it follows that the amount of functional SOD1 that could be recovered would also be maximised. But, determining how the protein can be refolded *in vitro* can be a complicated process and involves additional steps in protein handling which meant that the purification process would be more time consuming. In contrast to working from inclusion bodies, it would be easier to purify SOD1 protein from the soluble form because it is likely to be folded properly which would eliminate the need for refolding and so would be more time-efficient. However, working from soluble SOD1 protein meant that the protein yield would be lesser because SOD1 protein is expressed very poorly in the soluble form.

To assess which purification strategy would be more practical for use in the large scale protein preparation, a small scale purification preparation (2L culture) of wtSOD1 was performed. The purification strategies attempted are illustrated in Figure 3.3. wtSOD1 purification from inclusion bodies required two extra steps compared to purification directly from soluble wtSOD1 fractions. The two additional steps were the solubilisation of inclusion bodies and *in vitro* refolding. Inclusion bodies containing insoluble wtSOD1 protein were solubilised with 6M GdnHCl buffered in 50mM Tris-Cl, pH8.0 to release the proteins from the aggregated mass and to unfold the proteins so that these proteins can be refolded *in vitro*. The *in vitro* refolding step of wtSOD1 was adapted from (Leinweber *et al.* 2004)). The buffer used for refolding was 10mM Tris-Cl, pH8.0 containing 0.5mM β-mercaptoethanol (β-ME). Refolding was performed by dialysis of the solubilised proteins against the refolding buffer to allow the denaturants from the solubilising

Figure 3.3. Production and purification scheme for SOD1.

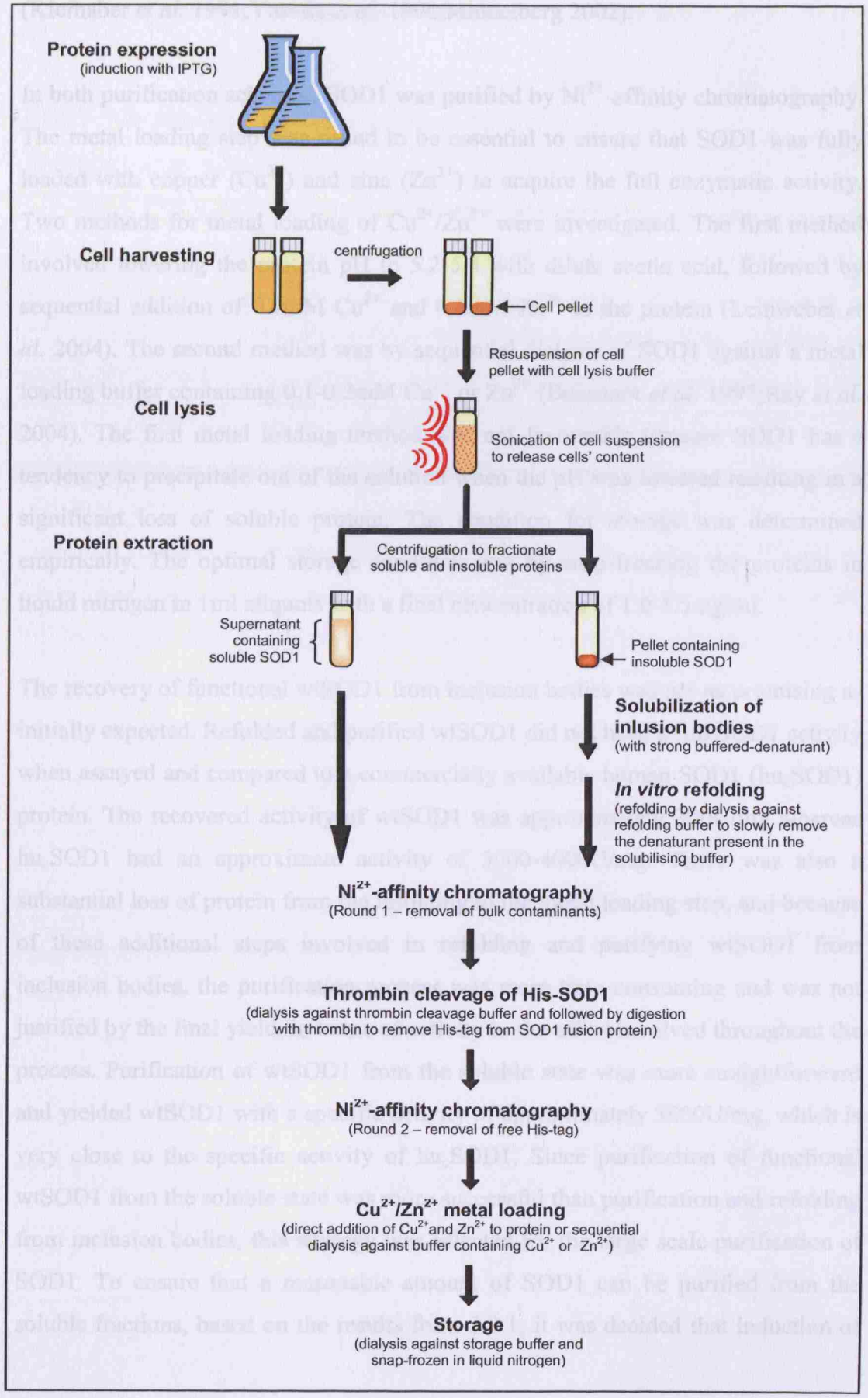

buffer to be removed slowly allowing SOD1 to refold with minimal aggregation (Kiefhaber *et al.* 1991;Yasuda *et al.* 1998;Middelberg 2002).

In both purification schemes, SOD1 was purified by Ni^{2+}-affinity chromatography. The metal loading step was found to be essential to ensure that SOD1 was fully loaded with copper (Cu^{2+}) and zinc (Zn^{2+}) to acquire the full enzymatic activity. Two methods for metal loading of Cu^{2+}/Zn^{2+} were investigated. The first method involved lowering the protein pH to 5.2-5.4 with dilute acetic acid, followed by sequential addition of 0.1mM Cu^{2+} and 0.1mM Zn^{2+} to the protein (Leinweber *et al.* 2004). The second method was by sequential dialysis of SOD1 against a metal loading buffer containing 0.1-0.2mM Cu^{2+} or Zn^{2+} (Boissinot *et al.* 1997;Ray *et al.* 2004). The first metal loading method was not favourable because SOD1 has a tendency to precipitate out of the solution when the pH was lowered resulting in a significant loss of soluble protein. The condition for storage was determined empirically. The optimal storage condition was by snap-freezing the proteins in liquid nitrogen in 1ml aliquots with a final concentration of 1.0-1.5mg/ml.

The recovery of functional wtSOD1 from inclusion bodies was not as promising as initially expected. Refolded and purified wtSOD1 did not have a full SOD1 activity when assayed and compared to a commercially available human SOD1 (hu_cSOD1) protein. The recovered activity of wtSOD1 was approximately 300U/mg whereas hu_cSOD1 had an approximate activity of 3000-4000U/mg. There was also a substantial loss of protein from the refolding to the metal loading step, and because of these additional steps involved in refolding and purifying wtSOD1 from inclusion bodies, the purification process was more time consuming and was not justified by the final yield, in terms of activity to the effort involved throughout the process. Purification of wtSOD1 from the soluble state was more straightforward and yielded wtSOD1 with a specific activity of approximately 3800U/mg, which is very close to the specific activity of hu_cSOD1. Since purification of functional wtSOD1 from the soluble state was more successful than purification and refolding from inclusion bodies, this strategy was selected for the large scale purification of SOD1. To ensure that a reasonable amount of SOD1 can be purified from the soluble fractions, based on the results from 3.3.1, it was decided that induction of

SOD1 expression with 1mM IPTG at room temperature (or lower at 18-20°C) over 24hrs was optimal to produce a reasonable amount of soluble SOD1.

3.3.3 Protein purification – yield and activity recovery

wtSOD1, mutSOD1 (G93A, G37R, A4V, G85R, D83G, D90A, and G114A) and chimaeric GFP-G93A proteins were expressed according to the conditions described in 3.3.2. SOD1 protein was extracted from an 8-10L culture, His-tag removed and was purified by Ni^{2+}-affinity chromatography (as outlined in Figure 3.3). The purification process of SOD1 was followed by assaying the enzymatic activity. The final yield of purified SOD1 was variable between the SOD1 mutants, which ranged from 15-150mg (1-7% of total soluble proteins in the crude extract) and was an average of 8-fold lower than the amount purified for wtSOD1. Table 3.1 gives a purification summary of all SOD1 purified showing the yield and recovery of activity from each purification step. Figure 3.4, 3.5 and 3.6 show representative SDS-PAGE gel images of the purification process of wtSOD1, G37R and GFP-G93A, respectively. Figure 3.7 shows an SDS-PAGE gel image of all the SOD1 protein purified with emphasis on the level of purity of each protein.

Table 3.1. Summary of human SOD1 protein purification. Protein yield is the percentage (%) of total protein at a purification step to the total protein at the start of purification from the crude extract (CE). Purification factor is calculated as the % of specific activity at a purification step to the initial specific activity in the CE.

$^{\delta}$Step	Volume (ml)	Total activity (U)	Total protein (mg)	Specific activity (U/mg)	Yield (%)	Purification factor
wtSOD1						
CE (supernatant)	115.0	688594.70	1835.86	375.08	100.0	1.0
NiNTA I	130.0	454209.60	899.47	504.97	49.0	1.3
His-tag removal	140.0	446989.20	813.68	549.34	44.3	1.5
NiNTA II	140.0	423679.20	813.68	520.70	44.3	1.4
Cu/Zn loading	135.0	416519.10	685.40	3761.51	37.3	10.0
G93A						
CE (supernatant)	180.0	184051.00	665.10	276.35	100.0	1.0
NiNTA I	175.0	94734.99	31.50	3007.46	4.7	10.9
His-tag removal	30.0	106413.89	28.03	3814.12	4.2	13.8
NiNTA II	30.0	54405.02	15.30	3627.00	2.3	13.1
Cu/Zn loading	15.0	28880.21	15.00	3850.69	2.3	13.9
G37R						
CE (supernatant)	285.0	218690.53	3451.52	63.36	100	1.0
NiNTA I	100.0	219734.67	112.36	1955.57	3.3	30.9
His-tag removal	105.0	240743.83	110.15	2185.51	3.2	34.5
NiNTA II	180.0	167720.33	71.28	2352.98	2.1	37.1
Cu/Zn loading	65.0	114353.68	84.50	2567.96	2.5	40.5
***A4V**						
CE (supernatant)	n/a	n/a	n/a	n/a	n/a	n/a
NiNTA I	52.0	52246.48	110.86	471.71	n/a	n/a
His-tag removal	59.0	44606.95	110.64	402.15	n/a	n/a
NiNTA II	63.0	33633.81	65.02	518.32	n/a	n/a
Cu/Zn loading	48.0	56452.80	72.96	1200.10	n/a	n/a
***G85R**						
CE (supernatant)	121.0	n/a	n/a	n/a	n/a	n/a
NiNTA I	95.0	87590.00	154.30	569.13	n/a	n/a
His-tag removal	97.0	4467.82	140.59	31.77	n/a	n/a
NiNTA II	135.0	5815.80	63.41	91.65	n/a	n/a
Cu/Zn loading	63.0	10098.90	91.35	286.25	n/a	n/a
D83G						
CE (supernatant)	120.0	21278.80	2322.21	9.16	100.0	1.0
NiNTA I	95.0	9.36	185.47	0.05	8.0	0.0
His-tag removal	97.0	596.62	213.26	2.80	9.2	0.3
NiNTA II	15.0	667.10	26.42	25.25	1.1	2.8
Cu/Zn loading	15.0	4724.38	20.20	233.91	0.9	25.5

δ Step : CE – Crude extract
NiNTA – Ni^{2+}-affinity chromatography
*A4V and G85R – Protein extraction and NiNTA I was performed by another laboratory member. Purifications notes for these steps were not available (n/a)

(*con't* from **Table 3.1**. Summary of SOD1 purification.)

$^{\delta}$Step	Volume (ml)	Total activity (U)	Total protein (mg)	Specific activity (U/mg)	Yield (%)	Purification factor
D90A						
CE (supernatant)	125.0	27427.61	2404.06	11.41	100.0	1.0
NiNTA I	48.0	7691.17	193.10	39.83	8.0	3.5
His-tag removal	50.0	8304.50	177.27	46.85	7.4	4.1
NiNTA II	40.0	10301.70	169.29	60.85	7.0	5.3
Cu/Zn loading	40.0	27424.75	165.76	158.04	6.9	13.9
G114A						
CE (supernatant)	160.0	73159.97	2234.98	32.73	100.0	1.00
NiNTA I	75.0	99081.10	174.51	567.78	7.8	17.35
His-tag removal	78.0	122190.50	159.69	765.16	7.1	23.37
NiNTA II	53.0	98371.09	112.02	878.18	5.0	26.83
Cu/Zn loading	58.0	127452.09	114.91	1109.16	5.1	33.88
GFP-G93A						
CE (supernatant)	120.0	185546.90	1870.13	99.22	100.0	1.0
NiNTA I	60.0	50860.13	80.97	628.11	4.3	6.3
His-tag removal	60.0	28036.82	58.06	482.90	3.1	4.9
GF-Sephacryl	7.5	47646.61	49.60	960.66	2.7	9.7
NiNTA II	13.0	27263.26	24.48	1113.67	1.3	11.2
Cu/Zn loading	12.5	34422.23	24.55	1402.29	1.3	14.1

δ Step : CE – Crude extract
NiNTA – Ni^{2+}-affiniiy chromatography
GF-Sephacryl – Gel filtration using Sephacryl 300-HR

Description for Figure 3.4, Figure 3.5 and Figure 3.6.

The soluble fractions from the crude cell extract containing soluble SOD1 was fractionated by Ni^{2+}-affinity chromatography (Round 1) to remove the bulk of contaminating proteins from the His-SOD1 protein. Eluted fractions containing the His-SOD1 protein and with the least contaminating proteins from Round 1 of Ni^{2+}-affinity chromatography were pooled. The pooled protein was dialysed against thrombin cleavage buffer. After dialysis, the pooled protein was incubated with thrombin to cleave the His-tag off the SOD1 protein. The free His-tag was removed by Ni^{2+}-affinity chromatography (Round 2). The flowthrough fractions from Round 2 of Ni^{2+}-affinity chromatography containing the untagged-SOD1 were pooled. The pooled protein was metal loaded with Cu^{2+} and Zn^{2+} by dialysis prior to storage in liquid nitrogen.

For reasons undetermined (in Figure 3.6), when His-GFP-G93A was subjected to thrombin cleavage, the GFP-tag was also cleaved from the G93A protein. Since there was still a substantial amount of intact GFP-G93A protein left, the intact GFP-G93A protein was recovered by gel filtration chromatography. Gel filtration chromatography fractionates molecules by size. Larger molecules will take a shorter time to run the gel filtration column length, therefore eluting first, whereas smaller molecules take a longer time and so will elute later.

Abbreviations used in figures:

M	– protein marker
C(bv)	– commercial bovine SOD1
C(hu)	– commercial human SOD1
S	– supernatant of crude extract (containing soluble SOD1)
FT	– flowthrough fractions
W	– wash fractions
E	– elution fractions
TX (pr)	– pre-thrombin cleavage
TX (pt)	– post-thrombin cleavage
Buff. A or B	– buffers used in Ni^{2+}-affinity chromatography (refer 2.2.5.1)
OD_{280}	– absorbance at 280nm
app.	– application

Figure 3.4. Purification of wtSOD1.

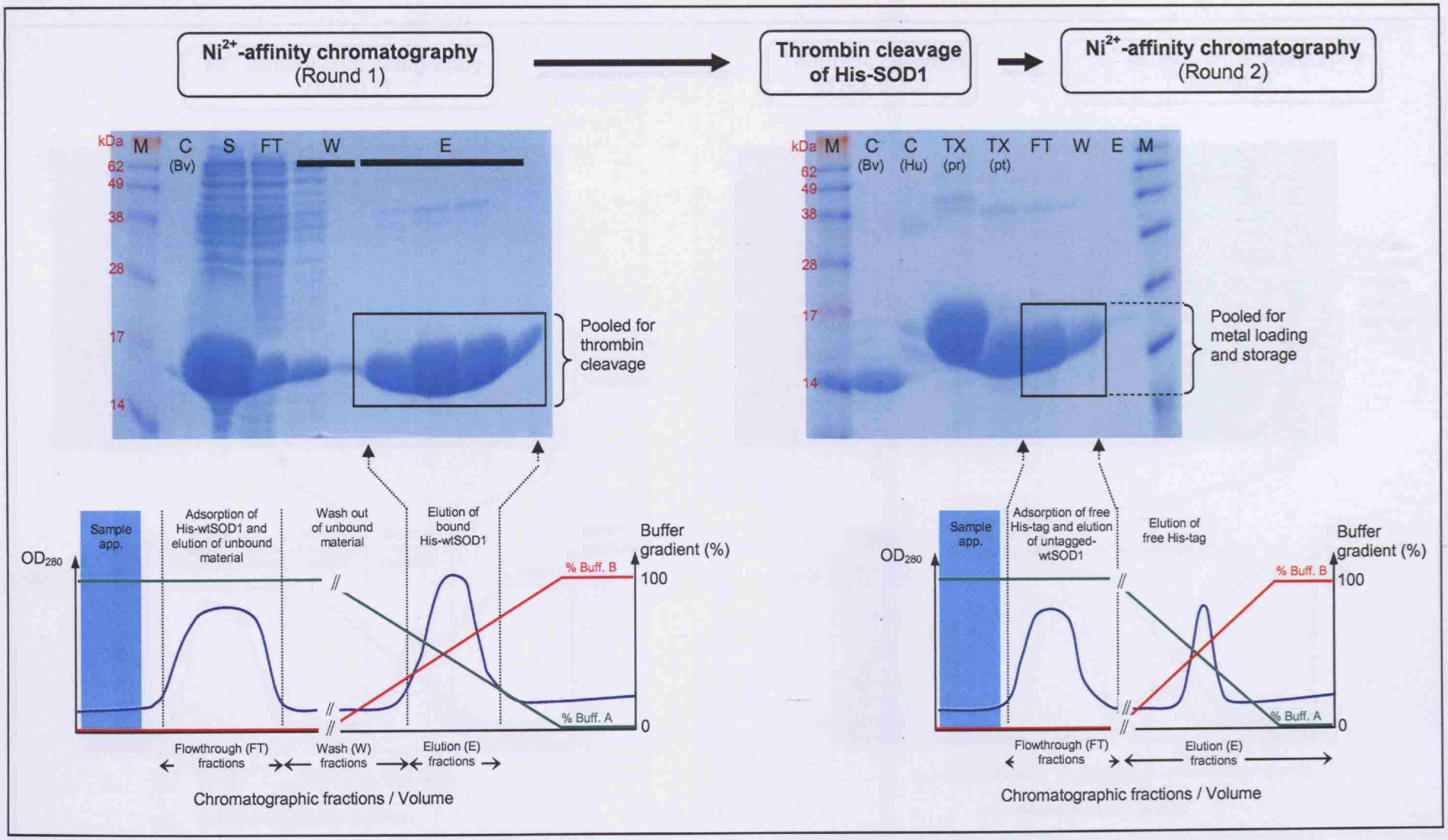

Figure 3.5. Purification of G37R.

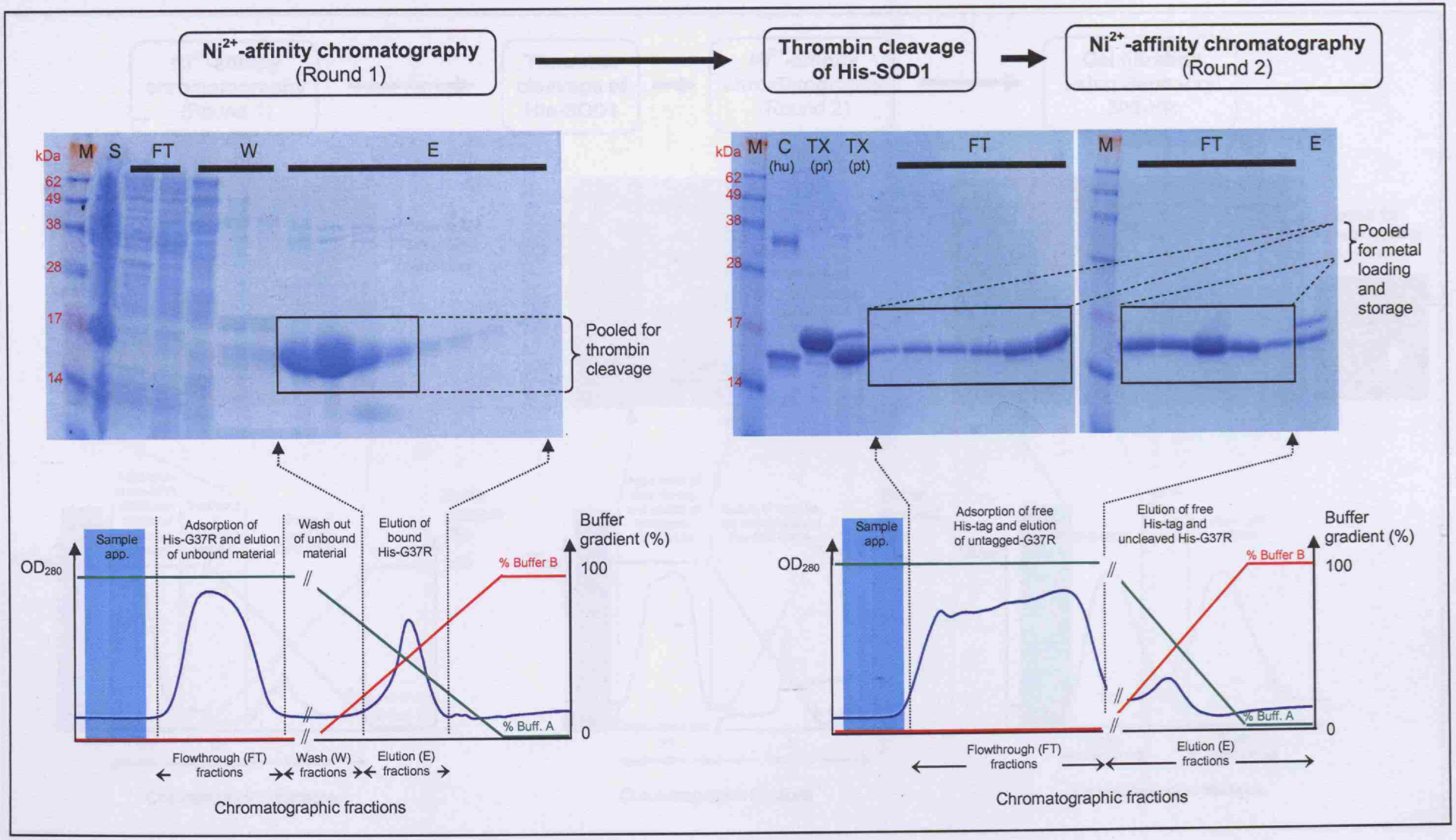

Figure 3.6. Purification of GFP-G93A.

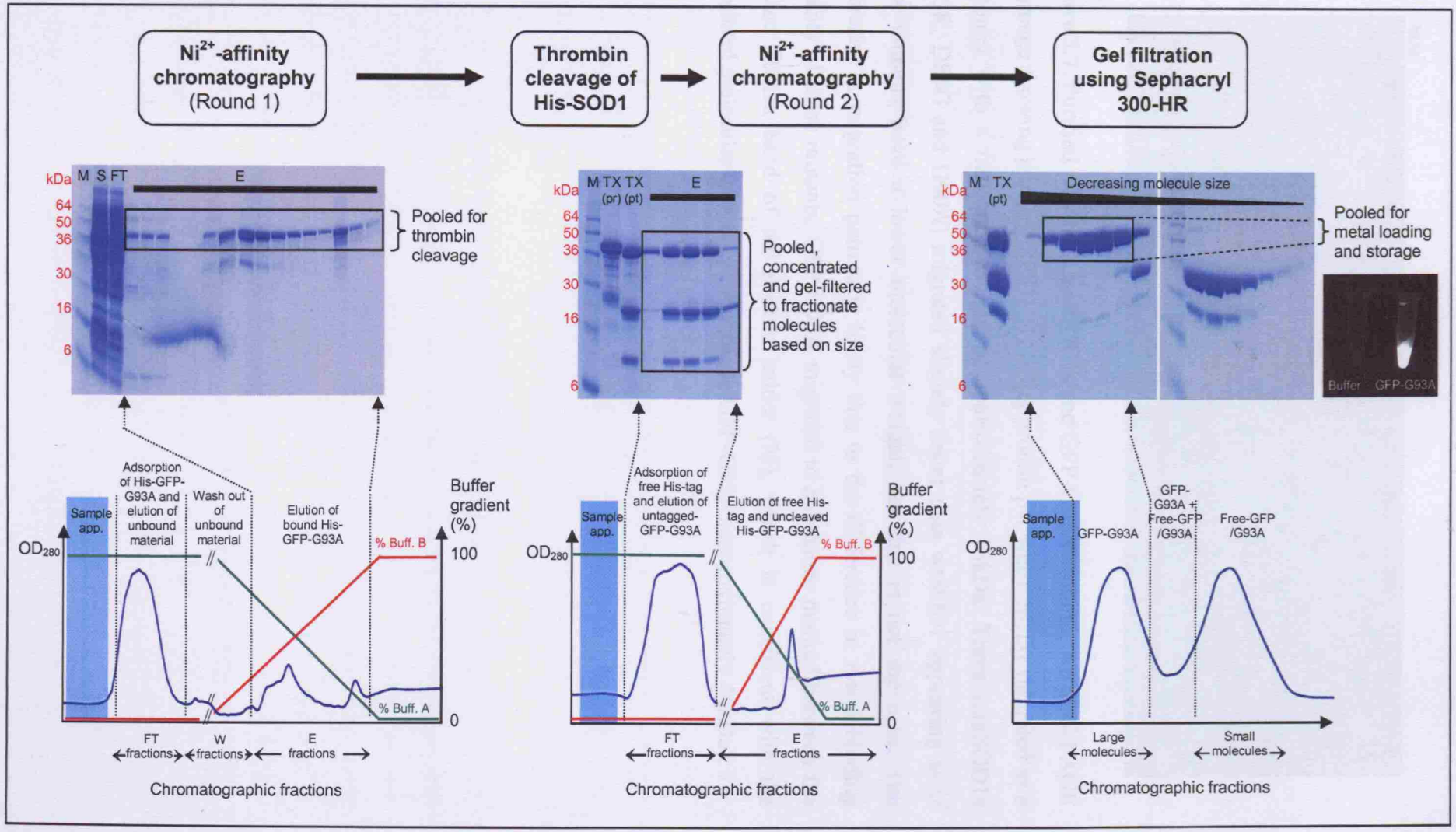

Figure 3.7. Purified wtSOD1, mutSOD1s and GFP-G93A proteins. An SDS-PAGE gel image showing purified SOD1 (12-15μg protein per well). SOD1 migrated as a monomer with a molecular weight of approximately 16kDa. Three mutSOD1s (G85R, D83G and D90A) migrated slightly faster than wtSOD1 appearing as if these mutants have a lower molecular weight, but this is not the case. The difference in migration pattern is likely due to the difference in metal binding capacity of these mutants. GFP-G93A migrated to a distance marked between the 36 and 50kDa band of the protein ladder (M), which is consistent with the calculated molecular weight of monomeric GFP-G93A (approximately 44kDa).

3.4 Discussion and conclusion

The expression and solubility results presented in Figure 3.2 show that mutSOD1 have a higher tendency to form aggregates compared to wtSOD1 even when expression of mutSOD1 and wtSOD1 was induced under the same conditions. These results are early indications that mutations in SOD1 cause some alterations to the biophysical and biochemical properties of the protein, and these alterations affect the protein folding of SOD1 upon synthesis in *E.coli*. This is more obvious when expression of SOD1 was induced at 37°C compared to induction at room temperature (RT; approximately 20-25°C). While the expression of wtSOD1 at either temperature did not affect the solubility of the protein, the expression of mutSOD1, G93A as an example shown in Figure 3.2 (c) and (d), was significantly influenced by the temperature of induction, indicating that mutSOD1 has a slower folding rate compared to wtSOD1. Expression of SOD1 at 37°C causes rapid overloading of SOD1 in *E. coli* but because mutSOD1 was not able to fold as efficiently and effectively as wtSOD1, more mutSOD1 was channelled to form inclusion bodies. However, the solubility of mutSOD1 was increased when mutSOD1 was expressed at a lower temperature likely because at lower temperature, the protein synthesis rate in *E. coli* was reduced resulting in a slower accumulation of mutSOD1, thus increasing the probability that more mutSOD1 can be folded correctly.

The SOD1 production and purification procedure was determined empirically, as described in 3.3.2, and it was concluded that purification of SOD1 from inclusion bodies was not a practical way forward. Purification of SOD1 directly from the soluble fraction yielded a reasonable amount of functional protein (Table 3.1) with very high purity, as qualitatively assessed from the SDS-PAGE gel image in Figure 3.7. The purification factor and yield varied from variant to variant emphasizing that wtSOD1 and each mutSOD1 is different from each other in their biophysical and biochemical properties. To confirm that the purified proteins are structurally and biochemically similar to SOD1 expressed in mammalian cells, the biophysical and biochemical properties of the purified SOD1 proteins were characterized and are presented in Chapter 4 SOD1 protein characterization.

Chapter 4 SOD1 protein characterization

4.1 Chapter aim

To confirm that the SOD1 proteins produced and purified from an *E. coli* expression system (described in Chapter 3 Production and purification of superoxide dismutase 1 (SOD1) are biophysically and biochemically similar to SOD1 proteins produced in eukaryotes.

4.2 Introduction

In any protein preparation, it is important to first characterize the protein obtained to ensure that the correct protein is purified before further work is carried out. Proteins can be characterized for their biophysical and biochemical properties and in the case of enzymes, specific activity is an important indicator of protein integrity. The resulting information provides clues to the conformational state and the functionality of the protein which can be used for comparison to known structures. For example, in the case of unknown protein function, this allows prediction of function based on comparison to known protein domains with known functions. Also, if the protein has been previously purified and characterized by others, this allows comparison to ensure that results produced from work on the protein are directly comparable to existing results reported by others.

There are several established techniques that can be used in characterizing the biophysical properties of a protein. Table 4.1 is a summary of some important biophysical properties that are available for use in assessing the quality of a protein preparation and the most frequently used methods for their determination (Geerlof *et al.* 2006). In this chapter, purified SOD1 proteins were characterized for their folding or structural state by circular dichroism (CD) and crystallization, protein stability by thermal denaturation using differential scanning fluorimetry (DSF), and dimeric integrity and oligomerization or aggregation property by

analytical ultracentrifugation (AUC). The enzymatic activity and the thiol status were also determined biochemically, as described in Chapter 2.

Table 4.1. Important biophysical properties for quality assessment of a protein preparation and the most frequently used methods for their determination. (Adapted from Geerlof *et al.* 2006). Methods used for SOD1 characterization are coloured in green.

Biophysical property	Methods used for its determination
Purity	SDS-PAGE Size-exclusion chromatography Mass spectrometry
Monodispersity, aggregation state	Dynamic light scattering Size-exclusion chromatography Analytical ultracentrifugation
Conformational state	Static light scattering Analytical ultracentrifugation
Folding state	Nuclear magnetic resonance spectroscopy Circular dichroism Fourier-transformed infrared spectroscopy
Stability	Differential scanning calorimetry Circular dichroism Differential scanning fluorimetry
Identity, modification	Mass spectrometry

4.3 Results

4.3.1 SOD1 enzymatic activity

The enzymatic activity of all purified SOD1 proteins was assessed using a SOD1 assay commercial kit (OxisResearch). The assay procedure is based on the SOD1-mediated increase of a chromophore from the auto-oxidation of an enzyme substrate provided with the kit. The chromophore has maximum absorbance at 525nm, which turns the reaction solution light orangish-pink upon production. The enzymatic activity of all proteins was in comparison to the activity of wtSOD1 and a commercial recombinant SOD1 protein (hucSOD1), the results of which are summarised in Table 4.2. With exception of G93A, all mutSOD1 proteins had lower enzymatic activity in comparison to wtSOD1. D83G, G85R and D90A had less than 10% activity in comparison to wtSOD1, whereas A4V, G114A and GFP-G93A had approximate activities of 30% of wtSOD1. The two mutSOD1 proteins which had higher activities were G93A (100%) and G37R (68%).

Table 4.2. Specific activity of SOD1 proteins purified.

SOD1 variant	SOD1 specific activity (units/mg)	% specific activity of wtSOD1
hu_cSOD1	3000-4000	80 - 105
wtSOD1	3800	100
G93A	3900	102
G37R	2600	68
A4V	1200	32
G85R	290	8
D83G*	230	6
D90A	160	4
G114A	1100	29
GFP-G93A	1400	37

As mentioned previously (refer to 1.3.2.2 on page 60), the true biological metal loading process *in vivo* is speculated from *in vitro* experiments, and so the actual *in vivo* metal complement of SOD1, whether all Cu^{2+} and Zn^{2+} sites are fully metallated or only partially metallated, is not known. The catalytic activity assayed for SOD1, whether produced and purified recombinantly or "as isolated" from SOD1-transfected cells (e.g. COS-1 cells, yeast) were shown to differ slightly depending on the type of assay used to measure the SOD1 activity and the degree of Cu^{2+} and Zn^{2+} metallation of SOD1 (Borchelt *et al.* 1994;Jacobsson *et al.* 2001;Valentine and Hart 2003;Doucette 2004;Valentine *et al.* 2005). Recombinantly produced and purified SOD1 proteins had slightly higher SOD1 activities than "as isolated" SOD1, likely due to differences in the degree of metallation. For example, the recombinantly purified G85R SOD1 mutant protein had 76% activity compared to wtSOD1 (Valentine *et al.* 2005) when fully complemented with Cu^{2+} and Zn^{2+}. However, when the activity of G85R was measured "as isolated" from cell lysates from G85R-transfected yeast, insect and COS-1 cells, "as isolated" G85R had an almost undetectable (Borchelt *et al.* 1994; Hayward *et al.* 2002) or very low, about 35% (Ratovitski *et al.* 1999), SOD1 activity.

Taking into account these factors which may influence the measurement of the actual SOD1 activity, and that the degree of metallation of SOD1 proteins produced in this thesis was not quantified, it was impossible to determine if the activities measured here were reflective of SOD1 having a full metal complement of Cu^{2+} and Zn^{2+} per dimer. Therefore, to make reasonable comparisons of results obtained here to published reports by others, SOD1 activities measured here were compared to published SOD1 activities of both recombinantly purified and "as isolated" SOD1 proteins. Results here were within an acceptable range of activities. It was concluded that the SOD1 proteins purified here were considered comparable for further use in subsequent characterization studies.

4.3.2 Structural profile with circular dichroism (CD)

Circular dichroism (CD) is a form of spectroscopy measuring the differential interaction of circularly polarized light with macromolecules (protein or nucleic acids) in solution, which gives information on the conformation of the macromolecules (Beychok 1966). Different molecular conformation will interact with the circularly polarized light differently and this gives rise to a characteristic CD spectrum for that conformation. CD measurements are usually measured at two sets of wavelength regions, which are 190-250nm (far-UV) and 250-360nm (near-UV). The far-UV CD spectrum of proteins reveals information on their secondary structures (2°) (α-helix, β-sheet or random coil conformation), whereas the near-UV CD spectrum provides information on their tertiary structure. While it is possible to qualitatively assign a particular 2° structure to a far-UV CD spectrum, it is not possible to do the same for near-UV CD spectrum which simply provides a measure of how much tertiary organisation a polypeptide chain has. Although CD measurements give information on the structural content of a protein, this method of structural determination only provides limited details of the actual three dimensional (3D) structures. The real power of CD is in analysing structural changes in a protein upon physical of chemical perturbation and how it behaves in solution, or in the comparison of the structure of an engineered protein to the parent protein. In this case, CD was used to compare the folding state of mutSOD1 to wtSOD1.

Purified SOD1 proteins (described Chapter 3) were measured for their CD properties at far-UV and near-UV wavelengths, as shown in Figure 4.1. Comparison of the far-UV CD spectra of all mutSOD1 proteins to wtSOD1, except for G85R and GFP-G93A, revealed that they had comparable CD spectra (negative peak of spectra at approximately 208-210nm) which, although not identical, showed similarities to far-UV CD spectra of proteins containing β-sheet conformation (negative and positive peaks of spectra at approximately 212nm and 196nm, respectively). This is consistent with previously published structures of SOD1 where monomeric SOD1 is composed of a beta-barrel structure of 8 beta-strands (Tainer *et al.* 1982;Getzoff *et al.* 1989). The far-UV CD spectrum of G85R

compared to wtSOD1 showed a deviation of negative peak to approximately 195nm, which was indicative of an increase in random coil conformation. The far-UV CD spectra of GFP-G93A was more characteristic of β-sheet conformation likely due to the relatively large size of the GFP protein (approximately 23kDa) compared to monomeric SOD1 (approximately 16kDa) and mainly composed of 11 beta-strands forming a beta-barrel structure (Tsien 1998).

The tertiary structures of purified SOD1 proteins were compared by assessing the near-UV CD spectrum of each protein to wtSOD1. The overlaid spectra of all mutSOD1 proteins to wtSOD1 showed spectral similarities, suggesting that regardless of the presence of mutations the overall tertiary conformation of SOD1 was not disrupted significantly. This was more apparent in G85R where although G85R had a disrupted secondary structure (Figure 4.1(a)), the tertiary structure was relatively preserved (Figure 4.1(b)). GFP-G93A had a significantly different near-UV CD spectrum to any of the non-GFP tagged SOD1 proteins due to the presence of the GFP tag (Figure 4.1(b)). The CD results presented here were mainly concerned with the overall conformations of the purified proteins and were only assessed qualitatively. Further analysis on the observed difference was not carried out as it was beyond the scope of this chapter and would qualify as a separate project.

Figure 4.1. Circular dichroism (CD) spectra of SOD1 proteins. a) Far-UV CD spectra at wavelength range of 190 – 250nm. All non-tagged SOD1 proteins, except G85R, shared similar CD spectra, which closely resembled spectra of proteins containing β-sheet conformation. The CD spectra of G85R more closely resembled CD spectra of proteins with random coil conformation suggestive that the G85R mutation in SOD1 caused a significant disruption to the β-sheet conformation. The CD spectra of GFP-G93A, although slightly different to spectra of non-tagged SOD1 proteins, also showed resemblance to spectra of proteins containing a β-sheet conformation. b) Near-UV CD spectra at wavelength range of 250 – 360nm. The near-UV CD spectra of all non-tagged SOD1 proteins were similar to each other suggesting a relatively preserved tertiary structure of SOD1 regardless of the presence of mutation. The tertiary structure of GFP-G93A is significantly different when compared to non-tagged SOD1 proteins. This is attributed to the relatively large GFP-tag which was not unexpected since the GFP-moiety is 1.4 fold larger in size than a single subunit of SOD1.

(*con't* from **Figure 4.1**. Circular dichroism (CD) spectra of SOD1 proteins)

a)

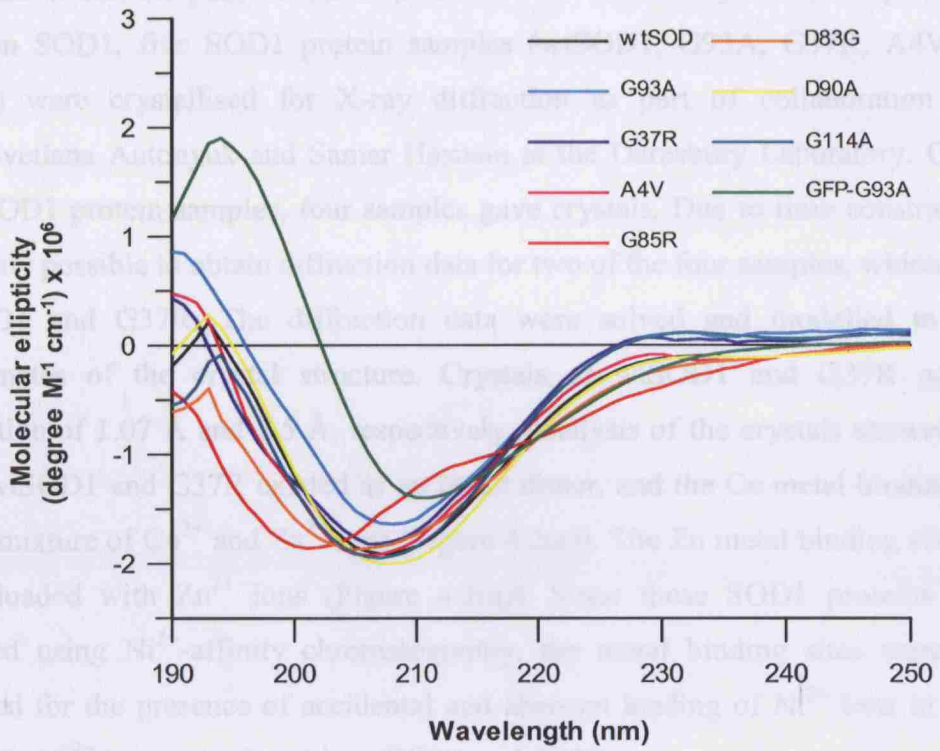

b)

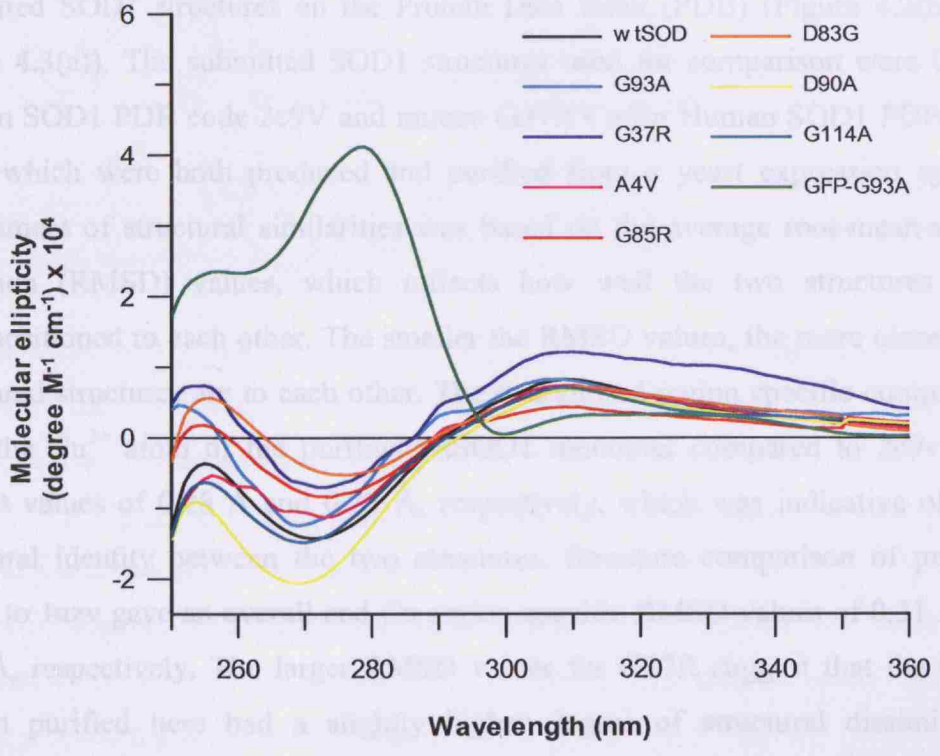

4.3.3 Crystal structure

To confirm that the purified SOD1 proteins were structurally similar to published data on SOD1, five SOD1 protein samples (wtSOD1, G93A, G37R, A4V and G85R) were crystallised for X-ray diffraction as part of collaboration with Drs. Svetlana Antonyuk and Samar Hasnain at the Daresbury Laboratory. Of the five SOD1 protein samples, four samples gave crystals. Due to time constraint, it was only possible to obtain diffraction data for two of the four samples, which were wtSOD1 and G37R. The diffraction data were solved and modelled to give coordinates of the crystal structure. Crystals of wtSOD1 and G37R gave a resolution of 1.07 Å and 2.5 Å, respectively. Analysis of the crystals showed that both wtSOD1 and G37R existed as an intact dimer, and the Cu metal binding site had a mixture of Cu^{2+} and Zn^{2+} ions (Figure 4.2(a)). The Zn metal binding site was fully loaded with Zn^{2+} ions (Figure 4.2(a)). Since these SOD1 proteins were purified using Ni^{2+}-affinity chromatography, the metal binding sites were also checked for the presence of accidental and aberrant loading of Ni^{2+} ions in these sites. No Ni^{2+} ions were found in wtSOD1 and G37R.

Coordinates for wtSOD1 and G37R obtained from the crystals were compared to submitted SOD1 structures on the Protein Data Bank (PDB) (Figure 4.2(b) and Figure 4.3(a)). The submitted SOD1 structures used for comparison were Cu/Zn Human SOD1 PDB code 2c9V and mutant G37R Cu/Zn Human SOD1 PDB code 1azv, which were both produced and purified from a yeast expression system. Assessment of structural similarities was based on the average root-mean-square deviation (RMSD) values, which reflects how well the two structures were superpositioned to each other. The smaller the RMSD values, the more closely the compared structures are to each other. The overall and region specific comparison circa the Cu^{2+} atom of the purified wtSOD1 monomer compared to 2c9v gave RMSD values of 0.28 Å and 0.22 Å, respectively, which was indicative of high structural identity between the two structures. Structure comparison of purified G37R to 1azv gave an overall and Cu region specific RMSD values of 0.31 Å and 0.38 Å, respectively. The larger RMSD values for G37R suggest that the G37R protein purified here had a slightly higher degree of structural dissimilarity,

although not statistically significant, which was apparent as a difference in the packing arrangement of G37R dimers in the crystals. From the G37R coordinates obtained from the crystals, the G37R mutation site was identified and located to the protein surface of the dimer (Figure 4.3(b)). With the exception of the absence of N-terminus acetylation of SOD1, the SOD1 proteins produced and purified here using an *E.coli* system had a comparable overall structure to the SOD1 proteins produced and purified in yeast.

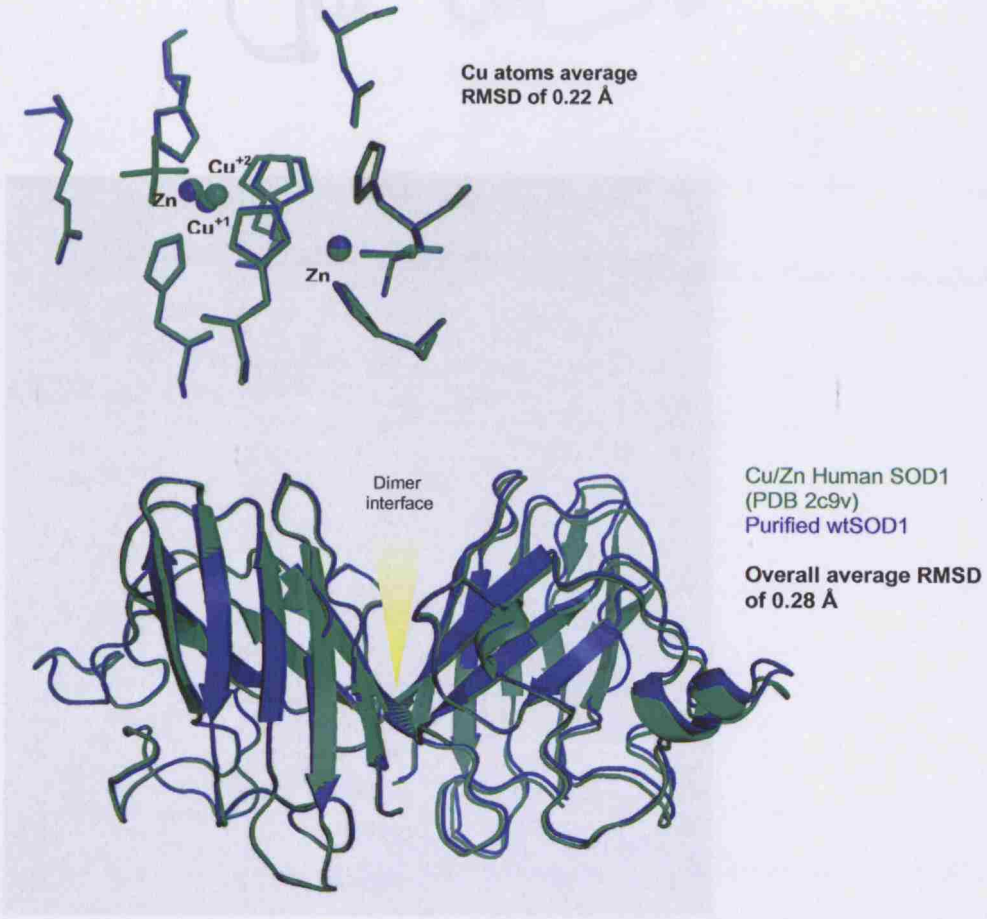

Figure 4.2. Overlay of Cu/Zn Human SOD1 PDB code 2c9v (green) to purified wtSOD1 (blue). a) Superposition of a monomer at the Cu and Zn metal binding site shown as a stick diagram. The RMSD value at the Cu atoms was calculated to be 0.22 Å. The Cu metal binding site was loaded with a mixture of Cu and Zn ions whereas the Zn metal binding site was fully loaded with Zn ions. b) Superposition of cartoon diagrams of an intact purified wtSOD1 to 2c9v (which was purified and produced from a yeast expression system). The global RMSD value calculated from the overlaid dimers was 0.28 Å.

a)

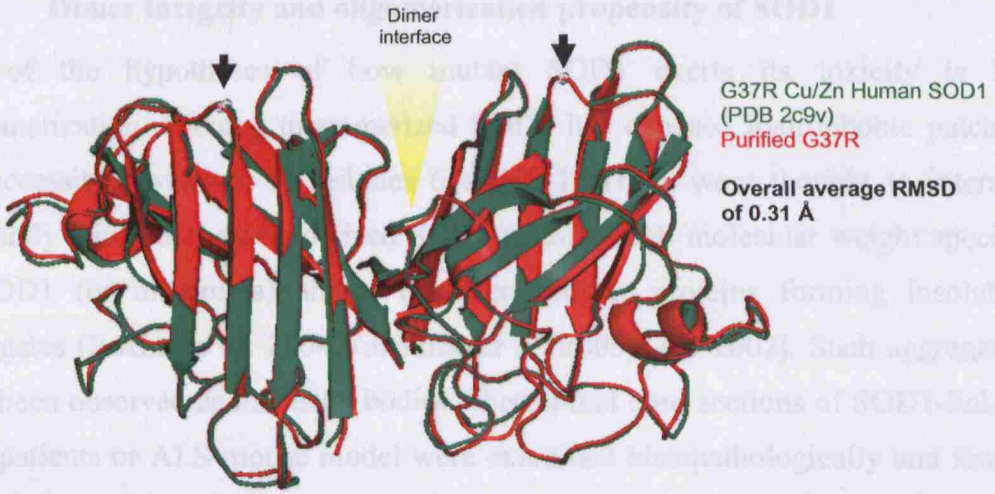

b)

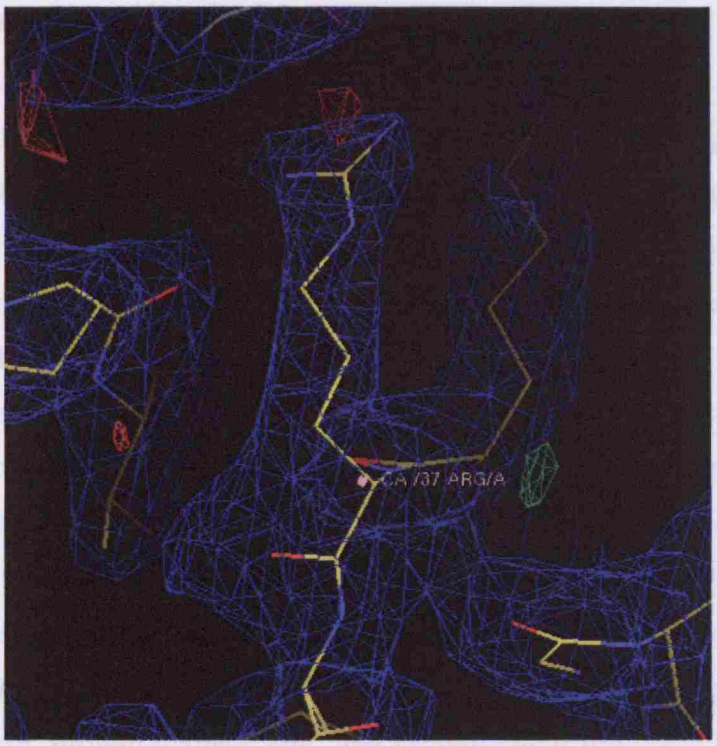

Figure 4.3. Structural profile of G37R. a) Superimposed cartoon diagrams of purified G37R (red) to G37R Cu/Zn Human SOD1 PDB code 1azv (green). The arrows are pointing to the G37R mutation site on the SOD1 dimer, which is located towards on the surface of the protein. The overall calculated RMSD value of the overlaid dimer was 0.31 Å. b) Electron density map of the mutation site at residue 37 (G37R).

4.3.4 Dimer integrity and oligomerization propensity of SOD1

One of the hypotheses of how mutant SOD1 exerts its toxicity is by monomerization whereby monomerized SOD1 has exposed hydrophobic patches and accessible cysteines at residues 6 and 111. These were thought to interact aberrantly with other monomerized SOD1 to form high molecular weight species of SOD1 (or oligomers) and/or to other cellular proteins forming insoluble aggregates (Rakhit *et al.* 2004;Valentine *et al.* 2005;Kato 2007). Such aggregates have been observed as inclusion bodies when spinal cord sections of SOD1-linked ALS patients or ALS mouse model were examined histopathologically and found to contain SOD1 when stained against a SOD1 antibody (Matsumoto *et al.* 1996;Shibata *et al.* 1996;Shibata *et al.* 1998;Shibata 2001;Rakhit *et al.* 2007;Shibata *et al.* 2007).

To determine the monomerization and oligomerization property of the purified SOD1 proteins, analytical ultracentrifugation (AUC) was employed. AUC is a technique which separates or redistributes proteins or macromolecules in solution when subjected to a centrifugal force based on the size and shape or conformation of the protein (correlated to the compactness or the hydrodynamic radii of proteins). There are two basic types of experiment with the AUC. They are the sedimentation velocity (SV) and sedimentation equilibrium (SE) experiments. SV experiments are useful in the identification of the oligomeric or aggregation state and the stoichiometry of heterogeneous interactions of proteins, whereas SE experiments are usually the method of choice for the molar mass determination and the study of self-association and heterogeneous interactions, such as protein-protein, protein-nucleic acid, and protein-small molecule binding (Lebowitz *et al.* 2002;Beckman Coulter 2008). Here, the sedimentation velocity (SV) based experiment of the AUC was employed to characterize the stability of SOD1 dimer and oligomerization state as well as to assess the heterogeneity of the purified SOD1 proteins. AUC experiments and fitting analyses (as described in Chapter 2) were performed by Samantha Jones (MRC Prion Unit, UK).

In order to determine if SOD1 undergoes a complex set of self-associations (oligomerization/aggregation) or self-dissociations (monomerization), AUC runs

were performed at three concentrations for each SOD1 protein, at 1:1, 1:2 and 1:10 of the stock concentration. The rationale behind this is that for a self-associating system, lowering the concentration sufficiently will cause SOD1 oligomers (if present) or dimers to dissociate into smaller species, which will sediment slower. However, if the protein is present in a variety of oligomers or stable as dimers that do not interconvert or monomerize, then dilution will have no effect on the proportion of SOD1 oligomers or dimers. SV results of all proteins are presented in Figure 4.4, where the sedimentation data were fitted to a continuous size distribution model (c(S)) from which the sedimentation coefficients of the protein were determined. Sedimentation coefficient, *s* (reported as Svedberg units, S), is directly proportional to the mass of SOD1 (M) and inversely proportional to the frictional coefficient (f), which is in turn a measure of effective size.

From Figure 4.4, independent of protein concentration, wtSOD1, G93A, G37R, D90A, G114A and GFP-G93A had a major peak with an approximate *s*-values of 2.8 – 3.1S and 5.3S for non-GFP tagged and GFP-tagged SOD1, respectively. To estimate the molecular weight of the species sedimenting at a particular *s*-values, the distribution in sedimentation coefficients derived from the c(S) distribution model was converted using another distribution model known as the molar mass distribution model (c(M)) (Lebowitz *et al.* 2002;Schuck 2008). The estimated molecular weights for SOD1 sedimenting at 2.8 – 3.1S and 5.3S were approximately 36kDa and 88kDa respectively, which corresponded to the size of a SOD1 dimer. A4V and D83G had one major peak at *s*-value of approximately 3.0S and a smaller peak at 1.8S and 1.2S, respectively, which corresponded to the size of a SOD1 monomer. These results were consistent with existing data by Doucette *et. al.* (Doucette *et al.* 2004) where SOD1 dimers were reported to sediment between 2.5 – 3.1S (variation in *s*-values of SOD1 dimers were dependent on the metal content and the presence of intrasubunit disulfide bonds), whereas SOD1 monomers sedimented at 1.4S or 1.8S (depending on the degree of unfolding of the monomers). G85R had multiple peaks which were independent of protein concentration, at 1.2S, 1.8S, 2.6S, 3.9S, 5.4S, 6.1S and 7.3S and had estimated average molecular weights of 12, 39, 73, 125 and 191kDa. From these SV profiles, it was demonstrated that the monomerization and oligomerization of SOD1 was

concentration independent, as shown for A4V, D83G and G85R where multiple peaks were present persistently even at a diluted protein concentration. All proteins except A4V, G85R and D83G exist almost exclusively as dimeric SOD1. A4V, G85R and D83G showed a higher propensity to monomerize. G85R had multiple peaks with *s*-values larger than *s*-values for dimeric SOD1. This was suggestive that the G85R mutation conferred the SOD1 protein to have a higher propensity to oligomerize.

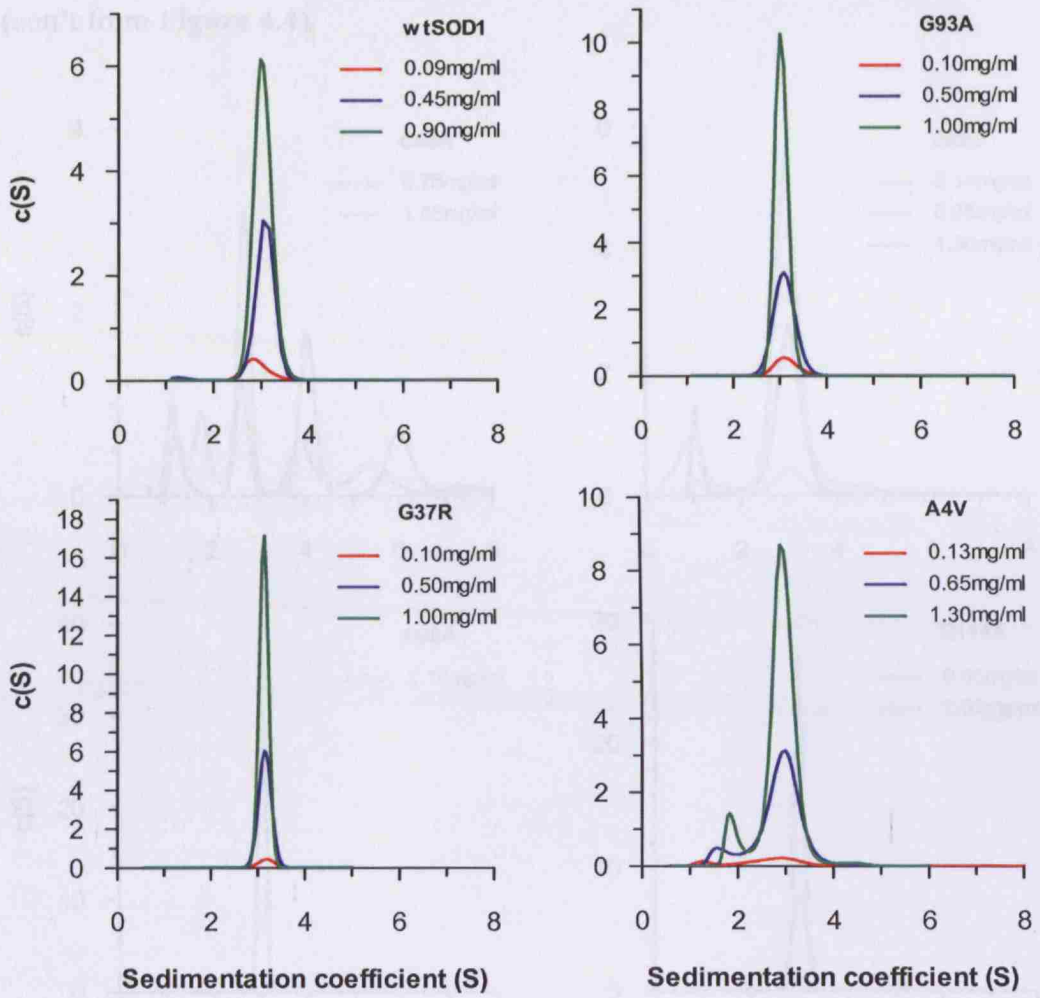

Figure 4.4. Sedimentation velocity profile of SOD1 proteins based on the continuous size-distribution model c(S)). Proteins were analysed at three concentrations. The analysis included all 200 scans acquired during the experimental runs, which were analysed using the Sedfit version 9.2 based on the continuous size distribution model (c(S) = y-axis) described elsewhere (Lebowitz *et al.* 2002;Schuck 2008). The larger the *s*-values (x-axis), the larger the size of the sedimenting protein species. Non-GFP tagged SOD1 dimers and monomers sedimented between 2.8 – 3.1S and 1.4 – 1.8S, respectively. GFP-G93A sedimented at 5.3S, which was estimated to be approximately 88kDa which corresponded to the size of dimeric GFP-G93A. All proteins except A4V, G85R and D83G existed almost exclusively as SOD1 dimers. A4V, G85R and D83G showed a higher propensity to monomerize. G85R had multiple peaks with *s*-values larger than *s*-values for dimeric SOD1, which was suggestive that G85R had a higher propensity to oligomerize.

(con't from **Figure 4.4**)

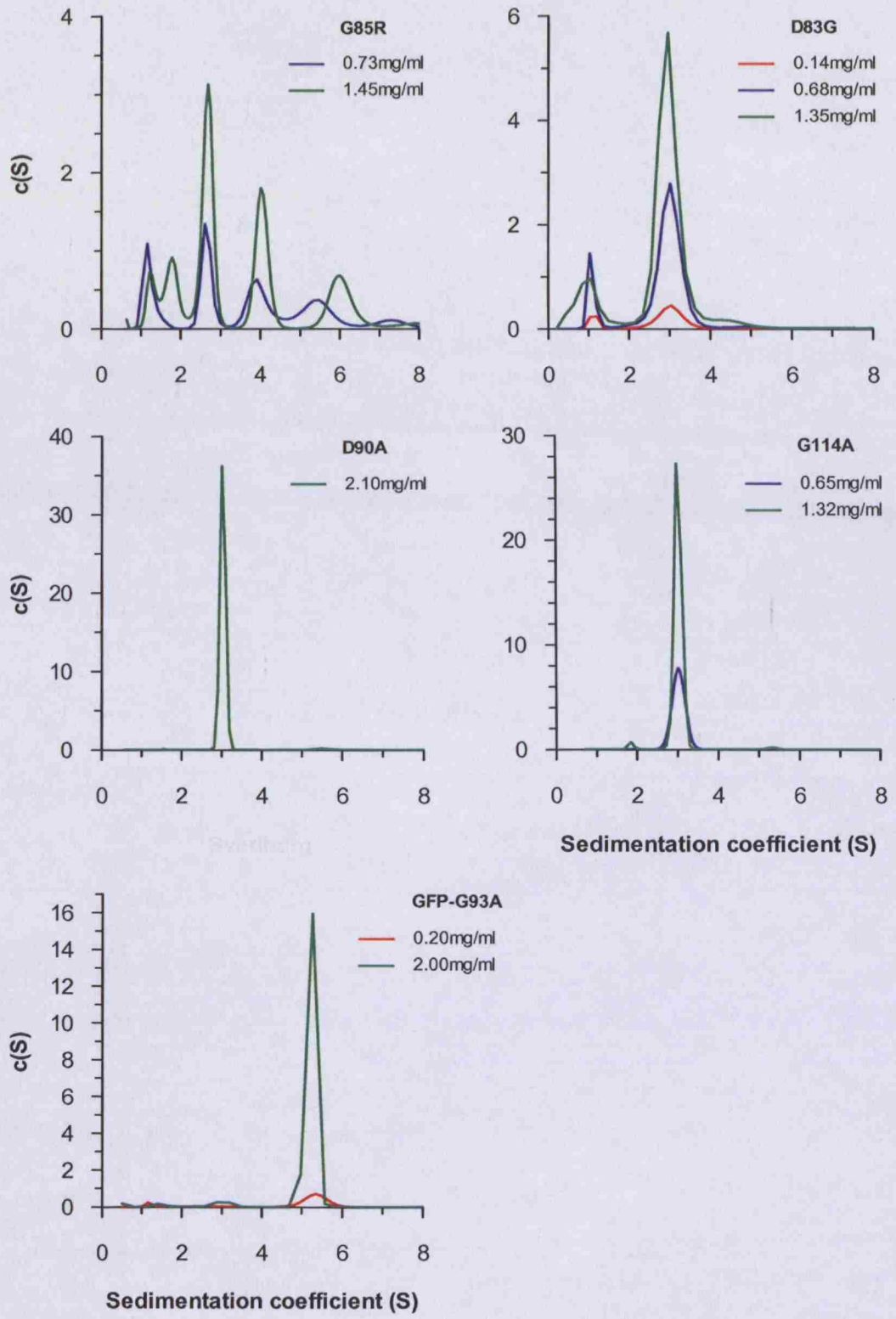

4.3.5 Thiol status

Native SOD1 has four cysteine residues (at residue 6, 57, 111 and 146) per monomer, where Cys57 and Cys146 are involved in the formation of an intrasubunit disulfide bond (S-S bond). Cys6 is located at the dimer interface (non-accessible sulfhydryl group, –SH group), whereas Cys111 is located on the connecting loop between beta-strand 6 and 7 (accessible –SH group). The thiol status of SOD1 proteins were assessed and are presented in Table 4.3. In the native state, all SOD1 proteins had no detectable free –SH group whereas when denatured, all except G85R and G114A, had one detectable free –SH group per monomer. Because of the location of Cys111 on the dimer surface, it was expected that each native SOD1 (both wtSOD1 and SOD1 mutants) monomer would have one free –SH group, however this was not the case.

Table 4.3. SOD1 thiol status. The number of free sulfhydryl (–SH group) was determined in native and denatured conditions. All native SOD1 proteins showed no detectable free –SH group. Denaturation of SOD1 exposed the otherwise inaccessible –SH group from Cys6. In the denatured state, all SOD1 variants, except for G85R and G114A which had no detectable free –SH group, had one detectable free –SH group when denatured in 6M GdnHCl.

SOD1 variant	No. free sulfhydryl /monomer	
	Native	Denatured
wtSOD1	0	1
G93A	0	1
G37R	0	1
A4V	0	1
G85R	0	0
D83G	0	1
D90A	0	1
G114A	0	0
GFP-G93A	0	1

4.3.6 SOD1 protein stability

To assess the stability of SOD1 proteins, the thermal stability of proteins was investigated by differential scanning fluorimetry (DSF), as described in Chapter 2 Materials and Methods. DSF is a method employing the use of a dye which can be excited and emission measured, upon binding of the dye to exposed hydrophobic patches of protein when the protein is thermally unfolded. Protein unfolding was monitored by following the change in fluorescence over time and temperature increment (unfolding of protein corresponds to increase in fluorescence intensity). Protein stability is expressed as apparent Tm, which refers to the apparent mid-point temperature (°C) where the ratio of unfolded (maximum fluorescence intensity) to folded proteins (minimum fluorescence intensity) is 1:1. The thermal stability of SOD1 proteins are summarized as shown in Table 4.4 and graphically presented in Figure 4.5. Taking the thermal stability of wtSOD1 as a reference, all SOD1 mutants (except GFP-G93A) had lower apparent Tm values which was expected due to the effect of mutation, and this was consistent with existing data shown by others (Roe *et al.* 1988;Rodriguez *et al.* 2002). When incubated with EDTA, the apparent Tm of all SOD1 proteins was lowered significantly demonstrating the importance of metals in conferring stability to SOD1 (green bars versus red bars in Figure 4.5). The thermal stability profile of GFP-G93A gave an unexpected result. Metallated GFP-G93A had an apparent Tm of 81°C which was 5°C and 12°C higher than the apparent Tm of metallated wtSOD1 and G93A, respectively. More strikingly is that when GFP-G93A was demetallated by incubation with EDTA, the apparent Tm was increased by almost 2°C which was not the usual effect seen in demetallation of any SOD1 variant, where demetallation significantly reduces the apparent Tm indicative of SOD1 destabilization upon loss of metal ions.

Table 4.4. Thermal stability of holo- and apo- SOD1 proteins. The thermal stability of wtSOD1 and SOD1 mutants was assessed at two concentrations (11μM and 33μM) and in the metallated and demetallated form (when incubated with EDTA which functioned as a metal chelator). Protein stability is expressed as apparent apparent Tm, which refers to the mid-point temperature (°C) where the ratio of unfolded to folded proteins is 1:1. Apparent Tm values reported are the average values ± SD obtained from n=3.

SOD1 variant	Apparent Tm (°C) (Holoenzyme)	Apparent Tm (°C) (Holoenzyme + 20mM EDTA)
33μM		
wtSOD1	75.5 ± 0.1	56.0 ± 0.0
G93A	68.7 ± 0.1	54.1 ± 0.0
G37R	69.6 ± 0.1	55.5 ± 0.0
A4V	70.8 ± 0.1	50.9 ± 0.1
D83G	54.9 ± 0.1	48.5 ± 0.1
D90A	73.1 ± 0.1	54.2 ± 0.1
G114A	67.0 ± 0.2	50.8 ± 0.2
GFP-G93A	81.2 ± 0.0	83.0 ± 0.2
11μM		
wtSOD1	73.8 ± 0.04	54.2 ± 0.1
G93A	67.8 ± 0.06	52.7 ± 0.0
G37R	68.7 ± 0.01	53.7 ± 0.0
A4V	69.7 ± 0.02	51.4 ± 0.2
D83G	57.4 ± 0.07	47.1 ± 0.1
D90A	71.5 ± 0.07	53.6 ± 0.0
G114A	66.1 ± 0.06	50.7 ± 0.3
GFP-G93A	79.2 ± 0.00	80.6 ± 0.0

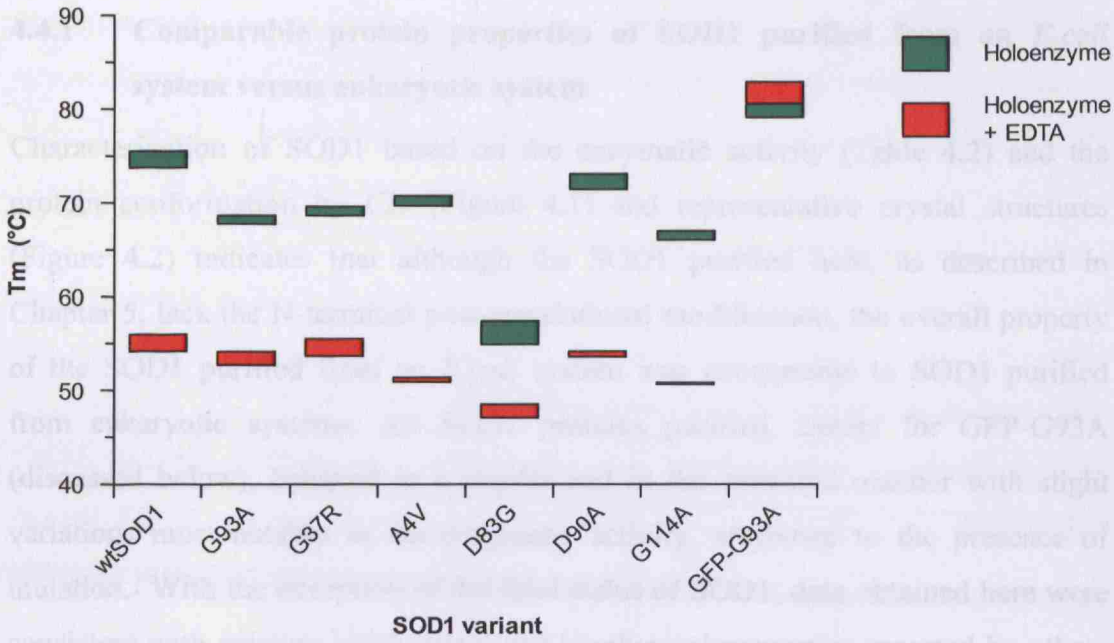

Figure 4.5. Graphical presentation of the thermal stability of SOD1 when incubated with and without EDTA. The green bars represent metallated SOD1 (holoezyme), whereas the red bars represent demetallated SOD1 (holoenzyme incubated with 20mM EDTA). The upper and lower limit of each bar represents the apparent Tm value of SOD1 at 33μM and 11μM, respectively. The gap between the lower and upper limit of each bar reflects the effect of protein concentration on the stability of the protein. The protein stability of SOD1 is not greatly influenced by protein concentration as there was only a 1-2°C change in apparent Tm of proteins at 33μM versus 11μM. From the graph, it is clearly demonstrated that demetallation causes significant reduction in protein stability of all non-GFP tagged SOD1 by approximately 20°C (except for D83G which had a 10°C reduction in apparent Tm). Metallated GFP-G93A had an apparent Tm value which was 5-6°C higher than the apparent Tm of metallated wtSOD1. Unexpectedly, demetallation of GFP-G93A caused an increase in the apparent Tm which was an unusual effect compared to the demetallation effect seen in the non-GFP tagged SOD1 proteins (decreased apparent Tm corresponds to decreased protein stability).

4.4 Discussion and conclusion

4.4.1 Comparable protein properties of SOD1 purified from an *E.coli* system versus eukaryotic system

Characterization of SOD1 based on the enzymatic activity (Table 4.2) and the protein conformation by CD (Figure 4.1) and representative crystal structures (Figure 4.2) indicates that although the SOD1 purified here, as described in Chapter 5, lack the N-terminal post-translational modification, the overall property of the SOD1 purified from an *E.coli* system was comparable to SOD1 purified from eukaryotic systems. All SOD1 proteins purified, except for GFP-G93A (discussed below), behaved in a similar and in the expected manner with slight variations most notably in the enzymatic activity, attributed to the presence of mutation. With the exception of the thiol status of SOD1, data obtained here were consistent with existing biochemical and biophysical properties reported by others (Strange *et al.* 2003;Valentine and Hart 2003;Doucette 2004;Hough *et al.* 2004;Hart 2006;Strange *et al.* 2006;Wang *et al.* 2007). Native SOD1 which was expected to have one free –SH group (Cys111) lacked any detectable thiols (Table 4.3). It is unlikely that the –SH group of Cys111 is involved in the formation of non-native intersubunit S-S bonds forming higher molecular weight species of SOD1 because this was inconsistent with the AUC data where wtSOD1 (and most SOD1 mutants) sedimented mainly as dimers. It is possible the thiol group of Cys111 was oxidised to the methoxide form and therefore unable to react with DTNB.

4.4.2 Differences in the biophysical and biochemical properties of GFP-G93A compared to non-GFP tagged SOD1 proteins

GFP-G93A has never been purified and characterized before. Data presented here are the first to report on the biophysical and biochemical properties of GFP-G93A. As show in Figure 4.1, the tertiary structure as determined by CD was significantly different compared to non-GFP tagged SOD1 proteins. In addition to the structural dissimilarity, although GFP-G93A exists as stable dimers as shown by AUC (Figure 4.4), metallated GFP-G93A differed in its enzymatic activity (only having

30% activity compared to wtSOD1 and G93A) and had an unexpected higher thermal stability compared to metallated wtSOD1 (Figure 4.5). In addition, for undetermined reasons, instead of being destabilized when GFP-G93A was demetallated with EDTA, loss of metal ions from GFP-G93A caused an increase in stability which was reflected as an increment in the apparent Tm. The increase of apparent Tm in GFP-G93A compared to wtSOD1 is likely due to the additional stability attributed to the GFP-moiety. It is also likely that because the GFP moiety is much more stable than SOD1, the unfolding of SOD1 was masked by GFP and so the actual stability of SOD1 tagged with GFP cannot be determined conclusively. The most important finding from these experiments is that GFP-G93A behaves differently biochemically and biophysically compared to non-tagged SOD1, which warrant caution on the use of models and experimental designs employing the use of GFP-tagged SOD1.

Chapter 5 Fibrillization is a generic misfolding property of SOD1

5.1 Chapter aim

To investigate if mutations in SOD1 predispose the protein to acquire an alternative misfolded but higher-ordered conformation rather than formation of unstructured aggregates which may be the toxic factor by which mutant SOD1 causes death to motor neurons.

5.2 Introduction

The presence of inclusion bodies or aggresomes is one of the neuropathological hallmarks of ALS. In SOD1-fALS patients, spinal cord sections examined by immuno-histochemistry contain aggregates that are reactive to anti-SOD1 antibodies (Kato 2007). More recent evidence has shown that in non-SOD1 ALS (fALS and sALS), aggregates also contain SOD1 (Nilsson *et al.* 2007). There is no marked difference in disease presentation and progression, either clinically or neuropathologically, between fALS and sALS (Gros-Louis *et al.* 2006). ALS presents itself as a neurodegenerative disease beginning insidiously as a focal weakness and atrophy of distal limbs or body region but progressively spread to other more proximal muscle groups over time (Ravits *et al.* 2007b). Loss of motor function appears to affect proximal motor units closest to the onset site, followed by more distal motor units and this correlates well with the observed gradient loss of motor neurons from the onset site (Ravits *et al.* 2007a). The disease usually starts abruptly, affecting mostly patients in their mid-life, and has a rapid disease progression (3-5years) ultimately leading to death due to respiratory failure. This pattern of disease progression suggests some form of cell-to-cell transmission of a toxic 'factor', where dying motor neurons (and possibly secondary contribution by microglia and astrocytes) harbouring the toxic 'factor' releases the toxic 'factor' to the extracellular microenvironment, from where it is taken up by neighbouring cells. Thus cell death spreads in a propagative manner from the onset site -- which

parallels the clinical observations made in ALS patients (i.e. gradient paralysis from distal to proximal muscles). Such a toxic 'factor' has not been identified, but it has been reported that SOD1 (predominantly SOD1 mutants, and to a lesser extent, wild type SOD1 (wtSOD1)) is secreted extracellularly (Urushitani *et al.* 2006;Gomes *et al.* 2007) and thus secreted SOD1 may be the toxic species responsible for the transmission of cytotoxicity.

Presently, it is agreed that variants of SOD1 exert toxicity by gaining a new biological function. One of the several current views is that this additional function involves an increase in the propensity of SOD1 to oligomerize with itself or with other proteins and thereby to form some type of aggregated species (Elam *et al.* 2003;Banci *et al.* 2007;Shaw and Valentine 2007). The hypothesis proposed here is that different mutSOD1s have varying tendencies to aggregate and it is the initial nucleation event of aggregation leading to formation of a stable protein 'seed' that is the critical point in the misfolding pathway, similar to prion disease. With the recent demonstration of the ability of neurons to be phagocytic (Bowen *et al.* 2007) and evidence of SOD1 being secreted from neurons, it became more convincing to test the protein aggregation theory proposed above within the prion paradigm. To test this hypothesis, fibrillization assays with varying solvent conditions (pH and chaotrope/denaturant concentration) were undertaken for wtSOD1, two MBR SOD1 mutants (G85R and D83G) and 5 WTL SOD1 mutants (G93A, G37R, A4V, D90A and G114A) and a GFP-tagged SOD1 mutant (GFP-G93A). The fibrillization ability of these proteins and the *in vivo* relevance of this property was demonstrated and are presented as follows.

5.3 Results

5.3.1 Parameters screened – conditions for fibrillization

To test if SOD1 could form fibrils, SOD1 proteins (wtSOD1, G93A, G37R, A4V, G85R, D83G, D90A, G114A, and GFP-G93A) were incubated in a matrix of varying solvent conditions (pH and chaotrope/denaturant concentration) to screen for conditions which could potentiate fibril formation. Fibril formation of SOD1 proteins was monitored by following the change in fluorescence of Thioflavin-T (ThT), as described in Chapter 2. Figure 5.1 shows the conditions screened (gradient concentration of GdnHCl from 0.0-3.0M and a pH range of pH4, 5, and 7.5) and conditions which were positive for a ThT fluorescence change indicative of formation of fibrils or some amyloid-like structures positive for ThT. Except for GFP-G93A, all SOD1 variants could form fibrils in at least one combination of conditions, with a higher propensity to form fibrils at pH4 in mild denaturing conditions (low GdnHCl concentration) and at pH5 in slightly harsher denaturing conditions (higher GdnHCl concentration).

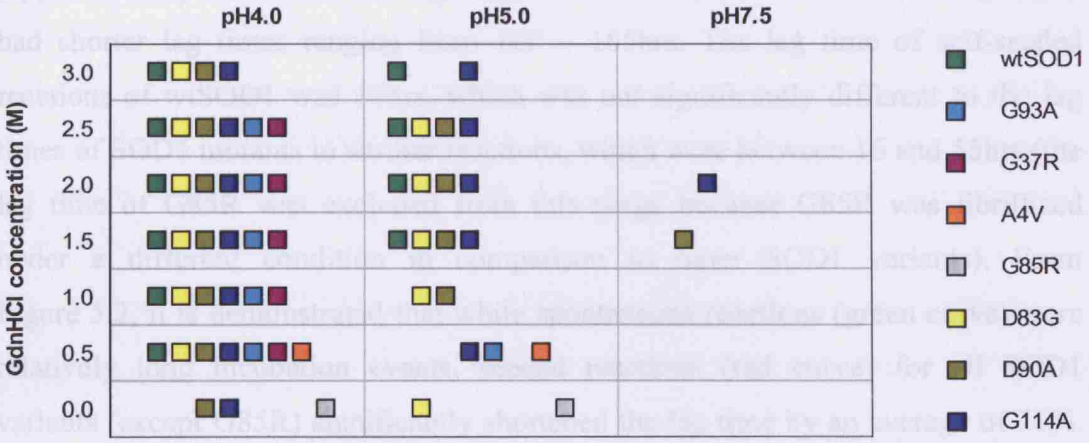

Figure 5.1. Fibrillization condition screen (pH versus denaturant concentration (GdnHCl)). SOD1 variants with higher stability could form fibrils under a wider fibrillization matrix (i.e. number of combinations of pH and denaturant strength) characterized by variation in lag times (wtSOD1 ■ = 10 combinations; G93A ■ = 6 combinations; G37R ■ = 5 combinations; A4V ■ = 2 combinations; G85R ■ = 2 combinations; D83G ■ = 11 combinations; D90A ■ = 12 combinations; G114A ■ = 13 combinations).

5.3.2 Kinetics of spontaneous and seeded fibrillization of SOD1

To study the kinetics of SOD1 fibrillization, a common fibrillization condition shared by most SOD1 variants was selected for subsequent fibrillization assays for spontaneous and seeded reactions. Except for G85R, fibrillization of all SOD1 proteins was carried out at pH4 with 0.5M GdnHCl. Fibrillization of G85R was carried out at pH5.0 with no denaturant. Spontaneous and seeded reactions were set up to characterise the lag time of each reaction and additionally for seeded reactions, to investigate if initial formation of SOD1 fibrils altered the ability to seed the formation of further fibrils in an autocatalytic cascade. The fibrillization lag times (equation described in Chapter 2) of each SOD1 variant were determined for each type of reaction, and are presented in Figure 5.2 and summarised in Table 5.1. Figure 5.2 shows the data fitted fibrillization curve of spontaneous and self-seeded reactions. Self-seeded (ss) reactions refer to the seeding of pre-formed fibril of a SOD1 variant to the same protein.

A lag time comparison of wtSOD1 fibrillization from spontaneous reactions (approximately 206hrs) to the lag times of mutSOD1s shows that all mutSOD1s had shorter lag times ranging from 100 – 165hrs. The lag time of self-seeded reactions of wtSOD1 was 16hrs, which was not significantly different to the lag times of SOD1 mutants in similar reactions, which were between 16 and 55hrs (the lag time of G85R was excluded from this range because G85R was fibrillized under a different condition in comparison to other SOD1 variants). From Figure 5.2, it is demonstrated that while spontaneous reactions (green curve) were relatively long incubation events, seeded reactions (red curve) for all SOD1 variants (except G85R) significantly shortened the lag time by an average of 70%. These findings confirm the generic property of SOD1, wtSOD1 and mutSOD1s, to form fibrils and once formed, these fibrils have the ability to initiate fibrillization in an autocatalytic manner.

Apart from the D90A mutation in SOD1 which has been reported in some populations (Scandinavian and Belgian) to cause fALS in an autosomal recessive manner (Robberecht *et al.* 1996;Aguirre *et al.* 1999;Winter *et al.* 2000), all other SOD1 mutations studied here give rise to dominantly inherited pattern of fALS.

Due to the difference in the nature of D90A mutation, it was initially expected that D90A might not be able to fibrillize at all, or would fibrillize but have different fibrillization properties compared to other mutSOD1s. Figure 5.2 shows that D90A behaved similarly to wtSOD1 and other mutSOD1s in its ability to fibrillize spontaneously and in the initiation of fibrillization in self-seeded reactions under similar conditions. Since there was no difference in the fibrillization properties of D90A in a homogenous set up, it was thought that the recessive nature of the D90A might be due to a modification of interaction between D90A and wtSOD1. To investigate if D90A behaves differently in the presence of wtSOD1 (heterogeneous mix), fibrillization assays were repeated for D90A mixed with wtSOD1 D90A/wtSOD1 in 1:1 protein ratio for spontaneous and self-seeded reactions. Due to time constraints and limited stock of purified proteins, it was possible to only include one SOD1 mutant, G93A, as a control where G93A was subjected to the same set up as D90A. Preformed fibrils of D90A and G93A were used as 'seed' for seeded reactions.

The spontaneous reactions of G93A/wtSOD1 and D90A/wtSOD1 had lag times of approximately 104hrs and 215hrs, respectively. The lag time for G93A/wtSOD1 was almost equivalent to the lag time for G93A (in a spontaneous reaction), whereas the lag time for D90A/wtSOD1 was more similar to the lag time observed for wtSOD1. The lag times for seeded reactions for both D90A/wtSOD1 and G93A/wtSOD1 were significantly shortened to approximately 44hrs, which were similar to other self-seeded reactions of SOD1 variants in a homogenous set up.

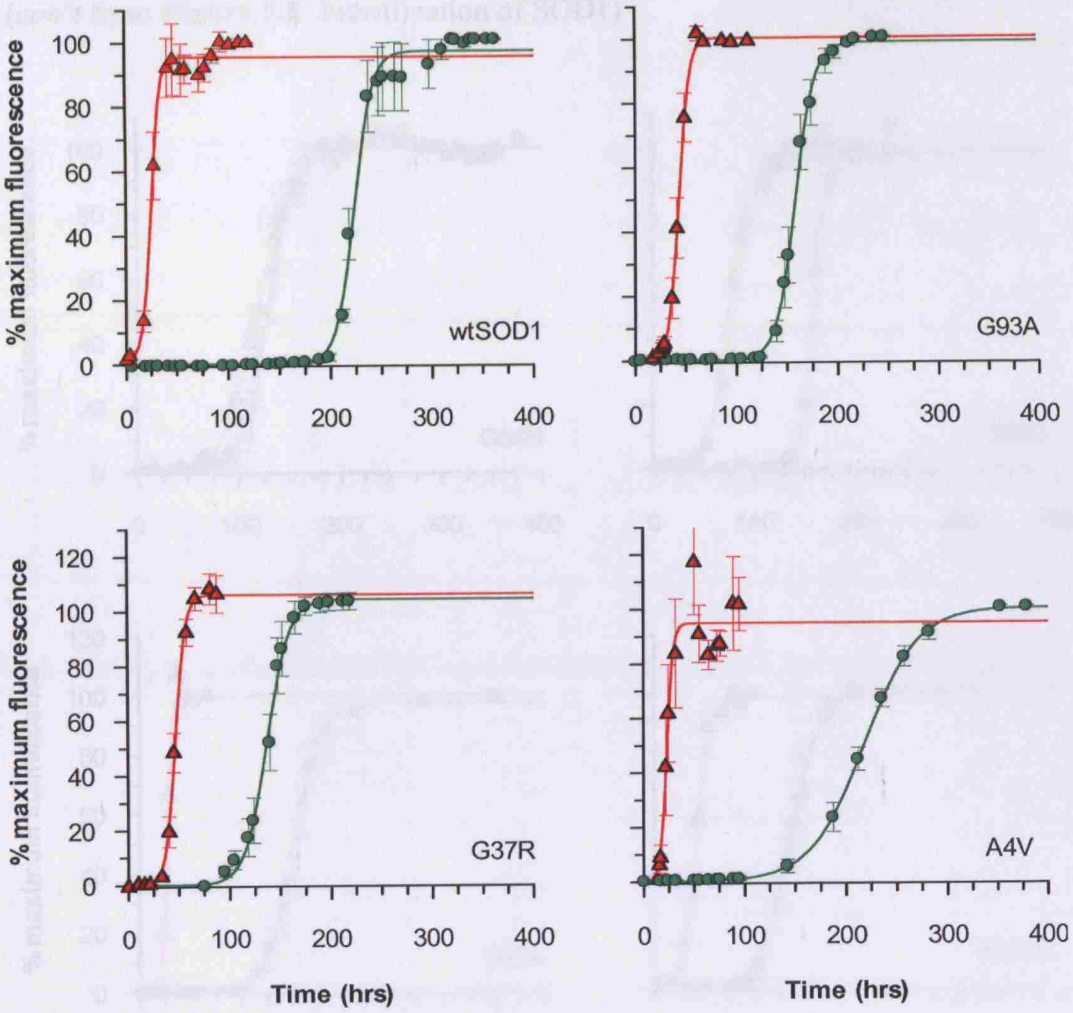

Figure 5.2. Fibrillization of SOD1. Spontaneous (green) and self-seeded (red) reactions for wtSOD1, G93A, G37R, A4V, G85R, D83G, D90A, and G114A. All SOD1 variants, except G85R were incubated at 37°C, at pH4 in mild denaturing condition (0.5M GdnHCl). Fibrillization of G85R was performed at pH5 with no denaturant. Fibril formation is reported as % maximum ThT relative fluorescence units (RFU) shown as a function of time (hrs). Data shown are average values from 6-10 replicates (± SEM) pooled from 2-3 independent assays. Seeded fibrillization reactions shortened the lag times by an average of 70% (except for G85R) compared to spontaneous reactions under similar conditions.

(*con't* from **Figure 5.2**. Fibrillization of SOD1)

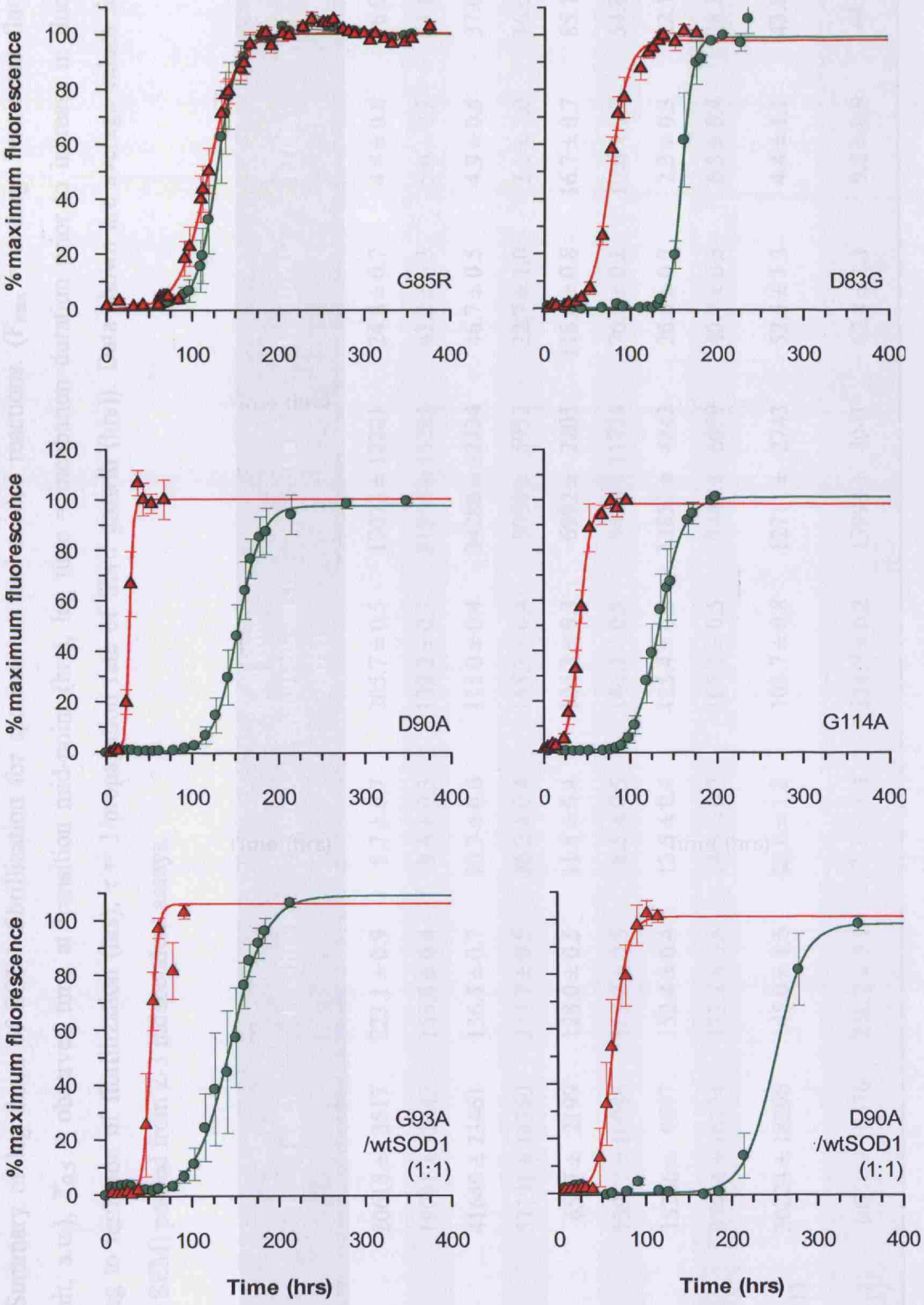

Table 5.1. Summary of lag times of SOD1 fibrillization for spontaneous and seeded reactions. (F_{max} = average maximum fluorescence (arbitrary unit, a.u.), $T_{0.5}$ = observed time at transition mid-point (hrs), lag time = incubation duration prior to increase in fluorescence corresponding to initiation of fibrillization (hrs), τ = 1/propagation rate of fibril growth (hrs)). Data shown are average values from 6-10 replicates (± SEM) pooled from 2-3 independent assays.

SOD1 Variant	F_{max} (a.u.)	$T_{0.5}$ (hrs)	τ (hrs)	Lag time (spontaneous) (hrs)	F_{max} (a.u.)	$T_{0.5}$ (hrs)	τ (hrs)	Lag time (self-seeded) (hrs)
wtSOD1	20618 ± 3517	223.1 ± 0.9	8.7 ± 0.7	205.7 ± 0.5	17073 ± 12201	24.8 ± 0.7	4.4 ± 0.6	16.0 ± 0.6
G93A	19041 ± 12443	158.4 ± 0.4	9.6 ± 0.3	139.2 ± 0.3	21964 ± 15221	43.2 ± 0.3	5.0 ± 0.2	33.1 ± 0.2
G37R	41649 ± 23461	136.5 ± 0.7	10.7 ± 0.6	115.0 ± 0.4	34286 ± 12334	46.7 ± 0.5	4.9 ± 0.5	37.0 ± 0.4
A4V	51191 ± 14760	217.7 ± 0.5	26.2 ± 0.4	165.3 ± 0.4	9080 ± 5952	22.7 ± 1.0	3.1 ± 1.0	16.6 ± 1.0
G85R	6507 ± 2199	128.0 ± 0.5	11.8 ± 0.4	104.3 ± 0.3	6992 ± 2205	118.4 ± 0.8	16.7 ± 0.7	85.1 ± 0.5
D83G	13917 ± 10986	159.2 ± 0.5	6.5 ± 0.5	146.1 ± 0.5	9486 ± 11724	76.0 ± 0.8	10.6 ± 0.7	54.8 ± 0.7
D90A	18286 ± 9607	152.4 ± 0.4	13.5 ± 0.4	125.4 ± 0.3	13852 ± 4843	26.6 ± 0.3	2.3 ± 0.3	22.1 ± 0.3
G114A	37494 ± 16124	133.7 ± 0.8	14.3 ± 0.7	105.1 ± 0.5	9445 ± 6059	40.7 ± 0.5	6.3 ± 0.4	28.1 ± 0.4
G93A/ wtSOD1 (1:1)	20224 ± 18296	145.0 ± 1.6	20.6 ± 1.2	103.7 ± 0.8	12711 ± 2743	52.5 ± 1.3	4.4 ± 1.1	43.8 ± 0.8
D90A/ wtSOD1 (1:1)	10710 ± 8576	250.2 ± 3.1	17.7 ± 1.4	214.7 ± 0.2	13993 ± 4041	62.8 ± 1.1	9.2 ± 0.9	44.5± 0.7

To investigate if pre-formed fibrils of mutSOD1s could initiate the fibrillization of wtSOD1, cross-seeded (cs) reactions were performed for all mutSOD1s in a similar set up as self-seeded reactions where pre-formed mutSOD1 fibrils were seeded to wtSOD1 instead to self. All fibrillization reactions were set up at pH4 with 0.5M GdnHCl. Cross-seeded reactions by all pre-formed mutSOD1 fibrils (except G85R) shortened the fibrillization lag time by an average of 90% (approximately 9 – 33hrs) in comparison to the lag time of wtSOD1 (spontaneous). Results for cross-seeded reactions are shown in Figure 5.3 and summarised in Table 5.2.

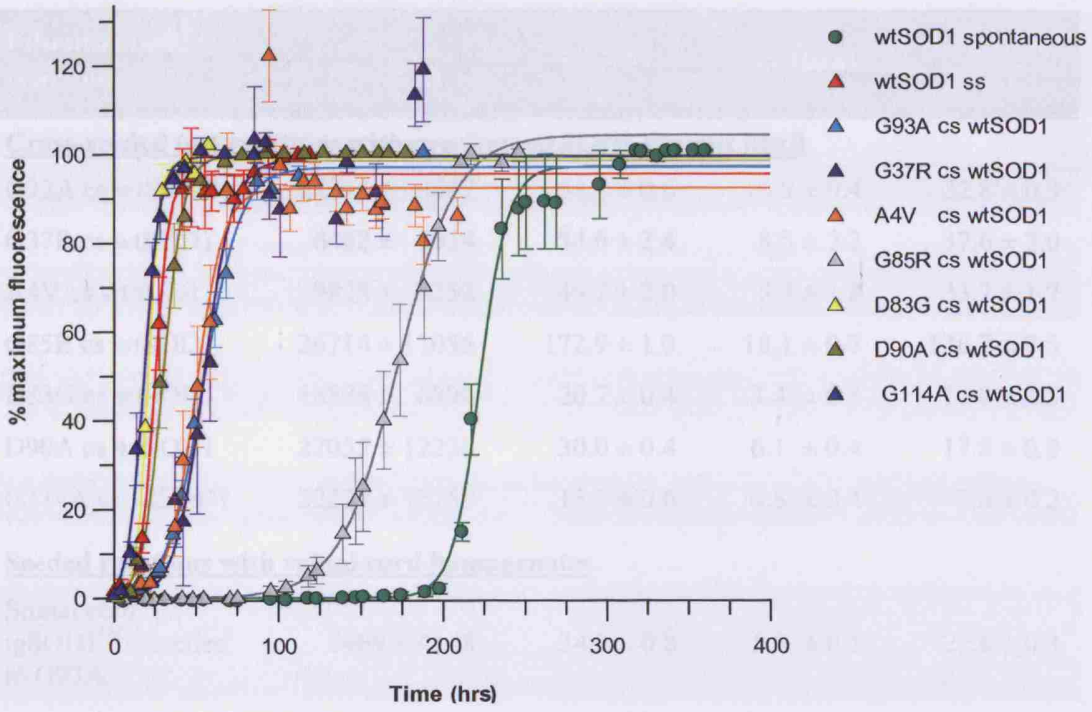

Figure 5.3. Cross-seeding fibrillization reactions of pre-formed fibrils of mutant SOD1 to wtSOD1 (pH4, 0.5M GdnHCl). Formation of fibrils is reported as % maximum ThT relative fluorescence units (RFU) shown as a function of time. Data shown are average values from 6-10 replicates (± SEM) pooled from 2-3 independent assays. Cross-seeding of G93A, G37R, A4V, D83G, D90A and G114A into wtSOD1 shortened lag time from ~206 hours to ~9 – 33 hours (lag time shortened by approximately 90%). G85R also showed the same effect but not as significant as the other mutants (33% reduction in lag time).

Table 5.2. Summary of lag times of SOD1 fibrillization for seeded reactions with pre-formed fibril of SOD1 mutants to wtSOD1 and with spinal cord homogenates to G93A and wtSOD1. (F_{max} = average maximum fluorescence (arbitrary unit, a.u.), $T_{0.5}$ = observed time at transition mid-point (hrs), lag time = incubation duration prior to initiation of fibrillization (hrs), τ = 1/propagation rate of fibril growth (hrs), $tgSOD1^{G93A}$ = transgenic SOD1 mice carrying the G93A mutation, $tgSOD1^{wtSOD1}$ = transgenic wtSOD1 overexpressor mice and $non\text{-}tg^{wt}$ = non-transgenic mice, n/a = not available). Data shown are average values from 6-10 replicates (± SEM) pooled from 2-3 independent assays.

Fibrillization reaction	F_{max} (a.u.)	$T_{0.5}$ (hrs)	τ (hrs)	Lag time (hrs)
Cross-seeded (cs) reactions with pre-formed SOD1 mutant fibril				
G93A cs wtSOD1	22214 ± 9547	54.6 ± 0.6	10.9 ± 0.4	32.8 ± 0.3
G37R cs wtSOD1	6482 ± 5934	54.6 ± 2.4	8.5 ± 2.2	37.6 ± 2.0
A4V cs wtSOD1	9828 ± 4252	49.7 ± 2.0	8.3 ± 1.8	33.2 ± 1.7
G85R cs wtSOD1	26714 ± 11056	172.9 ± 1.0	18.1 ± 0.7	136.7 ± 0.5
D83G cs wtSOD1	18828 ± 6890	20.7 ± 0.4	3.4 ± 0.5	14.0 ± 0.5
D90A cs wtSOD1	22055 ± 12236	30.0 ± 0.4	6.1 ± 0.4	17.8 ± 0.3
G114A cs wtSOD1	22222 ± 13750	18.3 ± 0.6	4.8 ± 0.4	8.6 ± 0.2
Seeded reactions with spinal cord homogenates				
Spinal cord $tgSOD1^{G93A}$ seeded to G93A	7469 ± 4148	34.3 ± 0.8	5.8 ± 0.5	22.6 ± 0.3
Spinal cord $non\text{-}tg^{wt}$ seeded to G93A	2702 ± 444	111.1 ± 1.9	15.0 ± 1.4	81.1 ± 0.9
Spinal cord $tgSOD1^{wtSOD1}$ seeded to G93A	2077 ± 366	115.6 ± 2.5	14.8 ± 2.1	86.0 ± 1.7
Spinal cord $tgSOD1^{G93A}$ seeded to wtSOD1	2140 ± 690	78.0 ± 0.5	11.0 ± 0.4	56.0 ± 0.3
Spinal cord $non\text{-}tg^{wt}$ seeded to wtSOD1	1352 ± 114	n/a	n/a	n/a
Spinal cord $tgSOD1^{wtSOD1}$ seeded to wtSOD1	1621 ± 210	n/a	n/a	n/a

5.3.3 *In vivo* relevance of fibrillization with spinal cord homogenates

In sections 5.3.1 and 5.3.2, it was demonstrated that SOD1 has a generic property of forming amyloid *in vitro,* as described in the ThT assay. To investigate the *in vivo* relevance of these *in vitro* results, fibrillization assays were repeated for G93A and wtSOD1 seeded with spinal cord homogenates from transgenic SOD1 mice carrying the G93A mutation ($tgSOD1^{G93A}$), transgenic wtSOD1 overexpressor mice ($tgSOD1^{wtSOD1}$) and non-transgenic littermates ($non\text{-}tg^{wt}$). Spinal cords used were from animals at 120 days old corresponding to the end-stage age of $tgSOD1^{G93A}$ mice. Results from these spinal cord homogenate seeded reactions are shown in Figure 5.4 and the lag times are summarised in Table 5.2. Seeded reactions of G93A and wtSOD1 by $tgSOD1^{G93A}$ spinal cord homogenates initiated fibrillization at approximately 23hrs and 56hrs which were comparable to the lag time of self-seeded reaction of G93A and cross-seeded reaction of G93A to wtSOD1, with a small deviation of 10-15hrs. Seeded reaction with $tgSOD1^{wtSOD1}$ and $non\text{-}tg^{wt}$ spinal cord homogenates to G93A had lag times of approximately 81hrs and 86hrs respectively, whereas there was no significant ThT fluorescence change in seeded reaction of $non\text{-}tg^{wt}$ spinal cord homogenates to wtSOD1 which was indicative of the absence of fibrillization.

To test for the specificity of the observed seeding effect using spinal cord homogenates of $tgSOD1^{G93A}$, in addition to using spinal cord homogenates of $tgSOD1^{wtSOD1}$ and $non\text{-}tg^{wt}$, spinal cord homogenates of non-ALS related mouse models or human samples were included as controls. The controls used were spinal cord homogenates from Prion RML mice, huntingtin transgenic mice (N171-82Q), and human brain homogenate archived from an FTD3 patient (FTD3 is acronym for frontal temporal dementia linked to chromosome 3 (OMIM 2006)). These additional controls showed no significant ThT fluorescence change when seeded to G93A or wtSOD1, indicating that the seeding effect which gave rise to the change in ThT fluorescence and shortened lag time observed in $tgSOD1^{G93A}$ spinal cord seeded reactions were specific and likely due to the presence of a species of SOD1 which behaved similarly to pre-formed SOD1 fibrils, formed *in vitro*, when seeded to self or to wtSOD1.

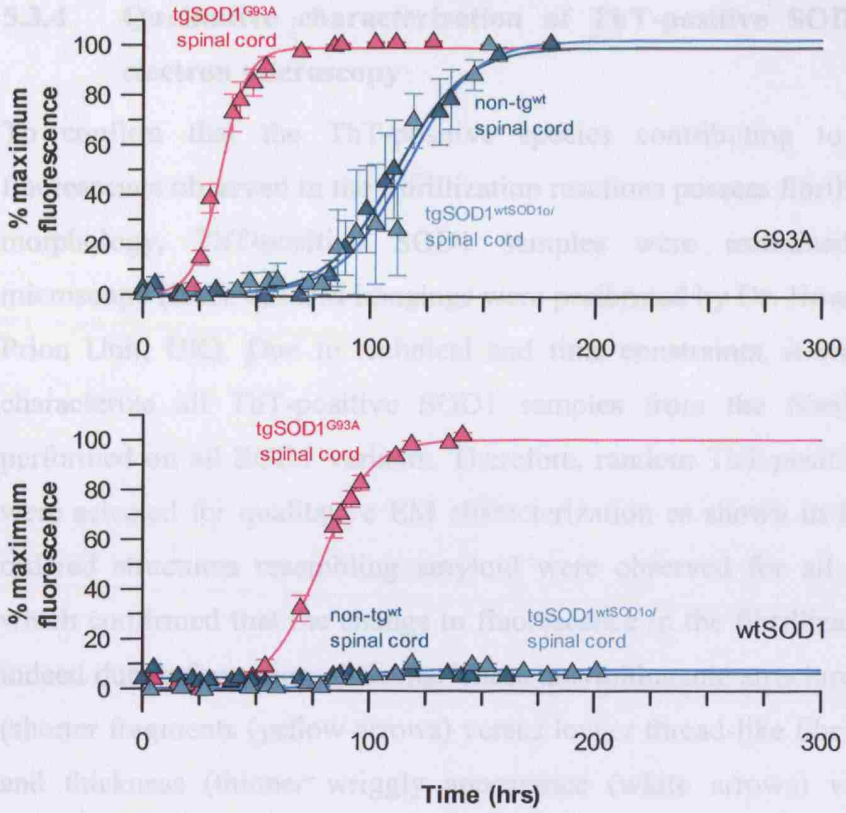

Figure 5.4. Fibrillization reactions of G93A (top graph) and wtSOD1 (bottom graph) seeded with spinal cord homogenates from 120 days old tgSOD1^{G93A}, tgSOD1^{wtSOD1} and non-tg^{wt} mice. Seeded reactions with tgSOD1^{G93A} spinal cord homogenates to G93A and wtSOD1 shortened the lag time to approximately 23hrs and 56hrs respectively, which were comparable to seeded reactions by pre-formed G93A fibrils to self and wtSOD1 (Table 5.1). The lag times of seeded reactions by tgSOD1^{wtSOD1} and non-tg^{wt} spinal cord homogenates to G93A were 1.5 – 3.5 fold longer than the lag times of seeded reactions by tgSOD1^{G93A} spinal cord homogenates. Seeding with tgSOD1^{wtSOD1} and non-tg^{wt} spinal cord homogenates to wtSOD1 did not give rise to any ThT fluorescence change indicating absence of fibril formation. Additional spinal cord controls were used to test for seeding specificity for the observed change in fluorescence in tgSOD1^{G93A} spinal cord homogenate seeded reactions. These were spinal cord homogenates from Prion RML mice, huntingtin transgenic mice (N171-82Q), and brain homogenate from an archived sample from an FTD3 patient. No significant change in ThT fluorescence in these reactions was observed (data not shown). Data shown are average values from 4-10 replicates (± SEM) pooled from 2-3 independent assays.

5.3.4 Qualitative characterization of ThT-positive SOD1 species under electron microscopy

To confirm that the ThT-positive species contributing to the increase in fluorescence observed in the fibrillization reactions possess fibrillar or amyloid-like morphology, ThT-positive SOD1 samples were examined under electron microscopy (EM). All EM imagings were performed by Dr. Howard Tattum (MRC Prion Unit, UK). Due to technical and time constraints, it was not possible to characterize all ThT-positive SOD1 samples from the fibrillization reactions performed on all SOD1 variants. Therefore, random ThT-positive SOD1 samples were selected for qualitative EM characterization as shown in Figure 5.5. Higher ordered structures resembling amyloid were observed for all samples analysed which confirmed that the change in fluorescence in the fibrillization reactions was indeed due to formation of fibrils. These amyloidogenic structures varied in length (shorter fragments (yellow arrows) versus longer thread-like fibrils (green arrows)) and thickness (thinner wriggly appearance (white arrows) versus thicker 2-3 intertwined fibrils (red arrows)) and occasionally, a less structured morphology was also observed in some ThT-positive SOD1 samples. An example of this less structured morphology is shown in Figure 5.5(e) where G85R ThT-positive species mostly appeared as spherical aggregates and some with a donut-like appearance. The significance of the difference in morphologies is currently unknown, but the common property observed in all ThT-positive SOD1 samples was the increase in the propensity of these structurally altered SOD1 proteins to clump together or to aggregate, regardless of the adopted morphology of the ThT-positive species.

Figure 5.5. Representative electron micrographs of SOD1 fibrils from spontaneous and seeded reactions (self-seeded and cross-seeded with pre-formed fibril/oligomer or with spinal cord tissue homogenate). Samples from fibrillization reactions of : a) – c) A4V spontaneous, self-seeded and cross-seeded to wtSOD1, d) G37R spontaneous, e) – f) G85R spontaneous and self-seeded, g) – i) G93A spontaneous and tgSOD1^{G93A} spinal cord homogenate seeded. All spontaneous, self- and cross-seeded reactions for all SOD1 variants were carried out at pH4 with 0.5M GdnHCl, except for G85R which was carried out at pH5 without any denaturant. Shorter fibrillar fragments are indicated by yellow arrows, which were observed in all samples. Green arrows point to longer and continuous fibrillar threads, whereas white arrows point to thinner and wriggly appearing SOD1 species (possibly shorter oligomers). Blue arrows in e) point to a less structured morphology of G85R ThT-positive species (most appear as spherical aggregates but some have a donut-like appearance) which morphology was also occasionally observed in other SOD1 fibrillar samples. Red arrows in h) and i) point to the flexion points of what appears to be 2-3 fibrils twisted together to form a thicker fibrillar thread or fragment. All SOD1 fibril samples which were qualitatively characterized under EM showed a common property of increased propensity to clump together or to aggregate, regardless of the morphology of the ThT-positive species.

(*con't* from **Figure 5.5**. Representative electron micrographs (EM) of SOD1 fibrils from spontaneous and seeded reactions (self-seeded and cross-seeded with pre-formed fibril/oligomer or with spinal cord tissue homogenate).

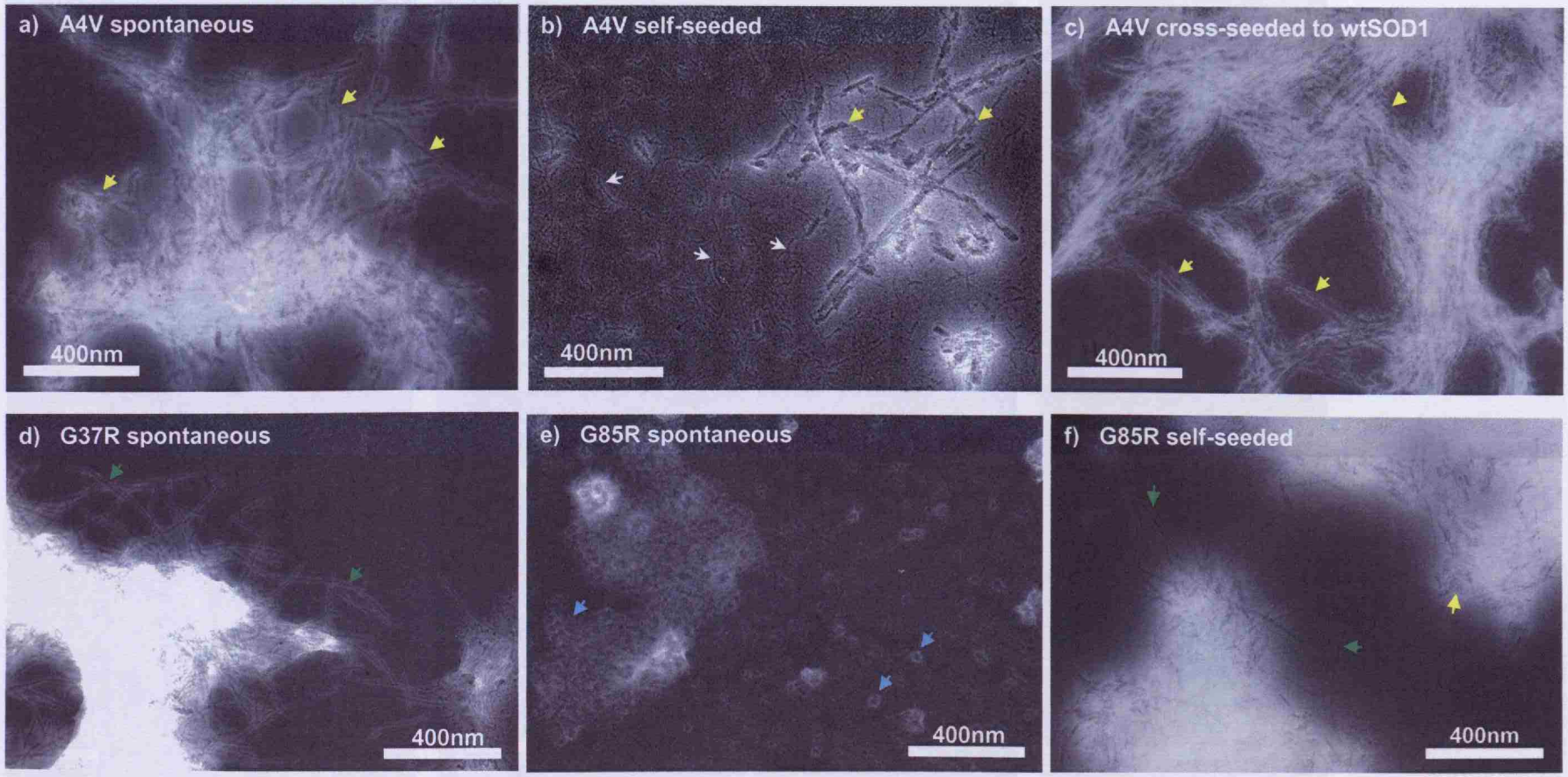

(*con't* from **Figure 5.5**. Representative electron micrographs (EM) of SOD1 fibrils from spontaneous and seeded reactions (self-seeded and cross-seeded with pre-formed fibril/oligomer or with spinal cord tissue homogenate).

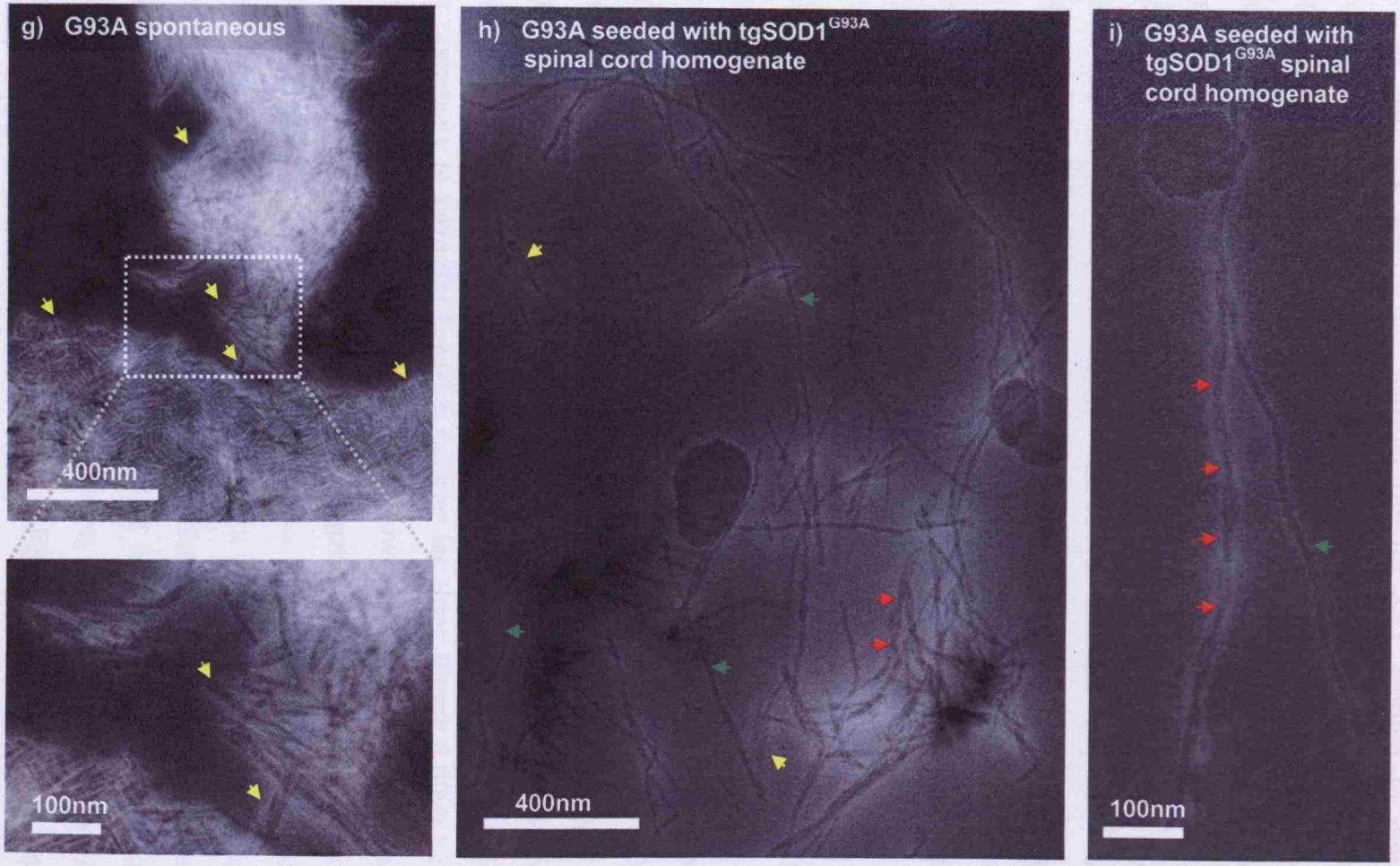

5.4 Discussion and conclusion

5.4.1 Correlation of SOD1 stability to fibrillization propensity

Proteins were screened against a matrix of varying pH and denaturant strength (GdnHCl concentration), and a range of conditions were found to potentiate the fibrillization of wtSOD1 and SOD1 mutants (Figure 5.1). Parallel to other amyloidogenic proteins, it was found that SOD1 variants (both wtSOD1 and mutant SOD1) could form fibrils more readily at low pH, in conditions that maybe encountered during lysosomal degradation. The spectrum of GdnHCl-induced destabilizing conditions at a fixed pH suggests that fibril formation is a conformation-dependent process, with some limited degree of unfolding and destabilization required to expose critical interaction domains required for oligomerization. Noticeably, SOD1 variants with higher protein stability could form fibrils over a broader range of fibrillization conditions but with a predictable trend whereby lag time for fibril formation was inversely proportional to denaturing activity (data not shown).

This is in agreement with the observed shorter lag time of SOD1 variants with lower protein stability (reflected by the melting temperature, apparent Tm ((C), characterized in Chapter 4). By plotting apparent Tm values against the fibrillization propagation rates and lag times of all SOD1 variants for both spontaneous and seeded reactions (Figure 5.6), the fibrillization propensity of SOD1 to protein stability was correlated. In spontaneous fibrillization reactions, SOD1 variants with lower protein stability (reflected by lower apparent Tm values) had a higher propensity to form fibrils earlier (shorter lag time; Figure 5.6(b)) but with no significant change in the propagation rate. However, in seeded reactions, the reverse appears to be the case where the propagation rate is dependent on protein stability (Figure 5.6(a)) with a relatively narrow range of lag times shared by all SOD1 variants. From Figure 5.6 and Table 5.1, it appears that there is some degree of clustering of SOD1 variants with relation to the propagation rates, where wtSOD1, G93A, G37R, A4V, D90A and G114A had faster propagation rates in seeded reactions in comparison to spontaneous reactions, whereas G85R and D83G and behaved in the opposite manner having a faster propagation rate in

spontaneous reaction than in seeded reaction. This is likely due to the effect of mutations whereby SOD1 with G93A, G37R, A4V, D90A and G114A mutations have similar metal binding capacity (and therefore similar enzymatic activity and protein stability) to wtSOD1. These SOD1 are grouped as WTL mutants. The G85R and D83G mutations in SOD1 (unpublished SOD1 linked fALS mutation) are mutations circa the metal binding site having reduced enzymatic activity and lowered protein stability, thus grouped as MBR mutants. Although the significance of this difference in fibrillization property between WTL and MBR mutants is not understood, the most important finding here is that destabilization of SOD1 is a factor which potentiates SOD1 to form fibrils. This is in line with the aggregation theory proposed by others where destabilization of SOD1 promotes formation of aggregates which were claimed to be detrimental to motor neurons (Brown, Jr. 1998;Cleveland and Liu 2000;Fukada *et al.* 2001;Andersen *et al.* 2004;Furukawa and O'Halloran 2005;Sato *et al.* 2005;Tiwari and Hayward 2005). Here, it is clearly demonstrated that formation of fibrils is an alternative misfolding property of destabilized SOD1 forming higher ordered structures with intrinsic ability to autocatalyze formation of more fibrils contrary to formation of poorly-defined or unstructured aggregates.

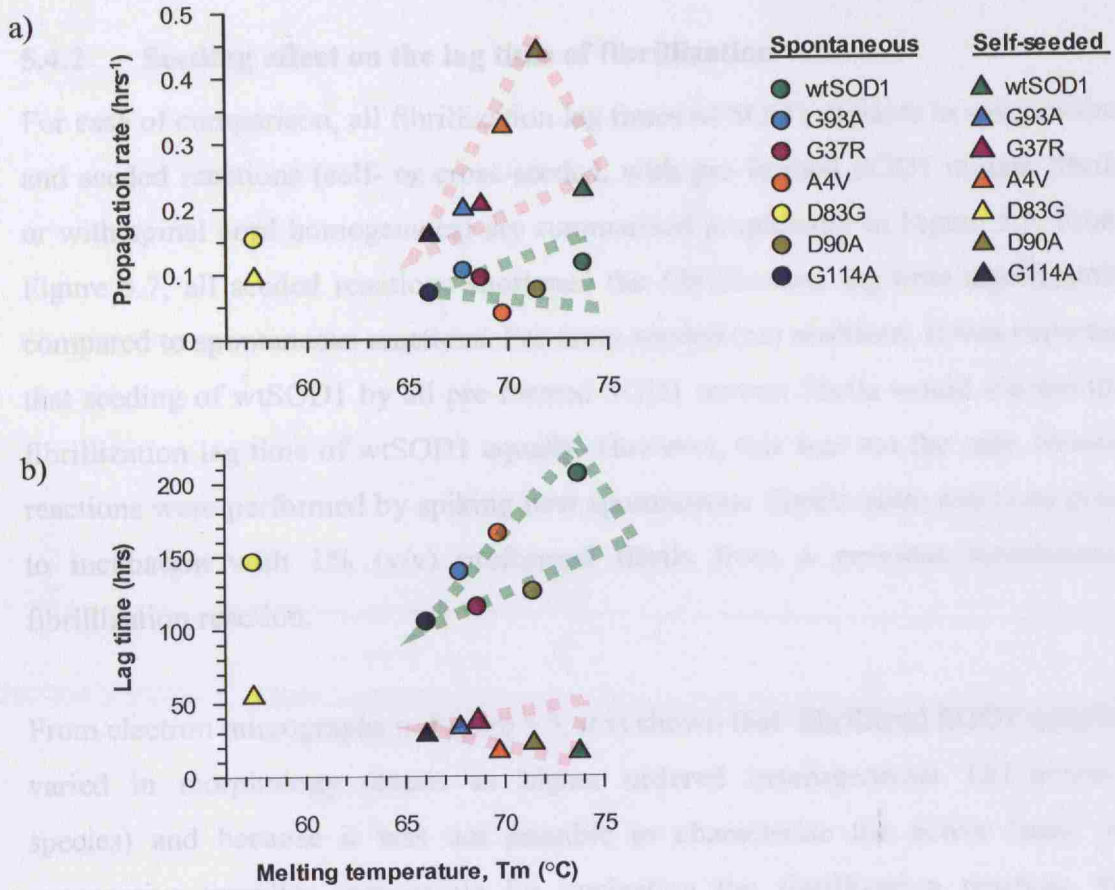

Figure 5.6. Effect of protein stability on the lag time and propagation rate of SOD1 fibrillization for spontaneous and self-seeded reactions. Graphs showing the correlation of SOD1 stability (expressed as melting temperature, apparent Tm (°C)) to a) propagation rate (hrs^{-1}) and b) lag time (hrs). In spontaneous reactions, the propagation rate was not affected by the protein stability whereas in seeded reactions, the more stable the protein, the faster the propagation rate. In terms of lag time, destabilized SOD1 variants had shorter lag times in spontaneous reactions, whereas seeded reactions initiated fibrillization at significantly shorter (than spontaneous reactions) but similar lag times. From the graphs, it appears to be that there is some degree of clustering of fibrillization parameters to the stability of SOD1 (clustering highlighted by light green and light red triangles). G93A, G37R, A4V, D90A and G114A are classified as wild-type like (WTL) mutants whereas G85R and D83G are classified as metal binding region (MBR) mutants. (Tm data for G85R was not determined, thus it was not possible to include the G85R fibrillization lag time and propagation rate in the graphs).

5.4.2 Seeding effect on the lag time of fibrillization

For ease of comparison, all fibrillization lag times of SOD1 variants in spontaneous and seeded reactions (self- or cross-seeded, with pre-formed SOD1 mutant fibrils or with spinal cord homogenates) are summarised graphically in Figure 5.7. From Figure 5.7, all seeded reactions shortened the fibrillization lag time significantly compared to spontaneous reactions. For cross-seeded (cs) reactions, it was expected that seeding of wtSOD1 by all pre-formed SOD1 mutant fibrils would shorten the fibrillization lag time of wtSOD1 equally. However, this was not the case. Seeded reactions were performed by spiking new spontaneous fibrillization reactions prior to incubation with 1% (v/v) preformed fibrils from a previous spontaneous fibrillization reaction.

From electron micrographs in Figure 5.5, it is shown that fibrillized SOD1 samples varied in morphology (exists as higher ordered heterogeneous ThT-positive species) and because it was not possible to characterise the active 'seed' or propagative template responsible for nucleating the fibrillization reaction, the actual amount of the active 'seed' used to spike the seeded reactions cannot be determined. Therefore, it is likely that the difference in the lag times observed in cross-seeded reactions by different pre-formed SOD1 mutant fibrils was due to the variation in the actual concentration of active 'seed' used to spike the seeded reactions. This is also likely to be the case for seeded reactions with spinal cord homogenates (tgSOD1^{G93A} seeded to G93A and wtSOD1) and in self-seeded reactions. To obtain more accurate lag times from seeded reactions, the active 'seed' must first be characterised so that seeded reactions can be spiked with a standardized concentration of active 'seed'. However, since this undertaking was beyond the work of this thesis, the fibrillization results from seeded reactions presented here are only semi-quantitative serving only to demonstrate the ability of SOD1, once misfolded to acquire some form of propagative conformation, to further catalyze formation of more fibrils.

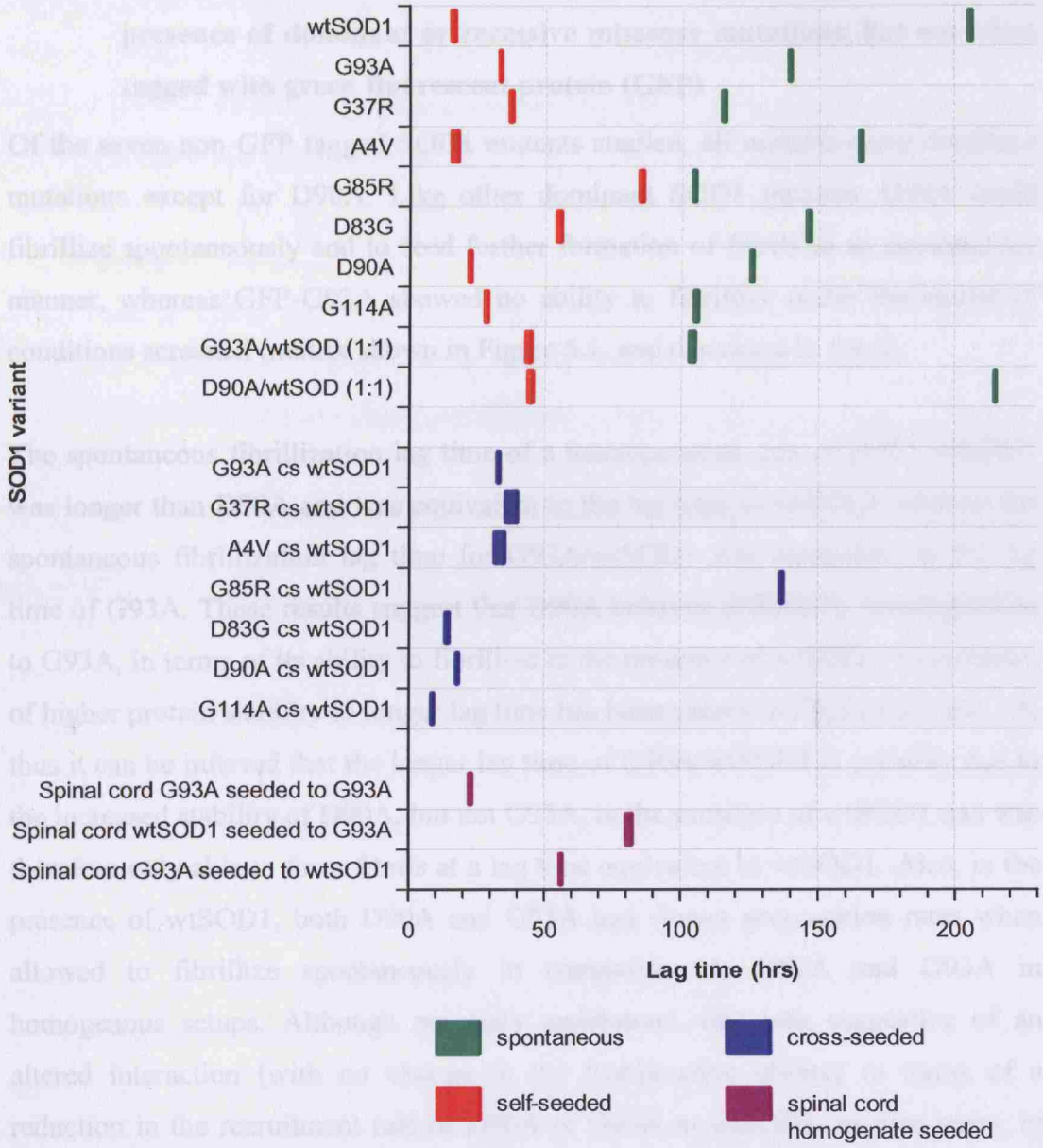

Figure 5.7. Graphical summary of fibrillization lag times of SOD1 in spontaneous and seeded reactions. Spontaneous and self-seeded reactions for wtSOD1, G93A, G37R, A4V, G85R, D83G, D90A, and G114A are plotted on the top portion of the graph, whereas the bottom portion of the graph shows lag times from spinal cord homogenate seeded reactions to G93A. All SOD1 variants, except G85R were incubated at 37°C, at pH4 in mild denaturing condition (0.5M GdnHCl). Fibrillization of G85R was performed at pH5 with no denaturant. (ss = self-seeded, cs = cross-seeded).

5.4.3 Fibrillization is a common property of SOD1 regardless of the presence of dominant or recessive missense mutations, but not when tagged with green fluorescent protein (GFP)

Of the seven non-GFP tagged SOD1 mutants studied, all mutants carry dominant mutations except for D90A. Like other dominant SOD1 mutants, D90A could fibrillize spontaneously and to seed further formation of fibrils in an autocatalytic manner, whereas GFP-G93A showed no ability to fibrillize under the matrix of conditions screened (matrix shown in Figure 5.1, and discussed in 5.4.4).

The spontaneous fibrillization lag time of a heterogeneous mix of D90A/wtSOD1 was longer than D90A and was equivalent to the lag time of wtSOD1 whereas the spontaneous fibrillization lag time for G93A/wtSOD1 was equivalent to the lag time of G93A. These results suggest that D90A behaved differently in comparison to G93A, in terms of its ability to fibrillize in the presence of wtSOD1. Correlation of higher protein stability to longer lag time has been shown in Figures 5.1 and 5.6, thus it can be inferred that the longer lag time of D90A/wtSOD1 is possibly due to the increased stability of D90A, but not G93A, in the presence of wtSOD1 and was therefore only able to form fibrils at a lag time equivalent to wtSOD1. Also, in the presence of wtSOD1, both D90A and G93A had slower propagation rates when allowed to fibrillize spontaneously in comparison to D90A and G93A in homogenous setups. Although not fully understood, this was suggestive of an altered interaction (with no change in the fibrillization ability) in terms of a reduction in the recruitment rate of D90A or G93A to wtSOD1, or vice versa, in the propagation or elongation of fibrils. These effects were abolished when seeded with pre-formed fibrils which further supports the notion that fibrillization of SOD1 is a propagative event upon nucleation by a SOD1 conformer which serves as a template.

There are two possible mechanisms of how D90A may cause disease in a recessive pattern:

1. The D90A mutation may cause SOD1 to acquire an altered protein property possibly in terms of how D90A interacts with itself or with wtSOD1 in

comparison to other mutSOD1s. This change in protein-protein interaction (mutSOD1-mutSOD1 or mutSOD1-wtSOD1) may modify or reduce the toxicity of D90A. This altered degree of toxicity means that in order for D90A to cause disease, both copies of the SOD1 gene need to be mutated to produce sufficient amounts of mutant protein to cause the equivalent toxic effect exerted by other dominant SOD1 mutants when only one copy is mutated.

2. The recessive phenotype of D90A is due to a strong modification (possibly by a protective factor) of the toxic effect of mutSOD1, which otherwise would manifest as a dominant disease.

Results shown thus far appear to be in agreement with the former where D90A in the presence of wtSOD1 fibrillized less readily in comparison to G93A. Since, only one control was used for this comparison, the conclusion drawn here is limited to only the effects seen for D90A and G93A. To confirm these findings, this work needs to be repeated for other SOD1 mutants to determine if the observed alteration in the protein-protein interaction of mutSOD-wtSOD1 is a common property shared by other dominant mutSOD1s. However, the latter mechanism cannot be ruled out because it has been shown that D90A can present as a dominant mutation with a full penetrance of the ALS phenotype (Robberecht *et al.* 1996;Jonsson *et al.* 2002). Also, in heterozygous relatives of D90A homozygous patients (Mezei *et al.* 1999), some abnormalities in the motor system have been observed. Collectively, these reported clinical findings are indicative of some kind of toxicity modification, although the phenotype-modifying factor is not yet determined. Therefore, it is likely that the two mechanisms mentioned above work in concert to each other rather than being mutually exclusive.

For the completion of this discussion, it is important to note that mutations implicated in fALS are mostly missense mutations (single amino acid substitutions), although some deletions, insertions and C-terminal truncations have been identified (Wroe 2008). Here, the mutSOD1s studied all carry missense mutations, and have all been shown to possess the intrinsic ability to form fibrils regardless of the nature of the mutation (whether dominant or recessive). In order

to further support the hypothesis that SOD1 fibrillization is the toxic process in conferring toxicity to motor neurons, it is therefore essential to characterize the ability of other mutSOD1s with different types of mutations in forming fibrils in a similar manner as mutSOD1s with missense mutations.

5.4.4 GFP-G93A does not firm fibrils *in vitro*

The inability of GFP-G93A to form fibrils was not unexpected because it has been shown in Chapter 4 that GFP-G93A differed significantly in its biochemical and biophysical properties when compared to non-GFP tagged SOD1. Therefore, results presented in this chapter reinforce the caution highlighted previously warranting the use of models and experimental designs employing the use of GFP-tagged SOD1.

5.4.5 Evidence of fibrillizing-accelerating species in tgSOD1^{G93A} mouse

Seeded reactions clearly demonstrate that SOD1 fibrils possess the ability to seed the formation of further fibrils in an autocatalytic manner, shown as a significant reduction of lag time (in both self-seeded and cross-seeded reactions) compared to spontaneous reactions under similar conditions (Figure 5.2 and Figure 5.3). Remarkably a similar seeding effect was observed using tissue homogenates from tgSOD1^{G93A} mice which was capable of stimulating fibrillization of wild type protein as well as mutant. This suggests the presence of a propagative-SOD1 conformer or 'template' in these homogenates, possibly pre-fibrillar aggregates present in the sample as residual material or produced from partial dissociation of the monomers from fibrils, as previously shown to be the case for other proteins not related to SOD1 (Baglioni *et al.* 2006). It has also been shown previously that Thioflavin-S-positive inclusions were evident in mouse models that express the G37R, G85R and G93A variants of human SOD1 (Wang *et al.* 2002) which adds support to the hypothesis proposed in this chapter.

5.4.6 Fibrillization of SOD1 as a possible mechanism in causing ALS

Mutations in SOD1 have long been implicated in familial cases of ALS, however the altered biological function that results in toxicity of this mutant protein and leads to disease pathology remains obscure. The ability to form self-propagating amyloid fibrils is a common property for all SOD1 variants (wtSOD1, G93A, G37R, A4V, G85R, D83G, D90A and G114A) which is likely to be the misfolding pathway that generates toxicity.

The main results described here confirm the generic property of SOD1 in forming amyloid-like structures or aggregates. Because the conditions used to characterize the fibrillization kinetics of SOD1 were not physiological, the relevance of these *in vitro* conditions to *in vivo* conditions needs to be verified. The finding by Banci and colleagues (Banci *et al.* 2007;Banci *et al.* 2008) showing that apo-wildtype SOD1 could form ThT-binding structures under a more physiological condition (pH7.0), but with a very long lag time of 7 months (~ 5100hrs), supports the results in this study that fibrillization is a generic and intrinsic misfolding property of SOD1 independent of the conditions used. It is likely that a more physiological fibrillization condition may have been found if the fibrillization assay performed here was conducted over a longer time frame (over months instead of 1-2weeks). To demonstrate the relevance of these *in vitro* fibrillization conditions to *in vivo* conditions in a cell, further work is needed to screen for conditions more similar to the cellular environment to include those encountered in the cellular environment, particularly those associated with the endosomal and lysosomal pathways.

The present findings parallel clinical observations of disease progression in humans and in mouse models. Classical human ALS cases display a long latent pre-clinical phase with disease onset in mid-life, and usually a rapid disease progression with death occurring within 2-5 years; a phenotype mirrored in ALS mouse models (Turner and Talbot 2008). The late onset of disease is analogous to the long lag time in spontaneous fibrillization reactions suggesting nucleation and the establishment of fibril seeds is the rate-limiting step. Furthermore, the aggression of the disease upon onset is consistent with the *in vitro* fibrillization profile, where

by once fibrils are formed further recruitment and oligomerization of SOD1 is a rapid process limited only by substrate concentration.

Based upon the findings: the phagocytic capacity of motor neurons (Bowen *et al.* 2007), the ability of SOD1 to be secreted from cells (Teoh *et al.* 2005;Turner *et al.* 2005;Urushitani *et al.* 2006;Gomes *et al.* 2007;Santillo *et al.* 2007), non-cell autonomous toxicity of mutant SOD1 (Clement *et al.* 2003;Boillee *et al.* 2006a;Di Giorgio *et al.* 2007), the acquisition of mutant properties by wtSOD1 when oxidized or misfolded (Ezzi *et al.* 2007) and on the clinical observation of disease focality, spread of paralysis and gradient motor neuron loss in the spinal cord from onset site (Ravits *et al.* 2007a;Ravits *et al.* 2007b), a mechanism of disease pathogenesis arising from the generic property of SOD1 to form amyloid is proposed.

The proposed mechanism is that the toxicity of mutant SOD1 may be transferred from one cell to another in a propagative manner in line with the non-cell autonomous theory involving motor neurons, microglia and astrocytes (illustrated in Figure 5.8). In accrued deranged cellular and microenvironment conditions, the highly abundant cellular protein SOD1, promoted by mutations, can form stable amyloid fibrils associated with self-propagating amyloidogenic seeds. It is hypothesized that the toxic SOD1 conformers are formed as part of this replication process analogous to the proposed formation of toxic species in other protein misfolding disorders such as prion disease (Collinge and Clarke 2007). Cytotoxicity is likely to arise from a multiple-hit phenomenon, where a combination of triggers in the cell and possibly environmental factors are required to tip over the cellular microenvironment that may favour and initiate the formation and accumulation of these conformers. These toxic species may then impair or cause further dysfunction of cellular functions and regulatory systems, which ultimately stresses the cell to a point of no return resulting in cell death. The release of these toxic conformers, either from the abnormal secretion by motor neurons, microglia, or astrocytes, or as accidental release during cell death, into the microenvironment may have direct or indirect effect on neighbouring cells. The uptake of these toxic conformers by secondary neurons may give rise to

propagative-like cell death (clinically observed as progressive paralysis from distal to proximal limbs). Cell death of motor neurons could be potentiated further by possible paracrine and autocrine effects (if released from astrocytes or microglia) of the toxic SOD1 conformer, resulting in the activation of microglial and astrocytes.

All these events would be postulated to work in an autocatalytic cascade, resulting in a progressive loss of cells from the site of onset. The impact of this proposed mechanism is exciting because it points towards the possibility of a practical approach of treatment in ALS, both familial and sporadic cases, in slowing down or even halting disease progression even after onset by identifying compounds that can inhibit amyloid formation either by stabilizing the native conformation of SOD1 or directly inhibiting the fibrillization process.

Figure 5.8. Proposed mechanism of cell-to-cell transmission of SOD1 toxicity. Initiation of disease requires 'multiple-hits' to motor neurons and glia cells, which may arise from purely physiological events (e.g.: free radical generation from mitochondria) or from exposure to xenobiotics (e.g.: cycad toxin). Early 'hits' are usually sub-lethal, and although compensated for, effect of assaults are accumulated over time. Cumulated assaults cause motor neurons and/or glia to reach a point where the cell's homeostatic balance and maintenance is completely disrupted (e.g.: protein misfolding and inhibition of the protein degradation machinery, alteration in the mitochondria redox state, chaperone imbalance, etc) resulting in the inability of cells to cope with further stress. In the case of SOD1, mutation in SOD1 is a predisposition for misfolding/oligomerization under various conditions causing further destabilization (e.g.: oxidative stress, deranged microenvironment resulting in loss of Cu/Zn, etc). Under similar stress conditions, wtSOD1 may be misfolded but would require a synergistic combination of destabilizing factors.

❶ Dimeric SOD1 secreted constitutively and in regulated manner. (Ca^{2+}, ATP and/or depolarization-dependent)(Mondola *et al.* 1996;Turner *et al.* 2005;Urushitani *et al.* 2006;Gomes *et al.* 2007;Mondola *et al.* 2007;Santillo *et al.* 2007).

❷ SOD1 oligomers may be formed extracellularly (in deranged extracellular microenvironment) or secreted as oligomers (by motor neurons, astrocytes or microglia).

❸ Oligomers may cause activation of astrocytes and microglia (release of cytokines, NO, superoxide, etc), and may cause dysfunction of synaptic maintenance (eg: glutamate uptake, Ca^{2+} fluctuation, K^{+} buffering, brain pH regulation, etc)

❹ Oligomers may be taken up by neighbouring cells, and serve as 'seed' to form more oligomers/fibrils.

❺ Oligomers may disrupt /alter other organelle and cellular functions:
Mitochondria, proteasome, chaperone, endomembrane network, axonal transport, Ca^{2+} regulation, pH regulation, etc.
Disruption accentuates dysregulated cellular homeostasis, resulting in death over time.

❻ Minute amounts of SOD1 oligomers may be transported to terminal end initiating autocatalytic cascade of oligomerization, which may directly affect synaptic homeostasis and the buffering of synaptic microenvironment between motor neurons and astrocytes.

More SOD1 may be secreted, and the cycle of cell-to-cell transmission of SOD1 oligomer continues.
This positive-feedback loop amplifies damage and promotes propagation of disease from onset site.

(*con't from* **Figure 5.8**. Proposed mechanism of cell-to-cell transmission of SOD1 toxicity.)

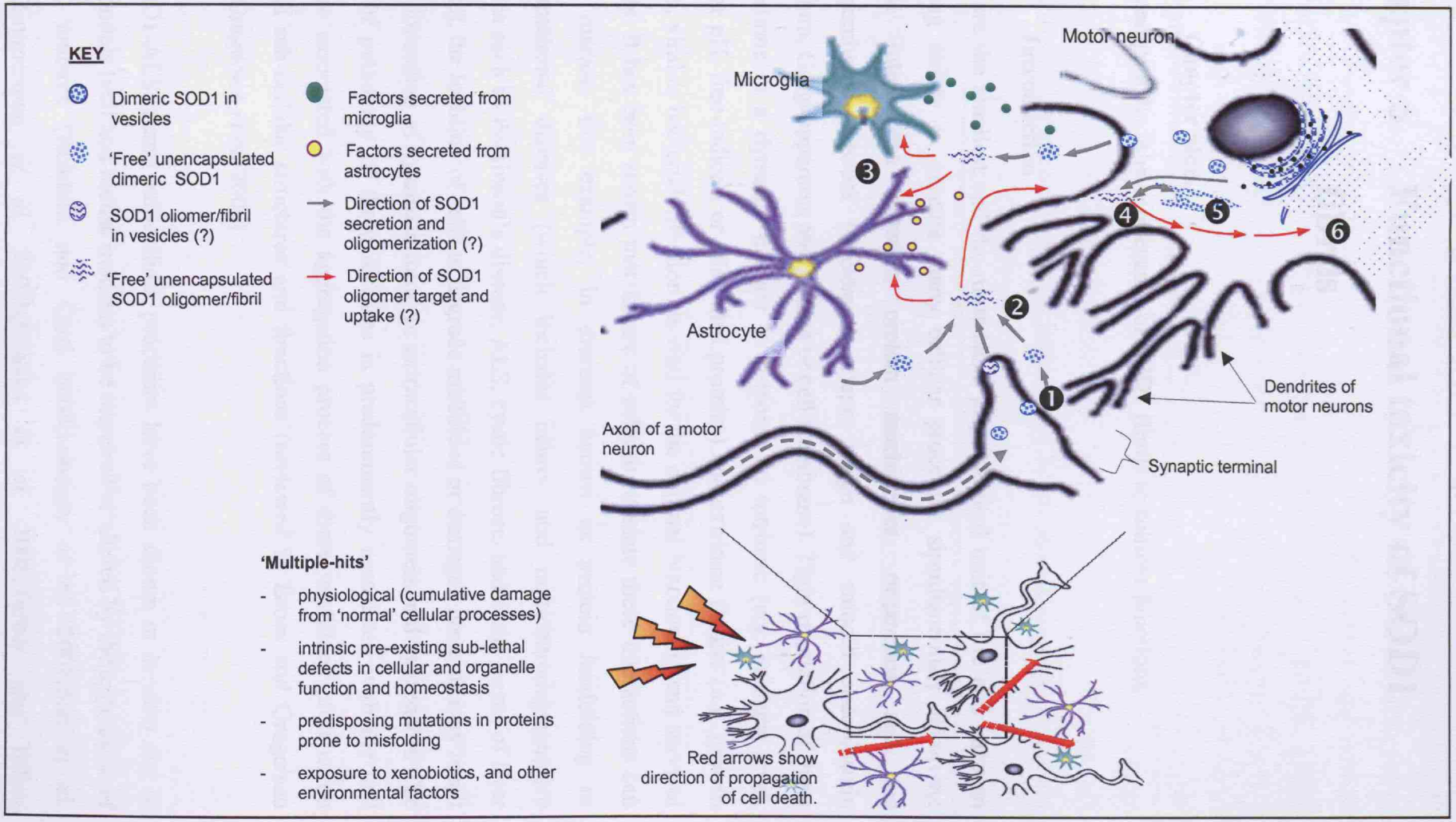

Chapter 6 Functional toxicity of SOD1 fibrils

6.1 Chapter aims

To investigate the *in vivo* relevance of SOD1 fibrils to cellular functions.

6.2 Introduction

Cells are the smallest and the most basic physiological unit of life and have an amazing ability to execute many cellular processes simultaneously involving diverse interactions between protein machineries, organelles and the endomembrane network (nuclear envelope, rough and smooth endoplasmic reticulum, Golgi apparatus and plasma or cell membrane). Tight regulation of these interactions in a dynamic manner in response to intrinsic (e.g. calcium level, cellular pH, free-radicals or misfolded proteins) and extrinsic factors (e.g. growth factors, viral or bacterial infection) is vital for the optimal functioning and survival of cells. It has been shown that failure of cells to regulate these interactions can cause disease. For example, in diseases known as protein misfolding or conformational diseases (which includes neuro- and non-neurodegenerative diseases such as Parkinson's disease, ALS, cystic fibrosis and some forms of liver disease), the inability of cells to degrade misfolded or damaged proteins may result in the formation of cytotoxic intra- or extracellular oligomers and aggregates. The basis of pathology of these diseases is predominantly associated with the cell damage associated with the aggregation process of these misfolded proteins on various sub-cellular structures and functions (reviewed in Bross and Gregersen 2003;Gregersen *et al.* 2006).

In SOD1-ALS, many sub-cellular processes have been shown in *in vitro* and *in vivo* models (cell and mouse models) to be impaired or altered by the expression of SOD1 mutants (Bendotti and Carri 2004;Lobsiger *et al.* 2007;Son *et al.* 2007;Zimmerman *et al.* 2007b;Cassina *et al.* 2008;Turner and Talbot

2008;Yamanaka *et al.* 2008) and reviewed in (Bendotti and Carri 2004). Some examples of impaired sub-cellular processes include inhibition of proteasome activity, impaired chaperone function, mitochondria dysfunction and axonal transport disruption. However, the toxic conformer/species of mutant SOD1 responsible for these alterations has not yet been identified. In Chapter 5, it was shown that *in vitro* formation of fibrils is a generic property of SOD1. Here, to investigate the functional toxicity of SOD1 fibrils (here on, SOD1 fibrils refer to all conformations of SOD1 which may exist in fibrillar samples), *in vitro* assays were undertaken to test the effects of these fibrils on the protein degradation machinery with a focus on the 26S proteasome (26S proteasomal assay; carried out in collaboration with Pelagia Derizoitis at the MRC Prion Unit, UK), membrane integrity (liposomal assays) and on the ability to induce aggregation of SOD1 expressed in cultured cells (*in vivo* modelling of SOD1 fibrillization). Results of these experiments are presented as follows.

6.3 Results

6.3.1 *In vitro* activity enhancement of the 26S proteasome by SOD1 fibrils

One of the cellular hallmarks observed in many protein misfolding diseases, ALS included, is a reduction in the ability of cells to clear misfolded protein leading to accumulation of these proteins as intra- or extracellular inclusions or aggregates (Brown, Jr. 1998;Pasinelli *et al.* 1998;Stieber *et al.* 2000;Bross and Gregersen 2003;Rakhit *et al.* 2004;Gregersen *et al.* 2006). The failure to clear misfolded proteins may be associated with the impairment of the 26S proteasome function (here on, simply referred to as 26S). To investigate if SOD1 fibrils have inhibitory effects on 26S function, SOD1 fibrils were incubated with 26S and the proteolytic activities of all three 26S sites (chymotrypsin-like, trypsin-like and caspase-like) were assayed by use of a fluorogenic assay, as described in Chapter 2.

It was found that the assay was sensitive to changes in pH resulting in the inactivation of 26S prior to the addition of samples (personal communication Deriziotis, P. (Kristiansen *et al.* 2007)), therefore it was necessary to extensively dialyse all samples of SOD1 fibrils (which were fibrillized at low pH) and native

SOD1 (as controls) against the proteasome assay buffer, 50mM Tris-Cl, pH7.5. To test if the pre-formed fibrils dialysed against the proteasome buffer retained similar seeding properties to undialysed fibrils, seeded fibrillization reactions using dialysed fibrils were performed. Dialysed G93A and A4V fibrils were used as test samples in self-seeded fibrillization reactions. The lag times were similar to the lag times of self-seeded fibrillization reactions using undialysed seeds (data not shown). This confirms that dialysis of the fibrils against the proteasome buffer did not alter the property of the critical species in the SOD1 fibril preparation in terms of autocatalytic formation of fibrils. Therefore, it follows that whatever results obtained from the 26S assay were unlikely due to artefacts arising from conformational changes in the dialysed samples of SOD1 fibrils.

Figure 6.1 shows that variants of SOD1 fibrils (red bars) caused significant enhancement of 26S activities at all three proteolytic sites when compared to buffer only control (blue bar gives maximum (100%) proteolytic activity of 26S proteasome). To test for specificity of the enhancement effect, aggregated lysozyme (by incubation with 50mM DTT for 1hr at 37°C) was included in the assays (Kristiansen *et al.* 2007). Aggregated lysozyme (purple bars) had no effect on 26S activity at any proteolytic sites, which suggests that the enhancement effect by SOD1 was specific.

The degree of activity enhancement by all variants of SOD1 fibrils varied from 16 – 150% for chymotrypsin-like activity, 63 – 380% for trypsin-like activity and 16 – 240% for caspase-like activity. Strikingly, native G85R and D83G had enhancement of chymotrypsin-, trypsin- and caspase-like activities by 140%, 350%, 220% and 70%, 160%, 120%, respectively for each SOD1 variant. wtSOD1, G93A and G37R did not alter the 26S activities at any of the sites in the native conformation. A4V, D90A and G114A showed more variability where these native SOD1 variants caused an increase in proteolytic activities at selective sites. Native D90A enhanced the chymotrypsin- and trypsin-like activities by approximately 8% and 90%, respectively, whereas there was approximately a 16% increase in the chymotrypsin-like activity and 40% increase in the trypsin-like activity induced by native G114 and A4V, respectively.

Figure 6.1. Enhancement of 26S activities at chymotrypsin-, trypsin- , and caspase-like proteolytic sites. All % of activities of all samples (green and red bars) were compared to the % maximum activity of 26S when treated with buffer (26S only control = blue bar)). Aggregated lysozyme had no effect on 26S activity at any proteolytic sites, which suggests that the enhancement effect by SOD1 was specific. Fibrillar forms of all SOD1 variants caused an enhancement of 26S activity at all three proteolytic sites. Native SOD1 variants showed more variability. Native G85R and D83G had an increase in activity at all three proteolytic sites whereas native D90A, G114A and A4V had selective enhancement of activities at either one or both chymotrypsin- and trypsin-like proteolytic sites. Data represent average values ± SEM (n=3 for protein samples, n=6 for buffer control, and n=8 for aggregated lysozyme). (Asterisks located above bars denote p-values calculated using the two-tailed Student t-test, where * = $p < 0.05$ and ** = $p < 0.01$. Asterisks are colour-coded red (fibril) or green (native) to match the corresponding bar description.)

(*con't* from **Figure 6.1**. Enhancement of 26S activities at chymotrypsin- (top graph), trypsin- (middle graph), and caspase-like (bottom graph) proteolytic sites.)

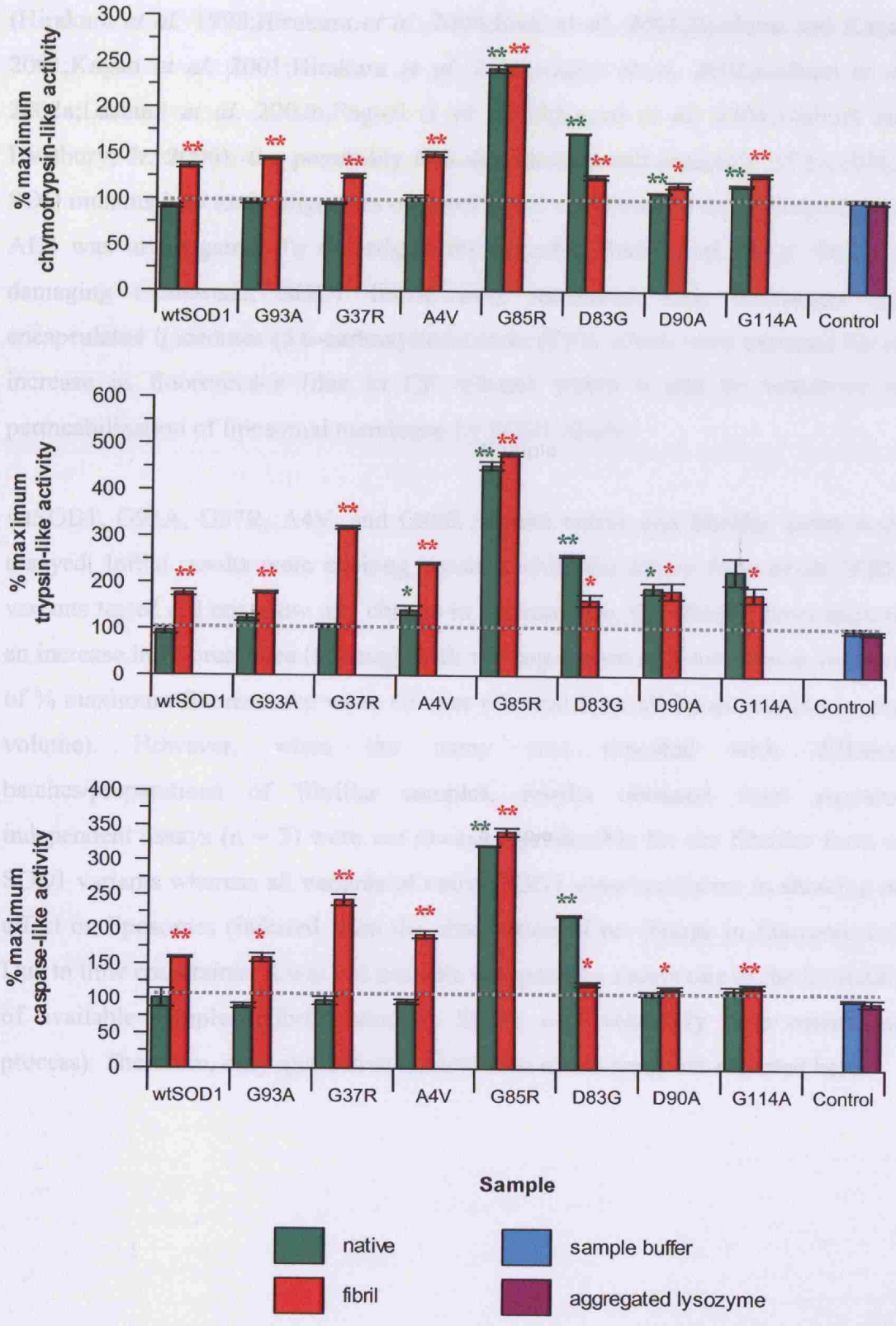

6.3.2 Effect of SOD1 fibrils on membrane

Because toxic pores have been recently implicated in the pathogenic mechanism of other neurodegenerative diseases such as Parkinson's and Alzheimer's disease (Hirakura *et al.* 1998;Hirakura *et al.* 2000;Ende *et al.* 2001;Hirakura and Kagan 2001;Kagan *et al.* 2001;Hirakura *et al.* 2002;Kagan *et al.* 2002;Lashuel *et al.* 2002a;Lashuel *et al.* 2002b;Foguel *et al.* 2003;Kayed *et al.* 2004;Lashuel and Lansbury, Jr. 2006), the possibility that the aberrant self-assembly of misfolded SOD mutants into toxic oligomers or pores might contribute to the pathogenesis of ALS was investigated. To investigate the potential toxicity of SOD1 fibrils in damaging membrane, SOD1 fibrils were incubated with fluorescent dye encapsulated liposomes (5,6-carboxyfluorescein (CF)) which were assessed for an increase in fluorescence (due to CF release) which would be indicative of permeabilization of liposomal membrane by SOD1 fibrils.

wtSOD1, G93A, G37R, A4V, and G85R of both native and fibrillar forms were assayed. Initial results were exciting because while the native form of all SOD1 variants tested did not show any change in fluorescence, the fibrillar form showed an increase in fluorescence (although with varying degree of fluorescence, in terms of % maximum fluorescence when CF was released from all liposomes in reaction volume). However, when the assay was repeated with different batches/preparations of fibrillar samples, results obtained from repeated independent assays (n = 3) were not always reproducible for the fibrillar form of SOD1 variants whereas all variants of native SOD1 were consistent in showing no effect on liposomes (inferred from the observation of no change in fluorescence). Due to time constraints, it was not possible to repeat the assays due to the limitation of available samples (fibrillization of SOD1 is a relatively time consuming process). Therefore, only qualitative observations of the assay are reported here.

6.3.3 Incubation of PC12 expressing GFP-G93A with pre-formed G93A fibrils showed evidence of SOD1 fibrils uptake but no formation of G93A fibril-induced GFP-G93A aggregation in PC12 cells.

To investigate the seeding effect of pre-formed fibrils in cells, nerve growth factor (NGF)-differentiated PC12 cells expressing GFP-G93A were incubated with pre-formed G93A fibrils tagged with a fluorescent dye, Alexa555 (G93A-fibril^{Alexa555}). To compare the uptake specificity of dye to labelled fibrils, Alexa555$^{free\text{-}dye}$ and native G93A labelled with Alexa555 (G93A-fibril^{Alexa555}) were included as controls. Cells were assessed for G93A-fibril^{Alexa555}-induced GFP-G93A aggregation over 48 – 96hrs, which would be observed as co-localization of red (G93A-fibril^{Alexa555}) and green fluorescent (GFP-G93A) aggregates in cells when examined under fluorescence microscopy. Figure 6.2 shows that incubated 'seeds' of G93A-fibril^{Alexa555} were taken up by PC12 cells and were observed to localise in the peri-nuclear region. Uptake of Alexa555$^{free\text{-}dye}$ and G93A-native^{Alexa555} was also observed, but to a lesser degree and appeared more diffuse in the cytoplasm. No GFP-G93A aggregation was observed even after 96hrs incubation in treated (with Alexa555$^{free\text{-}dye}$, G93A-fibril^{Alexa555} and G93A-fibril^{Alexa555}) or non-treated (as negative control; data not shown) PC12 cells. GFP-G93A was expressed homogenously throughout the cytoplasm. This meant that under non-stressed experimental conditions, as carried out here, the expressed GFP-G93A protein in PC12 cells do not readily form aggregates, and aggregation was not induced when 'seeds' of G93A-fibril^{Alexa555} were incubated with these cells.

Figure 6.2. Representative confocal images of PC12 cells at 48hrs incubation with Alexa555$^{free\text{-}dye}$, G93A-native^{Alexa555} and G93A-fibril^{Alexa555}. Expressed GFP-G93A proteins (green – expressed homogenously throughout the cytoplasm) in transfected PC12 cells were not observed to aggregate in treated a) Alexa555$^{free\text{-}dye}$, b) G93A-native^{Alexa555} and c) G93A-fibril^{Alexa555} or untreated preparations (data not shown). Uptake of Alexa555$^{free\text{-}dye}$, G93A-native^{Alexa555} and G93A-fibril^{Alexa555} were evident in all PC12 treated cells (GFP-G93A transfected or non-transfected). However, the degree of uptake and distribution pattern of Alexa555$^{free\text{-}dye}$ and G93A-native^{Alexa555} was different from G93A-fibril^{Alexa555}. The degree of Alexa555$^{free\text{-}dye}$ and G93A-native^{Alexa555} uptake into cells was less and appeared more diffuse in the cytoplasm compared to a more localised distribution of G93A-fibril^{Alexa555} around the nuclei. (DAPI = nuclear staining (blue); Scale bar = 20μm)

(*con't* from **Figure 6.2**. Confocal images of PC12 cells at 48hrs incubation with Alexa555$^{free\text{-}dye}$, G93A-native^{Alexa555} and G93A-fibril^{Alexa555}.)

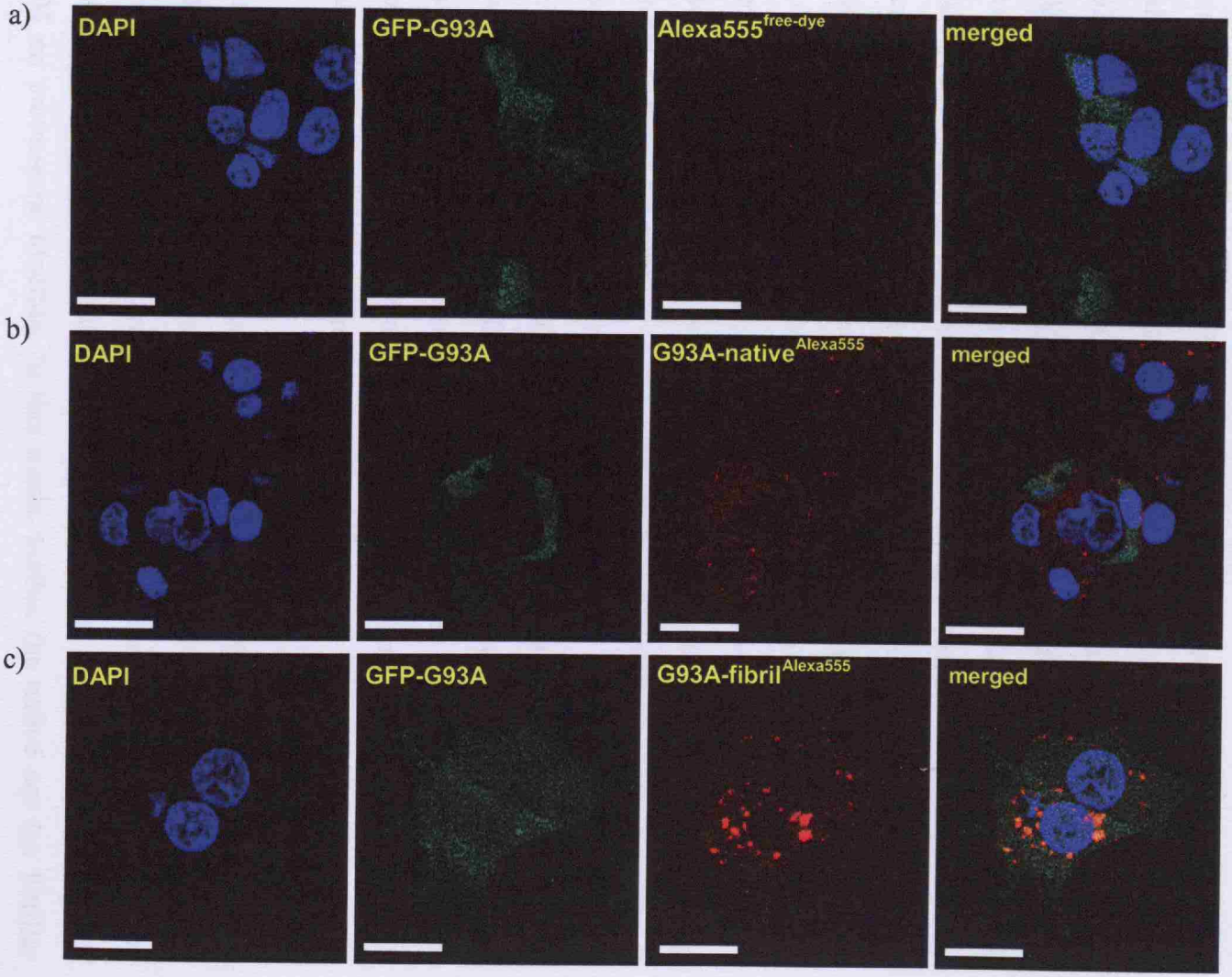

6.4 Discussion and conclusion

6.4.1 Novel effect of SOD1 on the 26S proteasome

In vitro and *in vivo* proteolytic changes in 20S or 26S have been shown to be induced by non-physiological and physiological agents such as detergents (e.g. SDS, Triton X-100), fatty acids (e.g. oleic acid, linolenic acid), cations (e.g. Mg^{2+}, Zn^{2+}, Ca^{2+}), oxidants (e.g. H_2O_2, $FeSO_4$-EDTA-ascorbate), enzymes (e.g. insulin-degrading enzyme, 170kDa-endogenous human platelet 20S activator) and natural or synthetic hydrophobic peptides (e.g. Suc-LLVY-mna, Suc-FLF-mna) (Saitoh *et al.* 1989;Arribas and Castano 1990;Djaballah and Rivett 1992;Djaballah *et al.* 1993;Yukawa *et al.* 1993;Strack *et al.* 1996;Hamel *et al.* 1998;Kisselev *et al.* 2002;Papapostolou *et al.* 2002;Kadowaki and Kanazawa 2003;Kisselev *et al.* 2003;Vigouroux *et al.* 2003;Thomas *et al.* 2005). Of interest is the reported increase in the proteolytic activities at all three proteolytic sites (independently and possibly cooperatively with each other) in a concentration dependent manner, where the activities were shown to increase over a low concentration range until a critical concentration was reached, by which further increase in concentration resulted in the inhibition of activities. Although the mechanism of the reported effect is unclear, it has been proposed that the alteration or modulation of 20S proteolytic activities by these agents may be associated with conformational changes, induced by binding of these agents to a non-catalytic site, resulting in selective changes in the proteolytic subunits of the 20S complex (Djaballah *et al.* 1993;Strack *et al.* 1996;Schmidtke *et al.* 2000;Kisselev *et al.* 2002). Therefore, it is possible that the effect of SOD1 on 26S activity enhancement observed here may be due to an induced allosteric modulation of 26S (or the 20S core) by one or several SOD1 conformers found in the fibrillar and some native SOD1 samples. Further work is necessary to investigate this effect.

Of importance to note is that results obtained from the 26S assay employed for the work carried out in this chapter only reflects the capacity of the proteolytic sites in cleaving the fluorogenic substrates and not on the degradation rate of SOD1 (native or fibrils). Results here are in contrast to existing reports on the inhibitory effect of SOD1 on proteasome function. In this thesis, neither the native nor the fibrillar

form of SOD1 variants was found to be inhibitory to 26S. Possible explanations for this discrepancy are discussed in the following section.

6.4.2 Implications of 26S proteasome activity enhancement by SOD1 fibrils in the pathogenesis of motor neuron death in ALS

The enhancement effect observed from the *in vitro* 26S assay induced by the fibrillar form of all SOD1 and some native SOD1 variants (A4V, G85R, D83G, D90A and G114A) was unexpected. Impairment of 26S proteasome function has been the acceptable theme in the pathogenesis of ALS (Urushitani *et al.* 2002;Puttaparthi *et al.* 2003;Kabashi *et al.* 2004;Kabashi and Durham 2006;Koyama *et al.* 2006) and other neurodegenerative protein misfolding diseases (Lopez *et al.* 2003;Lindersson *et al.* 2004;Goswami *et al.* 2006;Cecarini *et al.* 2007;Kristiansen *et al.* 2007) based on the presence of inclusions in affected regions of the nervous system in humans and in disease mouse models. In ALS, impairment of 26S function was thought to be caused by direct inhibition by mutant SOD1 (possibly in the misfolded form). Ineffective clearance of mutant SOD1 by 26S via the proteasome-ubiquitin system (UPS) results in the accumulation and formation of toxic SOD1 aggregates which may amplify further inhibition of 26S in a negative feedback manner. These toxic aggregates of mutant SOD1 were also postulated to cause damage to other cellular functions, whether as physical obstruction or via biochemical interference with cellular biochemical pathways, which collectively are detrimental to neuronal survival over a period of time (reviewed in (Hart 2006;Kabashi and Durham 2006).

Results presented in this chapter, are in contrast to the current working hypothesis on how impairment of 26S function contributes to the pathogenesis of ALS. Although purely speculative, it is possible that while the initial enhancement of activity of 26S induced by minute amounts of SOD1 fibrils (300nM of SOD1 incubated with 26S) is beneficial in the short term presumably to clear misfolded SOD1, over-enhancement induced by the accumulation of SOD1 fibrils over time (i.e. increase in concentration of misfolded SOD1) may eventually cause inhibitory conformational changes in the 26S subunits resulting in a decrease in the overall

protein degradation capacity of 26S (observed as reduced 26S activity). This is not an unreasonable speculation for reasons mentioned earlier, in 6.4.1 (concentration dependent increment of 20S of 26S activities at low concentrations followed by a concentration dependent decline at higher concentrations). Therefore, it may be possible that enhancement of 26S activity is an early event preceding the loss of 26S activity. Furthermore, it is important to note that most cellular and mouse models of ALS employ the over expression of SOD1 to model some properties of the disease (e.g.: formation of inclusions or aggregates). This meant that these models are overloaded with misfolded proteins thereby over-working the 26S from very early in the disease course, which may mask the initial (and possibly transient) increase of proteasome activity prior to the loss of activity.

Also, the increase in degradation capacity induced by misfolded SOD1 is unlikely to be specific to only the clearance of misfolded SOD1. This meant that other essential cellular proteins might also be degraded at a higher rate causing imbalance to the steady-state protein dynamics within the proteome leading to promotion of cell death. Moreover, it has also been shown that impairment of the UPS has profound inhibitory effects on the overall rates of protein synthesis (Ding *et al.* 2006) and this, although serves as a cell's initial response in preventing protein accumulation which is protective and reversible, can cause irreversible and pathological damage after prolonged periods of inhibition due to the persistent decrease in the synthesis of crucial and protective proteins (reviewed in (Ding *et al.* 2007).

To support the speculations made here, further work is needed. It would be interesting to investigate if the *in vitro* effect of 26S activity enhancement is 'real' in cellular or mouse models of ALS expressing lower amounts of mutant SOD1. If parallel *in vivo* effects to the *in vitro* results are found, then proteomic analysis to investigate the steady-state protein dynamics in these models (at different disease stages, particularly at the pre-symptomatic stage) would be useful in identifying the early and detrimental (and possibly subtle) changes in protein homeostasis in affected motor neurons which will give new information on the possible disease mechanism involved even before the appearance of any overt cellular dysfunction.

6.4.3 Possible but inconclusive membrane damaging effects of SOD1 fibrils

From the liposomal assays, it was not possible to draw any definitive conclusions on the effects of SOD1 fibrils in damaging membranes due to the varying results obtained from different preparations/batches of SOD1 fibrils. Due to time constraints, it was not possible to carry out further experiments to explain the discrepancies observed between assays. But, a possible explanation for this is that the SOD1 conformers which may be the damaging species to the membranes (whether as pore-forming structures or by causing general loss of liposomal membrane integrity) are likely to be present in varying amounts in different fibrillar preparations, thus the degree of fluorescence change (from CF release from liposome) is dependent on what is present in each sample. Since it was not possible to control for the homogeneity of SOD1 conformers/species in the fibrillar samples used (fibrillized SOD1 samples varied in morphology existing as higher order heterogeneous ThT-positive species as shown in Figure 5.5), the possibility of a conformer with a specific morphology formed during fibrillization being able to cause membrane damage cannot be ruled out definitively. It would only be possible to determine the effect of SOD1 fibrils on membranes if the different SOD1 species in the fibrillar samples are characterized and the experiments repeated with a homogenous preparation of SOD1 fibrils.

6.4.4 GFP-G93A does not form aggregates readily in cultured PC12 cells

GFP-G93A expressed in PC12 cells showed that it did not readily form any obvious aggregates when treated with or without G93A-fibril^{Alexa555} even after prolonged incubation. This was consistent with results presented in Chapter 4 and 5 where GFP-G93A was shown to be a protein with very high thermal stability and does not readily form fibrils *in vitro*. The absence of induction of GFP-G93A aggregation by G93A-fibril^{Alexa555} was not unexpected, but the absence of any GFP-G93A aggregates altogether was somewhat unexpected because of previous reports by others showing that GFP-G93A aggregation was a common property in GFP-G93A transfected cells (neuronal and non-neuronal cells) (Takeuchi *et al.* 2002b;Matsumoto *et al.* 2005;Matsumoto *et al.* 2006;Di Giorgio *et al.* 2007;Hetz *et al.* 2007;Urushitani *et al.* 2008). In an attempt to dissect the discrepancy of the

results found here to published work by others, through personal communication with Fox, S. (Matsumoto *et al.* 2005), it was made apparent that the formation of GFP-G93A aggregates was an inducible property of GFP-G93A transfected PC12 cells when stressed by treating the cells with a proteasome inhibitor (an important piece of information which was not mentioned in the published paper). With this acquired piece of information and the present findings in this chapter showing the absence of GFP-G93A aggregation in non-stressed PC12 cells (which complements the demonstrated differences in the biochemical and fibrillization properties of GFP-G93A compared to non-GFP tagged SOD1) the proposed caution, mentioned in previous chapters, on the use of GFP-tagged SOD1 in any experimental design is further supported here.

6.4.5 Possible implications of SOD1 fibril uptake

Although GFP-G93A aggregation in GFP-G93A transfected and differentiated PC12 cells was not induced when incubated with G93A-fibril^{Alexa555}, the striking finding from these experiments was the ability of PC12 cells to endocytose G93A-fibril^{Alexa555}. Although further investigation as to how and why SOD1 fibrils are endocytosed and the determination of endocytosis specificity is needed to understand the implications of this uptake on cellular survival, these preliminary findings are supportive of the proposed mechanism of cell-to-cell transmission of SOD1 toxicity, as explained in Chapter 5 in Figure 5.8, where one of the key themes of the proposed mechanism is the ability to propagate toxicity via uptake and release of the toxic SOD1 conformer/species by one cell (or localised group of cells) to neighbouring cells.

Chapter 7 Mariusz characterization

7.1 Chapter aim

To characterize phenotypically and to identify the gene mutated in an ENU (N-ethyl-N-nitrosourea) mutagenized mouse strain named Mariusz.

7.2 Introduction

Mutations induced in mice using ENU are usually point mutations and can occur throughout the entire genome (Concepcion *et al.* 2004). Mutations induced can give rise to dominant or recessive phenotypes, depending on the nature of the mutation in the gene involved. Genome wide screens for dominant or recessive mutations begin with ENU treatment of male mice (G_0), resulting in generation of mutations in their spermatogonial stem cells. These mice are then mated to wildtype females to generate F1 progeny (G_1), which will be heterozygous for the mutation. G_1 mice can then be screened for abnormalities if the phenotype of interest is caused by a dominant mutation. However, if the phenotype of interest is caused by a recessive mutation, G_1 mice are then entered into various breeding regimes (backcrossing and/or intercrossing) to generate mice homozygous for the mutation manifesting with recessive phenotypes.

Screening of mutant mice with recessive mutations is a more costly process compared to screening for dominant mutations, which is one reason why there are far fewer recessive disease mouse models. However, many human diseases display a recessive mode of inheritance, and it is for this reason that generation and screens for recessive mutants are essential to study and understand the genetic nature of recessive diseases in humans. Mariusz is a result of such a recessive screen carried out at the Mammalian Genetics Unit, MRC at Harwell and was identified in a screen for recessive mutant mice with low grip strength.

The Mariusz positional cloning project was initiated by Professor Neil Dear in 2004 at Harwell. In 2006, in collaboration with Professor Elizabeth Fisher (Institute of Neurology, UCL), the task of mapping the mutation was undertaken, which by then, the inheritance pattern (7.3.1), preliminary and secondary phenotype (7.3.2) of the mouse strain had been characterized and the initial location of the mutation had been mapped to the proximal region of chromosome 18 (7.3.3).

7.3 Results

Initial phenotype characterization and mapping were carried out by Professor Neil Dear and colleagues. Results figures 7.1, 7.2, 7.3, 7.4 and 7.7 were reproduced with permission and included in this thesis so that a more complete description of the project can be presented in this chapter.

7.3.1 Inheritance pattern

Two BALB/c males (G_0(a) and G_0(b)) were ENU mutagenized and were mated with C3H/HeJ females. Resulting F1 offpsring (female G_1(a) and male G_1(b)) from G_0 matings were intercrossed, producing G2 offspring. G2 females were backcrossed to G1(b) males and the resulting G3 offspring were screened for low grip strength. The low grip strength phenotype showed a typical autosomal recessive inheritance pattern with no evidence of sex bias. The initial pedigree is shown in Figure 7.1. Homozygous mice carrying the mutation were produced by intercrossing heterozygotes, maintained on a C3H/HeJ background.

7.3.2 Phenotypic screening and preliminary characterization

Mariusz mice were screened for low grip strength and were compared against wildtype littermates to generate baseline values. Grip strength (arbitrary force units, AFU) was measured for forelimbs only and on all four limbs (both forelimbs and hindlimbs) (Figure 7.2). Mariusz mice recorded an average forelimb grip strength value of 29.2 ± 8.1 AFU and forelimbs and hindlimbs value of 47.6 ± 16.6 AFU. These values were significantly lower than recorded baseline values from

wildtype littermates by an average of 68%. The phenotype was obvious by 6 weeks of age based on quantitative measurements on the grip strength meter. Mariusz mice were also observed to struggle weakly and have a tendency to cross their hindlimbs in a "cramping" manner when suspended by their tail (Figure 7.1). This "cramping" phenotype is indicative of neuromuscular weakness.

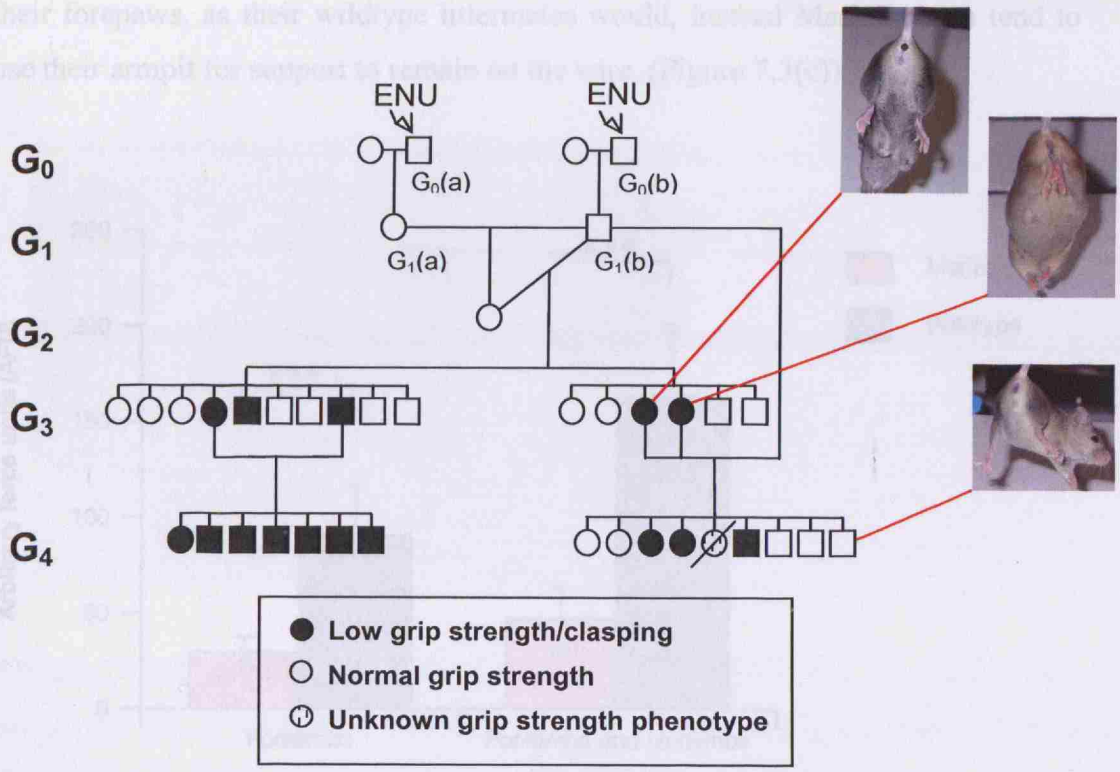

Figure 7.1. Mariusz pedigree showing a classical autosomal recessive inheritance pattern. G_3 generation was screened for recessive mutation by systematic and comprehensive phenotype screens. Representative photographs showing "cramping" phenotype of Mariusz mice compared to unaffected animals.

Mice with low grip strength were screened for additional neurobehavioral phenotypes. The two tests used for this additional screen were the MoRAG test and the wire manoeuvre test. For proprietary reasons, only a summary of results of the two tests is included in this thesis. Summary of results was obtained from Dr. Valter Tucci and Professor Neil Dear. MoRAG is a test designed to assess the

ability of the mouse to perform reaching and grasping actions. The ability to do so is a reflection of muscular and neurological functions (Tucci *et al.* 2007). Mariusz mice showed a clear abnormal grasping (Figure 7.3(b)) ability. These mice were able to extend their arms and hands to reach for the food target, but were not able to close theirs hands to grasp the food (Figure 7.3(a), and Video 7.1). Consistent with the grip strength results, Mariusz mice also performed poorly in the wire manoeuvre test. In this test, Mariusz mice were unable to hold on to the wire with their forepaws, as their wildtype littermates would, instead Mariusz mice tend to use their armpit for support to remain on the wire. (Figure 7.3(c)).

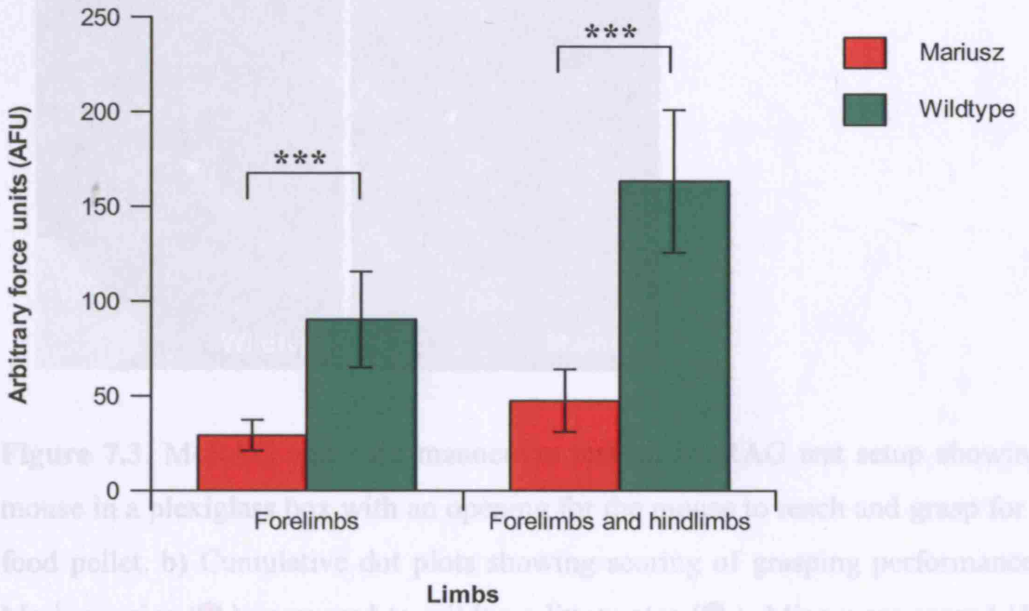

Figure 7.2. Muscular phenotype of Mariusz mice. Grip strength of Mariusz mice (n=27) and wildtype littermates (n=30) was measured using a grip strength meter. An average of 5 measurements was obtained from each mouse for each limb group. Each bar represents the average value (in arbitrary force units) ± SD. The difference in grip strength between Mariusz mice and wildtype littermates is highly significant with $p<10^{-14}$ at $\alpha = 0.05$ (t-test: Two sample assuming unequal variance).

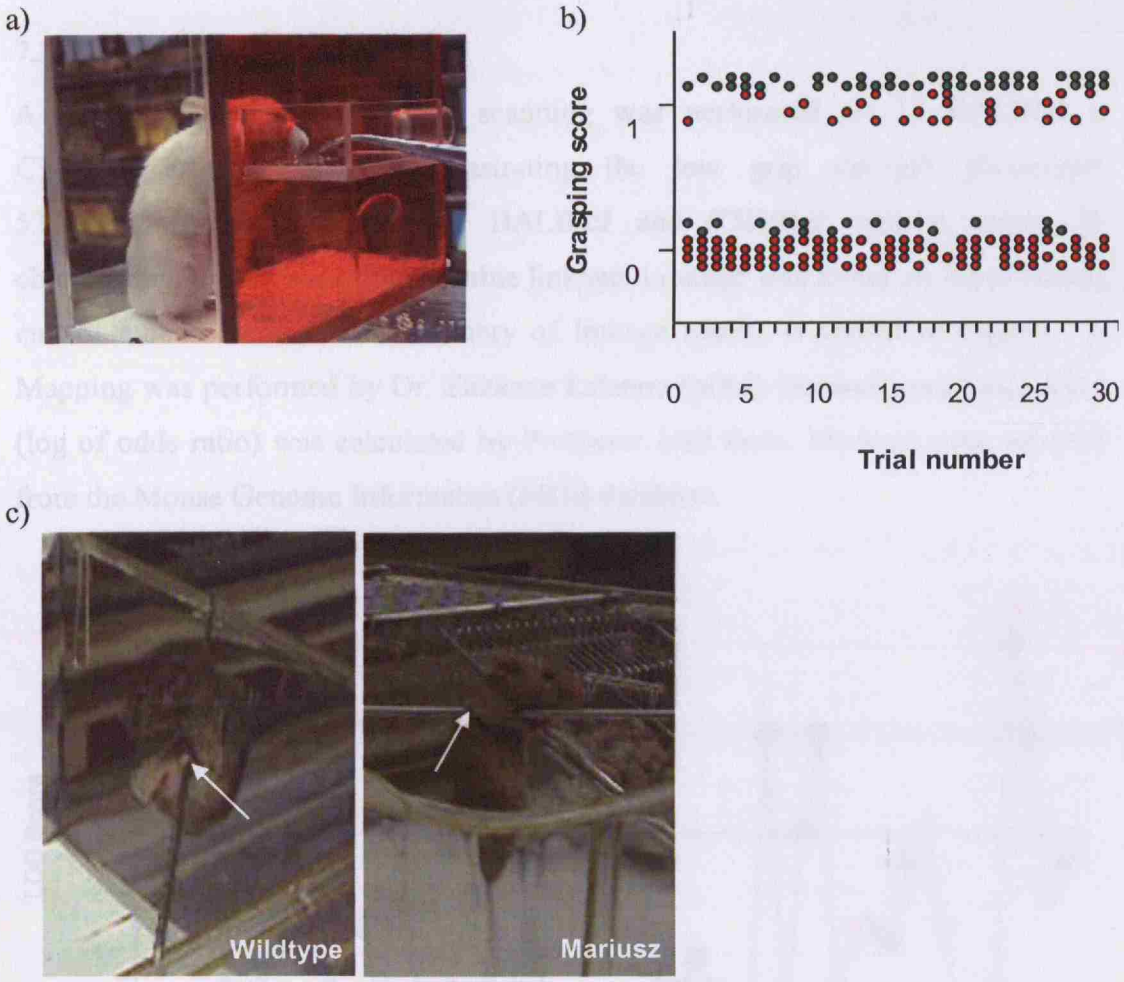

Figure 7.3. MoRAG and wire manoeuvre test. a) MoRAG test setup showing a mouse in a plexiglass box with an opening for the mouse to reach and grasp for the food pellet. b) Cumulative dot plots showing scoring of grasping performance of Mariusz mice (●) compared to wildtype littermates (●). Mice were scored '1' if they succeeded in grasping the food pellet, and scored '0' if they failed to grasp. Mariusz mice (n=4) and wildtype littermates (n=2) were tested for 30 trials over 2 days. From the graph, it is obvious that Mariusz mice have poorer grasping performance compared to wildtype littermates. c) Wire manoeuvre test demonstrating the difference in paw and arm use to support body weight when suspended on wire. Mariusz mice use their arms, whereas wildtype littermates use their paws (indicated by arrows) to stay on the wire.

7.3.3 Mapping

A low resolution genome-wide scanning was performed on 13 BALB/cJ x C3H/HeJ affected mice demonstrating the low grip strength phenotype. 53 polymorphic SNPs between BALB/cJ and C3H/HeJ, spaced across 19 chromosomes, were used to determine linkage. Linkage was found on the proximal end of chromosome 18. A summary of linkage results is shown in Figure 7.4. Mapping was performed by Dr. Zuzanne Lalanne (MRC, Harwell) and LOD score (log of odds ratio) was calculated by Professor Neil Dear. Markers were selected from the Mouse Genome Informatics (MGI) database.

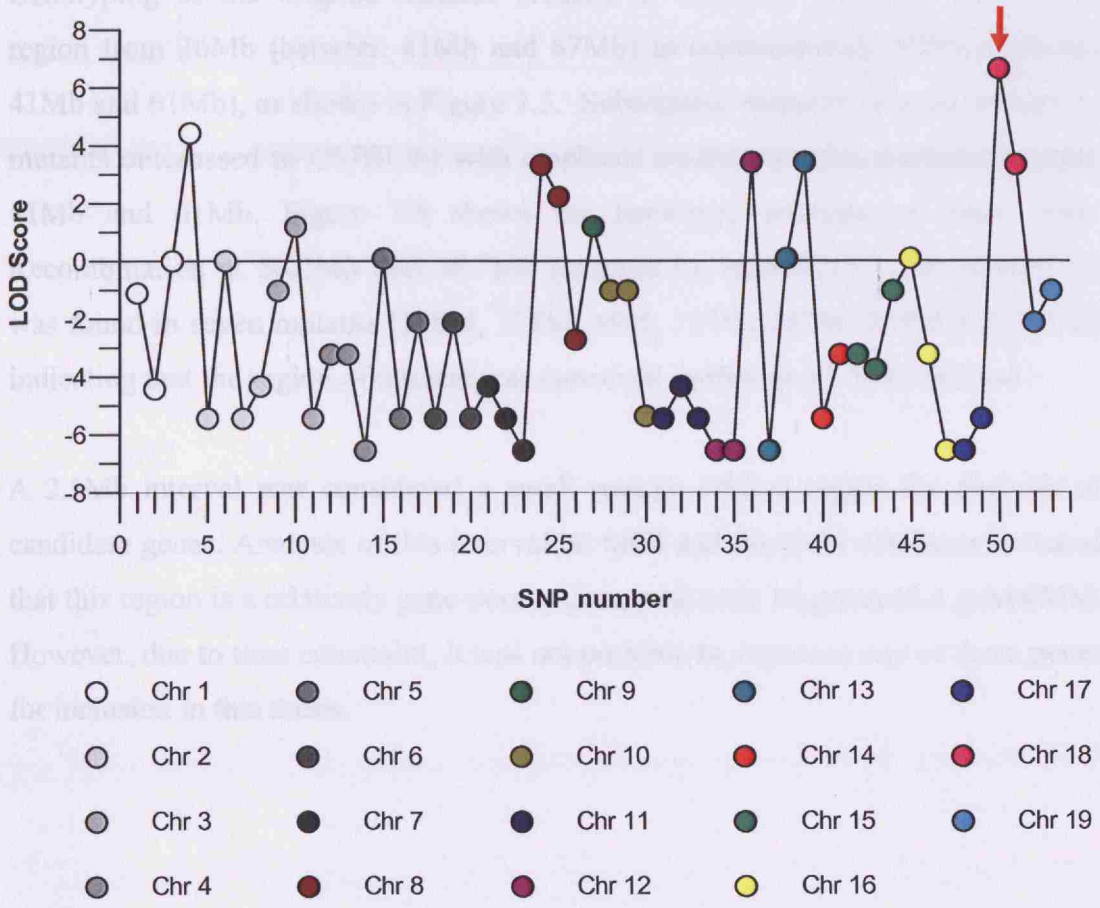

Figure 7.4. A genome wide scan for linkage was performed on 13 affected mice presenting the Mariusz phenotype (C3H/HeJ x BALB/c). 53 SNPs were used, and linkage was determined to be on chromosome 18 (red arrow), with the highest LOD score of >6.0 corresponding to a SNP at 62Mb. Each set of coloured circles corresponds to a set of SNPs on the same chromosome.

Initial fine mapping was performed by genotyping of microsatellite markers and SNPs which were polymorphic for BALB/cJ and C3H/HeJ between 41Mb and 67Mb on chromosome 18. However, because there was a common haplotype block between 45Mb and 56Mb in BALB/cJ and C3H/HeJ, it was not possible to fine map further on the C3H/HeJ background. To overcome this problem, Mariusz mice were outcrossed to C57BL/6J to generate more recombinants with informative markers from C57BL/6J. The markers used and the polymorphisms between BALB/cJ, C3H/HeJ and C57BL/6J are summarized in Table 7.1, and in full detail in Appendix A.

Genotyping of the original mutants crossed to C3H/HeJ narrowed the critical region from 26Mb (between 41Mb and 67Mb) to approximately 20Mb (between 41Mb and 61Mb), as shown in Figure 7.5. Subsequent mapping was performed on mutants outcrossed to C57BL/6J with emphasis on polymorphic markers between 41Mb and 61Mb. Figure 7.6 shows the haplotype analysis of these mice. Recombination at 56.2Mb and 58.7Mb (marked by rs13483373 and rs6309214) was found in seven mutants (128M, 177M, 49M, 127M, 147M, 278M and 301M) indicating that the region of interest was narrowed further to a 2.5Mb interval.

A 2.5Mb interval was considered a small enough critical region for analysis of candidate genes. Analysis of this interval on MGI and Ensembl databases revealed that this region is a relatively gene-poor region, with only 16 genes (6.4 genes/Mb). However, due to time constraint, it was not possible to sequence any of these genes for inclusion in this thesis.

Table 7.1. Microsatellite markers and SNPs polymorphic for BALB/cJ and C3H/HeJ or C57BL/6J. Markers were selected from MGI database. Map positions of microsatellite markers were based on Ensembl/NCBI build 36, and SNP positions were based on Ensemble/dbSNP128.

Marker	Location (bp)	Polymorphism (size or nucleotide)		
		BALB/cJ	C3H/HeJ	C57BL/6J
D18Mit177	41108480	196	168	172
D18Mit202	43517266	143	143	111
D18Mit105	53209717	149	149	137
D18Mit123	56095974	125	122	116
rs13483373	56201703	G	A	A
D18Mit238	57147126	122	126	122
D18Mit124	57582856	149	139	151
rs6309214	57616306	C	C	T
D18Mit181	58120164	146	150	150
rs8239209	58169287	C	T	C
D18Mit52	58462984	130	132	140
rs6338896	58717533	C	T	T
D18Mit28	60303417	222	224	222
rs13483389	60867522	C	T	T
D18Mit78	60934044	132	134	134
D18Mit51	61264745	154	198	198
D18Mit152	62062136	148	142	142
D18Mit139	62535609	128	126	124
rs4231898	62663769	A	C	C
D18Mit161	65803001	163	167	169
D18Mit209	67091136	86	122	124

Figure 7.5. Haplotype analysis of original Mariusz mutants on BALB/cJ x C3H/HeJ. Number in each cell denotes genotype (0 = BALB/cJ, 1 = C3H/HeJ, 2 = BALB/cJ x C3H/HeJ). Each cell is coloured with a different colour corresponding to the genotype.

Marker Location (bp)		**D18Mit177** 41108480	**rs13483373** 56201703	**D18Mit124** 57582856	**rs8239209** 58169287	**D18Mit78** 60934044	**D18Mit51** 61264745	**rs4231898** 62663769	**D18Mit209** 67091136
Mouse ID	**Phenotype**								
1.4f	Mariusz	0	0	0	0	2	2	2	2
6.3c	Mariusz	1	0	0	0	2	2	2	2
8.2a	Mariusz	1	0	0	0	2	2	2	2
2.6i	Mariusz	2	0	0	0	0	2	2	2
2.11	Mariusz	2	0	*fail	0	0	0	*fail	2
2.6d	Mariusz	2	0	0	0	0	2	*fail	2
2.6j	Mariusz	2	0	0	0	0	2	0	2
6.3h	Mariusz	1	0	0	0	0	0	0	2
14.1f	Mariusz	1	0	0	0	0	0	0	2
8.5b	Mariusz	1	0	0	0	0	0	*fail	2
15.1f	Mariusz	1	*fail	0	0	0	0	0	2
7.7b	Mariusz	1	*fail	0	0	0	0	0	2
7.8e	Mariusz	1	*fail	0	*fail	0	0	0	2
15.2b	Mariusz	1	*fail	0	*fail	0	0	0	0
5.5b	Wildtype	1	2	*fail	2	2	2	2	2

* Indicate failed genotyping at this locus.
Markers failed in genotyping: D18Mit123, D18Mit238, D18Mit181, D18Mit52, D18Mit28, D18Mit152, D18Mit139, and D18Mit161

Figure 7.6. Haplotype analysis of Mariusz mutants outcrossed to C57BL/6J. Number in each cell denotes genotype (0 = BALB/cJ, 1 = C57BL/6J, 2 = BALB/cJ x C57BL/6J). Each cell is coloured with a different colour corresponding to the genotype. Black bar highlights the 2.5Mb critical interval.

Marker Location (bp)		**D18Mit202** 43517266	**D18Mit105** 53209717	**rs13483373** 56201703	**rs6309214** 57616306	**rs6338896** 58717533	**rs13483389** 60867522
Mouse ID	**Phenotype**						
49M	Mariusz	0	0	0	0	2	2
127M	Mariusz	0	0	0	0	2	2
147M	Mariusz	0	0	0	0	2	2
278M	Mariusz	0	0	0	0	2	2
301M	Mariusz	0	0	0	0	2	2
84M	Mariusz	0	0	0	0	0	2
85M	Mariusz	0	0	0	0	0	2
106M	Mariusz	0	0	0	0	0	2
240M	Mariusz	0	0	0	0	0	2
128M	Mariusz	2	2	2	0	0	0
177M	Mariusz	2	2	2	0	0	0
242M	Wildtype	2	2	2	2	2	0
206M	Wildtype	1	2	2	2	2	0
176M	Wildtype	1	1	2	2	2	0
202M	Wildtype	1	1	1	1	1	0

7.4 Discussion and conclusion

Although it is beyond the scope of this thesis to present a detailed phenotypic characterization of Mariusz mice, for completion purpose of this discussion it is important to mention that in addition to weak grip strength, Mariusz mice also exhibit digit abnormalities in their hindlimbs when examined under X-ray and when stained with Alcian Blue/Alizarin Red (Figure 7.7) (personal communication with Professor Neil Dear). The phenotype penetrance of digit abnormalities is 100% but the expressivity is variable. The expressivity can be in combinations of either one or more of triphalangy of the big toe and syndactyly of two or more adjacent digits.

Based on these phenotypes, it was possible to search for parallel abnormalities observed in human disorders which may give additional clues as to which gene, when mutated, may be responsible for the Mariusz phenotype. It was found that syndactyly is a relatively common congenital malformation of the hand (Percival and Sykes 1989) often with no known genetic basis and there is also a human syndrome that has similar abnormalities to Mariusz, known as Poland's syndrome. The syndrome is either spontaneous or has a familial genetic basis. Patients with Poland's syndrome have unilateral hypoplasia of their upper limbs and chest muscles, and also syndactyly (Fokin and Robicsek 2002).

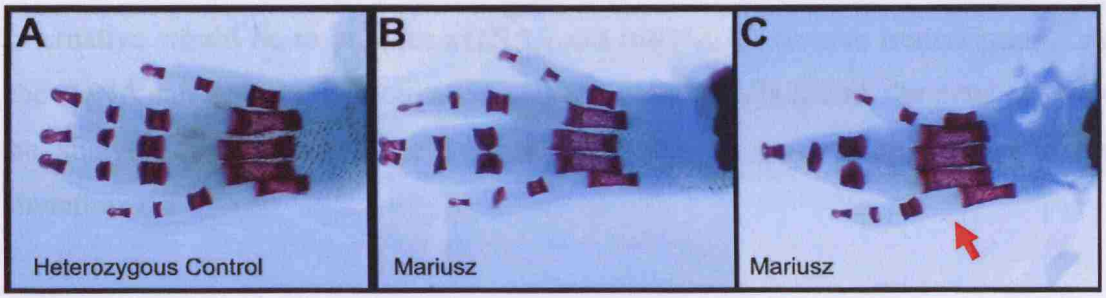

Figure 7.7. Examples of digit abnormalities observed in Mariusz mice. Images show hindlimbs of P7 mice stained with Alcian Blue/Alizarin Red. Alcian Blue/Alizarin Red is a differential stain for bone (purple) and cartilage (blue) (McLeod 1980;Kimmel and Trammell 1981). a) Littermate heterozygous control, b) Mariusz soft tissue syndactyly of toes 3 and 4, c) Syndactyly of toes 2, 3, and 4 with fusion of the distal phalanges (red arrow). (Figure from Professor Neil Dear).

Taken together and from searches through the Ensembl database (Figure 7.8), 5 of 16 genes found within the narrowed critical region were likely candidates, based on their reported or predicted protein functions, phenotypes of knockout mouse models or previously reported implications in humans (Table 7.2). The 5 genes are fibrillin 2 (*Fbn2*), multiple EGF-like-domains 10 (*Megf10*), GRAM domain containing 3 (*Gramd3*), aldehyde dehydrogenase family 7, member A1 (*Aldh7a1*) and cortexin 3 (*Ctxn3*). Homozygous null mice for lamin B1 (*Lmnb1*) display neonatal lethality (OMIM 2007b), thus making *Lmnb1* a less likely candidate since the recessive mutation in Mariusz is not lethal. Other genes seem to be less likely because they have not been reported to be involved in any neurological or musculoskeletal functions. However, it is not possible to rule out definitively the involvement of any of these genes until they are sequenced to confirm that there are indeed no mutations.

Although the mutation was not found in the course of this study, the fine mapping results obtained thus far will be useful to facilitate future work of candidate gene sequencing. With the shortlisted genes in hand, the next step is to sequence the top 5 priority genes, and to follow through with the remaining genes. This can be done by sequencing each exon (inclusive of a short stretch, at least 30bp, of flanking intronic sequence) in a gene to detect any protein coding sequence and splice donor/acceptor mutations. However, for genes with many exons, an example is the *Fbn2* gene with 65 exons, this is not an economical and efficient approach. The alternative would be to produce cDNA from mRNA by reverse transcription, and the cDNA can be directly sequenced. Once the mutation is found, the gene can then be analysed to determine the normal and defective gene function due to the mutation.

Figure 7.8. Critical interval of Mariusz between 56.2Mb and 58.7Mb. Snapshot was taken from Ensembl database (www.ensembl.org).

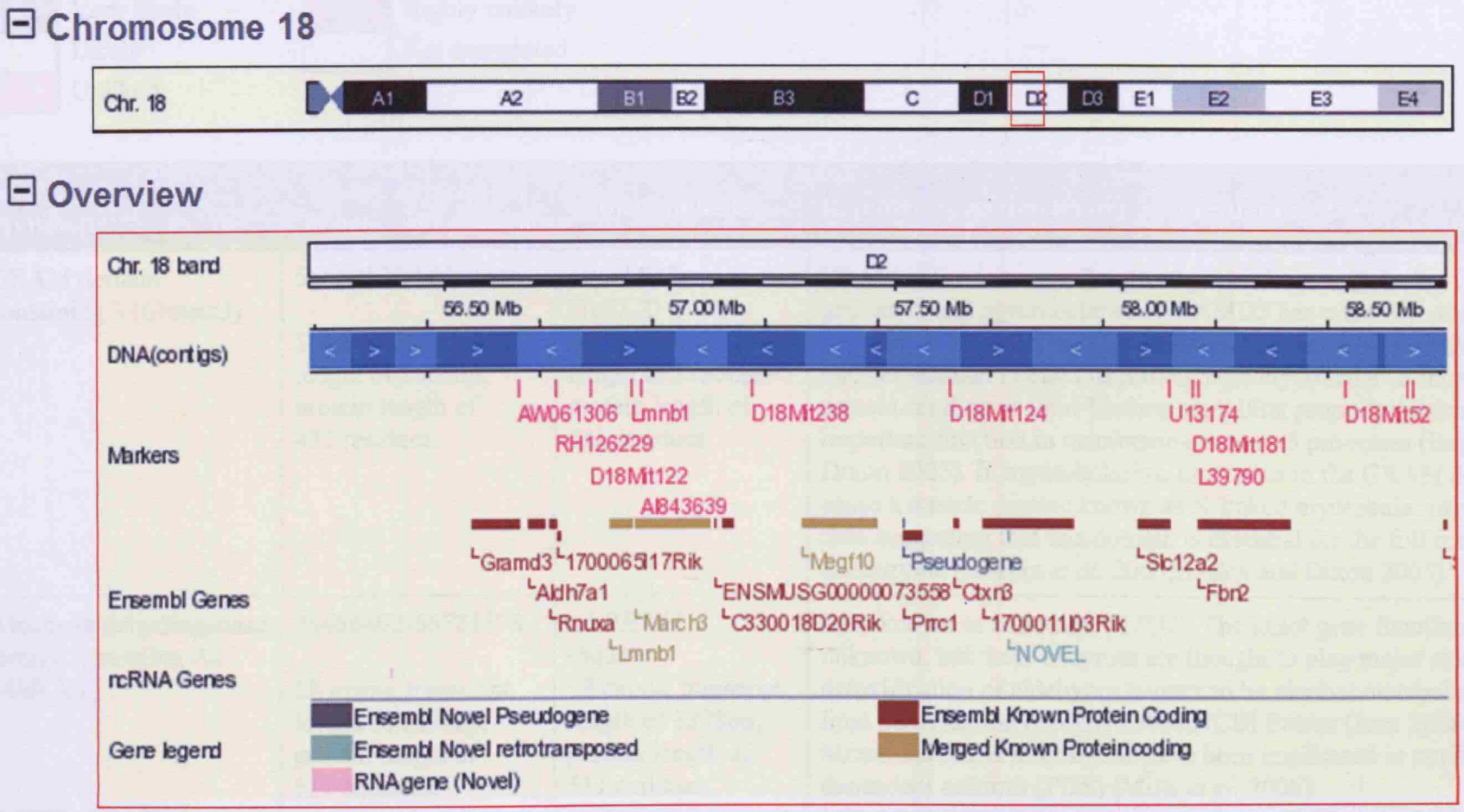

Table 7.2. Description of genes (from Ensembl database) and human homologues with reported or predicted gene function(s). Each row is coloured to indicate likelihood of mutation being found in the corresponding gene that might be responsible for the Mariusz phenotype.

Very likely
Likely
Unlikely
Highly unlikely
Not designated

Mouse gene name (Symbol)	Locus, description of gene and protein	Human homologue	Reported gene function(s)/ implications in disease
GRAM domain containing 3 (*Gramd3*)	56560139-56663446 14 exons, transcript length of 2605bp, protein length of 432 residues.	*GRAMD3* (5q23.2) 14 exons, transcript length of 2895bp, protein length of 432 residues	GRAM is the acronym for glucosyltransferases, Rab-like GTPase activators and myotubularins. GRAMD3 has unknown protein function, but prediction of the protein function based on the GRAM domain is that this protein is likely to have an intracellular protein-binding or lipid-binding signalling property, which has an important function in membrane-associated processes (Begley and Dixon 2005). In myotubularins, mutations in the GRAM domain cause a muscle disease known as X-linked myotubular myopathy, thus suggesting that this domain is essential for the full function of the enzyme (Doerks *et al.* 2000;Begley and Dixon 2005).
Aldehyde dehydrogenase family 7, member A1 (*Aldh7a1*)	56686402-56721878 18 exons, transcript length of 1824bp, protein length of 511 residues.	*ALDH7A1* (5q31) 18 exons, transcript length of 1878bp, protein length of 511 residues.	Also known as antiquitin (*ATQ1*). The exact gene function is unknown, but these enzymes are thought to play major role in detoxification of aldehydes generated by alcohol metabolism and lipid peroxidation (OMIM 2007a;NCBI Entrez Gene 2008a). Mutations found in this gene have been implicated in pyridoxine-dependent seizures (PDS) (Mills *et al.* 2006).

Mouse gene name (Symbol)	Locus, description of gene and protein	Human homologue	Reported gene function(s)/ implications in disease
RNA U, small nuclear RNA export adaptor (Rnuxa)	56732665-56747156 5 exons, transcript length of 1543bp, protein length of 385 residues.	*RNUXA* (5q23.2) 5 exons, transcript length of 1751bp, protein length of 394 residues.	Also known as phosphorylated adaptor for RNA export (*PHAX*). Functions as a regulator in small nuclear RNA (snRNA) nuclear export (OMIM 2001). *RNUXA* has been shown to be involved with the SMN complex in the assembly of small nuclear ribonucleoprotein (snRNP) (Massenet *et al.* 2002).
Lamin B1 (*Lmnb1*)	56867467-56913076 11 exons, transcript length of 2841bp, protein length of 588 residues.	*LMNB1* (5q23.3). 11 exons, transcript length of 2882bp, protein length of 586 residues.	Lamin is a component of the interphase nuclear lamina which is required for the maintenance of nuclear shape and mechanical integrity. Homozygous null mice display neonatal lethality with defects in lungs and bones (respiratory distress, abnormal lung, craniofacial, and skeletal morphology, impaired ossification, reduced embryo size). Cultured fibroblast from mutant embryos also showed impaired cellular proliferation and differentiation, premature senescence and abnormal nuclear morphology (OMIM 2007b).
Membrane-associated ring finger (C3HC4) 3 (*March3*)	56921370-57085202 4 exons, transcript length of 860bp, protein length of 253 residues.	*MARCH3* (5q23.2) 5 exons, transcript length of 1797bp, protein length of 253 residues.	Also known as E3 ubiquitin-protein ligase MARCH3. The exact protein function is undetermined. The predicted function based on predicted motifs and domain is that this protein maybe involved in mRNA turnover and stability (OMIM 2008).

Mouse gene name (Symbol)	Locus, description of gene and protein	Human homologue	Reported gene function(s)/ implications in disease
Multiple EGF-like-domains 10 (*Megf10*)	57292744-57457118 25 exons, transcript length of 7511bp, protein length of 1147 residues.	*MEGF10* (5q33) 26 exons, transcript length of 7524bp, protein length of 1140 residues.	The exact gene function is undetermined. *MEGF10*, expressed mainly in brain, has been shown to interact with clathrin assembly protein complex 2 medium chain, which is involved in endosome trafficking and in the formation of large vacuoles (Suzuki and Nakayama 2007)
Proline-rich coiled-coil 1 (*Prrc1*)	57514395-57552373 9 exons, transcript length of 4793bp, protein length of 443 residues.	*PRRC1* (5q23.2) 9 exons, transcript length of 4658bp, protein length of 445 residues.	Gene function is undetermined.
Cortexin 3 (*Ctxn3*)	57628181-57637763 2 exons, transcript length of 1406bp, protein length of 80 residues.	*CTXN3* (5q23.2) 3 exons, transcript length of 1660bp, protein length of 81 residues.	Gene function is undetermined. *CTXN* is highly conserved across species and is selectively expressed in kidney and brain, indicating specific involvement of this protein in kidney and brain tissue function (NCBI Entrez Gene 2008b).

Mouse gene name (Symbol)	Locus, description of gene and protein	Human homologue	Reported gene function(s)/ implications in disease
Solute carrier family 12, member 2 (*Slc12a2*)	58037369-58106475 27 exons, transcript length of 7483bp, protein length of 1206 residues.	*SLC12A2* (5q23.3) 27 exons, transcript length 6859bp, protein length of 1212 residues.	Also known as sodium-potassium-chloride transporter 1 (*NKCC1*). Functions in aiding movement of chloride across secretory and absorptive epithelia. Knockout models causes deafness in mice (Dixon *et al.* 1999).
Fibrillin 2 (*Fbn2*)	58168277-58369580 65 exons, transcript length of 10480bp, protein length of 2907 residues.	*FBN2* (5q23-q31) 65 exons, transcript length of 10724bp, protein length of 2912 residues.	*FBN2* is developmentally expressed and plays an essential role in directing elastic fibre formation. Mutations in this gene have been implicated in congenital contractural arachnodactyly (OMIM 2005). Knockout model has syndactyly (Chaudhry *et al.* 2001).
Solute carrier family 27 (fatty acid transporter), member 6 (*Slc27a6*)	58715894-58772523 10 exons, transcript length of 2598bp, protein length of 619 residues.	*SLC27A6* (5q23-q31) 10 exons, transcript length of 2838bp, protein length of 619 residues.	Also known as fatty acid transport protein 6 (*FATP6*). Functions in facilitating uptake of long fatty acids (OMIM 2004). *SLC27A6* has been implicated in the pathogenesis of lipid-related cardiac disorders (NCBI Entrez Gene 2008c).

Chapter 8 Arl - New mouse strain of motor neuron dysfunction

8.1 Chapter aim

Abnormal rear legs (Arl) is a new mouse strain of motor neuron dysfunction and is allelic to another neurodegenerative mouse model called Legs at odd angles (Loa). The aim of this thesis chapter was to investigate if the Arl mice have a more severe disease phenotype compared to the Loa mice in terms of their retrograde axonal transport function.

8.2 Introduction

The axonal transport system in motor neurons plays an important role in making sure that motor neurons have an efficient intracellular network in communicating survival signals, organelles (mitochondria), subcellular organelles (membranous vesicles carrying growth factors or neurotransmitters) and cytosolic proteins or elements of the cytoskeletal matrix (Schwartz and Westbrook 2000) between the cell body and the distal end of the axon.

Trafficking of cargoes from the cell body towards the axon terminal is known as anterograde transport, whereas the reverse movement is known as retrograde transport. Classically, axonal transport is grouped based on the bulk speed of cargo movements. Cargoes transported at more than 400mm/day is categorized as fast axonal transport and slow axonal transport has speeds between 0.2 and 5mm/day (Schwartz and Westbrook 2000). Kinesin (anterograde) and cytoplasmic dynein (retrograde) are the main molecular motors responsible for the movement of both fast and slow axonal transport.

Mutations in the kinesin and dynein motors have been implicated in several neurodegenerative diseases. Examples of diseases caused by mutations in some members of the kinesin superfamily are hereditary spastic paraplegia (HSP) and

Charcot-Marie-Tooth disease (CMT) which were caused by mutations in KIF5A and KIF1Bβ, respectively (De Vos *et al.* 2008). Of interest in this chapter are the mutations in the dynein machinery responsible for retrograde axonal transport (rAT). The dynein machinery is made up of the cytoplasmic dynein (a multisubunit complex containing dynein heavy, intermediate and light intermediate chains) and dynactin (Hirokawa 1998). It has been shown that mutations in the dynactin subunit $p150^{Glued}$ are causal in a form of motor neuron disease (Puls *et al.* 2003;Munch *et al.* 2004) and mutations in the dynein heavy chain (*Dync1h1*) in mice cause motor neuron degeneration (Hafezparast *et al.* 2003). The Legs at odd angles (Loa) and Cramping 1 (Cra1) mice are examples of neurodegenerative mouse models which have mutations in *Dync1h1*.

Abnormal rear legs (Arl), is a novel mouse strain with a different point mutation in *Dync1h1* (W1206R). In the initial examination of homozygous Arl mice (*Arl/Arl*) it was observed that the embryonic development of these mice were severely impaired compared to homozygous Loa mice (*Loa/Loa*) (Schiavo, G. unpublished data). Based on this observation, it was hypothesized that the heterozygous Arl (*Arl/+*) mice might have a more severe phenotype compared to the heterozygous Loa (*Loa/+*) mice in terms of their axonal transport function. To confirm this hypothesis, in collaboration with Dr. Matthew Golding at the Cancer Research UK London Research Institute, the motor neuron rAT function, in terms of the rate of cargo trafficking, of *Arl/+* mice was investigated and compared to previously published rAT rate of *Loa/+* mice (Kieran *et al.* 2005).

8.3 Results

8.3.1 Normal axonal transport rate in *Arl/+* mice

The retrograde axonal transport rate in E13.5 embryonic motor neurons from *Arl/+* mice and wildtype littermates was monitored using an established protocol (Kieran *et al.* 2005) based on the uptake of exogenously applied fluorescently labelled tetanus toxin (TeNT-Hc-Alexa488). TeNT-Hc-Alexa488 served as carriers which were monitored in real-time and videoed using low light microscopy. From the movies captured from imaging, the movements of these carriers were tracked and the velocities and displacements were calculated and plotted in a speed-distribution profile, as shown in Figure 8.1. The relative frequency was calculated by dividing the number of single movements at a specific speed by the total number of single movements.

Motor neurons from 8 *Arl/+* mice and 3 wildtype littermate embryos were used to monitor the rAT rate. From Figure 8.1, it is shown that there is no significant difference in the movement of carriers between motor neurons from wildtype and *Arl/+* mice. Figure 8.2 is reproduced from published results in (Kieran *et al.* 2005) showing the rAT rates in embryonic motor neurons from *Loa/+*,SOD1^{G93A}, and tgSOD1^{G93A} mice (*Loa/+*,SOD1^{G93A} mice are offsprings from the mating of *Loa/+* to tgSOD1^{G93A} mice). By comparing Figure 8.1 and Figure 8.2, it seems as if there is a slight difference in the overall pattern of the carrier speed distribution profile. However, this difference is not significant. In the experiments carried out for this thesis, in order to generate data which will be directly comparable to previously reported data, shown in Figure 8.2, results obtained here were collated and analysed from two independent experiments. In each experiment, motor neurons from wildtype littermates were included and used for the direct comparison to motor neurons from *Arl/+* mice. Therefore, the slight gross overall difference in the pattern of the speed distribution profile between motor neurons from *Loa/+* and *Arl/+* mice is negligible when compared to their respective wildtype littermate controls. The tracking of the carriers was performed by a single operator and blind to genotype, which was later decoded, to ensure that additional bias in carrier tracking was minimised.

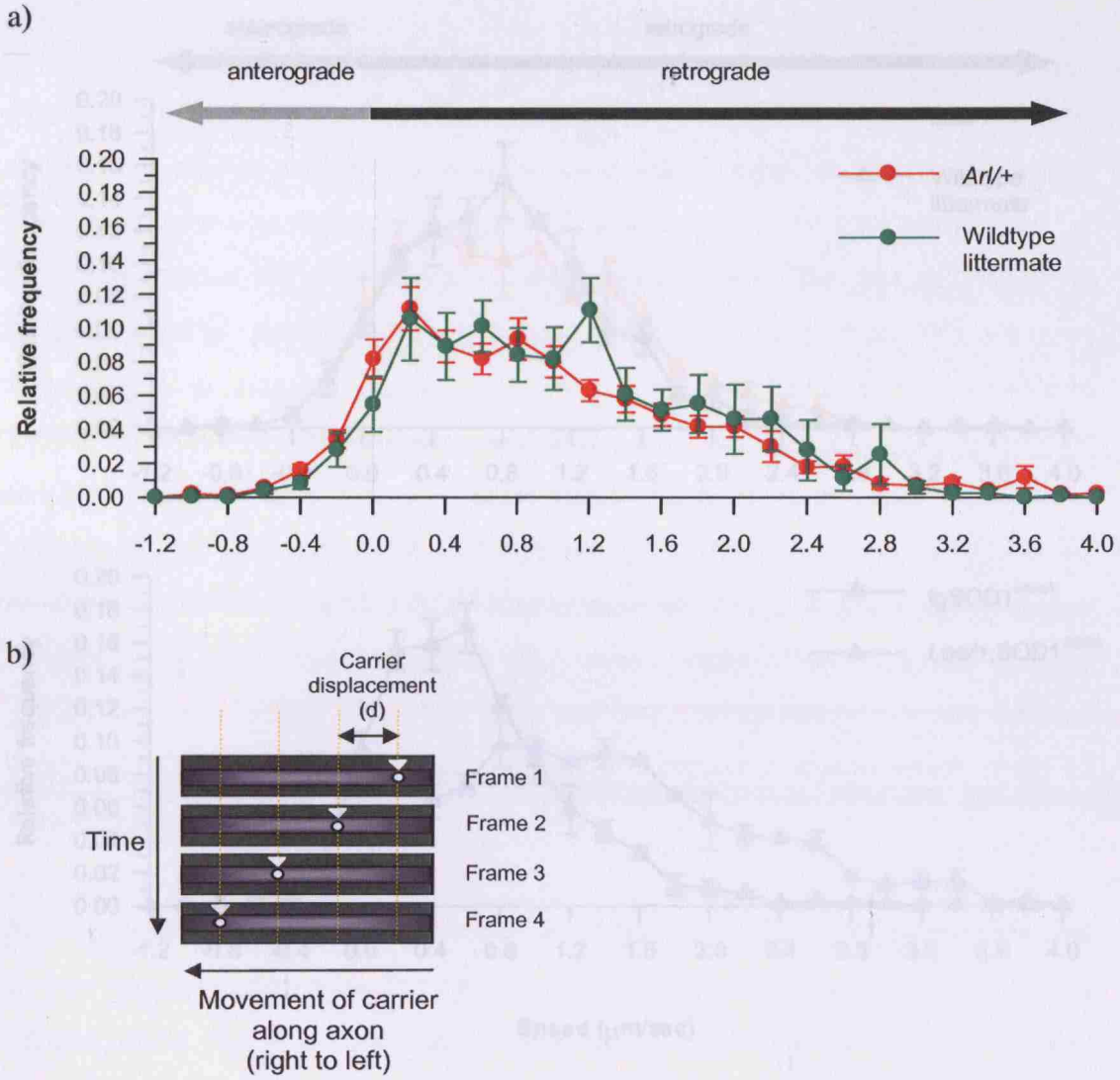

Figure 8.1. Speed profile of axonal TeNT Hc-compartment of motor neurons from wildtype and *Arl/+* E13.5 embryos. The relative frequency on the y-axis was calculated by dividing the number of single movements at a specific speed by the total number of single movements. a) The relative frequency and speed of TeNT-Hc-Alexa488 carriers in *Arl/+* (n=8 embryos, 2348 single movements from 233 carriers) motor neurons is very similar to wildtype (n=3 embryos, 993 single movements from 87 carriers) motor neurons. Single movements of TeNT Hc-Alexa 488 carriers were plotted against their relative frequency. Retrograde transport is conventionally shown as positive, anterograde as negative and pauses during movement are grouped at 0µm/sec. b) A schematic illustrating tracking of single movements of a carrier (white circles) by following carrier displacements (arrow heads) in consecutive frames.

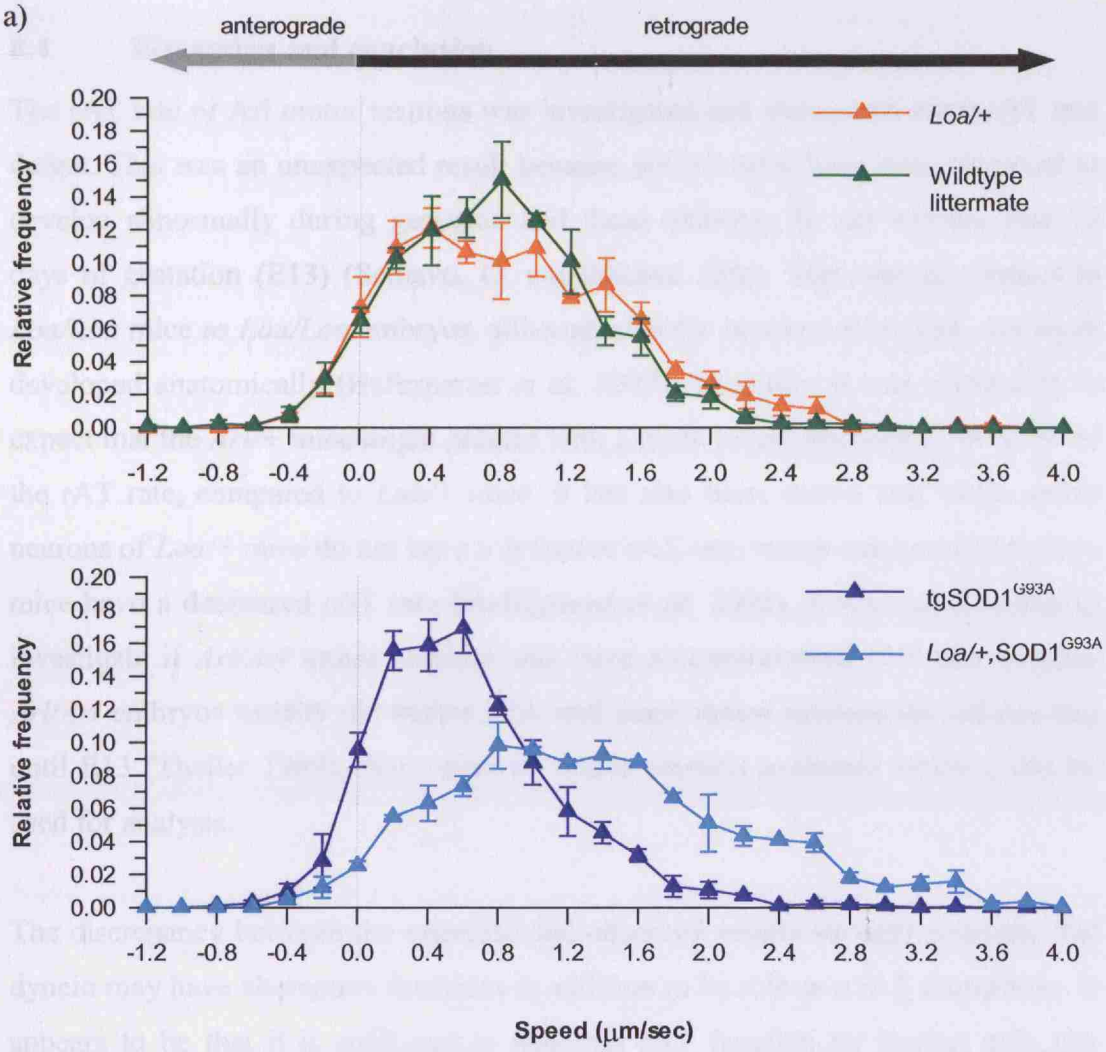

Figure 8.2. Speed profile of axonal TeNT-Hc-compartment of motor neurons from wildtype, *Loa*/+, tgSOD1^{G93A} and *Loa*/+,SOD1^{G93A} E13.5 embryos (Kieran *et al.* 2005). The average frequency and speed of TeNT-Hc-Alexa488 carriers in *Loa*/+ (n=3 embryos) motor neurons is very similar to wildtype (n=3 embryos) motor neurons. A change in rAT rate was determined by a change in the distribution curve of the speed profile when compared to the speed profile of wildtype motor neurons. A shift in the distribution curve to the right indicates an increase in rAT rate, whereas a decrease is represented by a shift to the left. From the bottom graph, there is a shift in the distribution curve compared to wildtype. There is a significant decrease and increase of rAT rate in tgSOD1^{G93A} (n=4 embryos) and *Loa*/+,SOD1^{G93A} (n=2 embryos) motor neurons, respectively. Retrograde transport is conventionally shown as positive, anterograde as negative and pauses during movement are grouped at 0μm/sec.

8.4 Discussion and conclusion

The rAT rate of Arl motor neurons was investigated and showed no overt rAT rate defect. This was an unexpected result because *Arl/Arl* mice have been observed to develop abnormally during gestation and these embryos do not survive past 13 days of gestation (E13) (Schiavo, G. unpublished data). This was in contrast to *Loa/Loa* mice as *Loa/Loa* embryos, although also die *in utero* or at birth, are more developed anatomically (Hafezparast *et al.* 2003). Therefore it was reasonable to expect that the *Arl/+* mice might present with a more severe phenotype, in terms of the rAT rate, compared to *Loa/+* mice. It has also been shown that while motor neurons of *Loa/+* mice do not have a defective rAT rate, motor neurons of *Loa/Loa* mice have a decreased rAT rate (Hafezparast *et al.* 2003). It was not possible to investigate if *Arl/Arl* motor neurons also have a compromised rAT rate because *Arl/Arl* embryos usually die before E13, and since motor neurons do not develop until E13 (Theiler 1989), there were no motor neurons available which could be used for analysis.

The discrepancy between the expected and observed results strongly suggests that dynein may have alternative functions in addition to its role as a rAT transporter. It appears to be that it is sufficient to maintain rAT function by having only one normal *Dync1h1* gene. Therefore, it may be possible that the neurodegenerative motor neuron phenotype might be caused by a secondary effect of the dysfunctional dynein on other cellular processes or homeostasis. Evidence supporting this possibility is the unexplainable interaction of an anti-oxidant protein, SOD1, with mutant dynein which resulted in an improved motor neuron disease phenotype in tgSOD1^{G93A} mice. This secondary effect appears to be mutation dependent, because although both Arl and Loa mice have mutations in the same gene, they clearly differ developmentally (when present in a homozygous state) but not in their rAT function in heterozygous animals. In addition, *Loa/+* and *Arl/+* mice have a normal lifespan ((Hafezparast *et al.* 2003) and unpublished data) indicating that although the mutation does cause dysfunction of motor neurons, it is unlikely solely due to the impairment of TeNT-Hc compartment based rAT because these animals do not have an observable rAT rate defect. This suggests

that impairment of the TeNT-Hc compartment based rAT alone is not sufficient to cause motor neuron dysfunction and it is possible that there could be other yet to be discovered "non-axonal" dynein-mediated roles which may be integral in survival maintenance. One possibility of such a "non-axonal" dynein-mediated role could be in the maintenance of mitochondrial membrane potential as it has been found that mitochondria in motor neurons of tgSOD1^{G93A} and *Loa*/+ mice have different polarization states (Bros, V., Greensmith, L. and Fisher E.M., unpublished data). As this is purely speculative, more work to investigate this possibility is necessary to fully understand the converging mechanisms involved in motor neuron survival.

From the work carried out in this chapter, it can be concluded that in terms of rAT function based on the rate of cargo trafficking, the *Arl*/+ mice do not have a more severe disease phenotype compared to the *Loa*/+ mice. It is also important to stress that although it appears that the rAT rate is not affected in the motor neurons of *Arl*/+ and *Loa*/+ mice, this is only true for the tracked compartment which is equivalent to the retrograde transport of small vesicles or endosomes, including the transport of nerve growth factor (NGF) (Lalli and Schiavo 2002). It is also known that mitochondria, although also transported by dynein, are transported and regulated differently from the transport of vesicles (Liu *et al.* 2007). Thus, the conclusion drawn here that there is no rAT defect only applies to transport of vesicles, and not for mitochondria.

Chapter 9 General discussion and future work

9.1 Looking at ALS from within the prion paradigm

ALS has been shown to arise from protein misfolding and shows many similarities to other protein misfolding neurodegenerative diseases like Alzheimer's and Parkinson's disease. These diseases are grouped together under the name of protein conformational disorders (Soto 2001). This group of diseases shows many biochemical, genetic, and neuropathological features supporting the idea that all protein misfolding and aggregation processes have the intrinsic possibility for transmissibility, although not necessarily in terms of human transmission, but certainly in terms of disease progression and spread within the same individual via cell-to-cell transmission of the toxic misfolded protein. Some indications supporting the idea are (Soto *et al.* 2006):

1) the presence of abnormal aggregates usually found in the main and neighbouring brain regions most damaged by the disease
2) mutations in the gene encoding for the misfolded protein produce inherited forms of the disease
3) transgenic animals expressing the human mutant gene for the misfolded protein develop some of the typical neuropathological and clinical characteristics of the human disease
4) misfolded protein aggregates produced *in vitro* are neurotoxic capable of inducing apoptosis

Results from *in vitro* fibrillization experiments, presented in this thesis, clearly support the 'seeding-nucleation' model which is frequently used to explain the infectious nature of prions. Furthermore, the *in vivo* relevance was demonstrated in seeding reactions using spinal cord homogenates of endstage tgSOD1^{G93A} mice where SOD1 oligomerization was accelerated suggesting that a 'seed' capable of causing SOD1 to oligomerize was present in the spinal cord homogenates of these

mice. An immunization study by Urushitani and colleagues showed that by immunizing tgSOD1^{G93A} mice with anti-human SOD1 antibody, mutSOD1 was cleared in the spinal cord and this was accompanied by alleviation of ALS symptoms and prolongation of the lifespan in these mice (Urushitani *et al.* 2007). This experiment shows remarkable similarities to other prion experiments, where it was demonstrated that immunotherapy treatment of anti-prion protein in prion-infected mice prolonged survival, and in some cases prevented disease progression even after clinical onset (Kalinke *et al.* 2006;Song *et al.* 2008).

In prion diseases, how these infectious proteins travel from extra-CNS sites to the CNS is unclear, but is thought that they travel via the peripheral nerves into the CNS, and from there cause propagative cell death (Heikenwalder *et al.* 2007). The clinical progression of ALS is one that starts asymmetrically affecting one part of the body and appears to cause 'spread' of disease to other parts of the body. On the cellular level, a gradient of motor neuron loss is also evident where loss is greatest at the onset site followed by neighbouring regions in the spinal cord (Ravits *et al.* 2007a;Ravits *et al.* 2007b). This shows similarities to the pattern of prion-induced cell death, and suggests that the propagative motor neuron death in SOD1-linked ALS, due to potentially toxic SOD1 oligomers, may follow a similar route. This raises the question of whether the architectural organisation of the motor system in the CNS has a role to play in causing the gradient pattern of motor neuron death in ALS.

9.2 Anatomical and genetic complexity of the CNS – is there a connection to disease focality and progression of ALS

If one considers how the motor system is organised in the CNS, an interesting observation with possible relevance to the pattern of ALS disease progression can be made from reviewing how lower motor neurons in the spinal cord (at different segments i.e. cervical, thoracic, lumbar, sacral and coccyx, and motor neurons located either medially or laterally of the ventral horn) make their connections with the upper motor neurons in the motor region of the cerebral cortex and the brainstem. To describe this observation, some background on the anatomical organization of the motor system in the CNS is necessary; main points of interest are obtained from the textbook Principles of Neural Science by Kandel *et al.* (2000), and are summarised briefly in paragraphs to follow and illustrated in Figures 9.1, 9.2 and 9.3.

The motor system is controlled via a three-level hierarchical organization, made up of the spinal cord, brain stem and the forebrain (motor and non-motor areas of the cerebral cortex). The motor areas can influence the spinal cord either directly or through the descending systems of the brain stem. All three levels are under the influence of two independent subcortical systems, which are the basal ganglia and the cerebellum, which both exert influence on the cerebral cortex through the relay nuclei in the thalamus but act directly on motor neurons in the brain stem (Figure 9.1). Although their precise contribution to motor action is still not clear, the cerebellum and basal ganglia are necessary for smooth movement and posture.

In the spinal cord, motor neurons (existing in clusters called motor nuclei forming longitudinal columns extending over 1 to 4 segments of the spinal cord) are organised spatially according to a proximal-distal rule where motor nuclei innervating the most proximal muscles (e.g. axial muscles of neck and back, shoulder girdle) lie most medially within the spinal cord while those innervating more distal muscles (e.g. elbow, wrist and digit muscles) are located progressively more laterally (Figure 9.2). These motor nuclei are interconnected across segments of the spinal by propriospinal interneurons (PI), where short PIs have shorter axons

interconnecting the lateral motor nuclei over fewer segments compared to long PIs with longer axons that branch extensively interconnecting the medial motor nuclei across several segments. Some long PIs extend through the entire length of the spinal cord therefore enabling coordination of movements of muscles involved in posture. The upper motor neurons (UMN) make connections with the lower motor neurons (LMN) via two pathways of descending bundles of UMN fibres called the lateral- and ventral-corticospinal tracts (Figure 9.3). Similar to the spatial organization rule for motor neurons, the lateral-corticospinal tracts terminate at the dorsolateral motor nuclei whereas the ventral-corticospinal tracts terminate at the ventromedial motor nuclei.

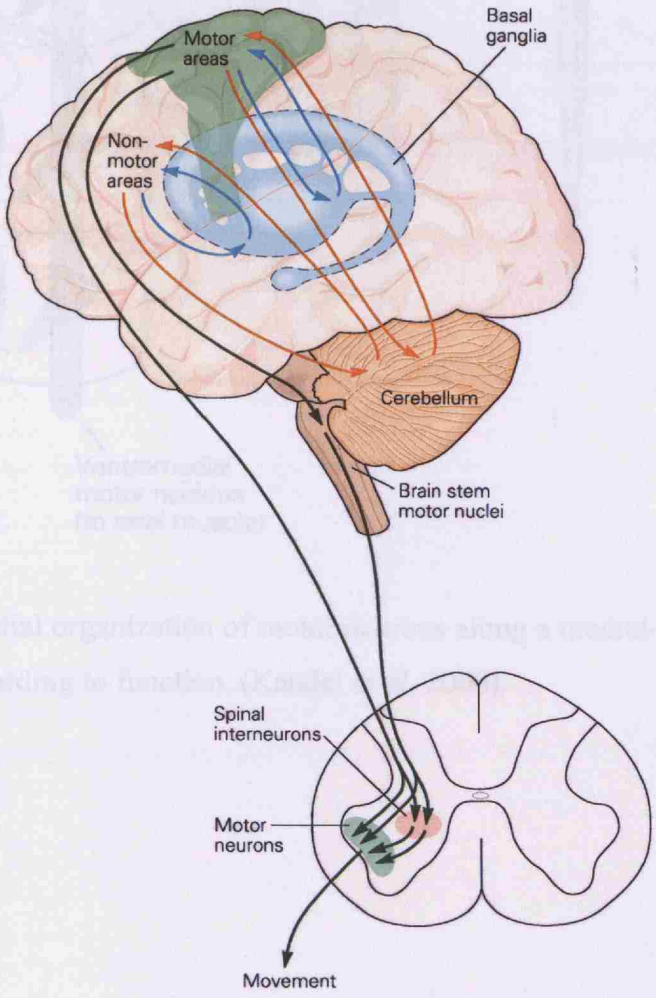

Figure 9.1. Hierarchical organization of movement at three levels of control – the spinal cord, brainstem and the forebrain. (Kandel *et al.* 2000).

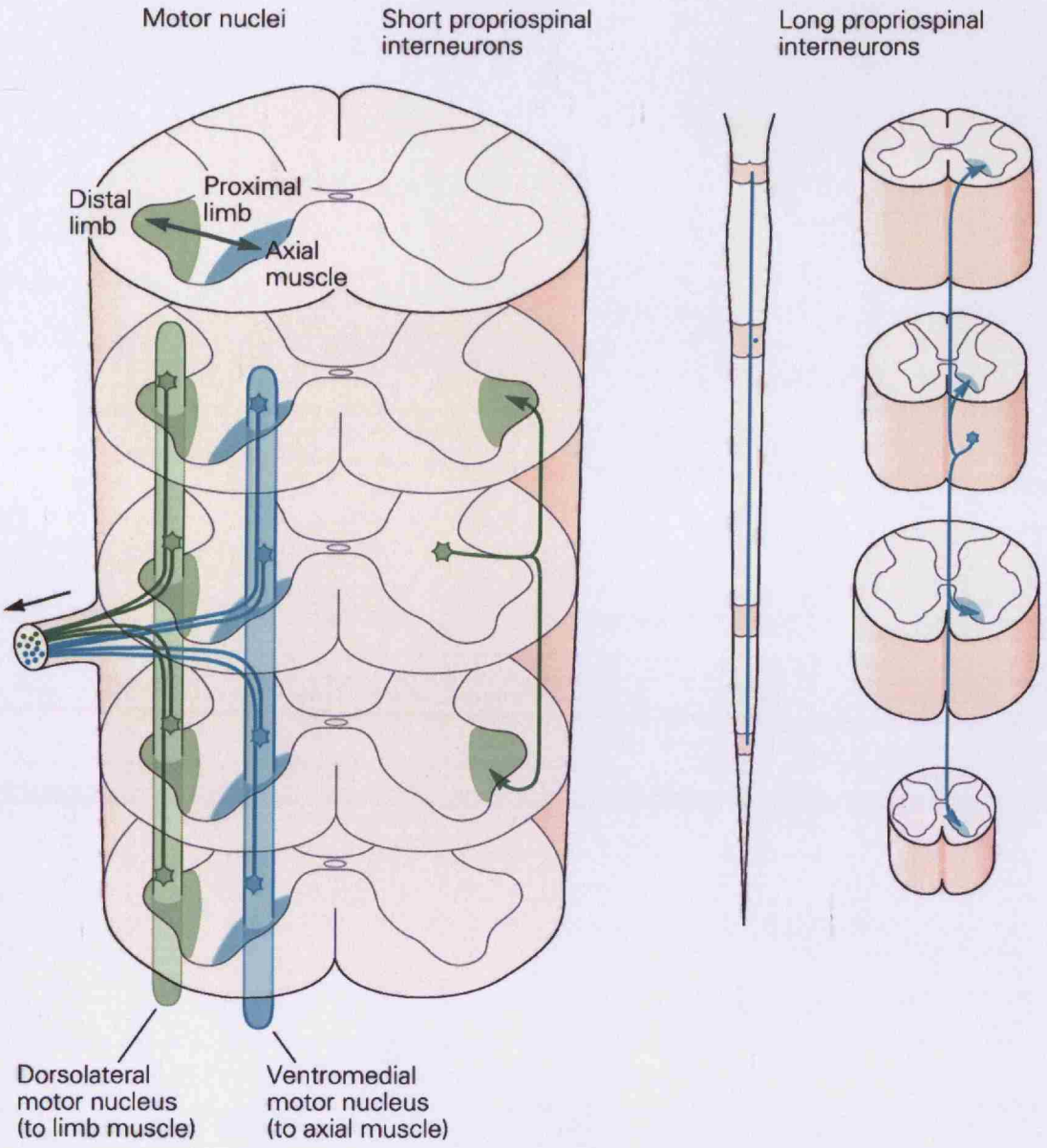

Figure 9.2. Spatial organization of motor neurons along a medial-lateral axis in the spinal cord according to function. (Kandel *et al.* 2000).

Figure 9.3. Spinal cord tracts. a) A cross-sectional view of the spinal cord showing the location of different fiber bundles (tracts) and run along the spinal cord. b) Descending pathways by which the motor cortex directly controls the motor neurons in the spinal cord. The ventralcorticol spinal tract (left) originates from the motor cortex of Broadmann area 4 and 6 and terminates bilaterally and sends collaterals to the medial pathways from the brainstem. The lateral corticolspinal tract originates in from two motor and three sensory areas which cross as the pyramidal decussation before descending to the dorsolateral column and terminating in the spinal gray matter. (Figures from Kandel *et al.* 2000).

(*con't* from **Figure 9.3.** Spinal cord tracts)

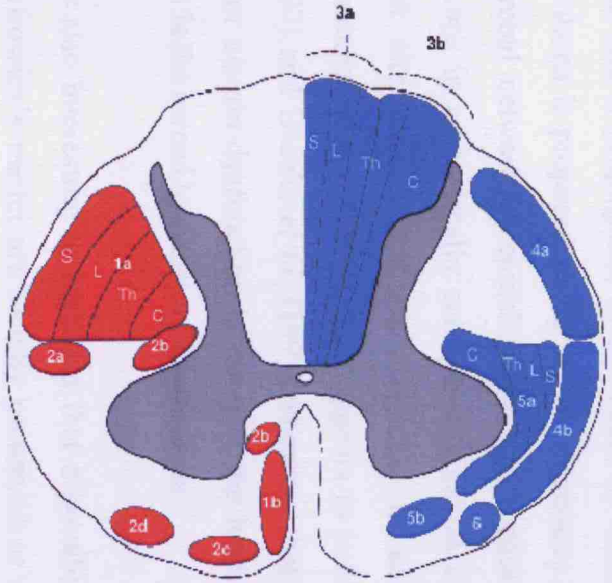

Motor and decending (efferent) pathways (left, red)

1. Pyramidal Tracts
1a. Lateral corticospinal tract
1b. Anterior corticospinal tract
2. Extrapyramidal Tracts
2a. Rubrospinal tract
2b. Reticulospinal tract
2c. Vestibulospinal tract
2d. Olivospinal tract

Somatotopy Abbreviations:
S: Sacral, **L: Lumbar**
Th: Thoracic, **C: Cervical**

Sensory and ascending (afferent) pathways (right, blue)

3. Dorsal Column Medial Lemniscus System
3a. Gracile fasciculus
3b. Cuneate fasciculus
4. Spinocerebellar Tracts
4a. Posterior spinocerebellar tract
4b. Anterior spinocerebellar tract
5. Anterolateral System
5a. Lateral spinothalamic tract
5b. Anterior spinothalamic tract

6. Spino-olivary fibers

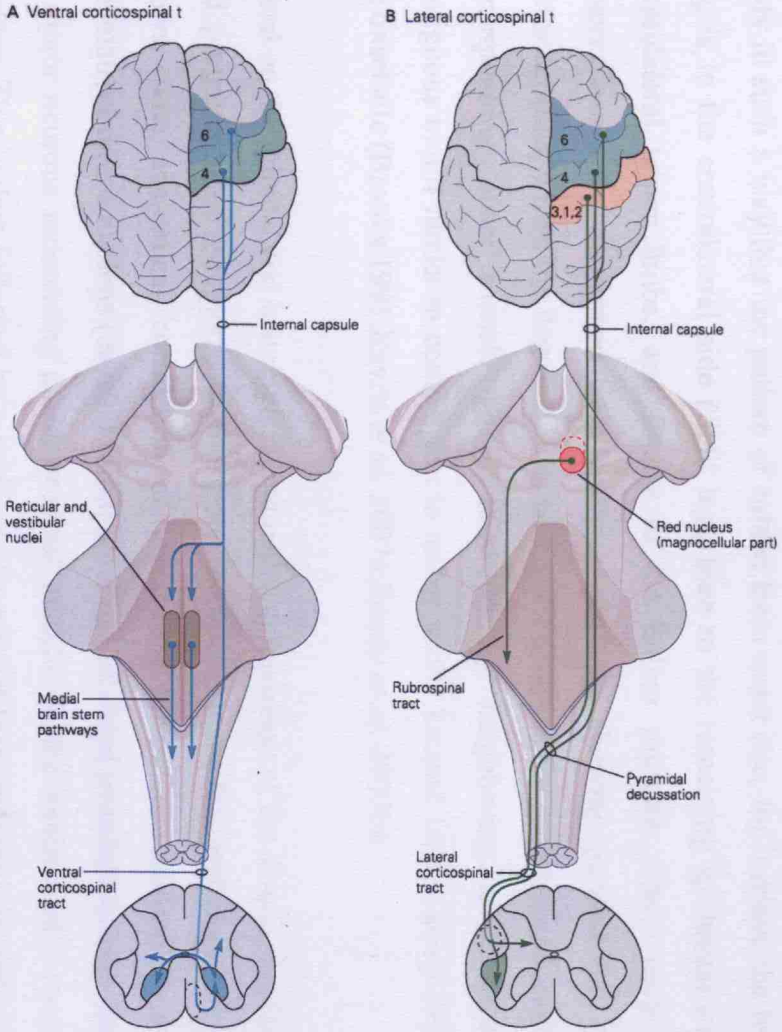

As mentioned previously, ALS is a progressive disorder with initial symptoms starting focally at one onset site, usually asymmetric, and it involves weakness in more distal extremities, followed by spread of symptoms to adjacent parts of the body in such a way that the pattern of spread from onset site, for instance the left leg, is to the contralateral side (right leg), then to the remaining ipsilateral and contralateral upper limbs, and finally to the bulbar muscles. These clinical observations were confirmed by histological findings showing parallel loss of motor neurons, where the degree of loss was more severe at the motor nuclei of the corresponding onset muscle group followed by neighboring anatomically contiguous motor nuclei in comparison to motor nuclei located farther away from the onset site (Brooks 1991;Ravits *et al.* 2007a;Ravits *et al.* 2007b).

Based on the clinical and histological findings, a comparison of the disease focality and progression of symptoms to the motor system (Figure 9.2 and Figure 9.3) shows some anatomical correlation of initial loss of motor neurons in the dorsolateral motor nucleus (causing initial paralysis of distal muscles) to later loss of motor neurons innervating more proximal muscles in the ventromedial motor nucleus. This is then followed by a gradient of neuronal loss 'moving' towards the upper motor neurons. In light of these observations, this correlation is suggestive of some sort of propagation of cell death by transmission of a 'factor' (which from this thesis is proposed to be SOD1 oligomers) from cell to cell, possibly via the neuronal network of spinal tracts, which could be used to explain why motor neurons in anatomically contiguous areas in the spinal cord (dorsolateral) from onset site are affected more quickly in comparison to more distant areas (ventromedial and UMN). This appears to hold true as reported by Ravits *et al.* (2007) and Brooks *et al.* (1991), showing that the spread to contiguous areas of motor neuron dysfunction is faster at the lumbar, cervical and brainstem regions than is the spread to non-contiguous areas.

It is also interesting to highlight that a possible reason why the oculomotor and Onufrowicz's nuclei are usually preserved or only mildly affected in ALS, and phrenic nerves innervating the respiratory muscles are only affected towards the terminal stages of the disease is because these motor neurons are located in the

ventromedial motor nuclei columns (Mannen *et al.* 1977;Schroder 1981;de Carvalho *et al.* 1996;Donzelli *et al.* 1998;Mannen 2000), and therefore 'rank' lower in the 'transmission-list' to be affected in the course of propagative neuronal death.

Based on the anatomical and neural involvement of the non-motor regions in the motor system organization, it becomes less surprising that other complications are sometimes seen in ALS patients. An example is the concurrent symptom of parkinsonism proceeding ALS onset. Since the substantia nigra is part of the basal ganglia and makes connections with the motor neurons via the anatomical network, it is therefore more likely to expect, than not, that nigral neurons will also be affected in the course of disease propagation.

What determines which muscle group is affected first at onset? No one really knows why and what causes death of a selective pool of motor neurons, giving rise to the clinically observed asymmetrical and focal onset appearance of muscle paralysis. A possible determinant of selective death of the motor pool lies in the genetic complexity of the CNS. Recently, it has been found that human brain cells (both neurons and non-neuronal cells) can be aneuploid and that the resulting genetic mosaicism is a normal feature of the human CNS (Rehen *et al.* 2001;Kingsbury *et al.* 2005;Rehen *et al.* 2005;Mosch *et al.* 2007). However, the biological consequences of neural aneuploidy is yet to be determined, it is possible that the presence of even a few genomically distinct neurons (likely with *de novo* mutations) with altered physiology could have substantial effects on networks formed by interconnected cells or may become 'sick' and initiate damaging propagative effects to other cells thereby causing disease. Therefore, at the organism level, these permanent genomic changes might contribute to physiological and behavioural variation among individuals not accounted for by classical genetics (Rehen *et al.* 2001) which if disease-causing may give rise to apparently sporadic origin, as with sALS, whereas at the cellular level, this could contribute to the unexplainable and initial death of selective pools of motor neurons.

9.3 Implications of SOD1 fibrillization in ALS therapeutics

Based on the main finding of SOD1, wildtype and mutants, having the intrinsic propensity to fibrillize, a 'seeding-nucleation' disease model with similarities to Prion disease is proposed (as illustrated in Figure 9.4). From this SOD1 fibrillization model, there are four main key steps which are crucial in the initiation and propagation of SOD1 toxicity and cell death. The steps are:

1. SOD1 destabilization and *protein misfolding* (formation of 'seeds')
2. *Propagation* of misfolded SOD1 (i.e. fibril growth)
3. Extracellular *release* of toxic SOD1 conformers ('seed', oligomers or fibrils)
4. *Uptake* of toxic SOD1 conformers by neighboring cells (cell-to-cell transmission of toxicity and propagative cell death)

The proposed model from the work presented in this thesis has important therapeutic implication in ALS because these key steps are also possible intervention points which can be exploited for ALS therapeutics. Table 9.1 gives an overview of the underlying concept and possible therapeutic strategies for each intervention point. Some supporting examples from other protein misfolding diseases which have successfully employed a similar approach is also included in Table 9.1 to give an idea of the practicality of such an approach. The results from the work carried out here on SOD1 fibrillization and speculation in this thesis as to how this might be toxic to motor neurons favour the possibility of using immunotherapy as an approach in treating potentially both SOD1 and non-SOD1 linked ALS. This is because wtSOD1 was also found to behave similarly to mutSOD1 in its oligomerization property under certain conditions, thus it is possible that for non-SOD1 linked cases, the same pathogenic mechanism may apply.

Based on the points discussed in 9.1 and 9.2, ALS shares many similarities to Prion disease, where both are considered protein conformational diseases and share a similar disease transmission pattern and misfolded protein-propagation property.

Therefore, it is not unreasonable to propose that work on SOD1 should be handled with caution, and be treated as potentially infectious, especially when in the oligomeric or fibrillar state, until proven otherwise.

Figure 9.4. Seeding-nucleation disease model illustrating the possible propagation pathway of misfolded SOD1. Under certain unfavorable conditions in the cell, SOD1 protein may become destabilized (labeled ❶). These destabilized SOD1 intermediates may form aggregates, and it is this initial nucleation event of aggregation leading to the formation of a stable 'seed' that is the critical point in the misfolding pathway, similar to Prion disease. These 'seeds' serve as a template for the conversion of destabilized intermediates to form more 'seeds' (labeled ❷) and for fibril growth (labeled ❸). The formed oligomers/fibrils may become dissociated to produce more SOD1 'seeds', thus producing even more oligomers/fibrils in an autocatalytic manner. The inset box (dotted lines) (labeled ❹) represents the possible SOD1 conformers that may be secreted or released extracellularly and taken up by neighbouring cells. When taken up by a secondary neighboring cell, the cycle of ❷-❸-❹ is repeated, resulting in the propagation and accumulation of SOD1 oligomer/fibril in the secondary cell.

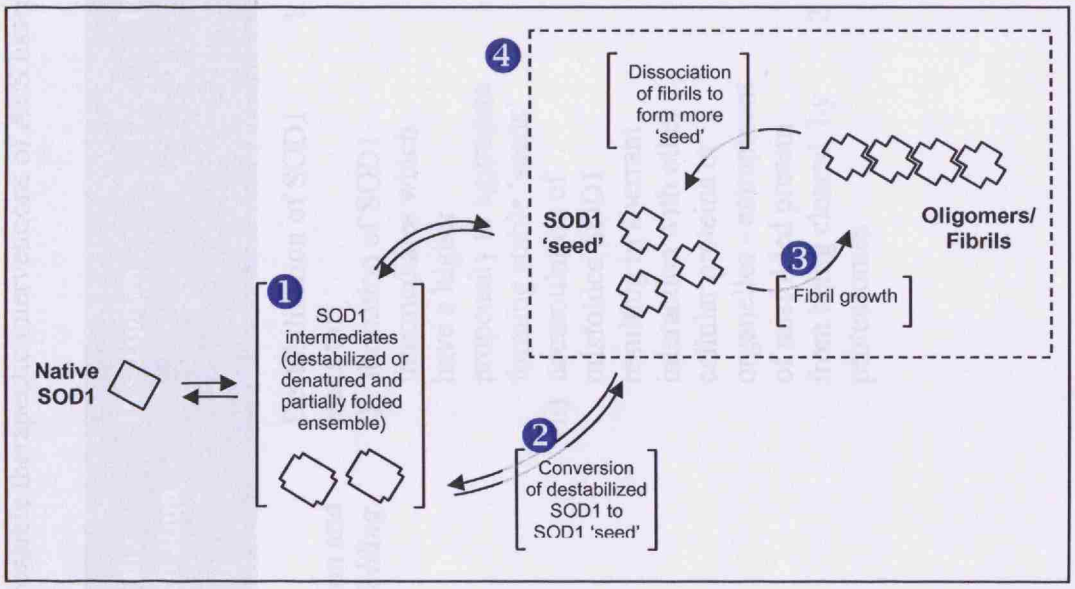

Table 9.1. Possible therapeutic interventions of ALS based on the SOD1 fibrillization seeding-nucleation disease model.

Key step in the seeding-nucleation model	Description	Possible therapeutic intervention	Some examples of intervention strategy from other protein misfolding diseases
SOD1 destabilization and *protein misfolding*	Destabilization of SOD1 leads to: i) formation of SOD1 intermediates which have a higher propensity to aggregate forming stable 'seeds' ii) accumulation of misfolded SOD1 resulting in aberrant interaction with other cellular proteins or organelles - entrapment of misfolded protein from being cleared by proteasomes	1. To stabilize mutant SOD1 with small molecules to reduce the propensity to misfold and aggregate. In Ray *et al.* (2005), in a drug screening effort to look for mutSOD1-stabilizing compounds, some small molecules were discovered to significantly increase the stability and to inhibit *in vitro* aggregation of mutSOD1s. *In vivo* testing on the efficacy of such an approach is currently underway (Ray SS; personal communication) 2. To use chemical chaperones to: - stabilize protein and prevent mis-translocation to other organelles (e.g. mitochondria) - decrease the concentration of aggregation prone species by promoting protein degradation	Stabilizing the native conformation (with small molecules) to inhibit misfolding and aggregation of monomeric and oligomeric species on the misfolding pathway has been shown to be effective in reducing transthyretin (TTR) amyloidogenesis (Miroy *et al.* 1996). 1-deoxy-galactonojirimycin, a potent competitive inhibitor of α-galactosidase A (α -Gal A) was used to rescue the misfolding and mistrafficking associated with certain Fabry-disease-causing mutations. It acts as a chemical chaperone in stabilizing, facilitating the proper folding and trafficking of a-Gal A variants to the lysosome (Fan *et al.* 1999).

Key step in the seeding-nucleation model	Description	Possible therapeutic intervention	Some examples of intervention strategy from other protein misfolding diseases
Propagation of misfolded SOD1	Accumulation of fibrils due to autocatalytic growth can as act as a sink for accumulation of misfolded protein and formation of larger insoluble aggregates. Aggregates might be toxic to the cell and may also interact aberrantly with other cellular proteins or cellular organelles.	1. To destabilise misfolded SOD1 or SOD1 'seeds' to prevent propagation and fibrillar growth 2. To alter the conformation of misfolded SOD1 or SOD1 'seeds' - exposing new epitopes that may be recognized as a signal by the protein degradation machinery to clear the misfolded protein 3. To design a dominant-negative SOD1 mimetic aimed to disrupt protein-protein interaction of misfolded SOD1 (i.e. to prevent conversion of SOD1 intermediates to SOD1 'seeds' and to inhibit fibril growth)	Amyloid binding dye Congo red is known to bind PrP 27-30 fibers *in vitro* and reduce PrP^{Sc} concentrations in a cellular model of disease (Sellarajah *et al.* 2004). Dominant-negative variants of PrP^{C} were shown to slow or stop PrP^{Sc} replication in cell culture and in transgenic animals. Based on these findings, it may be possible that small molecules designed to mimic this dominant-negative effect can also block PrP^{Sc} replication in cell culture (Telling *et al.* 1995).

Key step in the seeding-nucleation model	Description	Possible therapeutic intervention	Some examples of intervention strategy from other protein misfolding diseases
Extracellular *release* of toxic SOD1 conformers (misfolded intermediates, 'seed', oligomers or fibrils)	Release of potentially toxic SOD1 conformers extracellularly can cause a more distal damage from release site because these conformers are free to diffuse to other contiguous motor neuron nuclei. Also, these conformers may activate astrocytes and microglia causing a severe inflammatory-mediated damage.	1. To inhibit the abnormal secretory/ excretory pathway of SOD1 2. To stabilize (with ligands) or to remove SOD1 conformers (use of antibodies i.e. immunotherapy (Urushitani *et al.* 2007)) when secreted to prevent extracellular misfolding and propagation of toxic species	Active immunization of APP transgenic mice (Alzheimer's disease mouse model) overexpressing Aβ with Aβ peptides showed that deposits that would ordinarily accumulate were cleared in these mice (Spooner *et al.* 2002). Antibody studies suggest show that antibodies binding cell-surface PrP^{C} inhibit PrP^{Sc} formation in a dose-dependent manner, abolishment of prion replication and rapid clearance of pre-existing PrP^{Sc} suggesting that clearance of PrP could slow or cure prion (Peretz *et al.* 2001).

Key step in the seeding-nucleation model	Description	Possible therapeutic intervention	Some examples of intervention strategy from other protein misfolding diseases
Uptake of toxic SOD1 conformers by neighboring cells	Cell-to-cell transmission of toxicity and propagation of cell death	1. To prevent uptake by inhibiting SOD1 from interacting with receptors (if uptake is via a specific receptor-mediated pathway) 2. To modify the intracellular transport of 'ingested' SOD1 conformers so that these conformers may be directed to chaperones for refolding or to be degraded	-

9.4 Future work - unresolved aspect of SOD1 fibrillization

The results presented in this thesis on SOD1 fibrillization are only preliminary findings. There are many more unresolved aspects which need to be investigated. Some aspects which are thought to be of immediate importance in validating these preliminary results are highlighted in the sections to follow.

9.4.1 Characterization of SOD1 fibrils

The two main questions under this sub-heading that need to be addressed are:

1. What is the actual toxic species generated from the *in vitro* fibrillization experiments? Which oligomeric state is toxic and the 'active seed' responsible for the seeding effect seen in the seeded reactions?
2. Are there structural alterations or masking of SOD1 epitopes, usually recognized by commercial human SOD1 antibodies, when SOD1 is in the oligomeric or fibrillar state?

Determining which of the oligomeric or misfolded species formed in the in vitro fibrillization assay which harbors cellular toxicity is important. This is because by knowing the structure of the toxic SOD1 conformer, this may provide a structural basis for an effective drug design, for instance in the design of a SOD1 dominant-negative peptidomimetic that can inhibit propagation of misfolded SOD1. The second reason why it is necessary to characterize the structures of SOD1 conformers formed during fibrillization, is to determine if fibrillization of SOD1 has caused alterations in the 'usual epitopes' recognized by commercial human SOD1 antibodies. This has important implications because if the 'usual epitopes' are lost, this would mean that the available antibody to detect SOD1 (in the native form) is not a useful antibody to detect SOD1 in the oligomeric/fibrillar state, thus raising the question of the validity of results reported by others claiming that the inclusions in non-SOD1 linked ALS do not contain SOD1. If the 'usual epitopes' are lost, then a new antibody to detect SOD1 oligomers/fibrils will have to be generated and the reported experiments should be repeated with the appropriate antibody against oligomeric/fibrillar SOD1.

To characterize each SOD1 conformer formed in the fibrillization assay, each conformer must be isolated via fractionation (eg. by size) and the seeding ability of each isolate should be tested. Also, a dotblot for each isolated fraction should be performed for the SOD1 antibody to determine if the 'usual epitopes' of SOD1 are still present.

9.4.2 Investigation of the effects of SOD1 *in vivo*

The toxicity and effects of SOD1 oligomers/fibrils are still unknown. Several aspects of toxicity which have implications in ALS therapeutics need to be addressed:

1. Can the ALS mouse model develop an earlier disease onset if inoculated with exogenous SOD1 oligomer/fibril?
2. How are mutant SOD1 (native, oligomeric or fibrillar forms) endocytosed/taken up by neighbouring cells? Which pathways - specific receptor interaction vs. non-specific phagocytosis?
3. What other proteins do SOD1 oligomers/fibrils interact with?
4. Are oligomeric/fibrillar SOD1 aberrantly sublocalised in the cell?

9.4.3 Determination of conditions for SOD1 fibrillization *in vivo*

The cell is made up of many compartments bound by membranes, and so each compartment has a unique microenvironment. For example, the endoplasmic reticulum has an almost neutral pH, at pH 7.2, whereas the lysosomal compartment has an acidic pH, at pH5 (Wu *et al.* 2000). Because the fibrillization conditions used were non-physiological, the questions to address here are:

1. What are the conditions in the cell which can cause SOD1 to oligomerize/fibrillize?
2. Where is SOD1 misfolded in the cell?
3. Does SOD1 gets secreted in the native state, but gets misfolded/oligomerise when in the extracellular environment?

To answer these questions, the development of an appropriate cell model with targeted expression of SOD1 to specific cellular compartments might be useful to

investigate under what cellular conditions endogenously expressed SOD1 can form fibrils/oligomerize. Also, in developing such a model, the effects of SOD1 fibrils/oligomers formed (if any) in the cell can also be investigated directly.

9.5 Conclusion

From the work presented in this thesis, it appears possible that the focal nature and pathogenesis of ALS may be explained by a 'seeding-nucleation' model for SOD1 comparable to that seen in Prion disease. Therefore, it is hopeful that new therapies, based in this model can be developed for the treatment and possible cure of ALS at some point in the not so distant future.

BIBLIOGRAPHY

Abalkhail H., Mitchell J., Habgood J., Orrell R. and de B. J. (2003) A new familial amyotrophic lateral sclerosis locus on chromosome 16q12.1-16q12.2. *Am. J. Hum. Genet.* **73,** 383-389.

Abe K., Pan L. H., Watanabe M., Kato T. and Itoyama Y. (1995) Induction of nitrotyrosine-like immunoreactivity in the lower motor neuron of amyotrophic lateral sclerosis. *Neurosci. Lett.* **199,** 152-154.

Abe K., Pan L. H., Watanabe M., Konno H., Kato T. and Itoyama Y. (1997) Upregulation of protein-tyrosine nitration in the anterior horn cells of amyotrophic lateral sclerosis. *Neurol. Res.* **19,** 124-128.

Adamek D., Tomik B., Pichor A., Kaluza J. and Szczudlik A. (2002) The heterogeneity of neuropathological changes in amyotrophic lateral sclerosis. A review of own autopsy material. *Folia Neuropathol.* **40,** 119-124.

Aguirre T., Matthijs G., Robberecht W., Tilkin P. and Cassiman J. J. (1999) Mutational analysis of the Cu/Zn superoxide dismutase gene in 23 familial and 69 sporadic cases of amyotrophic lateral sclerosis in Belgium. *Eur. J. Hum. Genet.* **7,** 599-602.

Al-Chalabi A., Andersen P. M., Nilsson P., Chioza B., Andersson J. L., Russ C., Shaw C. E., Powell J. F. and Leigh P. N. (1999) Deletions of the heavy neurofilament subunit tail in amyotrophic lateral sclerosis. *Hum. Mol. Genet.* **8,** 157-164.

Al-Chalabi A., Scheffler M. D., Smith B. N., Parton M. J., Cudkowicz M. E., Andersen P. M., Hayden D. L., Hansen V. K., Turner M. R., Shaw C. E., Leigh P. N. and Brown R. H., Jr. (2003) Ciliary neurotrophic factor genotype does not influence clinical phenotype in amyotrophic lateral sclerosis. *Ann. Neurol.* **54,** 130-134.

Albers D. S. and Beal M. F. (2000) Mitochondrial dysfunction and oxidative stress in aging and neurodegenerative disease. *J. Neural. Transm. Suppl* **59,** 133-154.

Alexander G. M., Erwin K. L., Byers N., Deitch J. S., Augelli B. J., Blankenhorn E. P. and Heiman-Patterson T. D. (2004) Effect of transgene copy number on survival in the G93A SOD1 transgenic mouse model of ALS. *Brain Res. Mol. Brain Res.* **130,** 7-15.

Alexander M. D., Traynor B. J., Miller N., Corr B., Frost E., McQuaid S., Brett F. M., Green A. and Hardiman O. (2002) "True" sporadic ALS associated with a novel SOD-1 mutation. *Ann. Neurol.* **52,** 680-683.

Anand P., Parrett A., Martin J., Zeman S., Foley P., Swash M., Leigh P. N., Cedarbaum J. M., Lindsay R. M., Williams-Chestnut R. E. and . (1995) Regional changes of ciliary neurotrophic factor and nerve growth factor levels in post mortem spinal cord and cerebral cortex from patients with motor disease. *Nat. Med.* **1,** 168-172.

Andersen P. M. (2001) Genetics of sporadic ALS. *Amyotroph. Lateral. Scler. Other Motor Neuron Disord.* **2 Suppl 1,** S37-S41.

Andersen P. M. (2006) Amyotrophic lateral sclerosis associated with mutations in the CuZn superoxide dismutase gene. *Curr. Neurol. Neurosci. Rep.* **6,** 37-46.

Andersen P. M., Restagno G., Stewart H. G. and Chio A. (2004) Disease penetrance in amyotrophic lateral sclerosis associated with mutations in the SOD1 gene. *Ann. Neurol.* **55,** 298-299.

Andreadou E., Kapaki E., Kokotis P., Paraskevas G. P., Katsaros N., Libitaki G., Petropoulou O., Zis V., Sfagos C. and Vassilopoulos D. (2008) Plasma glutamate and glycine levels in patients with amyotrophic lateral sclerosis. *In vivo* **22,** 137-141.

Annesi G., Savettieri G., Pugliese P., D'Amelio M., Tarantino P., Ragonese P., La B., V, Piccoli T., Civitelli D., Annesi F., Fierro B., Piccoli F., Arabia G., Caracciolo M., Ciro C., I and Quattrone A. (2005) DJ-1 mutations and parkinsonism-dementia-amyotrophic lateral sclerosis complex. *Ann. Neurol.* **58,** 803-807.

Aoki M., Lin C. L., Rothstein J. D., Geller B. A., Hosler B. A., Munsat T. L., Horvitz H. R. and Brown R. H., Jr. (1998) Mutations in the glutamate transporter EAAT2 gene do not cause abnormal EAAT2 transcripts in amyotrophic lateral sclerosis. *Ann. Neurol.* **43,** 645-653.

Arce V., Garces A., de B. B., Filippi P., Henderson C., Pettmann B. and deLapeyriere O. (1999) Cardiotrophin-1 requires LIFRbeta to promote survival of mouse motoneurons purified by a novel technique. *J. Neurosci. Res.* **55,** 119-126.

Armon C. (2001) Environmental risk factors for amyotrophic lateral sclerosis. *Neuroepidemiology* **20,** 2-6.

Armon C. (2004) Excess incidence of ALS in young Gulf War veterans. *Neurology* **63,** 1986-1987.

Armon C. (2005) Acquired nucleic acid changes may trigger sporadic amyotrophic lateral sclerosis. *Muscle Nerve* **32,** 373-377.

Armon C. (2007) Sports and trauma in amyotrophic lateral sclerosis revisited. *J. Neurol. Sci.* **262,** 45-53.

Armon C., Kurland L. T., Daube J. R. and O'Brien P. C. (1991) Epidemiologic correlates of sporadic amyotrophic lateral sclerosis. *Neurology* **41,** 1077-1084.

Arribas J. and Castano J. G. (1990) Kinetic studies of the differential effect of detergents on the peptidase activities of the multicatalytic proteinase from rat liver. *J. Biol. Chem.* **265,** 13969-13973.

Baglioni S., Casamenti F., Bucciantini M., Luheshi L. M., Taddei N., Chiti F., Dobson C. M. and Stefani M. (2006) Prefibrillar amyloid aggregates could be generic toxins in higher organisms. *J. Neurosci.* **26,** 8160-8167.

Baloh R. H., Rakowicz W., Gardner R. and Pestronk A. (2007) Frequent atrophic groups with mixed-type myofibers is distinctive to motor neuron syndromes. *Muscle Nerve* **36,** 107-110.

Banack S. A. and Cox P. A. (2003) Biomagnification of cycad neurotoxins in flying foxes: implications for ALS-PDC in Guam. *Neurology* **61,** 387-389.

Banci L., Bertini I., Boca M., Girotto S., Martinelli M., Valentine J. S. and Vieru M. (2008) SOD1 and amyotrophic lateral sclerosis: mutations and oligomerization. *PLoS. ONE.* **3,** e1677.

Banci L., Bertini I., Durazo A., Girotto S., Gralla E. B., Martinelli M., Valentine J. S., Vieru M. and Whitelegge J. P. (2007) Metal-free superoxide dismutase forms soluble oligomers under physiological conditions: a possible general mechanism for familial ALS. *Proc. Natl. Acad. Sci. U. S. A* **104,** 11263-11267.

Barber S. C., Mead R. J. and Shaw P. J. (2006) Oxidative stress in ALS: a mechanism of neurodegeneration and a therapeutic target. *Biochim. Biophys. Acta* **1762,** 1051-1067.

Beaulieu J. M., Nguyen M. D. and Julien J. P. (1999) Late onset of motor neurons in mice overexpressing wild-type peripherin. *J. Cell Biol.* **147,** 531-544.

Beckman Coulter (2008) Introduction to Analytical Ultracentrifugation, Beckman Coulter.

Beers D. R., Henkel J. S., Xiao Q., Zhao W., Wang J., Yen A. A., Siklos L., McKercher S. R. and Appel S. H. (2006) Wild-type microglia extend survival in PU.1 knockout mice with familial amyotrophic lateral sclerosis. *Proc. Natl. Acad. Sci. U. S. A* **103,** 16021-16026.

Begley M. J. and Dixon J. E. (2005) The structure and regulation of myotubularin phosphatases. *Curr. Opin. Struct. Biol.* **15,** 614-620.

Ben H. M., Hentati F. and Ben H. C. (1990) Giant axonal neuropathy with inherited multisystem degeneration in a Tunisian kindred. *Neurology* **40,** 245-250.

Bendotti C. and Carri M. T. (2004) Lessons from models of SOD1-linked familial ALS. *Trends Mol. Med.* **10,** 393-400.

Bergmann M. (1993) Motor neuron disease/amyotrophic lateral sclerosis--lessons from ubiquitin. *Pathol. Res. Pract.* **189,** 902-912.

Bergmann M., Volpel M. and Kuchelmeister K. (1995) Onuf's nucleus is frequently involved in motor neuron disease/amyotrophic lateral sclerosis. *J. Neurol. Sci.* **129,** 141-146.

Berkers C. R., Verdoes M., Lichtman E., Fiebiger E., Kessler B. M., Anderson K. C., Ploegh H. L., Ovaa H. and Galardy P. J. (2005) Activity probe for *in vivo* profiling of the specificity of proteasome inhibitor bortezomib. *Nat. Methods* **2,** 357-362.

Bertram L. and Tanzi R. E. (2005) The genetic epidemiology of neurodegenerative disease. *J. Clin. Invest.* **115,** 1449-1457.

Beychok S. (1966) Circular dichroism of biological macromolecules. *Science* **154,** 1288-1299.

Boillee S., Vande V. C. and Cleveland D. W. (2006a) ALS: a disease of motor neurons and their nonneuronal neighbors. *Neuron* **52,** 39-59.

Boillee S., Yamanaka K., Lobsiger C. S., Copeland N. G., Jenkins N. A., Kassiotis G., Kollias G. and Cleveland D. W. (2006b) Onset and Progression in Inherited ALS Determined by Motor Neurons and Microglia. *Science* **312,** 1389-1392.

Boissinot M., Karnas S., Lepock J. R., Cabelli D. E., Tainer J. A., Getzoff E. D. and Hallewell R. A. (1997) Function of the Greek key connection analysed using circular permutants of superoxide dismutase. *EMBO J.* **16,** 2171-2178.

Borchelt D. R., Lee M. K., Slunt H. S., Guarnieri M., Xu Z. S., Wong P. C., Brown R. H., Jr., Price D. L., Sisodia S. S. and Cleveland D. W. (1994) Superoxide dismutase 1 with mutations linked to familial amyotrophic lateral sclerosis possesses significant activity. *Proc. Natl. Acad. Sci U. S. A* **91,** 8292-8296.

Borthwick G. M., Johnson M. A., Ince P. G., Shaw P. J. and Turnbull D. M. (1999) Mitochondrial enzyme activity in amyotrophic lateral sclerosis: implications for the role of mitochondria in neuronal cell death. *Ann. Neurol.* **46,** 787-790.

Boston-Howes W., Gibb S. L., Williams E. O., Pasinelli P., Brown R. H., Jr. and Trotti D. (2006) Caspase-3 cleaves and inactivates the glutamate transporter EAAT2. *J. Biol. Chem.* **281,** 14076-14084.

Bowen S., Ateh D. D., Deinhardt K., Bird M. M., Price K. M., Baker C. S., Robson J. C., Swash M., Shamsuddin W., Kawar S., El-Tawil T., Roos J., Hoyle A., Nickols C. D., Knowles C. H., Pullen A. H., Luthert P. J., Weller R. O., Hafezparast M., Franklin R. J., Revesz T., King R. H., Berninghausen O., Fisher E. M., Schiavo G. and Martin J. E. (2007) The phagocytic capacity of neurones. *Eur. J. Neurosci.* **25,** 2947-2955.

Bowling A. C., Schulz J. B., Brown R. H., Jr. and Beal M. F. (1993) Superoxide dismutase activity, oxidative damage, and mitochondrial energy metabolism in familial and sporadic amyotrophic lateral sclerosis. *J. Neurochem.* **61,** 2322-2325.

Brockington A., Wokke B., Nixon H., Hartley J. and Shaw P. J. (2007) Screening of the transcriptional regulatory regions of vascular endothelial growth factor receptor 2 (VEGFR2) in amyotrophic lateral sclerosis. *BMC. Med. Genet.* **8,** 23.

Brooks B. R. (1991) The role of axonal transport in neurodegenerative disease spread: a meta-analysis of experimental and clinical poliomyelitis compares with amyotrophic lateral sclerosis. *Can. J. Neurol. Sci.* **18,** 435-438.

Bross P. and Gregersen N. (2003) *Protein misfolding and disease: principles and protocols*. Humana Press, New Jersey.

Brown R. H., Jr. (1998) SOD1 aggregates in ALS: cause, correlate or consequence? *Nat. Med.* **4,** 1362-1364.

Browne S. E., Bowling A. C., Baik M. J., Gurney M., Brown R. H., Jr. and Beal M. F. (1998) Metabolic dysfunction in familial, but not sporadic, amyotrophic lateral sclerosis. *J. Neurochem.* **71,** 281-287.

Bruening W., Roy J., Giasson B., Figlewicz D. A., Mushynski W. E. and Durham H. D. (1999) Up-regulation of protein chaperones preserves viability of cells expressing toxic Cu/Zn-superoxide dismutase mutants associated with amyotrophic lateral sclerosis. *J. Neurochem.* **72,** 693-699.

Bruijn L. I., Becher M. W., Lee M. K., Anderson K. L., Jenkins N. A., Copeland N. G., Sisodia S. S., Rothstein J. D., Borchelt D. R., Price D. L. and Cleveland D. W. (1997) ALS-linked SOD1 mutant G85R mediates damage to astrocytes and promotes rapidly progressive disease with SOD1-containing inclusions. *Neuron* **18,** 327-338.

Carvalho M., Schwartz M. S. and Swash M. (1995) Involvement of the external anal sphincter in amyotrophic lateral sclerosis. *Muscle Nerve* **18,** 848-853.

Cassina P., Cassina A., Pehar M., Castellanos R., Gandelman M., de L. A., Robinson K. M., Mason R. P., Beckman J. S., Barbeito L. and Radi R. (2008) Mitochondrial dysfunction in SOD1G93A-bearing astrocytes promotes motor neuron degeneration: prevention by mitochondrial-targeted antioxidants. *J. Neurosci.* **28,** 4115-4122.

Cecarini V., Ding Q. and Keller J. N. (2007) Oxidative inactivation of the proteasome in Alzheimer's disease. *Free Radic. Res.* **41,** 673-680.

Chancellor A. M. and Warlow C. P. (1992) Adult onset motor neuron disease: worldwide mortality, incidence and distribution since 1950. *J. Neurol. Neurosurg. Psychiatry* **55,** 1106-1115.

Chang J. L., Lomen-Hoerth C., Murphy J., Henry R. G., Kramer J. H., Miller B. L. and Gorno-Tempini M. L. (2005) A voxel-based morphometry study of patterns of brain atrophy in ALS and ALS/FTLD. *Neurology* **65,** 75-80.

Chang-Hong R., Wada M., Koyama S., Kimura H., Arawaka S., Kawanami T., Kurita K., Kadoya T., Aoki M., Itoyama Y. and Kato T. (2005) Neuroprotective effect of oxidized galectin-1 in a transgenic mouse model of amyotrophic lateral sclerosis. *Exp. Neurol.* **194,** 203-211.

Chaudhry S. S., Gazzard J., Baldock C., Dixon J., Rock M. J., Skinner G. C., Steel K. P., Kielty C. M. and Dixon M. J. (2001) Mutation of the gene encoding fibrillin-2 results in syndactyly in mice. *Hum. Mol. Genet.* **10,** 835-843.

Chen D., Shen L., Wang L., Lu A., Zhang H., Zhang X., Zhang Y., Shui W., Li L., Fan D. and Zhang J. (2007) Association of polymorphisms in vascular endothelial growth factor gene with the age of onset of amyotrophic lateral sclerosis. *Amyotroph. Lateral. Scler.* **8,** 144-149.

Chen W., Saeed M., Mao H., Siddique N., Dellefave L., Hung W. Y., Deng H. X., Sufit R. L., Heller S. L., Haines J. L., Pericak-Vance M. and Siddique T. (2006) Lack of association of VEGF promoter polymorphisms with sporadic ALS. *Neurology* **67,** 508-510.

Chen Y. Z., Bennett C. L., Huynh H. M., Blair I. P., Puls I., Irobi J., Dierick I., Abel A., Kennerson M. L., Rabin B. A., Nicholson G. A., uer-Grumbach M., Wagner K., De J. P., Griffin J. W., Fischbeck K. H., Timmerman V., Cornblath D. R. and Chance P. F. (2004) DNA/RNA helicase gene mutations in a form of juvenile amyotrophic lateral sclerosis (ALS4). *Am. J. Hum. Genet.* **74,** 1128-1135.

Chevalier-Larsen E. and Holzbaur E. L. (2006) Axonal transport and neurodegenerative disease. *Biochim. Biophys. Acta* **1762,** 1094-1108.

Chio A., Benzi G., Dossena M., Mutani R. and Mora G. (2005) Severely increased risk of amyotrophic lateral sclerosis among Italian professional football players. *Brain* **128,** 472-476.

Choi J., Rees H. D., Weintraub S. T., Levey A. I., Chin L. S. and Li L. (2005) Oxidative modifications and aggregation of Cu,Zn-superoxide dismutase associated with Alzheimer and Parkinson diseases. *J. Biol. Chem.* **280,** 11648-11655.

Chou S. M. (1997) Neuropathology of amyotrophic lateral sclerosis: new perspectives on an old disease. *J. Formos. Med. Assoc.* **96,** 488-498.

Clement A. M., Nguyen M. D., Roberts E. A., Garcia M. L., Boillee S., Rule M., McMahon A. P., Doucette W., Siwek D., Ferrante R. J., Brown R. H., Jr., Julien J. P., Goldstein L. S. and Cleveland D. W. (2003) Wild-type nonneuronal cells extend survival of SOD1 mutant motor neurons in ALS mice. *Science* **302,** 113-117.

Cleveland D. W. and Liu J. (2000) Oxidation versus aggregation - how do SOD1 mutants cause ALS? *Nat. Med.* **6,** 1320-1321.

Collard J. F., Cote F. and Julien J. P. (1995) Defective axonal transport in a transgenic mouse model of amyotrophic lateral sclerosis. *Nature* **375,** 61-64.

Collard J. F. and Julien J. P. (1995) A simple test to monitor the motor dysfunction in a transgenic mouse model of amyotrophic lateral sclerosis. *J. Psychiatry Neurosci.* **20,** 80-82.

Collinge J. and Clarke A. R. (2007) A general model of prion strains and their pathogenicity. *Science* **318,** 930-936.

Concepcion D., Seburn K. L., Wen G., Frankel W. N. and Hamilton B. A. (2004) Mutation rate and predicted phenotypic target sizes in ethylnitrosourea-treated mice. *Genetics* **168,** 953-959.

Cookson M. R. and Shaw P. J. (1999) Oxidative stress and motor neurone disease. *Brain Pathol.* **9,** 165-186.

Corbo M. and Hays A. P. (1992) Peripherin and neurofilament protein coexist in spinal spheroids of motor neuron disease. *J. Neuropathol. Exp. Neurol.* **51,** 531-537.

Corrado L., D'Alfonso S., Bergamaschi L., Testa L., Leone M., Nasuelli N., Momigliano-Richiardi P. and Mazzini L. (2006) SOD1 gene mutations in Italian patients with Sporadic Amyotrophic Lateral Sclerosis (ALS). *Neuromuscul. Disord.* **16,** 800-804.

Cote F., Collard J. F. and Julien J. P. (1993) Progressive neuronopathy in transgenic mice expressing the human neurofilament heavy gene: a mouse model of amyotrophic lateral sclerosis. *Cell* **73,** 35-46.

Couillard-Despres S., Zhu Q., Wong P. C., Price D. L., Cleveland D. W. and Julien J. P. (1998) Protective effect of neurofilament heavy gene overexpression in motor neuron disease induced by mutant superoxide dismutase. *Proc. Natl. Acad. Sci. U. S. A* **95,** 9626-9630.

Cox P. A. and Sacks O. W. (2002) Cycad neurotoxins, consumption of flying foxes, and ALS-PDC disease in Guam. *Neurology* **58,** 956-959.

Cronin S., Hardiman O. and Traynor B. J. (2007) Ethnic variation in the incidence of ALS: a systematic review. *Neurology* **68,** 1002-1007.

Cudkowicz M. E., Kenna-Yasek D., Sapp P. E., Chin W., Geller B., Hayden D. L., Schoenfeld D. A., Hosler B. A., Horvitz H. R. and Brown R. H. (1997) Epidemiology of mutations in superoxide dismutase in amyotrophic lateral sclerosis. *Ann. Neurol.* **41,** 210-221.

Curti D., Malaspina A., Facchetti G., Camana C., Mazzini L., Tosca P., Zerbi F. and Ceroni M. (1996) Amyotrophic lateral sclerosis: oxidative energy metabolism and calcium homeostasis in peripheral blood lymphocytes. *Neurology* **47,** 1060-1064.

Dal Canto M. C. and Gurney M. E. (1995) Neuropathological changes in two lines of mice carrying a transgene for mutant human Cu,Zn SOD, and in mice overexpressing wild type human SOD: a model of familial amyotrophic lateral sclerosis (FALS). *Brain Res.* **676,** 25-40.

Dal Canto M. C. and Gurney M. E. (1997) A low expressor line of transgenic mice carrying a mutant human Cu,Zn superoxide dismutase (SOD1) gene develops pathological changes that most closely resemble those in human amyotrophic lateral sclerosis. *Acta Neuropathol. (Berl)* **93,** 537-550.

Dantuma N. P., Lindsten K., Glas R., Jellne M. and Masucci M. G. (2000) Short-lived green fluorescent proteins for quantifying ubiquitin/proteasome-dependent proteolysis in living cells. *Nat. Biotechnol.* **18,** 538-543.

Daube J. R. (2000) Electrodiagnostic studies in amyotrophic lateral sclerosis and other motor neuron disorders. *Muscle Nerve* **23,** 1488-1502.

de Carvalho M., Matias T., Coelho F., Evangelista T., Pinto A. and Luis M. L. (1996) Motor neuron disease presenting with respiratory failure. *J. Neurol. Sci.* **139 Suppl,** 117-122.

de Girolami U., Frosch M. P. and Anthony D. C. (1999) The Central Nervous System, in *Robbin's Pathologic Basis of Disease,* (Cotran R. S., Kumar V., Collins T. and Robbins S. L., eds), pp. 1293-1358. W.B. Saunders Company, Philadelphia.

De Jonghe P., uer-Grumbach M., Irobi J., Wagner K., Plecko B., Kennerson M., Zhu D., De V. E., Van G., V, Nicholson G., Hartung H. P. and Timmerman V. (2002) Autosomal dominant juvenile amyotrophic lateral sclerosis and distal hereditary motor neuronopathy with pyramidal tract signs: synonyms for the same disorder? *Brain* **125,** 1320-1325.

De Vos K. J., Grierson A. J., Ackerley S. and Miller C. C. J. (2008) Role of Axonal Transport in Neurodegenerative Diseases. *Ann. Rev. Neuroscience* **31.**

del Aguila M. A., Longstreth W. T., Jr., McGuire V., Koepsell T. D. and van B. G. (2003) Prognosis in amyotrophic lateral sclerosis: a population-based study. *Neurology* **60,** 813-819.

Deng H. X., Shi Y., Furukawa Y., Zhai H., Fu R., Liu E., Gorrie G. H., Khan M. S., Hung W. Y., Bigio E. H., Lukas T., Dal Canto M. C., O'Halloran T. V. and Siddique T. (2006) Conversion to the amyotrophic lateral sclerosis phenotype is associated with intermolecular linked insoluble aggregates of SOD1 in mitochondria. *Proc. Natl. Acad. Sci. U. S. A* **103,** 7142-7147.

Desai J. and Swash M. (1999) Extrapyramidal involvement in amyotrophic lateral sclerosis: backward falls and retropulsion. *J. Neurol. Neurosurg. Psychiatry* **67,** 214-216.

Di Giorgio F. P., Carrasco M. A., Siao M. C., Maniatis T. and Eggan K. (2007) Non-cell autonomous effect of glia on motor neurons in an embryonic stem cell-based ALS model. *Nat. Neurosci.* **10,** 608-614.

Di Trapani G., David P., La C. A., Tonali P. and Laurienzo P. (1987) Light and ultrastructural studies in sural biopsies of the pseudopolyneuropathic form of ALS. *Adv. Exp. Med. Biol.* **209,** 111-119.

Dickson D. W., Josephs K. A. and mador-Ortiz C. (2007) TDP-43 in differential diagnosis of motor neuron disorders. *Acta Neuropathol. (Berl)* **114,** 71-79.

DiDonato M., Craig L., Huff M. E., Thayer M. M., Cardoso R. M., Kassmann C. J., Lo T. P., Bruns C. K., Powers E. T., Kelly J. W., Getzoff E. D. and Tainer J. A. (2003) ALS mutants of human superoxide dismutase form fibrous aggregates via framework destabilization. *J. Mol. Biol.* **332,** 601-615.

Ding Q., Cecarini V. and Keller J. N. (2007) Interplay between protein synthesis and degradation in the CNS: physiological and pathological implications. *Trends Neurosci.* **30,** 31-36.

Ding Q., Dimayuga E., Markesbery W. R. and Keller J. N. (2006) Proteasome inhibition induces reversible impairments in protein synthesis. *FASEB J.* **20,** 1055-1063.

Dixon M. J., Gazzard J., Chaudhry S. S., Sampson N., Schulte B. A. and Steel K. P. (1999) Mutation of the Na-K-Cl co-transporter gene Slc12a2 results in deafness in mice. *Hum. Mol. Genet.* **8,** 1579-1584.

Djaballah H. and Rivett A. J. (1992) Peptidylglutamyl-peptide hydrolase activity of the multicatalytic proteinase complex: evidence for a new high-affinity site, analysis of cooperative kinetics, and the effect of manganese ions. *Biochemistry* **31,** 4133-4141.

Djaballah H., Rowe A. J., Harding S. E. and Rivett A. J. (1993) The multicatalytic proteinase complex (proteasome): structure and conformational changes associated with changes in proteolytic activity. *Biochem. J.* **292,** 857-862.

Doble A. and Kennel P. (2000) Animal models of amyotrophic lateral sclerosis. *Amyotroph. Lateral. Scler. Other Motor Neuron Disord.* **1,** 301-312.

Doerks T., Strauss M., Brendel M. and Bork P. (2000) GRAM, a novel domain in glucosyltransferases, myotubularins and other putative membrane-associated proteins. *Trends Biochem. Sci.* **25,** 483-485.

Donzelli R., Marinkovic S., Brigante L., Nikodijevic I., Maiuri F. and de D. O. (1998) The oculomotor nuclear complex in humans. Microanatomy and clinical significance. *Surg. Radiol. Anat.* **20,** 7-12.

Doucette P. A. (2004) Biophysical Studies of Human Copper-Zinc Superoxide Dismutase and Mutants Associated with the Neurodegenerative Disease Amyotrophic Lateral Sclerosis. *UCLA Department of Chemistry and Biochemistry* **PhD thesis.**

Doucette P. A., Whitson L. J., Cao X., Schirf V., Demeler B., Valentine J. S., Hansen J. C. and Hart P. J. (2004) Dissociation of human copper-zinc superoxide dismutase dimers using chaotrope and reductant. Insights into the molecular basis for dimer stability. *J. Biol. Chem.* **279,** 54558-54566.

Dubois M., Lalonde R., Julien J. P. and Strazielle C. (2005a) Mice with the deleted neurofilament of low-molecular-weight (Nefl) gene: 1. Effects on regional brain metabolism. *J. Neurosci. Res.* **80,** 741-750.

Dubois M., Strazielle C., Julien J. P. and Lalonde R. (2005b) Mice with the deleted neurofilament of low molecular weight (Nefl) gene: 2. Effects on motor functions and spatial orientation. *J. Neurosci. Res.* **80,** 751-758.

Dupuis L., Gonzalez de Aguilar J. L., Oudart H., de T. M., Barbeito L. and Loeffler J. P. (2004) Mitochondria in amyotrophic lateral sclerosis: a trigger and a target. *Neurodegener. Dis.* **1,** 245-254.

Eisen A., Mezei M. M., Stewart H. G., Fabros M., Gibson G. and Andersen P. M. (2008) SOD1 gene mutations in ALS patients from British Columbia, Canada: clinical features, neurophysiology and ethical issues in management. *Amyotroph. Lateral. Scler.* **9,** 108-119.

El-Kadi A. M., Soura V. and Hafezparast M. (2007) Defective axonal transport in motor neuron disease. *J. Neurosci. Res.* **85,** 2557-2566.

Elam J. S., Taylor A. B., Strange R., Antonyuk S., Doucette P. A., Rodriguez J. A., Hasnain S. S., Hayward L. J., Valentine J. S., Yeates T. O. and Hart P. J. (2003) Amyloid-like filaments and water-filled nanotubes formed by SOD1 mutant proteins linked to familial ALS. *Nat. Struct. Biol.* **10,** 461-467.

Elder G. A., Friedrich V. L., Jr., Bosco P., Kang C., Gourov A., Tu P. H., Lee V. M. and Lazzarini R. A. (1998) Absence of the mid-sized neurofilament subunit decreases axonal calibers, levels of light neurofilament (NF-L), and neurofilament content. *J. Cell Biol.* **141,** 727-739.

Elder G. A., Friedrich V. L., Jr., Margita A. and Lazzarini R. A. (1999a) Age-related atrophy of motor axons in mice deficient in the mid-sized neurofilament subunit. *J. Cell Biol.* **146,** 181-192.

Elder G. A., Friedrich V. L., Jr., Pereira D., Tu P. H., Zhang B., Lee V. M. and Lazzarini R. A. (1999b) Mice with disrupted midsized and heavy neurofilament genes lack axonal neurofilaments but have unaltered numbers of axonal microtubules. *J. Neurosci. Res.* **57,** 23-32.

Elliott J. L. (1999) Experimental models of amyotrophic lateral sclerosis. *Neurobiol. Dis.* **6,** 310-320.

Ellis C. M., Suckling J., Amaro E Jr, Bullmore E. T., Simmons A., Williams S. C. and Leigh P. N. (2001) Volumetric analysis reveals corticospinal tract degeneration and extramotor involvement in ALS. *Neurology* **57,** 1571-1578.

Ellman G. L. (1958) A colorimetric method for determining low concentrations of mercaptans. *Arch. Biochem. Biophys.* **74,** 443-450.

Ellman G. L. (1959) Tissue sulfhydryl groups. *Arch. Biochem. Biophys.* **82,** 70-77.

Ende N., Chen R. and Ende-Harris D. (2001) Human umbilical cord blood cells ameliorate Alzheimer's disease in transgenic mice. *J. Med.* **32,** 241-247.

Ezzi S. A., Urushitani M. and Julien J. P. (2007) Wild-type superoxide dismutase acquires binding and toxic properties of ALS-linked mutant forms through oxidation. *J. Neurochem.* **102,** 170-178.

Fan J. Q., Ishii S., Asano N. and Suzuki Y. (1999) Accelerated transport and maturation of lysosomal alpha-galactosidase A in Fabry lymphoblasts by an enzyme inhibitor. *Nat. Med.* **5,** 112-115.

Fernandez-Santiago R., Sharma M., Mueller J. C., Gohlke H., Illig T., Anneser J., Munch C., Ludolph A., Kamm C. and Gasser T. (2006) Possible gender-dependent association of vascular endothelial growth factor (VEGF) gene and ALS. *Neurology* **66,** 1929-1931.

Ferrante R. J., Shinobu L. A., Schulz J. B., Matthews R. T., Thomas C. E., Kowall N. W., Gurney M. E. and Beal M. F. (1997) Increased 3-nitrotyrosine and oxidative damage in mice with a human copper/zinc superoxide dismutase mutation. *Ann. Neurol.* **42,** 326-334.

Figlewicz D. A., Krizus A., Martinoli M. G., Meininger V., Dib M., Rouleau G. A. and Julien J. P. (1994) Variants of the heavy neurofilament subunit are associated with the development of amyotrophic lateral sclerosis. *Hum. Mol. Genet.* **3,** 1757-1761.

Foguel D., Suarez M. C., Ferrao-Gonzales A. D., Porto T. C., Palmieri L., Einsiedler C. M., Andrade L. R., Lashuel H. A., Lansbury P. T., Kelly J. W. and Silva J. L. (2003) Dissociation of amyloid fibrils of alpha-synuclein and transthyretin by pressure reveals their reversible nature and the formation of water-excluded cavities. *Proc. Natl. Acad. Sci U. S. A* **100,** 9831-9836.

Fokin A. A. and Robicsek F. (2002) Poland's syndrome revisited. *Ann. Thorac. Surg.* **74,** 2218-2225.

Fray A. E., Ince P. G., Banner S. J., Milton I. D., Usher P. A., Cookson M. R. and Shaw P. J. (1998) The expression of the glial glutamate transporter protein EAAT2 in motor neuron disease: an immunohistochemical study. *Eur. J. Neurosci.* **10,** 2481-2489.

Fridovich I. (1999) Fundamental aspects of reactive oxygen species, or what's the matter with oxygen? *Ann. N. Y. Acad. Sci* **893,** 13-18.

Fujita K., Yamauchi M., Shibayama K., Ando M., Honda M. and Nagata Y. (1996) Decreased cytochrome c oxidase activity but unchanged superoxide dismutase and glutathione peroxidase activities in the spinal cords of patients with amyotrophic lateral sclerosis. *J. Neurosci. Res.* **45,** 276-281.

Fukada K., Nagano S., Satoh M., Tohyama C., Nakanishi T., Shimizu A., Yanagihara T. and Sakoda S. (2001) Stabilization of mutant Cu/Zn superoxide dismutase (SOD1) protein by coexpressed wild SOD1 protein accelerates the disease progression in familial amyotrophic lateral sclerosis mice. *Eur. J. Neurosci.* **14,** 2032-2036.

Furukawa Y. and O'Halloran T. V. (2005) Amyotrophic lateral sclerosis mutations have the greatest destabilizing effect on the apo- and reduced form of SOD1, leading to unfolding and oxidative aggregation. *J. Biol. Chem.* **280,** 17266-17274.

Geerlof A., Brown J., Coutard B., Egloff M. P., Enguita F. J., Fogg M. J., Gilbert R. J., Groves M. R., Haouz A., Nettleship J. E., Nordlund P., Owens R. J., Ruff M., Sainsbury S., Svergun D. I. and Wilmanns M. (2006) The impact of protein characterization in structural proteomics. *Acta Crystallogr. D. Biol. Crystallogr.* **62,** 1125-1136.

Gellera C., Colombrita C., Ticozzi N., Castellotti B., Bragato C., Ratti A., Taroni F. and Silani V. (2008) Identification of new ANG gene mutations in a large cohort of Italian patients with amyotrophic lateral sclerosis. *Neurogenetics.* **9,** 33-40.

Georgesco M., Salerno A. and Camu W. (1997) Somatosensory evoked potentials elicited by stimulation of lower-limb nerves in amyotrophic lateral sclerosis. *Electroencephalogr. Clin. Neurophysiol.* **104,** 333-342.

Getzoff E. D., Tainer J. A., Stempien M. M., Bell G. I. and Hallewell R. A. (1989) Evolution of CuZn superoxide dismutase and the Greek key beta-barrel structural motif. *Proteins* **5,** 322-336.

Giess R., Goetz R., Schrank B., Ochs G., Sendtner M. and Toyka K. (1998) Potential implications of a ciliary neurotrophic factor gene mutation in a German population of patients with motor neuron disease. *Muscle Nerve* **21,** 236-238.

Gomes C., Keller S., Altevogt P. and Costa J. (2007) Evidence for secretion of Cu,Zn superoxide dismutase via exosomes from a cell model of amyotrophic lateral sclerosis. *Neurosci. Lett.* **428,** 43-46.

Gong Y. H., Parsadanian A. S., Andreeva A., Snider W. D. and Elliott J. L. (2000) Restricted expression of G86R Cu/Zn superoxide dismutase in astrocytes results in astrocytosis but does not cause motoneuron degeneration. *J. Neurosci.* **20,** 660-665.

Goodall E. F., Greenway M. J., van M., I, Carroll C. B., Hardiman O. and Morrison K. E. (2005) Association of the H63D polymorphism in the hemochromatosis gene with sporadic ALS. *Neurology* **65,** 934-937.

Goswami A., Dikshit P., Mishra A., Mulherkar S., Nukina N. and Jana N. R. (2006) Oxidative stress promotes mutant huntingtin aggregation and mutant huntingtin-dependent cell death by mimicking proteasomal malfunction. *Biochem. Biophys. Res. Commun.* **342,** 184-190.

Greene L. A. and Tischler A. S. (1976) Establishment of a noradrenergic clonal line of rat adrenal pheochromocytoma cells which respond to nerve growth factor. *Proc. Natl. Acad. Sci. U. S. A* **73,** 2424-2428.

Greenway M. J., Alexander M. D., Ennis S., Traynor B. J., Corr B., Frost E., Green A. and Hardiman O. (2004) A novel candidate region for ALS on chromosome 14q11.2. *Neurology* **63,** 1936-1938.

Greenway M. J., Andersen P. M., Russ C., Ennis S., Cashman S., Donaghy C., Patterson V., Swingler R., Kieran D., Prehn J., Morrison K. E., Green A., Acharya K. R., Brown R. H., Jr. and Hardiman O. (2006) ANG mutations segregate with familial and 'sporadic' amyotrophic lateral sclerosis. *Nat. Genet.* **38,** 411-413.

Gregersen N., Bross P., Vang S. and Christensen J. H. (2006) Protein Misfolding and Human Disease. *Ann. Rev. Genomic Hum. Gen.***7,** 103-124.

Gregory R., Mills K. and Donaghy M. (1993) Progressive sensory nerve dysfunction in amyotrophic lateral sclerosis: a prospective clinical and neurophysiological study. *J. Neurol.* **240,** 309-314.

Gros-Louis F., Gaspar C. and Rouleau G. A. (2006) Genetics of familial and sporadic amyotrophic lateral sclerosis. *Biochim. Biophys. Acta* **1762,** 956-972.

Gros-Louis F., Lariviere R., Gowing G., Laurent S., Camu W., Bouchard J. P., Meininger V., Rouleau G. A. and Julien J. P. (2004) A frameshift deletion in peripherin gene associated with amyotrophic lateral sclerosis. *J. Biol. Chem.* **279,** 45951-45956.

Gubbay S. S., Kahana E., Zilber N., Cooper G., Pintov S. and Leibowitz Y. (1985) Amyotrophic lateral sclerosis. A study of its presentation and prognosis. *J. Neurol.* **232,** 295-300.

Gurney M. E., Pu H., Chiu A. Y., Dal Canto M. C., Polchow C. Y., Alexander D. D., Caliendo J., Hentati A., Kwon Y. W., Deng H. X. and . (1994) Motor neuron degeneration in mice that express a human Cu,Zn superoxide dismutase mutation. *Science* **264,** 1772-1775.

Hafezparast M., Klocke R., Ruhrberg C., Marquardt A., hmad-Annuar A., Bowen S., Lalli G., Witherden A. S., Hummerich H., Nicholson S., Morgan P. J., Oozageer R., Priestley J. V., Averill S., King V. R., Ball S., Peters J., Toda T., Yamamoto A., Hiraoka Y., Augustin M., Korthaus D., Wattler S., Wabnitz P., Dickneite C., Lampel S., Boehme F., Peraus G., Popp A., Rudelius M., Schlegel J., Fuchs H., Hrabe de A. M., Schiavo G., Shima D. T., Russ A. P., Stumm G., Martin J. E. and Fisher E. M. (2003) Mutations in dynein link motor neuron degeneration to defects in retrograde transport. *Science* **300,** 808-812.

Hamel F. G., Bennett R. G. and Duckworth W. C. (1998) Regulation of multicatalytic enzyme activity by insulin and the insulin-degrading enzyme. *Endocrinology* **139,** 4061-4066.

Hammad M., Silva A., Glass J., Sladky J. T. and Benatar M. (2007) Clinical, electrophysiologic, and pathologic evidence for sensory abnormalities in ALS. *Neurology* **69,** 2236-2242.

Hand C. K., Khoris J., Salachas F., Gros-Louis F., Lopes A. A., Mayeux-Portas V., Brewer C. G., Brown R. H., Jr., Meininger V., Camu W. and Rouleau G. A. (2002) A novel locus for familial amyotrophic lateral sclerosis, on chromosome 18q. *Am. J. Hum. Genet.* **70,** 251-256.

Hart P. J. (2006) Pathogenic superoxide dismutase structure, folding, aggregation and turnover. *Curr. Opin. Chem. Biol.* **10,** 131-138.

Haverkamp L. J., Appel V. and Appel S. H. (1995) Natural history of amyotrophic lateral sclerosis in a database population Validation of a scoring system and a model for survival prediction. *Brain* **118,** 707-719.

Hayashi H. and Kato S. (1989) Total manifestations of amyotrophic lateral sclerosis. ALS in the totally locked-in state. *J. Neurol. Sci.* **93,** 19-35.

Hayashi H., Kato S. and Kawada A. (1991) Amyotrophic lateral sclerosis patients living beyond respiratory failure. *J. Neurol. Sci.* **105,** 73-78.

Hayashi H., Kato S., Kawada T. and Tsubaki T. (1987) Amyotrophic lateral sclerosis: oculomotor function in patients in respirators. *Neurology* **37,** 1431-1432.

Hayes D. B., Laue T. M. and Philo J. (2003) SEDNTERP (Sedimentation Utility Software), Amgen Corp..

Hayward C., Colville S., Swingler R. J. and Brock D. J. (1999) Molecular genetic analysis of the APEX nuclease gene in amyotrophic lateral sclerosis. *Neurology* **52,** 1899-1901.

Hayward L. J., Rodriguez J. A., Kim J. W., Tiwari A., Goto J. J., Cabelli D. E., Valentine J. S. and Brown R. H., Jr. (2002) Decreased metallation and activity in subsets of mutant superoxide dismutases associated with familial amyotrophic lateral sclerosis. *J. Biol. Chem.* **277,** 15923-15931.

Heads T., Pollock M., Robertson A., Sutherland W. H. and Allpress S. (1991) Sensory nerve pathology in amyotrophic lateral sclerosis. *Acta Neuropathol.* **82,** 316-320.

Heikenwalder M., Julius C. and Aguzzi A. (2007) Prions and peripheral nerves: a deadly rendezvous. *J. Neurosci. Res.* **85,** 2714-2725.

Hentati A., Bejaoui K., Pericak-Vance M. A., Hentati F., Speer M. C., Hung W. Y., Figlewicz D. A., Haines J., Rimmler J., Ben H. C. and . (1994) Linkage of recessive familial amyotrophic lateral sclerosis to chromosome 2q33-q35. *Nat. Genet.* **7,** 425-428.

Hentati A., Ouahchi K., Pericak-Vance M. A., Nijhawan D., Ahmad A., Yang Y., Rimmler J., Hung W., Schlotter B., Ahmed A., Ben H. M., Hentati F. and Siddique T. (1998) Linkage of a commoner form of recessive amyotrophic lateral sclerosis to chromosome 15q15-q22 markers. *Neurogenetics.* **2,** 55-60.

Hetz C., Thielen P., Fisher J., Pasinelli P., Brown R. H., Korsmeyer S. and Glimcher L. (2007) The proapoptotic BCL-2 family member BIM mediates motoneuron loss in a model of amyotrophic lateral sclerosis. *Cell Death. Differ.* **14,** 1386-1389.

Higgins C. M., Jung C. and Xu Z. (2003) ALS-associated mutant SOD1G93A causes mitochondrial vacuolation by expansion of the intermembrane space and by involvement of SOD1 aggregation and peroxisomes. *BMC. Neurosci.* **4,** 16.

Hirakura Y., Azimov R., Azimova R. and Kagan B. L. (2000) Polyglutamine-induced ion channels: a possible mechanism for the neurotoxicity of Huntington and other CAG repeat diseases. *J. Neurosci. Res.* **60,** 490-494.

Hirakura Y., Carreras I., Sipe J. D. and Kagan B. L. (2002) Channel formation by serum amyloid A: a potential mechanism for amyloid pathogenesis and host defense. *Amyloid.* **9,** 13-23.

Hirakura Y. and Kagan B. L. (2001) Pore formation by beta-2-microglobulin: a mechanism for the pathogenesis of dialysis associated amyloidosis. *Amyloid.* **8,** 94-100.

Hirakura Y., Satoh Y., Hirashima N., Suzuki T., Kagan B. L. and Kirino Y. (1998) Membrane perturbation by the neurotoxic Alzheimer amyloid fragment beta 25-35 requires aggregation and beta-sheet formation. *Biochem. Mol. Biol. Int.* **46,** 787-794.

Hirano A. (1991) Cytopathology of amyotrophic lateral sclerosis. *Adv. Neurol.* **56,** 91-101.

Hirano A. (1996) Neuropathology of ALS: an overview. *Neurology* **47,** S63-S66.

Hirano A., Donnenfeld H., Sasaki S. and Nakano I. (1984) Fine structural observations of neurofilamentous changes in amyotrophic lateral sclerosis. *J Neuropathol. Exp. Neurol.* **43,** 461-470.

Hirokawa N. (1998) Kinesin and dynein superfamily proteins and the mechanism of organelle transport. *Science* **279,** 519-526.

Hoffman E. K., Wilcox H. M., Scott R. W. and Siman R. (1996) Proteasome inhibition enhances the stability of mouse Cu/Zn superoxide dismutase with mutations linked to familial amyotrophic lateral sclerosis. *J. Neurol. Sci.* **139,** 15-20.

Hosler B. A., Siddique T., Sapp P. C., Sailor W., Huang M. C., Hossain A., Daube J. R., Nance M., Fan C., Kaplan J., Hung W. Y., Kenna-Yasek D., Haines J. L., Pericak-Vance M. A., Horvitz H. R. and Brown R. H., Jr. (2000) Linkage of familial amyotrophic lateral sclerosis with frontotemporal dementia to chromosome 9q21-q22. *JAMA* **284,** 1664-1669.

Hough M. A., Grossmann J. G., Antonyuk S. V., Strange R. W., Doucette P. A., Rodriguez J. A., Whitson L. J., Hart P. J., Hayward L. J., Valentine J. S. and Hasnain S. S. (2004) Dimer destabilization in superoxide dismutase may result in disease-causing properties: structures of motor neuron disease mutants. *Proc. Natl. Acad. Sci. U. S. A* **101,** 5976-5981.

Howland D. S., Liu J., She Y., Goad B., Maragakis N. J., Kim B., Erickson J., Kulik J., DeVito L., Psaltis G., DeGennaro L. J., Cleveland D. W. and Rothstein J. D. (2002) Focal loss of the glutamate transporter EAAT2 in a transgenic rat model of SOD1 mutant-mediated amyotrophic lateral sclerosis (ALS). *Proc. Natl. Acad. Sci U. S. A* **99,** 1604-1609.

Ince P. G. and Codd G. A. (2005) Return of the cycad hypothesis - does the amyotrophic lateral sclerosis/parkinsonism dementia complex (ALS/PDC) of Guam have new implications for global health? *Neuropathol. Appl. Neurobiol.* **31,** 345-353.

Inoue H., Tsukita K., Iwasato T., Suzuki Y., Tomioka M., Tateno M., Nagao M., Kawata A., Saido T. C., Miura M., Misawa H., Itohara S. and Takahashi R. (2003) The crucial role of caspase-9 in the disease progression of a transgenic ALS mouse model. *EMBO J.* **22,** 6665-6674.

Isaacs J. D., Dean A. F., Shaw C. E., Al-Chalabi A., Mills K. R. and Leigh P. N. (2007) Amyotrophic lateral sclerosis with sensory neuropathy: part of a multisystem disorder? *J. Neurol. Neurosurg. Psychiatry* **78,** 750-753.

Jaarsma D., Haasdijk E. D., Grashorn J. A., Hawkins R., van D. W., Verspaget H. W., London J. and Holstege J. C. (2000) Human Cu/Zn superoxide dismutase (SOD1) overexpression in mice causes mitochondrial vacuolization, axonal degeneration, and premature motoneuron death and accelerates motoneuron disease in mice expressing a familial amyotrophic lateral sclerosis mutant SOD1. *Neurobiol. Dis.* **7,** 623-643.

Jaarsma D., Teuling E., Haasdijk E. D., De Zeeuw C. I. and Hoogenraad C. C. (2008) Neuron-specific expression of mutant superoxide dismutase is sufficient to induce amyotrophic lateral sclerosis in transgenic mice. *J. Neurosci.* **28,** 2075-2088.

Jablecki C. K., Berry C. and Leach J. (1989) Survival prediction in amyotrophic lateral sclerosis. *Muscle Nerve* **12,** 833-841.

Jackson M., Steers G., Leigh P. N. and Morrison K. E. (1999) Polymorphisms in the glutamate transporter gene EAAT2 in European ALS patients. *J. Neurol* **246,** 1140-1144.

Jacobsson J., Jonsson P. A., Andersen P. M., Forsgren L. and Marklund S. L. (2001) Superoxide dismutase in CSF from amyotrophic lateral sclerosis patients with and without CuZn-superoxide dismutase mutations. *Brain* **124,** 1461-1466.

Jacomy H., Zhu Q., Couillard-Despres S., Beaulieu J. M. and Julien J. P. (1999) Disruption of type IV intermediate filament network in mice lacking the neurofilament medium and heavy subunits. *J. Neurochem.* **73,** 972-984.

Jonsson P. A., Backstrand A., Andersen P. M., Jacobsson J., Parton M., Shaw C., Swingler R., Shaw P. J., Robberecht W., Ludolph A. C., Siddique T., Skvortsova V. I. and Marklund S. L. (2002) CuZn-superoxide dismutase in D90A heterozygotes from recessive and dominant ALS pedigrees. *Neurobiol. Dis.* **10,** 327-333.

Jonsson P. A., Graffmo K. S., Andersen P. M., Brannstrom T., Lindberg M., Oliveberg M. and Marklund S. L. (2006a) Disulphide-reduced superoxide dismutase-1 in CNS of transgenic amyotrophic lateral sclerosis models. *Brain* **129,** 451-464.

Jonsson P. A., Graffmo K. S., Brannstrom T., Nilsson P., Andersen P. M. and Marklund S. L. (2006b) Motor neuron disease in mice expressing the wild type-like D90A mutant superoxide dismutase-1. *J. Neuropathol. Exp. Neurol.* **65,** 1126-1136.

Julien J. P., Cote F. and Collard J. F. (1995) Mice overexpressing the human neurofilament heavy gene as a model of ALS. *Neurobiol. Aging* **16,** 487-490.

Julien J. P. and Kriz J. (2006) Transgenic mouse models of amyotrophic lateral sclerosis. *Biochim. Biophys. Acta.* **1762,** 1013-1024.

Julien J. P. and Mushynski W. E. (1998) Neurofilaments in health and disease. *Prog. Nucleic Acid Res. Mol. Biol.* **61,** 1-23.

Julien J. P. and Beaulieu J. M. (2000) Cytoskeletal abnormalities in amyotrophic lateral sclerosis: beneficial or detrimental effects? *J. Neurol. Sci.* **180,** 7-14.

Kaal E. C., Vlug A. S., Versleijen M. W., Kuilman M., Joosten E. A. and Bar P. R. (2000) Chronic mitochondrial inhibition induces selective motoneuron death *in vitro*: a new model for amyotrophic lateral sclerosis. *J. Neurochem.* **74,** 1158-1165.

Kabashi E., Agar J. N., Taylor D. M., Minotti S. and Durham H. D. (2004) Focal dysfunction of the proteasome: a pathogenic factor in a mouse model of amyotrophic lateral sclerosis. *J. Neurochem.* **89,** 1325-1335.

Kabashi E. and Durham H. D. (2006) Failure of protein quality control in amyotrophic lateral sclerosis. *Biochim. Biophys. Acta* **1762,** 1038-1050.

Kabashi E., Valdmanis P. N., Dion P., Spiegelman D., McConkey B. J., Vande V. C., Bouchard J. P., Lacomblez L., Pochigaeva K., Salachas F., Pradat P. F., Camu W., Meininger V., Dupre N. and Rouleau G. A. (2008) TARDBP mutations in individuals with sporadic and familial amyotrophic lateral sclerosis. *Nat. Genet.* **40,** 572-574.

Kadowaki M. and Kanazawa T. (2003) Amino acids as regulators of proteolysis. *J. Nutr.* **133,** 2052S-2056S.

Kagan B. L., Hirakura Y., Azimov R. and Azimova R. (2001) The channel hypothesis of Huntington's disease. *Brain Res. Bull.* **56,** 281-284.

Kagan B. L., Hirakura Y., Azimov R., Azimova R. and Lin M. C. (2002) The channel hypothesis of Alzheimer's disease: current status. *Peptides* **23,** 1311-1315.

Kalinke U., Bach P., Konig M. and Buchholz C. J. (2006) Vaccination against prion diseases. *Discov. Med.* **6,** 29-34.

Kandel E. R., Schwartz J. H. and Jessell T. M. (2000) *Principles of Neural Science.* McGraw-Hill, New York.

Katayama S., Watanabe C., Noda K., Ohishi H., Yamamura Y., Nishisaka T., Inai K., Asayama K., Murayama S. and Nakamura S. (1999) Numerous conglomerate inclusions in slowly progressive familial amyotrophic lateral sclerosis with posterior column involvement. *J. Neurol. Sci.* **171,** 72-77.

Kato S. (2008) Amyotrophic lateral sclerosis models and human neuropathology: similarities and differences. *Acta Neuropathol.* **115,** 97-114.

Kato S., Oda M. and Tanabe H. (1993) Diminution of dopaminergic neurons in the substantia nigra of sporadic amyotrophic lateral sclerosis. *Neuropathol. Appl. Neurobiol.* **19,** 300-304.

Kato S., Sumi-Akamaru H., Fujimura H., Sakoda S., Kato M., Hirano A., Takikawa M. and Ohama E. (2001) Copper chaperone for superoxide dismutase co-aggregates with superoxide dismutase 1 (SOD1) in neuronal Lewy body-like hyaline inclusions: an immunohistochemical study on familial amyotrophic lateral sclerosis with SOD1 gene mutation. *Acta Neuropathol.* **102,** 233-238.

Kato S., Takikawa M., Nakashima K., Hirano A., Cleveland D. W., Kusaka H., Shibata N., Kato M., Nakano I. and Ohama E. (2000) New consensus research on neuropathological aspects of familial amyotrophic lateral sclerosis with superoxide dismutase 1 (SOD1) gene mutations: inclusions containing SOD1 in neurons and astrocytes. *Amyotroph. Lateral. Scler. Other Motor Neuron Disord.* **1,** 163-184.

Kawamura Y., Dyck P. J., Shimono M., Okazaki H., Tateishi J. and Doi H. (1981) Morphometric comparison of the vulnerability of peripheral motor and sensory neurons in amyotrophic lateral sclerosis. *J Neuropathol. Exp. Neurol.* **40,** 667-675.

Kawashima T., Doh-ura K., Kikuchi H. and Iwaki T. (2001) Cognitive dysfunction in patients with amyotrophic lateral sclerosis is associated with spherical or crescent-shaped ubiquitinated intraneuronal inclusions in the parahippocampal gyrus and amygdala, but not in the neostriatum. *Acta Neuropathol.* **102,** 467-472.

Kayed R., Sokolov Y., Edmonds B., McIntire T. M., Milton S. C., Hall J. E. and Glabe C. G. (2004) Permeabilization of Lipid Bilayers Is a Common Conformation-dependent Activity of Soluble Amyloid Oligomers in Protein Misfolding Diseases. *J. Biol. Chem.* **279,** 46363-46366.

Khabazian I., Bains J. S., Williams D. E., Cheung J., Wilson J. M., Pasqualotto B. A., Pelech S. L., Andersen R. J., Wang Y. T., Liu L., Nagai A., Kim S. U., Craig U. K. and Shaw C. A. (2002) Isolation of various forms of sterol beta-D-glucoside from the seed of Cycas circinalis: neurotoxicity and implications for ALS-parkinsonism dementia complex. *J. Neurochem.* **82,** 516-528.

Kiefhaber T., Rudolph R., Kohler H. H. and Buchner J. (1991) Protein aggregation *in vitro* and *in vivo*: a quantitative model of the kinetic competition between folding and aggregation. *Biotechnology (N. Y.)* **9,** 825-829.

Kieran D., Hafezparast M., Bohnert S., Dick J. R., Martin J., Schiavo G., Fisher E. M. and Greensmith L. (2005) A mutation in dynein rescues axonal transport defects and extends the life span of ALS mice. *J. Cell Biol.* **169,** 561-567.

Kieran D., Kalmar B., Dick J. R., Riddoch-Contreras J., Burnstock G. and Greensmith L. (2004) Treatment with arimoclomol, a coinducer of heat shock proteins, delays disease progression in ALS mice. *Nat. Med.* **10,** 402-405.

Kihira T., Yoshida S., Okamoto K., Kazimoto Y., Ookawa M., Hama K., Miwa H. and Kondo T. (2008) Survival rate of patients with amyotrophic lateral sclerosis in Wakayama Prefecture, Japan, 1966 to 2005. *J. Neurol. Sci.* **268,** 95-101.

Kihira T., Yoshida S., Yoshimasu F., Wakayama I. and Yase Y. (1997) Involvement of Onuf's nucleus in amyotrophic lateral sclerosis. *J. Neurol. Sci.* **147,** 81-88.

Kimmel C. A. and Trammell C. (1981) A rapid procedure for routine double staining of cartilage and bone in fetal and adult animals. *Stain Technol.* **56,** 271-273.

Kingsbury M. A., Friedman B., McConnell M. J., Rehen S. K., Yang A. H., Kaushal D. and Chun J. (2005) Aneuploid neurons are functionally active and integrated into brain circuitry. *Proc. Natl. Acad. Sci. U. S. A* **102,** 6143-6147.

Kisselev A. F., Garcia-Calvo M., Overkleeft H. S., Peterson E., Pennington M. W., Ploegh H. L., Thornberry N. A. and Goldberg A. L. (2003) The caspase-like sites of proteasomes, their substrate specificity, new inhibitors and substrates, and allosteric interactions with the trypsin-like sites. *J. Biol. Chem.* **278,** 35869-35877.

Kisselev A. F. and Goldberg A. L. (2005) Monitoring activity and inhibition of 26S proteasomes with fluorogenic peptide substrates. *Methods Enzymol.* **398,** 364-378.

Kisselev A. F., Kaganovich D. and Goldberg A. L. (2002) Binding of hydrophobic peptides to several non-catalytic sites promotes peptide hydrolysis by all active sites of 20 S proteasomes. Evidence for peptide-induced channel opening in the alpha-rings. *J. Biol. Chem.* **277,** 22260-22270.

Kong J. and Xu Z. (1998) Massive mitochondrial degeneration in motor neurons triggers the onset of amyotrophic lateral sclerosis in mice expressing a mutant SOD1. *J. Neurosci.* **18,** 3241-3250.

Kong J. and Xu Z. (2000) Overexpression of neurofilament subunit NF-L and NF-H extends survival of a mouse model for amyotrophic lateral sclerosis. *Neurosci. Lett.* **281,** 72-74.

Koyama S., Arawaka S., Chang-Hong R., Wada M., Kawanami T., Kurita K., Kato M., Nagai M., Aoki M., Itoyama Y., Sobue G., Chan P. H. and Kato T. (2006) Alteration of familial ALS-linked mutant SOD1 solubility with disease progression: its modulation by the proteasome and Hsp70. *Biochem. Biophys. Res. Commun.* **343,** 719-730.

Kristiansen M., Deriziotis P., Dimcheff D. E., Jackson G. S., Ovaa H., Naumann H., Clarke A. R., van Leeuwen F. W., Menendez-Benito V., Dantuma N. P., Portis J. L., Collinge J. and Tabrizi S. J. (2007) Disease-associated prion protein oligomers inhibit the 26S proteasome. *Mol. Cell* **26,** 175-188.

Kriz J., Meier J., Julien J. P. and Padjen A. L. (2000a) Altered ionic conductances in axons of transgenic mouse expressing the human neurofilament heavy gene: A mouse model of amyotrophic lateral sclerosis. *Exp. Neurol* **163,** 414-421.

Kriz J., Zhu Q., Julien J. P. and Padjen A. L. (2000b) Electrophysiological properties of axons in mice lacking neurofilament subunit genes: disparity between conduction velocity and axon diameter in absence of NF-H. *Brain Res.* **885,** 32-44.

Kurland L. T., Radhakrishnan K., Smith G. E., Armon C. and Nemetz P. N. (1992) Mechanical trauma as a risk factor in classic amyotrophic lateral sclerosis: lack of epidemiologic evidence. *J. Neurol. Sci.* **113,** 133-143.

Lalli G. and Schiavo G. (2002) Analysis of retrograde transport in motor neurons reveals common endocytic carriers for tetanus toxin and neurotrophin receptor p75NTR. *J. Cell Biol.* **156,** 233-239.

Lambrechts D., Poesen K., Fernandez-Santiago R., Al-Chalabi A., Del B. R., Van Vaught P. W., Khan S., Marklund S., Brockington A., van M., I, Anneser J., Shaw C., Ludolph A., Leigh N., Comi G., Gasser T., Shaw P. J., Morrison K., Andersen P., Van den Berg L. H., Thijs V., Siddique T., Robberecht W. and Carmeliet P. (2008) Meta-analysis of VEGF variations in ALS: increased susceptibility in male carriers of the -2578AA genotype. *J Med. Genet.* **E-pub 17 July 2008**.

Lambrechts D., Storkebaum E., Morimoto M., Del-Favero J., Desmet F., Marklund S. L., Wyns S., Thijs V., Andersson J., van M., I, Al-Chalabi A., Bornes S., Musson R., Hansen V., Beckman L., Adolfsson R., Pall H. S., Prats H., Vermeire S., Rutgeerts P., Katayama S., Awata T., Leigh N., Lang-Lazdunski L., Dewerchin M., Shaw C., Moons L., Vlietinck R., Morrison K. E., Robberecht W., Van B. C., Collen D., Andersen P. M. and Carmeliet P. (2003) VEGF is a modifier of amyotrophic lateral sclerosis in mice and humans and protects motoneurons against ischemic death. *Nat. Genet.* **34,** 383-394.

LaMonte B. H., Wallace K. E., Holloway B. A., Shelly S. S., Ascano J., Tokito M., Van W. T., Howland D. S. and Holzbaur E. L. (2002) Disruption of dynein/dynactin inhibits axonal transport in motor neurons causing late-onset progressive degeneration. *Neuron* **34,** 715-727.

Lariviere R. C. and Julien J. P. (2004) Functions of intermediate filaments in neuronal development and disease. *J. Neurobiol.* **58,** 131-148.

Lariviere R. C., Nguyen M. D., Ribeiro-da-Silva A. and Julien J. P. (2002) Reduced number of unmyelinated sensory axons in peripherin null mice. *J. Neurochem.* **81,** 525-532.

Lashuel H. A., Hartley D., Petre B. M., Walz T. and Lansbury P. T., Jr. (2002a) Neurodegenerative disease: amyloid pores from pathogenic mutations. *Nature* **418,** 291.

Lashuel H. A. and Lansbury P. T., Jr. (2006) Are amyloid diseases caused by protein aggregates that mimic bacterial pore-forming toxins? *Q. Rev. Biophys.* **39,** 167-201.

Lashuel H. A., Petre B. M., Wall J., Simon M., Nowak R. J., Walz T. and Lansbury P. T., Jr. (2002b) Alpha-synuclein, especially the Parkinson's disease-associated mutants, forms pore-like annular and tubular protofibrils. *J. Mol. Biol.* **322,** 1089-1102.

Lavine L., Steele J. C., Wolfe N., Calne D. B., O'Brien P. C., Williams D. B., KURLAND L. T. and Schoenberg B. S. (1991) Amyotrophic lateral sclerosis/parkinsonism-dementia complex in southern Guam: is it disappearing? *Adv. Neurol* **56,** 271-285.

Lebowitz J., Lewis M. S. and Schuck P. (2002) Modern analytical ultracentrifugation in protein science: a tutorial review. *Protein Sci.* **11,** 2067-2079.

Lee J. P., Gerin C., Bindokas V. P., Miller R., Ghadge G. and Roos R. P. (2002) No correlation between aggregates of Cu/Zn superoxide dismutase and cell death in familial amyotrophic lateral sclerosis. *J. Neurochem.* **82,** 1229-1238.

Lee M. K., Marszalek J. R. and Cleveland D. W. (1994) A mutant neurofilament subunit causes massive, selective motor neuron death: implications for the pathogenesis of human motor neuron disease. *Neuron* **13,** 975-988.

Leigh P. N., Dodson A., Swash M., Brion J. P. and Anderton B. H. (1989) Cytoskeletal abnormalities in motor neuron disease. An immunocytochemical study. *Brain* **112,** 521-535.

Leigh P. N. and Swash M. (1991) Cytoskeletal pathology in motor neuron diseases. *Adv. Neurol.* **56,** 115-124.

Leinweber B., Barofsky E., Barofsky D. F., Ermilov V., Nylin K. and Beckman J. S. (2004) Aggregation of ALS mutant superoxide dismutase expressed in Escherichia coli. *Free Rad. Biol. Med.* **36,** 911-918.

Lemmens R., Van H. A., Hersmus N., Geelen V., D'Hollander I., Thijs V., Van Den B. L., Carmeliet P. and Robberecht W. (2007) Overexpression of mutant superoxide dismutase 1 causes a motor axonopathy in the zebrafish. *Hum. Mol. Genet.* **16,** 2359-2365.

Leung C. L., He C. Z., Kaufmann P., Chin S. S., Naini A., Liem R. K., Mitsumoto H. and Hays A. P. (2004) A pathogenic peripherin gene mutation in a patient with amyotrophic lateral sclerosis. *Brain Pathol.* **14,** 290-296.

Li T. M., Alberman E. and Swash M. (1990) Clinical features and associations of 560 cases of motor neuron disease. *J. Neurol. Neurosurg. Psychiatry* **53,** 1043-1045.

Lindberg M. J., Bystrom R., Boknas N., Andersen P. M. and Oliveberg M. (2005) Systematically perturbed folding patterns of amyotrophic lateral sclerosis (ALS)-associated SOD1 mutants. *Proc. Natl. Acad. Sci. U. S. A* **102,** 9754-9759.

Lindberg M. J., Tibell L. and Oliveberg M. (2002) Common denominator of Cu/Zn superoxide dismutase mutants associated with amyotrophic lateral sclerosis: decreased stability of the apo state. *Proc. Natl. Acad. Sci U. S. A* **99,** 16607-16612.

Lindersson E., Beedholm R., Hojrup P., Moos T., Gai W., Hendil K. B. and Jensen P. H. (2004) Proteasomal inhibition by alpha-synuclein filaments and oligomers. *J. Biol. Chem.* **279,** 12924-12934.

Lindsay K. W. and Bone I. (1992) *Neurology and Neurosurgery Illustrated.* Churchill Livingstone, London.

Lino M. M., Schneider C. and Caroni P. (2002) Accumulation of SOD1 mutants in postnatal motoneurons does not cause motoneuron pathology or motoneuron disease. *J. Neurosci.* **22,** 4825-4832.

Liu D., Wen J., Liu J. and Li L. (1999a) The roles of free radicals in amyotrophic lateral sclerosis: reactive oxygen species and elevated oxidation of protein, DNA, and membrane phospholipids. *FASEB J.* **13,** 2318-2328.

Liu J., Lillo C., Jonsson P. A., Vande V. C., Ward C. M., Miller T. M., Subramaniam J. R., Rothstein J. D., Marklund S., Andersen P. M., Brannstrom T., Gredal O., Wong P. C., Williams D. S. and Cleveland D. W. (2004) Toxicity of familial ALS-linked SOD1 mutants from selective recruitment to spinal mitochondria. *Neuron* **43,** 5-17.

Liu J., Shinobu L. A., Ward C. M., Young D. and Cleveland D. W. (2005) Elevation of the Hsp70 chaperone does not effect toxicity in mouse models of familial amyotrophic lateral sclerosis. *J. Neurochem.* **93,** 875-882.

Liu J. J., Ding J., Wu C., Bhagavatula P., Cui B., Chu S., Mobley W. C. and Yang Y. (2007) Retrolinkin, a membrane protein, plays an important role in retrograde axonal transport. *Proc. Natl. Acad. Sci. U. S. A* **104,** 2223-2228.

Liu R., Narla R. K., Kurinov I., Li B. and Uckun F. M. (1999b) Increased hydroxyl radical production and apoptosis in PC12 neuron cells expressing the gain-of-function mutant G93A SOD1 gene. *Radiat. Res.* **151,** 133-141.

Lobsiger C. S., Boillee S. and Cleveland D. W. (2007) Toxicity from different SOD1 mutants dysregulates the complement system and the neuronal regenerative response in ALS motor neurons. *Proc. Natl. Acad. Sci U. S. A* **104,** 7319-7326.

Logroscino G., Traynor B. J., Hardiman O., Chio' A., Couratier P., Mitchell J. D., Swingler R. J., Beghi E. and for E. U. R. A. (2008) Descriptive epidemiology of amyotrophic lateral sclerosis: new evidence and unsolved issues. *J. Neurol. Neurosurg. Psychiatry* **79,** 6-11.

Lomen-Hoerth C., Murphy J., Langmore S., Kramer J. H., Olney R. K. and Miller B. (2003) Are amyotrophic lateral sclerosis patients cognitively normal? *Neurology* **60,** 1094-1097.

Lopez S. M., Pasquini L., Besio M. M., Pasquini J. M. and Soto E. (2003) Relationship between beta-amyloid degradation and the 26S proteasome in neural cells. *Exp. Neurol.* **180,** 131-143.

Luquin N., Yu B., Trent R. J., Morahan J. M. and Pamphlett R. (2008) An analysis of the entire SOD1 gene in sporadic ALS. *Neuromuscul. Disord.***18,** 545-552.

Maatkamp A., Vlug A., Haasdijk E., Troost D., French P. J. and Jaarsma D. (2004) Decrease of Hsp25 protein expression precedes degeneration of motoneurons in ALS-SOD1 mice. *Eur. J. Neurosci.* **20,** 14-28.

Mackenzie I. R. and Feldman H. (2003) The relationship between extramotor ubiquitin-immunoreactive neuronal inclusions and dementia in motor neuron disease. *Acta Neuropathol.* **105,** 98-102.

Malinowski D. P. and Fridovich I. (1979) Subunit association and side-chain reactivities of bovine erythrocyte superoxide dismutase in denaturing solvents. *Biochemistry* **18,** 5055-5060.

Mannen T. (2000) Neuropathological findings of Onuf's nucleus and its significance. *Neuropathology.* **20 Suppl,** S30-S33.

Mannen T., Iwata M., Toyokura Y. and Nagashima K. (1977) Preservation of a certain motoneurone group of the sacral cord in amyotrophic lateral sclerosis: its clinical significance. *J. Neurol. Neurosurg. Psychiatry* **40,** 464-469.

Mannen T., Iwata M., Toyokura Y. and Nagashima K. (1982) The Onuf's nucleus and the external anal sphincter muscles in amyotrophic lateral sclerosis and Shy-Drager syndrome. *Acta Neuropathol.* **58,** 255-260.

Manser C., Stevenson A., Banner S., Davies J., Tudor E. L., Ono Y., Nigel L. P., McLoughlin D. M., Shaw C. E. and Miller C. C. (2008) Deregulation of PKN1 activity disrupts neurofilament organisation and axonal transport. *FEBS Lett.* **582,** 2303-2308.

Martin L. J. (1999) Neuronal death in amyotrophic lateral sclerosis is apoptosis: possible contribution of a programmed cell death mechanism. *J. Neuropathol. Exp. Neurol* **58,** 459-471.

Massenet S., Pellizzoni L., Paushkin S., Mattaj I. W. and Dreyfuss G. (2002) The SMN complex is associated with snRNPs throughout their cytoplasmic assembly pathway. *Mol. Cell Biol.* **22,** 6533-6541.

Massman P. J., Sims J., Cooke N., Haverkamp L. J., Appel V. and Appel S. H. (1996) Prevalence and correlates of neuropsychological deficits in amyotrophic lateral sclerosis. *J. Neurol. Neurosurg. Psychiatry* **61,** 450-455.

Masu Y., Wolf E., Holtmann B., Sendtner M., Brem G. and Thoenen H. (1993) Disruption of the CNTF gene results in motor neuron degeneration. *Nature* **365,** 27-32.

Matsumoto G., Kim S. and Morimoto R. I. (2006) Huntingtin and mutant SOD1 form aggregate structures with distinct molecular properties in human cells. *J. Biol. Chem.* **281,** 4477-4485.

Matsumoto G., Stojanovic A., Holmberg C. I., Kim S. and Morimoto R. I. (2005) Structural properties and neuronal toxicity of amyotrophic lateral sclerosis-associated Cu/Zn superoxide dismutase 1 aggregates. *J. Cell Biol.* **171,** 75-85.

Matsumoto S., Kusaka H., Ito H., Shibata N., Asayama T. and Imai T. (1996) Sporadic amyotrophic lateral sclerosis with dementia and Cu/Zn superoxide dismutase-positive Lewy body-like inclusions. *Clin. Neuropathol.* **15,** 41-46.

Mattson M. P. (2003) Excitotoxic and excitoprotective mechanisms: abundant targets for the prevention and treatment of neurodegenerative disorders. *Neuromolecular. Med.* **3,** 65-94.

Matyja E., Naganska E., Taraszewska A. and Rafalowska J. (2005) The mode of spinal motor neurons degeneration in a model of slow glutamate excitotoxicity *in vitro*. *Folia Neuropathol.* **43,** 7-13.

McLeod M. J. (1980) Differential staining of cartilage and bone in whole mouse fetuses by alcian blue and alizarin red S. *Teratology* **22,** 299-301.

McNeely J. C. and Brown D. (1992) Laboratory evaluation of leukocytes, in *Clinical Hematology: Principles, Procedures, Correlations,* (Steine-Martin E. A., Lotspeich-Steininger C. A. and Koepke J. A., eds), pp. 318-323. Lippincott-Raven.

Meier J., Couillard-Despres S., Jacomy H., Gravel C. and Julien J. P. (1999) Extra neurofilament NF-L subunits rescue motor neuron disease caused by overexpression of the human NF-H gene in mice. *J. Neuropathol. Exp. Neurol.* **58,** 1099-1110.

Meyer T., Lenk U., Kuther G., Weindl A., Speer A. and Ludolph A. C. (1995) Studies of the coding region of the neuronal glutamate transporter gene in amyotrophic lateral sclerosis. *Ann. Neurol.* **37,** 817-819.

Mezei M., Andersen P. M., Stewart H., Weber M. and Eisen A. (1999) Motor system abnormalities in heterozygous relatives of a D90A homozygous CuZn-SOD ALS patient of finnish extraction. *J. Neurol. Sci.* **169,** 49-55.

Mezzapesa D. M., Ceccarelli A., Dicuonzo F., Carella A., De Caro M. F., Lopez M., Samarelli V., Livrea P. and Simone I. L. (2007) Whole-Brain and Regional Brain Atrophy in Amyotrophic Lateral Sclerosis. *AJNR Am. J. Neuroradiol.* **28,** 255-259.

Middelberg A. P. (2002) Preparative protein refolding. *Trends Biotechnol.* **20,** 437-443.

Mills P. B., Struys E., Jakobs C., Plecko B., Baxter P., Baumgartner M., Willemsen M. A., Omran H., Tacke U., Uhlenberg B., Weschke B. and Clayton P. T. (2006) Mutations in antiquitin in individuals with pyridoxine-dependent seizures. *Nat. Med.* **12,** 307-309.

Miroy G. J., Lai Z., Lashuel H. A., Peterson S. A., Strang C. and Kelly J. W. (1996) Inhibiting transthyretin amyloid fibril formation via protein stabilization. *Proc. Natl. Acad. Sci U. S. A* **93,** 15051-15056.

Mitne-Neto M., Ramos C. R., Pimenta D. C., Luz J. S., Nishimura A. L., Gonzales F. A., Oliveira C. C. and Zatz M. (2007) A mutation in human VAP-B--MSP domain, present in ALS patients, affects the interaction with other cellular proteins. *Protein Expr. Purif.* **55,** 139-146.

Mondola P., Annella T., Santillo M. and Santangelo F. (1996) Evidence for secretion of cytosolic CuZn superoxide dismutase by Hep G2 cells and human fibroblasts. *Int. J. Biochem. Cell Biol.* **28,** 677-681.

Mondola P., Seru R., Damiano S. and Santillo M. (2007) A new perspective on the role of CuZn superoxide dismutase (SOD1). *Cen. Eur. J. Biol.* **2,** 337-350.

Morris C. J. (1969) Human skeletal muscle fibre type grouping and collateral re-innervation. *J. Neurol. Neurosurg. Psychiatry* **32,** 440-444.

Morrison B. M., Morrison J. H. and Gordon J. W. (1998) Superoxide dismutase and neurofilament transgenic models of amyotrophic lateral sclerosis. *J. Exp. Zool.* **282,** 32-47.

Mosch B., Morawski M., Mittag A., Lenz D., Tarnok A. and Arendt T. (2007) Aneuploidy and DNA Replication in the Normal Human Brain and Alzheimer's Disease. *J. Neurosci.* **27,** 6859-6867.

Moulard B., Sefiani A., Laamri A., Malafosse A. and Camu W. (1996) Apolipoprotein E genotyping in sporadic amyotrophic lateral sclerosis: evidence for a major influence on the clinical presentation and prognosis. *J. Neurol. Sci.* **139 Suppl,** 34-37.

Mu X., He J., Anderson D. W., Trojanowski J. Q. and Springer J. E. (1996) Altered expression of bcl-2 and bax mRNA in amyotrophic lateral sclerosis spinal cord motor neurons. *Ann. Neurol* **40,** 379-386.

Mui S., Rebeck G. W., Kenna-Yasek D., Hyman B. T. and Brown R. H., Jr. (1995) Apolipoprotein E epsilon 4 allele is not associated with earlier age at onset in amyotrophic lateral sclerosis. *Ann. Neurol* **38,** 460-463.

Mulder D. W., Bushek W., Spring E., Karnes J. and Dyck P. J. (1983) Motor neuron disease (ALS): evaluation of detection thresholds of cutaneous sensation. *Neurology* **33,** 1625-1627.

Munch C., Rosenbohm A., Sperfeld A. D., Uttner I., Reske S., Krause B. J., Sedlmeier R., Meyer T., Hanemann C. O., Stumm G. and Ludolph A. C. (2005) Heterozygous R1101K mutation of the DCTN1 gene in a family with ALS and FTD. *Ann. Neurol.* **58,** 777-780.

Munch C., Sedlmeier R., Meyer T., Homberg V., Sperfeld A. D., Kurt A., Prudlo J., Peraus G., Hanemann C. O., Stumm G. and Ludolph A. C. (2004) Point mutations of the p150 subunit of dynactin (DCTN1) gene in ALS. *Neurology* **63,** 724-726.

Murakami T., Nagano I., Hayashi T., Manabe Y., Shoji M., Setoguchi Y. and Abe K. (2001) Impaired retrograde axonal transport of adenovirus-mediated *E. coli* LacZ gene in the mice carrying mutant SOD1 gene. *Neurosci. Lett.* **308,** 149-152.

Murch S. J., Cox P. A., Banack S. A., Steele J. C. and Sacks O. W. (2004) Occurrence of beta-methylamino-l-alanine (BMAA) in ALS/PDC patients from Guam. *Acta Neurol. Scand.* **110,** 267-269.

Nagai M., Aoki M., Miyoshi I., Kato M., Pasinelli P., Kasai N., Brown R. H., Jr. and Itoyama Y. (2001) Rats expressing human cytosolic copper-zinc superoxide dismutase transgenes with amyotrophic lateral sclerosis: associated mutations develop motor neuron disease. *J. Neurosci.* **21,** 9246-9254.

Nagai M., Re D. B., Nagata T., Chalazonitis A., Jessell T. M., Wichterle H. and Przedborski S. (2007) Astrocytes expressing ALS-linked mutated SOD1 release factors selectively toxic to motor neurons. *Nat. Neurosci.* **10,** 615-622.

NCBI Entrez Gene (2008a) ALDH7A1 aldehyde dehydrogenase 7 family, member A1 [Homo sapiens].

NCBI Entrez Gene (2008b) CTXN3 cortexin 3 [Homo sapiens].

NCBI Entrez Gene (2008c) SLC27A6 solute carrier family 27 (fatty acid transporter), member 6 [Homo sapiens].

Neumann M., Sampathu D. M., Kwong L. K., Truax A. C., Micsenyi M. C., Chou T. T., Bruce J., Schuck T., Grossman M., Clark C. M., McCluskey L. F., Miller B. L., Masliah E., Mackenzie I. R., Feldman H., Feiden W., Kretzschmar H. A., Trojanowski J. Q. and Lee V. M. (2006) Ubiquitinated TDP-43 in frontotemporal lobar degeneration and amyotrophic lateral sclerosis. *Science* **314,** 130-133.

Niesen F. H., Berglund H. and Vedadi M. (2007) The use of differential scanning fluorimetry to detect ligand interactions that promote protein stability. *Nat. Protoc.* **2,** 2212-2221.

Nilsson K. M., Jonsson A. P., Graffmo K. S., Andersen P., Marklund S. and Brannstrom T. (2007) Inclusions containing superoxide dismutase-1 are regularly present in amyotrophic lateral sclerosis patients lacking mutations in the enzyme, in *Neuroscience 2007,* San Diego, California.

Nishimura A. L., Mitne-Neto M., Silva H. C., Oliveira J. R., Vainzof M. and Zatz M. (2004a) A novel locus for late onset amyotrophic lateral sclerosis/motor neurone disease variant at 20q13. *J. Med. Genet.* **41,** 315-320.

Nishimura A. L., Mitne-Neto M., Silva H. C., Richieri-Costa A., Middleton S., Cascio D., Kok F., Oliveira J. R., Gillingwater T., Webb J., Skehel P. and Zatz M. (2004b) A mutation in the vesicle-trafficking protein VAPB causes late-onset spinal muscular atrophy and amyotrophic lateral sclerosis. *Am. J. Hum. Genet.* **75,** 822-831.

Novagen (2001) Protein Expression: Prokaryotic Expression: pET System Overview, Novagen.

Obata Y., Niikura T., Kanekura K., Hashimoto Y., Kawasumi M., Kita Y., Aiso S., Matsuoka M. and Nishimoto I. (2005) Expression of N19S-SOD1, an SOD1 mutant found in sporadic amyotrophic lateral sclerosis patients, induces low-grade motoneuronal toxicity. *J. Neurosci. Res.* **81,** 720-729.

Oeda T., Shimohama S., Kitagawa N., Kohno R., Imura T., Shibasaki H. and Ishii N. (2001) Oxidative stress causes abnormal accumulation of familial amyotrophic lateral sclerosis-related mutant SOD1 in transgenic Caenorhabditis elegans. *Hum. Mol. Genet.* **10,** 2013-2023.

Okamoto K., Hirai S., Iizuka T., Yanagisawa T. and Watanabe M. (1991a) Reexamination of granulovacuolar degeneration. *Acta Neuropathol.* **82,** 340-345.

Okamoto K., Hirai S., Ishiguro K., Kawarabayashi T. and Takatama M. (1991b) Light and electron microscopic and immunohistochemical observations of the Onuf's nucleus of amyotrophic lateral sclerosis. *Acta Neuropathol.* **81,** 610-614.

Okamoto K., Hirai S., Shoji M., Senoh Y. and Yamazaki T. (1990) Axonal swellings in the corticospinal tracts in amyotrophic lateral sclerosis. *Acta Neuropathol.* **80,** 222-226.

Okamoto K., Hirai S., Yamazaki T., Sun X. Y. and Nakazato Y. (1991c) New ubiquitin-positive intraneuronal inclusions in the extra-motor cortices in patients with amyotrophic lateral sclerosis. *Neurosci. Lett.* **129,** 233-236.

Okamoto K., Mizuno Y. and Fujita Y. (2008) Bunina bodies in amyotrophic lateral sclerosis. *Neuropathology.* **28,** 109-115.

Okumura H. (2003) Epidemiological and clinical patterns of western pacific amyotrophic lateral sclerosis (ALS) in Guam and sporadic ALS in Rochester, Minnesota, U.S.A. and Hokkaido, Japan: a comparative study. *Hokkaido Igaku Zasshi* **78,** 187-195.

OMIM (2001) RNA, U small muclear, export adaptor; RNUXA. *NCBI Entrez Gene* http://www.ncbi.nlm.nih.gov/entrez/dispomim.cgi?id=604924.

OMIM (2004) Solute carrier family 27 (Fatty acid transporter), member 6; SLC27A6. *NCBI Entrez Gene* http://www.ncbi.nlm.nih.gov/entrez/dispomim.cgi?id=604196.

OMIM (2005) Contractural arachnodactyly, congenital. *NCBI Entrez Gene* http://www.ncbi.nlm.nih.gov/entrez/dispomim.cgi?id=121050.

OMIM (2006) Frontotemporal Dementia, Chromosome 3-linked, FTD3. *NCBI Entrez Gene* http://www.ncbi.nlm.nih.gov/entrez/dispomim.cgi?id=600795.

OMIM (2007a) Aldehyde dehydrogenase 7 family, member A1; ALDH7A1. *NCBI Entrez Gene* http://www.ncbi.nlm.nih.gov/entrez/dispomim.cgi?id=107323.

OMIM (2007b) Lamin B1; LMNB1. *NCBI Entrez Gene* http://www.ncbi.nlm.nih.gov/entrez/dispomim.cgi?id=150340.

OMIM (2008) MARCH3 membrane-associated ring finger (C3HC4) 3 [Homo sapiens]. *NCBI Entrez Gene* http://www.ncbi.nlm.nih.gov/entrez/dispomim.cgi?id=600795.

Orrell R. W., Habgood J. J., Malaspina A., Mitchell J., Greenwood J., Lane R. J. and deBelleroche J. S. (1999) Clinical characteristics of SOD1 gene mutations in UK families with ALS. *J. Neurol. Sci.* **169,** 56-60.

Papapostolou D., Coux O. and Reboud-Ravaux M. (2002) Regulation of the 26S proteasome activities by peptides mimicking cleavage products. *Biochem. Biophy. Res. Comm.* **295,** 1090-1095.

Parkinson N., Ince P. G., Smith M. O., Highley R., Skibinski G., Andersen P. M., Morrison K. E., Pall H. S., Hardiman O., Collinge J., Shaw P. J. and Fisher E. M. (2006) ALS phenotypes with mutations in CHMP2B (charged multivesicular body protein 2B). *Neurology* **67,** 1074-1077.

Pasinelli P., Belford M. E., Lennon N., Bacskai B. J., Hyman B. T., Trotti D. and Brown R. H., Jr. (2004) Amyotrophic lateral sclerosis-associated SOD1 mutant proteins bind and aggregate with Bcl-2 in spinal cord mitochondria. *Neuron* **43,** 19-30.

Pasinelli P., Borchelt D. R., Houseweart M. K., Cleveland D. W. and Brown R. H., Jr. (1998) Caspase-1 is activated in neural cells and tissue with amyotrophic lateral sclerosis-associated mutations in copper-zinc superoxide dismutase. *Proc. Natl. Acad. Sci U. S. A.* **95,** 15763-15768.

Percival N. J. and Sykes P. J. (1989) Syndactyly: a review of the factors which influence surgical treatment. *J. Hand Surg. [Br.]* **14,** 196-200.

Peretz D., Williamson R. A., Kaneko K., Vergara J., Leclerc E., Schmitt-Ulms G., Mehlhorn I. R., Legname G., Wormald M. R., Rudd P. M., Dwek R. A., Burton D. R. and Prusiner S. B. (2001) Antibodies inhibit prion propagation and clear cell cultures of prion infectivity. *Nature* **412,** 739-743.

Pette D. (2001) Historical Perspectives: plasticity of mammalian skeletal muscle. *J. Appl. Physiol* **90,** 1119-1124.

Phillips J. P., Tainer J. A., Getzoff E. D., Boulianne G. L., Kirby K. and Hilliker A. J. (1995) Subunit-destabilizing mutations in Drosophila copper/zinc superoxide dismutase: neuropathology and a model of dimer dysequilibrium. *Proc. Natl. Acad. Sci U. S. A.* **92,** 8574-8578.

Piao Y. S., Wakabayashi K., Kakita A., Yamada M., Hayashi S., Morita T., Ikuta F., Oyanagi K. and Takahashi H. (2003) Neuropathology with clinical correlations of sporadic amyotrophic lateral sclerosis: 102 autopsy cases examined between 1962 and 2000. *Brain Pathol.* **13,** 10-22.

Plaitakis A., Constantakakis E. and Smith J. (1988) The neuroexcitotoxic amino acids glutamate and aspartate are altered in the spinal cord and brain in amyotrophic lateral sclerosis. *Ann. Neurol* **24,** 446-449.

Plato C. C., Garruto R. M., Galasko D., Craig U. K., Plato M., Gamst A., Torres J. M. and Wiederholt W. (2003) Amyotrophic lateral sclerosis and parkinsonism-dementia complex of Guam: changing incidence rates during the past 60 years. *Am. J. Epidemiol.* **157,** 149-157.

Portet F., Cadilhac C., Touchon J. and Camu W. (2001) Cognitive impairment in motor neuron disease with bulbar onset. *Amyotroph. Lateral. Scler. Other Motor Neuron Disord.* **2,** 23-29.

Pramatarova A., Laganiere J., Roussel J., Brisebois K. and Rouleau G. A. (2001) Neuron-specific expression of mutant superoxide dismutase 1 in transgenic mice does not lead to motor impairment. *J. Neurosci.* **21,** 3369-3374.

Pugdahl K., Fuglsang-Frederiksen A., de C. M., Johnsen B., Fawcett P. R., Labarre-Vila A., Liguori R., Nix W. A. and Schofield I. S. (2007) Generalised sensory system abnormalities in amyotrophic lateral sclerosis: a European multicentre study. *J. Neurol. Neurosurg. Psychiatry* **78,** 746-749.

Pugdahl K., Fuglsang-Frederiksen A., Johnsen B., de C. M., Fawcett P. R., Labarre-Vila A., Liguori R., Nix W. A. and Schofield I. S. (2008) A prospective multicentre study on sural nerve action potentials in ALS. *Clin. Neurophysiol.* **119,** 1106-1110.

Pullen A. H., Tucker D. and Martin J. E. (1997) Morphological and morphometric characterisation of Onuf's nucleus in the spinal cord in man. *J Anat.* **191,** 201-213.

Puls I., Jonnakuty C., LaMonte B. H., Holzbaur E. L., Tokito M., Mann E., Floeter M. K., Bidus K., Drayna D., Oh S. J., Brown R. H., Jr., Ludlow C. L. and Fischbeck K. H. (2003) Mutant dynactin in motor neuron disease. *Nat. Genet.* **33,** 455-456.

Puttaparthi K., Wojcik C., Rajendran B., DeMartino G. N. and Elliott J. L. (2003) Aggregate formation in the spinal cord of mutant SOD1 transgenic mice is reversible and mediated by proteasomes. *J. Neurochem.* **87,** 851-860.

Qureshi A. I., Wilmot G., Dihenia B., Schneider J. A. and Krendel D. A. (1996) Motor neuron disease with parkinsonism. *Arch. Neurol.* **53,** 987-991.

Rabin B. A., Griffin J. W., Crain B. J., Scavina M., Chance P. F. and Cornblath D. R. (1999) Autosomal dominant juvenile amyotrophic lateral sclerosis. *Brain* **122,** 1539-1550.

Rakhit R., Crow J. P., Lepock J. R., Kondejewski L. H., Cashman N. R. and Chakrabartty A. (2004) Monomeric Cu,Zn-superoxide dismutase is a common misfolding intermediate in the oxidation models of sporadic and familial amyotrophic lateral sclerosis. *J. Biol. Chem.* **279,** 15499-15504.

Rakhit R., Cunningham P., Furtos-Matei A., Dahan S., Qi X. F., Crow J. P., Cashman N. R., Kondejewski L. H. and Chakrabartty A. (2002) Oxidation-induced misfolding and aggregation of superoxide dismutase and its implications for amyotrophic lateral sclerosis. *J. Biol. Chem.* **277,** 47551-47556.

Rakhit R., Robertson J., Vande V. C., Horne P., Ruth D. M., Griffin J., Cleveland D. W., Cashman N. R. and Chakrabartty A. (2007) An immunological epitope selective for pathological monomer-misfolded SOD1 in ALS. *Nat. Med.* **13,** 754-759.

Ratovitski T., Corson L. B., Strain J., Wong P., Cleveland D. W., Culotta V. C. and Borchelt D. R. (1999) Variation in the biochemical/biophysical properties of mutant superoxide dismutase 1 enzymes and the rate of disease progression in familial amyotrophic lateral sclerosis kindreds. *Hum. Mol. Genet.* **8,** 1451-1460.

Ravits J., Laurie P., Fan Y. and Moore D. H. (2007a) Implications of ALS focality: rostral-caudal distribution of lower motor neuron loss postmortem. *Neurology* **68,** 1576-1582.

Ravits J., Paul P. and Jorg C. (2007b) Focality of upper and lower motor neuron degeneration at the clinical onset of ALS. *Neurology* **68,** 1571-1575.

Ray S. S., Nowak R. J., Strokovich K., Brown R. H., Jr., Walz T. and Lansbury P. T., Jr. (2004) An intersubunit disulfide bond prevents *in vitro* aggregation of a superoxide dismutase-1 mutant linked to familial amytrophic lateral sclerosis. *Biochemistry* **43,** 4899-4905.

Reaume A. G., Elliott J. L., Hoffman E. K., Kowall N. W., Ferrante R. J., Siwek D. F., Wilcox H. M., Flood D. G., Beal M. F., Brown R. H., Jr., Scott R. W. and Snider W. D. (1996) Motor neurons in Cu/Zn superoxide dismutase-deficient mice develop normally but exhibit enhanced cell death after axonal injury. *Nat. Genet.* **13,** 43-47.

Rehen S. K., Yung Y. C., McCreight M. P., Kaushal D., Yang A. H., Almeida B. S. V., Kingsbury M. A., Cabral K. M. S., McConnell M. J., Anliker B., Fontanoz M. and Chun J. (2005) Constitutional Aneuploidy in the Normal Human Brain. *J. Neurosci.* **25,** 2176-2180.

Rehen S. K., McConnell M. J., Kaushal D., Kingsbury M. A., Yang A. H. and Chun J. (2001) Chromosomal variation in neurons of the developing and adult mammalian nervous system. *Proc. Natl. Acad. Sci U. S. A.* **98,** 13361-13366.

Riddles P. W., Blakeley R. L. and Zerner B. (1979) Ellman's reagent: 5,5'-dithiobis(2-nitrobenzoic acid)--a reexamination. *Anal. Biochem.* **94,** 75-81.

Riddles P. W., Blakeley R. L. and Zerner B. (1983) Reassessment of Ellman's reagent. *Methods Enzymol.* **91,** 49-60.

Ripps M. E., Huntley G. W., Hof P. R., Morrison J. H. and Gordon J. W. (1995) Transgenic mice expressing an altered murine superoxide dismutase gene provide an animal model of amyotrophic lateral sclerosis. *Proc. Natl. Acad. Sci U. S. A.* **92,** 689-693.

Robberecht W., Aguirre T., Van Den B. L., Tilkin P., Cassiman J. J. and Matthijs G. (1996) D90A heterozygosity in the SOD1 gene is associated with familial and apparently sporadic amyotrophic lateral sclerosis. *Neurology* **47,** 1336-1339.

Rodriguez J. A., Shaw B. F., Durazo A., Sohn S. H., Doucette P. A., Nersissian A. M., Faull K. F., Eggers D. K., Tiwari A., Hayward L. J. and Valentine J. S. (2005) Destabilization of apoprotein is insufficient to explain Cu,Zn-superoxide dismutase-linked ALS pathogenesis. *Proc. Natl. Acad. Sci U. S. A.* **102,** 10516-10521.

Rodriguez J. A., Valentine J. S., Eggers D. K., Roe J. A., Tiwari A., Brown R. H., Jr. and Hayward L. J. (2002) Familial amyotrophic lateral sclerosis-associated mutations decrease the thermal stability of distinctly metallated species of human copper/zinc superoxide dismutase. *J. Biol. Chem.* **277,** 15932-15937.

Roe J. A., Butler A., Scholler D. M., Valentine J. S., Marky L. and Breslauer K. J. (1988) Differential scanning calorimetry of Cu,Zn-superoxide dismutase, the apoprotein, and its zinc-substituted derivatives. *Biochemistry* **27,** 950-958.

Roman G. C. (1996) Neuroepidemiology of amyotrophic lateral sclerosis: clues to aetiology and pathogenesis. *J. Neurol. Neurosurg. Psychiatry* **61,** 131-137.

Rosen A. D. (1978) Amyotrophic lateral sclerosis. Clinical features and prognosis. *Arch. Neurol.* **35,** 638-642.

Rosen D. R., Siddique T., Patterson D., Figlewicz D. A., Sapp P., Hentati A., Donaldson D., Goto J., O'Regan J. P. and Deng et a. (1993) Mutations in Cu/Zn superoxide dismutase gene are associated with familial amyotrophic lateral sclerosis. *Nature* **362,** 59-62.

Rothstein J. D. (1995) Excitotoxic mechanisms in the pathogenesis of amyotrophic lateral sclerosis. *Adv. Neurol.* **68,** 7-20.

Rothstein J. D., Van K. M., Levey A. I., Martin L. J. and Kuncl R. W. (1995) Selective loss of glial glutamate transporter GLT-1 in amyotrophic lateral sclerosis. *Ann. Neurol.* **38,** 73-84.

Ruddy D. M., Parton M. J., Al-Chalabi A., Lewis C. M., Vance C., Smith B. N., Leigh P. N., Powell J. F., Siddique T., Meyjes E. P., Baas F., de J., V and Shaw C. E. (2003) Two families with familial amyotrophic lateral sclerosis are linked to a novel locus on chromosome 16q. *Am. J. Hum. Genet.* **73,** 390-396.

Saitoh Y., Yokosawa H. and Ishii S. (1989) Sodium dodecyl sulfate-induced conformational and enzymatic changes of multicatalytic proteinase. *Biochem. Biophys. Res. Commun.* **162,** 334-339.

Sambrook J. and Russell D. W. (2001) *Molecular Cloning: A Laboratory Manual.* Cold Spring Harbor Laboratory Press.

Santillo M., Secondo A., Seru R., Damiano S., Garbi C., Taverna E., Rosa P., Giovedi S., Benfenati F. and Mondola P. (2007) Evidence of calcium- and SNARE-dependent release of CuZn superoxide dismutase from rat pituitary GH3 cells and synaptosomes in response to depolarization. *J. Neurochem.* **102,** 679-685.

Sapp P. C., Hosler B. A., Kenna-Yasek D., Chin W., Gann A., Genise H., Gorenstein J., Huang M., Sailer W., Scheffler M., Valesky M., Haines J. L., Pericak-Vance M., Siddique T., Horvitz H. R. and Brown R. H., Jr. (2003) Identification of two novel loci for dominantly inherited familial amyotrophic lateral sclerosis. *Am. J. Hum. Genet.* **73,** 397-403.

Sasaki N., Fukatsu R., Tsuzuki K., Hayashi Y., Yoshida T., Fujii N., Koike T., Wakayama I., Yanagihara R., Garruto R., Amano N. and Makita Z. (1998a) Advanced glycation end products in Alzheimer's disease and other neurodegenerative diseases. *Am J Pathol.* **153,** 1149-1155.

Sasaki S. and Iwata M. (1996) Ultrastructural study of synapses in the anterior horn neurons of patients with amyotrophic lateral sclerosis. *Neurosci. Lett.* **204,** 53-56.

Sasaki S. and Iwata M. (2007) Mitochondrial alterations in the spinal cord of patients with sporadic amyotrophic lateral sclerosis. *J. Neuropathol. Exp. Neurol.* **66,** 10-16.

Sasaki S., Komori T. and Iwata M. (2000) Excitatory amino acid transporter 1 and 2 immunoreactivity in the spinal cord in amyotrophic lateral sclerosis. *Acta Neuropathol.* **100,** 138-144.

Sasaki S., Komori T. and Iwata M. (2006) Neuronal inclusions in sporadic motor neuron disease are negative for alpha-synuclein. *Neurosci. Lett.* **397,** 15-19.

Sasaki S. and Maruyama S. (1992) Ultrastructural study of skein-like inclusions in anterior horn neurons of patients with motor neuron disease. *Neurosci. Lett.* **147,** 121-124.

Sasaki S., Ohsawa Y., Yamane K., Sakuma H., Shibata N., Nakano R., Kikugawa K., Mizutani T., Tsuji S. and Iwata M. (1998b) Familial amyotrophic lateral sclerosis with widespread vacuolation and hyaline inclusions. *Neurology* **51,** 871-873.

Sasaki S., Toi S., Shirata A., Yamane K., Sakuma H. and Iwata M. (2001) Immunohistochemical and ultrastructural study of basophilic inclusions in adult-onset motor neuron disease. *Acta Neuropathol.* **102,** 200-206.

Sasaki S., Yamane K., Sakuma H. and Maruyama S. (1989) Sporadic motor neuron disease with Lewy body-like hyaline inclusions. *Acta Neuropathol.* **78,** 555-560.

Sato T., Nakanishi T., Yamamoto Y., Andersen P. M., Ogawa Y., Fukada K., Zhou Z., Aoike F., Sugai F., Nagano S., Hirata S., Ogawa M., Nakano R., Ohi T., Kato T., Nakagawa M., Hamasaki T., Shimizu A. and Sakoda S. (2005) Rapid disease progression correlates with instability of mutant SOD1 in familial ALS. *Neurology* **65,** 1954-1957.

Schiffer D. and Fiano V. (2004) Astrogliosis in ALS: possible interpretations according to pathogenetic hypotheses. *Amyotroph. Lateral. Scler. Other Motor Neuron Disord.* **5,** 22-25.

Schmidt P. J., Kunst C. and Culotta V. C. (2000) Copper activation of superoxide dismutase 1 (SOD1) *in vivo*. Role for protein-protein interactions with the copper chaperone for SOD1. *J. Biol. Chem.* **275,** 33771-33776.

Schmidtke G., Emch S., Groettrup M. and Holzhutter H. G. (2000) Evidence for the Existence of a Non-catalytic Modifier Site of Peptide Hydrolysis by the 20 S Proteasome. *J. Biol. Chem.* **275,** 22056-22063.

Schmolck H., Mosnik D. and Schulz P. (2007) Rating the approachability of faces in ALS. *Neurology* **69,** 2232-2235.

Schochet S. S., Jr. and McCormick W. F. (1972) Ultrastructure of Hirano bodies. *Acta Neuropathol.* **21,** 50-60.

Schroder H. D. (1981) Onuf's nucleus X: a morphological study of a human spinal nucleus. *Anat. Embryol. (Berl)* **162,** 443-453.

Schuck P. (2008) Sedfit, http://www.analyticalultracentrifugation.com/default.htm.

Schwartz J. H. and Westbrook G. L. (2000) Synthesis and Trafficking of Neuronal Protein, in *Principles of Neural Science,* (Kandel E. R., Schwartz J. H. and Jessell T. M., eds), pp. 88-104. McGraw-Hill.

Sellarajah S., Lekishvili T., Bowring C., Thompsett A. R., Rudyk H., Birkett C. R., Brown D. R. and Gilbert I. H. (2004) Synthesis of analogues of Congo red and evaluation of their anti-prion activity. *J Med. Chem.* **47,** 5515-5534.

Sendtner M., Arakawa Y., Stockli K. A., Kreutzberg G. W. and Thoenen H. (1991) Effect of ciliary neurotrophic factor (CNTF) on motoneuron survival. *J Cell Sci Suppl* **15,** 103-109.

Shaw B. F. and Valentine J. S. (2007) How do ALS-associated mutations in superoxide dismutase 1 promote aggregation of the protein? *Trends Biochem. Sci.* **32,** 78-85.

Shaw C. A. and Wilson J. M. (2003) Analysis of neurological disease in four dimensions: insight from ALS-PDC epidemiology and animal models. *Neurosci. Biobehav. Rev.* **27,** 493-505.

Shaw P. J. (1999) Motor neurone disease. *BMJ* **318,** 1118-1121.

Shaw P. J., Forrest V., Ince P. G., Richardson J. P. and Wastell H. J. (1995a) CSF and plasma amino acid levels in motor neuron disease: elevation of CSF glutamate in a subset of patients. *Neurodegeneration.* **4,** 209-216.

Shaw P. J. and Ince P. G. (1997) Glutamate, excitotoxicity and amyotrophic lateral sclerosis. *J. Neurol.* **244 Suppl 2,** S3-14.

Shaw P. J., Ince P. G., Falkous G. and Mantle D. (1995b) Oxidative damage to protein in sporadic motor neuron disease spinal cord. *Ann. Neurol.* **38,** 691-695.

Shefner J. M., Tyler H. R. and Krarup C. (1991) Abnormalities in the sensory action potential in patients with amyotrophic lateral sclerosis. *Muscle Nerve* **14,** 1242-1246.

Shibata N. (2001) Transgenic mouse model for familial amyotrophic lateral sclerosis with superoxide dismutase-1 mutation. *Neuropathology.* **21,** 82-92.

Shibata N., Asayama K., Hirano A. and Kobayashi M. (1996) Immunohistochemical study on superoxide dismutases in spinal cords from autopsied patients with amyotrophic lateral sclerosis. *Dev. Neurosci.* **18,** 492-498.

Shibata N., Hirano A., Kobayashi M., Dal Canto M. C., Gurney M. E., Komori T., Umahara T. and Asayama K. (1998) Presence of Cu/Zn superoxide dismutase (SOD) immunoreactivity in neuronal hyaline inclusions in spinal cords from mice carrying a transgene for Gly93Ala mutant human Cu/Zn SOD. *Acta Neuropathol. (Berl)* **95,** 136-142.

Shibata N., Kawaguchi M., Uchida K., Kakita A., Takahashi H., Nakano R., Fujimura H., Sakoda S., Ihara Y., Nobukuni K., Takehisa Y., Kuroda S., Kokubo Y., Kuzuhara S., Honma T., Mochizuki Y., Mizutani T., Yamada S., Toi S., Sasaki S., Iwata M., Hirano A., Yamamoto T., Kato Y., Sawada T. and Kobayashi M. (2007) Protein-bound crotonaldehyde accumulates in the spinal cord of superoxide dismutase-1 mutation-associated familial amyotrophic lateral sclerosis and its transgenic mouse model. *Neuropathology.* **27,** 49-61.

Siddique T., Pericak-Vance M. A., Caliendo J., Hong S. T., Hung W. Y., Kaplan J., Kenna-Yasek D., Rimmler J. B., Sapp P., Saunders A. M., Scott W. K., Siddique N., Haines J. L. and Brown R. H. (1998) Lack of association between apolipoprotein E genotype and sporadic amyotrophic lateral sclerosis. *Neurogenetics.* **1,** 213-216.

Siklos L., Engelhardt J., Harati Y., Smith R. G., Joo F. and Appel S. H. (1996) Ultrastructural evidence for altered calcium in motor nerve terminals in amyotropic lateral sclerosis. *Ann. Neurol.* **39,** 203-216.

Son M., Puttaparthi K., Kawamata H., Rajendran B., Boyer P. J., Manfredi G. and Elliott J. L. (2007) Overexpression of CCS in G93A-SOD1 mice leads to accelerated neurological deficits with severe mitochondrial pathology. *Proc. Natl. Acad. Sci. U. S. A.* **104,** 6072-6077.

Song C. H., Furuoka H., Kim C. L., Ogino M., Suzuki A., Hasebe R. and Horiuchi M. (2008) Effect of intraventricular infusion of anti-prion protein monoclonal antibodies on disease progression in prion-infected mice. *J. Gen. Virol.* **89,** 1533-1544.

Soto C. (2001) Protein misfolding and disease; protein refolding and therapy. *FEBS Lett.* **498,** 204-207.

Soto C., Estrada L. and Castilla J. (2006) Amyloids, prions and the inherent infectious nature of misfolded protein aggregates. *Trends Biochem. Sci.* **31,** 150-155.

Spencer P. S., Palmer V. S. and Ludolph A. C. (2005) On the decline and etiology of high-incidence motor system disease in West Papua (southwest New Guinea). *Mov Disord.* **20 Suppl 12,** S119-S126.

Spooner E. T., Desai R. V., Mori C., Leverone J. F. and Lemere C. A. (2002) The generation and characterization of potentially therapeutic Abeta antibodies in mice: differences according to strain and immunization protocol. *Vaccine* **21,** 290-297.

Spreux-Varoquaux O., Bensimon G., Lacomblez L., Salachas F., Pradat P. F., Le F. N., Marouan A., Dib M. and Meininger V. (2002) Glutamate levels in cerebrospinal fluid in amyotrophic lateral sclerosis: a reappraisal using a new HPLC method with coulometric detection in a large cohort of patients. *J. Neurol. Sci.* **193,** 73-78.

Sreedharan J., Blair I. P., Tripathi V. B., Hu X., Vance C., Rogelj B., Ackerley S., Durnall J. C., Williams K. L., Buratti E., Baralle F., de B. J., Mitchell J. D., Leigh P. N., Al-Chalabi A., Miller C. C., Nicholson G. and Shaw C. E. (2008) TDP-43 mutations in familial and sporadic amyotrophic lateral sclerosis. *Science* **319,** 1668-1672.

Stathopulos P. B., Rumfeldt J. A., Scholz G. A., Irani R. A., Frey H. E., Hallewell R. A., Lepock J. R. and Meiering E. M. (2003) Cu/Zn superoxide dismutase mutants associated with amyotrophic lateral sclerosis show enhanced formation of aggregates *in vitro*. *Proc. Natl. Acad. Sci. U. S. A.* **100,** 7021-7026.

Stieber A., Gonatas J. O. and Gonatas N. K. (2000) Aggregation of ubiquitin and a mutant ALS-linked SOD1 protein correlate with disease progression and fragmentation of the Golgi apparatus. *J. Neurol. Sci.* **173,** 53-62.

Strack P. R., Waxman L. and Fagan J. M. (1996) Activation of the multicatalytic endopeptidase by oxidants. Effects on enzyme structure. *Biochemistry* **35,** 7142-7149.

Strange R. W., Antonyuk S., Hough M. A., Doucette P. A., Rodriguez J. A., Hart P. J., Hayward L. J., Valentine J. S. and Hasnain S. S. (2003) The structure of holo and metal-deficient wild-type human Cu, Zn superoxide dismutase and its relevance to familial amyotrophic lateral sclerosis. *J. Mol. Biol.* **328,** 877-891.

Strange R. W., Antonyuk S. V., Hough M. A., Doucette P. A., Valentine J. S. and Hasnain S. S. (2006) Variable metallation of human superoxide dismutase: atomic resolution crystal structures of Cu-Zn, Zn-Zn and as-isolated wild-type enzymes. *J. Mol. Biol.* **356,** 1152-1162.

Strom A. L., Shi P., Zhang F., Gal J., Kilty R., Hayward L. J. and Zhu H. (2008) Interaction of ALS-related mutant copper-zinc superoxide dismutase with the dynein-dynactin complex contributes to inclusion formation. *J. Biol. Chem.* **E-pub 30 May 2008.**

Strong M. J. (2003) The basic aspects of therapeutics in amyotrophic lateral sclerosis. *Pharmacol. Ther.* **98,** 379-414.

Strong M. J., Grace G. M., Orange J. B., Leeper H. A., Menon R. S. and Aere C. (1999) A prospective study of cognitive impairment in ALS. *Neurology* **53,** 1665.

Strong M. J. and Pattee G. L. (2000) Creatine and coenzyme Q10 in the treatment of ALS. *Amyotroph. Lateral. Scler. Other Motor Neuron Disord.* **1 Suppl 4,** 17-20.

Sutedja N. A., Sinke R. J., Van Vught P. W., Van der Linden M. W., Wokke J. H., Van Duijn C. M., Njajou O. T., Van der Schouw Y. T., Veldink J. H. and Van den Berg L. H. (2007) The association between H63D mutations in HFE and amyotrophic lateral sclerosis in a Dutch population. *Arch. Neurol.* **64,** 63-67.

Suthers G., Laing N., Wilton S., Dorosz S. and Waddy H. (1994) "Sporadic" motoneuron disease due to familial SOD1 mutation with low penetrance. *Lancet* **344,** 1773.

Suzuki E. and Nakayama M. (2007) MEGF10 is a mammalian ortholog of CED-1 that interacts with clathrin assembly protein complex 2 medium chain and induces large vacuole formation. *Exp. Cell Res.* **313,** 3729-3742.

Swash M. and Leigh N. (1992) Criteria for diagnosis of familial amyotrophic lateral sclerosis. European FALS Collaborative Group. *Neuromuscul. Disord.* **2,** 7-9.

Tabata R. C., Wilson J. M., Ly P., Zwiegers P., Kwok D., Van Kampen J. M., Cashman N. and Shaw C. A. (2008) Chronic Exposure to Dietary Sterol Glucosides is Neurotoxic to Motor Neurons and Induces an ALS-PDC Phenotype. *Neuromolecular. Med.* **10,** 24-39.

Tainer J. A., Getzoff E. D., Beem K. M., Richardson J. S. and Richardson D. C. (1982) Determination and analysis of the 2 A-structure of copper, zinc superoxide dismutase. *J. Mol. Biol.* **160,** 181-217.

Takahashi R., Yokoji H., Misawa H., Hayashi M., Hu J. and Deguchi T. (1994) A null mutation in the human CNTF gene is not causally related to neurological diseases. *Nat. Genet.* **7,** 79-84.

Takehisa Y., Ujike H., Ishizu H., Terada S., Haraguchi T., Tanaka Y., Nishinaka T., Nobukuni K., Ihara Y., Namba R., Yasuda T., Nishibori M., Hayabara T. and Kuroda S. (2001) Familial amyotrophic lateral sclerosis with a novel Leu126Ser mutation in the copper/zinc superoxide dismutase gene showing mild clinical features and lewy body-like hyaline inclusions. *Arch. Neurol.* **58,** 736-740.

Takeuchi H., Kobayashi Y., Ishigaki S., Doyu M. and Sobue G. (2002a) Mitochondrial localization of mutant superoxide dismutase 1 triggers caspase-dependent cell death in a cellular model of familial amyotrophic lateral sclerosis. *J. Biol. Chem.* **277,** 50966-50972.

Takeuchi H., Kobayashi Y., Yoshihara T., Niwa J., Doyu M., Ohtsuka K. and Sobue G. (2002b) Hsp70 and Hsp40 improve neurite outgrowth and suppress intracytoplasmic aggregate formation in cultured neuronal cells expressing mutant SOD1. *Brain Res.* **949,** 11-22.

Talbot K. (2004) Motor neuron disease. *Medicine* **32,** 105-107.

Tan C. F., Eguchi H., Tagawa A., Onodera O., Iwasaki T., Tsujino A., Nishizawa M., Kakita A. and Takahashi H. (2007) TDP-43 immunoreactivity in neuronal inclusions in familial amyotrophic lateral sclerosis with or without SOD1 gene mutation. *Acta Neuropathol.* **113,** 535-542.

Tandan R. and Bradley W. G. (1985) Amyotrophic lateral sclerosis: Part 1. Clinical features, pathology, and ethical issues in management. *Ann. Neurol.* **18,** 271-280.

Telling G. C., Scott M., Mastrianni J., Gabizon R., Torchia M., Cohen F. E., DeArmond S. J. and Prusiner S. B. (1995) Prion propagation in mice expressing human and chimeric PrP transgenes implicates the interaction of cellular PrP with another protein. *Cell* **83,** 79-90.

Teoh M. L., Turner P. V. and Evans D. H. (2005) Tumorigenic poxviruses up-regulate intracellular superoxide to inhibit apoptosis and promote cell proliferation. *J. Virol.* **79,** 5799-5811.

Teuchert M., Fischer D., Schwalenstoecker B., Habisch H. J., B÷ckers T. M. and Ludolph A. C. (2006) A dynein mutation attenuates motor neuron degeneration in SOD1G93A mice. *Exp. Neurol.* **198,** 271-274.

Theiler K. (1989) *The House Mouse - Atlas of Embryonic Development.* Springer-Verlag.

Theys P. A., Peeters E. and Robberecht W. (1999) Evolution of motor and sensory deficits in amyotrophic lateral sclerosis estimated by neurophysiological techniques. *J. Neurol.* **246,** 438-442.

Thomas A. R., Oosthuizen V. and Naude R. J. (2005) Differential effects of detergents, fatty acids, cations and heating on ostrich skeletal muscle 20S proteasome. *Comp Biochem. Physiol B Biochem. Mol. Biol.* **140,** 343-348.

Tiwari A. and Hayward L. J. (2003) Familial amyotrophic lateral sclerosis mutants of copper/zinc superoxide dismutase are susceptible to disulfide reduction. *J. Biol. Chem.* **278,** 5984-5992.

Tiwari A. and Hayward L. J. (2005) Mutant SOD1 instability: implications for toxicity in amyotrophic lateral sclerosis. *Neurodegener. Dis.* **2,** 115-127.

Tiwari A., Xu Z. and Hayward L. J. (2005) Aberrantly increased hydrophobicity shared by mutants of Cu,Zn-superoxide dismutase in familial amyotrophic lateral sclerosis. *J. Biol. Chem.* **280,** 29771-29779.

Tomkins J., Usher P., Slade J. Y., Ince P. G., Curtis A., Bushby K. and Shaw P. J. (1998) Novel insertion in the KSP region of the neurofilament heavy gene in amyotrophic lateral sclerosis (ALS). *Neuroreport* **9,** 3967-3970.

Tortarolo M., Veglianese P., Calvaresi N., Botturi A., Rossi C., Giorgini A., Migheli A. and Bendotti C. (2003) Persistent activation of p38 mitogen-activated protein kinase in a mouse model of familial amyotrophic lateral sclerosis correlates with disease progression. *Mol. Cell Neurosci.* **23,** 180-192.

Traynor B. J., Codd M. B., Corr B., Forde C., Frost E. and Hardiman O. M. (2000) Clinical features of amyotrophic lateral sclerosis according to the El Escorial and Airlie House diagnostic criteria: A population-based study. *Arch. Neurol.* **57,** 1171-1176.

Tsien R. Y. (1998) The green fluorescent protein. *Annu. Rev. Biochem.* **67,** 509-544.

Tu P. H., Gurney M. E., Julien J. P., Lee V. M. and Trojanowski J. Q. (1997) Oxidative stress, mutant SOD1, and neurofilament pathology in transgenic mouse models of human motor neuron disease. *Lab. Invest.* **76,** 441-456.

Tucci V., Achilli F., Blanco G., Lad H. V., Wells S., Godinho S. and Nolan P. M. (2007) Reaching and grasping phenotypes in the mouse (Mus musculus): a characterization of inbred strains and mutant lines. *Neuroscience* **147,** 573-582.

Tummala H., Jung C., Tiwari A., Higgins C. M., Hayward L. J. and Xu Z. (2005) Inhibition of chaperone activity is a shared property of several Cu,Zn-superoxide dismutase mutants that cause amyotrophic lateral sclerosis. *J. Biol. Chem.* **280,** 17725-17731.

Turner B. J., Atkin J. D., Farg M. A., Zang D. W., Rembach A., Lopes E. C., Patch J. D., Hill A. F. and Cheema S. S. (2005) Impaired extracellular secretion of mutant superoxide dismutase 1 associates with neurotoxicity in familial amyotrophic lateral sclerosis. *J. Neurosci.* **25,** 108-117.

Turner B. J. and Talbot K. (2008) Transgenics, toxicity and therapeutics in rodent models of mutant SOD1-mediated familial ALS. *Prog. Neurobiol.* **85,** 94-134.

Urushitani M., Ezzi S. A. and Julien J. P. (2007) Therapeutic effects of immunization with mutant superoxide dismutase in mice models of amyotrophic lateral sclerosis. *Proc. Natl. Acad. Sci. U. S. A.* **104,** 2495-2500.

Urushitani M., Ezzi S. A., Matsuo A., Tooyama I. and Julien J. P. (2008) The endoplasmic reticulum-Golgi pathway is a target for translocation and aggregation of mutant superoxide dismutase linked to ALS. *FASEB J.* **22,** 2476-2487.

Urushitani M., Kurisu J., Tsukita K. and Takahashi R. (2002) Proteasomal inhibition by misfolded mutant superoxide dismutase 1 induces selective motor neuron death in familial amyotrophic lateral sclerosis. *J. Neurochem.* **83,** 1030-1042.

Urushitani M., Sik A., Sakurai T., Nukina N., Takahashi R. and Julien J. P. (2006) Chromogranin-mediated secretion of mutant superoxide dismutase proteins linked to amyotrophic lateral sclerosis. *Nat. Neurosci.* **9,** 108-118.

Valentine J. S., Doucette P. A. and Zittin P. S. (2005) Copper-zinc superoxide dismutase and amyotrophic lateral sclerosis. *Annu. Rev. Biochem.* **74,** 563-593.

Valentine J. S. and Hart P. J. (2003) Misfolded CuZnSOD and amyotrophic lateral sclerosis. *Proc. Natl. Acad. Sci. U. S. A.* **100,** 3617-3622.

Van Deerlin V., Leverenz J. B., Bekris L. M., Bird T. D., Yuan W., Elman L. B., Clay D., Wood E. M., Chen-Plotkin A. S., Martinez-Lage M., Steinbart E., McCluskey L., Grossman M., Neumann M., Wu I. L., Yang W. S., Kalb R., Galasko D. R., Montine T. J., Trojanowski J. Q., Lee V. M., Schellenberg G. D. and Yu C. E. (2008) TARDBP mutations in amyotrophic lateral sclerosis with TDP-43 neuropathology: a genetic and histopathological analysis. *Lancet Neurol.* **7,** 409-416.

Van Den B. L., Van D. P., Bogaert E. and Robberecht W. (2006) The role of excitotoxicity in the pathogenesis of amyotrophic lateral sclerosis. *Biochim. Biophys. Acta* **1762,** 1068-1082.

Vande V. C., Miller T. M., Cashman N. R. and Cleveland D. W. (2008) Selective association of misfolded ALS-linked mutant SOD1 with the cytoplasmic face of mitochondria. *Proc. Natl. Acad. Sci U. S. A.* **105,** 4022-4027.

Vigouroux S., Farout L., Clavel S., Briand Y. and Briand M. (2003) Increased muscle proteasome activities in rats fed a polyunsaturated fatty acid supplemented diet. *The International Journal of Biochemistry & Cell Biology* **35,** 749-755.

Vijayvergiya C., Beal M. F., Buck J. and Manfredi G. (2005) Mutant superoxide dismutase 1 forms aggregates in the brain mitochondrial matrix of amyotrophic lateral sclerosis mice. *J. Neurosci.* **25,** 2463-2470.

Wang J., Caruano-Yzermans A., Rodriguez A., Scheurmann J. P., Slunt H. H., Cao X., Gitlin J., Hart P. J. and Borchelt D. R. (2007) Disease-associated mutations at copper ligand histidine residues of superoxide dismutase 1 diminish the binding of copper and compromise dimer stability. *J. Biol. Chem.* **282,** 345-352.

Wang J., Slunt H., Gonzales V., Fromholt D., Coonfield M., Copeland N. G., Jenkins N. A. and Borchelt D. R. (2003) Copper-binding-site-null SOD1 causes ALS in transgenic mice: aggregates of non-native SOD1 delineate a common feature. *Hum. Mol. Genet.* **12,** 2753-2764.

Wang J., Xu G., Gonzales V., Coonfield M., Fromholt D., Copeland N. G., Jenkins N. A. and Borchelt D. R. (2002) Fibrillar inclusions and motor neuron degeneration in transgenic mice expressing superoxide dismutase 1 with a disrupted copper-binding site. *Neurobiol. Dis.* **10,** 128-138.

Wang J., Xu G., Li H., Gonzales V., Fromholt D., Karch C., Copeland N. G., Jenkins N. A. and Borchelt D. R. (2005a) Somatodendritic accumulation of misfolded SOD1-L126Z in motor neurons mediates degeneration: alphaB-crystallin modulates aggregation. *Hum. Mol. Genet.* **14,** 2335-2347.

Wang J., Xu G., Slunt H. H., Gonzales V., Coonfield M., Fromholt D., Copeland N. G., Jenkins N. A. and Borchelt D. R. (2005b) Coincident thresholds of mutant protein for paralytic disease and protein aggregation caused by restrictively expressed superoxide dismutase cDNA. *Neurobiol. Dis.* **20,** 943-952.

Wang X. S., Lee S., Simmons Z., Boyer P., Scott K., Liu W. and Connor J. (2004) Increased incidence of the Hfe mutation in amyotrophic lateral sclerosis and related cellular consequences. *J. Neurol. Sci.* **227,** 27-33.

Watanabe M., Dykes-Hoberg M., Culotta V. C., Price D. L., Wong P. C. and Rothstein J. D. (2001) Histological evidence of protein aggregation in mutant SOD1 transgenic mice and in amyotrophic lateral sclerosis neural tissues. *Neurobiol. Dis.* **8,** 933-941.

Watanabe Y., Yasui K., Nakano T., Doi K., Fukada Y., Kitayama M., Ishimoto M., Kurihara S., Kawashima M., Fukuda H., Adachi Y., Inoue T. and Nakashima K. (2005) Mouse motor neuron disease caused by truncated SOD1 with or without C-terminal modification. *Brain Res. Mol. Brain Res.* **135,** 12-20.

Wheaton M. W., Salamone A. R., Mosnik D. M., McDonald R. O., Appel S. H., Schmolck H. I., Ringholz G. M. and Schulz P. E. (2007) Cognitive impairment in familial ALS. *Neurology* **69,** 1411-1417.

Wightman G., Anderson V. E., Martin J., Swash M., Anderton B. H., Neary D., Mann D., Luthert P. and Leigh P. N. (1992) Hippocampal and neocortical ubiquitin-immunoreactive inclusions in amyotrophic lateral sclerosis with dementia. *Neurosci. Lett.* **139,** 269-274.

Williams T. L., Shaw P. J., Lowe J., Bates D. and Ince P. G. (1995) Parkinsonism in motor neuron disease: case report and literature review. *Acta Neuropathol.* **89,** 275-283.

Wilson C. M., Grace G. M., Munoz D. G., He B. P. and Strong M. J. (2001) Cognitive impairment in sporadic ALS: a pathologic continuum underlying a multisystem disorder. *Neurology* **57,** 651-657.

Wilson J. M., Khabazian I., Wong M. C., Seyedalikhani A., Bains J. S., Pasqualotto B. A., Williams D. E., Andersen R. J., Simpson R. J., Smith R., Craig U. K., KURLAND L. T. and Shaw C. A. (2002) Behavioral and neurological correlates of ALS-parkinsonism dementia complex in adult mice fed washed cycad flour. *Neuromolecular. Med.* **1,** 207-221.

Winter S. M., Claus A., Oberwittler C., Volkel H., Wenzler S. and Ludolph A. C. (2000) Recessively inherited amyotrophic lateral sclerosis: a Germany family with the D90A CuZn-SOD mutation. *J. Neurol.* **247,** 783-786.

Wong P. C., Pardo C. A., Borchelt D. R., Lee M. K., Copeland N. G., Jenkins N. A., Sisodia S. S., Cleveland D. W. and Price D. L. (1995) An adverse property of a familial ALS-linked SOD1 mutation causes motor neuron disease characterized by vacuolar degeneration of mitochondria. *Neuron* **14,** 1105-1116.

Wood J. D., Beaujeux T. P. and Shaw P. J. (2003) Protein aggregation in motor neurone disorders. *Neuropathol. Appl. Neurobiol.* **29,** 529-545.

Worms P. M. (2001) The epidemiology of motor neuron diseases: a review of recent studies. *J. Neurol. Sci.* **191,** 3-9.

Wroe R. (2008) ALS Online Database (ALSOD). *http://alsod. iop. kcl. ac. uk/Als/index. aspx.*

Wu D., Yu W., Kishikawa H., Folkerth R. D., Iafrate A. J., Shen Y., Xin W., Sims K. and Hu G. F. (2007) Angiogenin loss-of-function mutations in amyotrophic lateral sclerosis. *Ann. Neurol.* **62,** 609-617.

Wu M. M., Llopis J., Adams S., McCaffery J. M., Kulomaa M. S., Machen T. E., Moore H. P. and Tsien R. Y. (2000) Organelle pH studies using targeted avidin and fluorescein-biotin. *Chem. Biol.* **7,** 197-209.

Wulfsberg E. A., Carrel R. E., Klisak I. J., O'Brien T. J., Sykes J. A. and Sparkes R. S. (1983) Normal superoxide dismutase-1 (SOD-1) activity with deletion of chromosome band 21q21 supports localization of SOD-1 locus to 21q22. *Hum. Genet.* **64,** 271-272.

Xiao S., McLean J. and Robertson J. (2006) Neuronal intermediate filaments and ALS: a new look at an old question. *Biochim. Biophys. Acta* **1762,** 1001-1012.

Xu Z., Cork L. C., Griffin J. W. and Cleveland D. W. (1993) Increased expression of neurofilament subunit NF-L produces morphological alterations that resemble the pathology of human motor neuron disease. *Cell* **73,** 23-33.

Yamanaka K., Boillee S., Roberts E. A., Garcia M. L., onis-Downes M., Mikse O. R., Cleveland D. W. and Goldstein L. S. (2008) Mutant SOD1 in cell types other than motor neurons and oligodendrocytes accelerates onset of disease in ALS mice. *Proc. Natl. Acad. Sci U. S. A.* **105,** 7594-7599.

Yang Y., Hentati A., Deng H. X., Dabbagh O., Sasaki T., Hirano M., Hung W. Y., Ouahchi K., Yan J., Azim A. C., Cole N., Gascon G., Yagmour A., Ben-Hamida M., Pericak-Vance M., Hentati F. and Siddique T. (2001) The gene encoding alsin, a protein with three guanine-nucleotide exchange factor domains, is mutated in a form of recessive amyotrophic lateral sclerosis. *Nat. Genet.* **29,** 160-165.

Yasuda M., Murakami Y., Sowa A., Ogino H. and Ishikawa H. (1998) Effect of additives on refolding of a denatured protein. *Biotechnol. Prog.* **14,** 601-606.

Yokoseki A., Shiga A., Tan C. F., Tagawa A., Kaneko H., Koyama A., Eguchi H., Tsujino A., Ikeuchi T., Kakita A., Okamoto K., Nishizawa M., Takahashi H. and Onodera O. (2008) TDP-43 mutation in familial amyotrophic lateral sclerosis. *Ann. Neurol.* **63,** 538-542.

Yoo H. Y., Kim S. S. and Rho H. M. (1999) Overexpression and simple purification of human superoxide dismutase (SOD1) in yeast and its resistance to oxidative stress. *J. Biotechnol.* **68,** 29-35.

Yoshida S., Uebayashi Y., Kihira T., Kohmoto J., Wakayama I., Taguchi S. and Yase Y. (1998) Epidemiology of motor neuron disease in the Kii Peninsula of Japan, 1989-1993: active or disappearing focus? *J. Neurol. Sci.* **155,** 146-155.

Yukawa M., Sakon M., Kambayashi J., Shiba E., Kawasaki T., Uemura Y., Murata K., Tanaka T., Nakayama T., Shibata H. and . (1993) Purification and characterization of endogenous protein activator of human platelet proteasome. *J. Biochem.* **114,** 317-323.

Zelko I. N., Mariani T. J. and Folz R. J. (2002) Superoxide dismutase multigene family: a comparison of the CuZn-SOD (SOD1), Mn-SOD (SOD2), and EC-SOD (SOD3) gene structures, evolution, and expression. *Free Radic. Biol. Med.* **33,** 337-349.

Zetterberg H., Jacobsson J., Rosengren L., Blennow K. and Andersen P. M. (2007) Cerebrospinal fluid neurofilament light levels in amyotrophic lateral sclerosis: impact of SOD1 genotype. *Eur. J. Neurol* **14,** 1329-1333.

Zhang F., Strom A. L., Fukada K., Lee S., Hayward L. J. and Zhu H. (2007) Interaction between familial amyotrophic lateral sclerosis (ALS)-linked SOD1 mutants and the dynein complex. *J. Biol. Chem.* **282,** 16691-16699.

Zhu Q., Couillard-Despres S. and Julien J. P. (1997) Delayed maturation of regenerating myelinated axons in mice lacking neurofilaments. *Exp. Neurol.* **148,** 299-316.

Zhu Q., Lindenbaum M., Levavasseur F., Jacomy H. and Julien J. P. (1998) Disruption of the NF-H gene increases axonal microtubule content and velocity of neurofilament transport: relief of axonopathy resulting from the toxin beta,beta'-iminodipropionitrile. *J. Cell Biol.* **143,** 183-193.

Zimmerman E. K., Eslinger P. J., Simmons Z. and Barrett A. M. (2007a) Emotional perception deficits in amyotrophic lateral sclerosis. *Cogn. Behav. Neurol* **20,** 79-82.

Zimmerman M. C., Oberley L. W. and Flanagan S. W. (2007b) Mutant SOD1-induced neuronal toxicity is mediated by increased mitochondrial superoxide levels. *J. Neurochem.* **102,** 609-618.

Zoccolella S., Beghi E., Palagano G., Fraddosio A., Guerra V., Samarelli V., Lepore V., Simone I. L., Lamberti P., Serlenga L., Logroscino G. and for the SLAP Registry (2008) Analysis of survival and prognostic factors in amyotrophic lateral sclerosis: a population based study. *J. Neurol. Neurosurg. Psychiatry* **79,** 33-37.

Zoccolella S., Palagano G., Fraddosio A., Russo I., Ferrannini E., Serlenga L., Maggio F., Lamberti S. and Iliceto G. (2002) ALS-plus: 5 cases of concomitant amyotrophic lateral sclerosis and parkinsonism. *Neurol. Sci.* **23 Suppl 2,** S123-S124.

APPENDICES

Appendix A Mariusz primers information

Appendix B Review on the origins and the uses of mouse outbred stock (Chia *et al.* 2005)

Appendix C Genealogy of Swiss mice (Supplementary data to Chia *et al.* 2005)

Appendix D The SOD1 transgene in the G93A mouse model of amyotrophic lateral sclerosis lies on distal mouse chromosome 12 (Achilli *et al.* 2005)

APPENDIX A **Mariusz primer information**

Marker	MGI Accession ID	Location (bp)	Primer sequence (5' to 3') (F= forward, R = Reverse)	Primer T_m (°C)	PCR T_A (°C)	5' fluorescent tag on F primer (if any)
D18Mit177	MGI:707005	41108480	F = CTGTAGTTTATCAGTTCACCCTGTG R = TGTGCTGTTAAACAAATATCTCTGG	58.4 55.5	58.0	none
D18Mit202	MGI:701499	43517266	F = CCCCTTGCAAAGATGGAGTA R = CATTTGCTAGTTTAGCAGGAAGC	63.8 62.9	63.0	none
D18Mit105	MGI:705199	53209717	F = CACAAGATCAAGCCAAGCAA R = GCTTCCTTCATGTAATATGTTTTCC	63.9 62.4	63.0	none
D18Mit123	MGI:701605	56095974	F = GGAATATATTACAGAAGAAAGCACAGG R = TCTGACACTGACTGGAACTACACA	62.8 60.8	62.0	Tet
D18Mit238	MGI:707294	57147126	F = TGTATCCTTTGTACTTAGAGACACAGC R = ACATGCCTGACAAATTTATTTGG	62.5 54.3	62.0	Tet
D18Mit124	MGI:701612	57582856	F = CCCAAATGGGGTGTCTTTTA R = CTGCCACACATTTGTGTGTATG	63.3 57.0	63.0	Hex
D18Mit181	MGI:706028	58120164	F = CTTGAACTTCCTTCACAAGAACTG R = AATCATGCTACTTGGAATGATAATG	62.9 52.8	62.0	Fam
D18Mit52	MGI:707654	58462984	F = TTCTCCTTTCTTCTGATAGATCCC R = TGTATGTATGTAGGAGTGTGTGCG	62.5 58.6	62.0	Fam

Marker	MGI Accession ID	Location (bp)	Primer sequence (5' to 3') (F= forward, R = Reverse)	Primer T_m (°C)	PCR T_A (°C)	5' fluorescent tag on F primer (if any)
D18Mit28	MGI:702449	60303417	F = TCTGCAATGAGACAACCACTG R = TTTCCCAACATAAAAAAGCTCC	64.0 54.8	63.0	Hex
D18Mit78	MGI:704060	60934044	F = GCATGATACAGACGGGGC R = TCCCATATGTTCCTTCCTGC	64.2 58.6	64.0	Fam
D18Mit51	MGI:707653	61264745	F = AACATGGTGGAAACCAACTACC R = AAGGGAAAGTCACCACATGC	59.1 59.2	59.0	none
D18Mit152	MGI:703067	62062136	F = CTGACCTCTTCCCACTCGAG R = CATGTTTGTTCCGAAGCATG	64.0 55.3	63.0	Hex
D18Mit139	MGI:707408	62535609	F = GTATTTGTATACAAGCAGGTATAGGGG R = ATGTGCATGGACACATAAGCA	62.4 56.6	62.0	Hex
D18Mit161	MGI:701238	65803001	F = TGACCAGCGTTTGATGGAT R = TTCCACAAGTTGTCAACTCCC	64.2 59.5	64.0	Fam
D18Mit209	MGI:701494	67091136	F = AAGTTGACAACCAAGATTAACTCTAGC R = AGACCACCTTTGTAAATGTCTGTG	57.3 58.1	58.0	none

Primer Tm was calculated using an online Primer Melting Temperature Calculator at http://www.sigma-genosys.com/calc/DNACalc.asp